Detection of Prostate Cancer Biomarker Using Molecularly Imprinted Polymers

A thesis submitted in accordance with the conditions

governing candidates for the degree of

Philosophiae Doctor in Cardiff University

By

Vibha Tamboli (M.S)

March 2017

Welsh School of Pharmacy and Pharmaceutical Sciences

Cardiff University

DECLARATION

This work has not been submitted in substance for any other degree or award at this or any other university or place of learning, nor is being submitted concurrently in candidature for any degree or other award.

Signed *Camboli*   Date.   08.08.2017

STATEMENT 1

This thesis is being submitted in partial fulfillment of the requirements for the degree of PhD

Signed *Camboli*   Date.   08.08.2017

STATEMENT 2

This thesis is the result of my own independent work/investigation, except where otherwise stated, and the thesis has not been edited by a third party beyond what is permitted by Cardiff University's Policy on the Use of Third Party Editors by Research Degree Students. Other sources are acknowledged by explicit references. The views expressed are my own.

Signed *Camboli*   Date.   08.08.2017

STATEMENT 3

I hereby give consent for my thesis, if accepted, to be available online in the University's Open Access repository and for inter-library loan, and for the title and summary to be made available to outside organizations.

Signed *Camboli*   Date.   08.08.2017

Bhagyashri, who designed and created some of the images in this thesis. At the end I would like to express special thanks to my husband, Amit who spent sleepless nights and weekends listening to my experiences, answering my queries, and pushing me through at moments when no one else was around.

Abbreviations:

1. AAm - Acrylamide
2. AIBN - Azobisisobutyronitrile
3. AFM - Atomic Force Microscopy
4. AMACR - Alpha-methylacyl - CoA racemase
5. Ag/AgCl - Silver/Silver Chloride
6. BLAST - Basic Local Alignment Search Tool
7. BPH   Benign Prostate Hyperplasia
8. BSA – Bovine Serum Albumin
9. CE – Counter Electrode
10. CMOS - Complementary Metal-oxide-semiconductor
11. CV – Cyclic Voltammetry
12. DAC - Dopaminechrome
13. DAQ- Dopamine Orthoquinone
14. DRE – Digital Rectal Examination
15. DMF – Dimethylformamide
16. DCM – Dichloromethane
17. DIEA - N,N- Diisopropylethylamine
18. DIPEA - N, N - Diisoproylethylamine
19. DMSO – Dimethylsulphoxide
20. DPV – Differential Pulse Voltammetry
21. E-MIPs - Electrochemical MIPs
22. EDC/NHS - 1-Ethyl-3-(3-dimethylaminopropyl)carbodiimide / N-Hydroxysuccinimide
23. EDL – Electrochemical Double Layer
24. EGDMA - Ethyleneglycoldimethycrylate
25. ELISA – Enzyme Linked Immunoabsorbent Assay
26. EIS – Electrochemical Impedance Spectroscopy
27. FET – Field Effect Transistors
28. FDA - Food and Drug Administration
29. Fmoc - 9-fluoromethoxycarbonyl
30. FTIR - Fourier Transform Infrared Spectroscopy
31. GCE – Glassy Carbon Electrode
32. HBTU - 2-(1H-benzotriazol-1-yl)-1,1,3,3-tetramethyluronium hexafluorophosphate
33. HATU - 1-[Bis(dimethylamino)methylene]-1H-1,2,3-triazolo[4,5-b]pyridinium 3-oxid hexafluorophosphate

34. HoBt - Hydroxybenzotriazole

35. HK2 – Human Kallikrein 2

36. HPAP – Human Prostatic Acid Phosphatase

37. HPLC –High Pressure Liquid Chromatography

38. HPLC-MS - High Pressure Liquid Chromatography Mass spectrometry

39. HSA – Human Serum Albumin

40. IF – Imprinting Factor

41. IHP - Inner Helmholtz Plane

42. IDT - Inter-Digital Transducers

43. KCN – Potassium Cyanide

44. LOD – Limit of Detection

45. LPS – Lipopolysaccharide

46. LDAC - Leucodopaminechrome

47. MAA – Methacrylic Acid

48. MBHA - 4-Methylbenzhydrylamine

49. MIP – Molecularly Imprinted Polymers

50. MOSFET - Metal-oxide-semiconductor field effect transistor

51. MUA – Mercaptoundecanoic Acid

52. NIP – Non-Imprinted Polymer

53. NMR – Nuclear Magnetic Resonance

54. OHP - Outer Helmholtz plane

55. PAP - Polyaminophenol

56. PCa - Prostate Cancer

57. PCA3 - Prostate Cancer Antigen 3

58. PDA – Polydopamine

59. PSA - Prostate Specific Antigen

60. PSMA – Prostate Specific Membrane Antigen

61. PyBop - Benzotriazol-1-yl-oxytripyrrolidinophosphonium hexafluorophosphate

62. PDMS - Polydimethylsiloxane

63. QCM - Quartz Crystal Microbalance

64. RE – Reference Electrode

65. SAM – Self Assembled Monolayer

66. SDS - Sodium Dodecyl Sulphate

67. SEM – Scanning Electron Microscopy

68. SELEX - Systematic Evolution of Ligands by Exponential Enrichment

69. SPSS – Solid Phase Peptide Synthesis

70. SPR - Surface Plasmon Resonance

71. TFA – Trifluoroacetic Acid
72. TBA - Tetrabutylammonium Hydroxide
73. TIPS - Triisopropylsilane
74. TRUS - Transrectal Ultrasound Scan
75. TLC – Thin Layer Chromatography
76. Trt – Triphenylmethyl
77. USPSTF - US Preventive Services Task Force
78. VP –Vinyl Pyridine
79. WE – Working Electrode
80. XPS - X-ray Photoelectron Spectroscopy

Summary

Successful treatment of prostate cancer (PCa) depends on early diagnosis and screening, which currently relies on the measurement of serum prostate specific antigen (PSA) levels. The overarching aim of the project was to generate molecularly imprinted polymers for PCa biomarkers, with subsequent integration with a sensing platform to allow for rapid, point of care detection and monitoring.

The initial work involved the use of simple PSA epitopes for epitope imprinting using conventional imprinting techniques. A four amino acid sequence from the C-terminus of PSA was imprinted with MAA, Aam and Urea monomers to obtain bulk imprinted polymers. Apparent Kd of 102 µM, 154 µM, 194 µM was obtained for MAA, AAm, Urea based bulk mini-MIPs respectively. Epitope imprinting was further developed using a surface imprinting approach, via electropolymersiation of dopamine to detect an epitopic sequence from pro-PSA. An improvement in Kd from bulk-imprinted polymers, with an apparent Kd of 2.9 µM was obtained with the surface electrochemical MIP sensor. However, both epitope imprinting technique lacked sensitivity to measure clinical relevant concentrations of PSA (nM range). As a consequence, a more sophisticated technique called hybrid imprinting was developed to build an electrochemical MIP sensor. Hybrid MIP imprinting utilised an aptamer with established affinity towards PSA to trap the aptamer-PSA complex into a surface grown electropolymer (polydopamine). The resulting aptamer lined polymer pockets exhibited high selectivity and affinity towards PSA (apparent Kd 0.3 nM). The apta-MIP sensor was also able to discriminate from a homologous protein (human Kallikrein 2) and was resilient to fouling from serum proteins. The apta-MIP sensor was further translated to a MOSFET device whereby successful detection of PSA at clinically relevant concentration was obtained in human plasma. Although good sensitivity and selectivity was obtained with the hybrid-MIP sensors, further research is required to understand the binding mechanism of the template to the MIP.

Table of Contents

List of Figures and Tables

1. Chapter: General Introduction

1.1. General Overview Of Project

Prostate Cancer (PCa) is one of the most common cancers in men in the UK, with over 40,000 new cases being diagnosed every year. One in every eight men suffers from prostate cancer in the UK.[1] Successful treatment of PCa depends on early diagnosis and screening, which currently relies on the measurement of serum prostate specific antigen (PSA) levels.[2] PSA is a 30 –32 KDa protein secreted by the prostate gland, levels of which are found elevated in men with PCa.[3] PSA alone does not have sufficient diagnostic or prognostic power to enable patient stratification and inform treatment decisions.[4] There is a need to develop a robust, sensitive and specific assay for prostate cancer detection. Monitoring the combination of different forms of PSA such as free PSA, total PSA and pro-PSA has been shown to improve assay specificity and sensitivity.[3,5] This project was aimed to generate molecularly imprinted polymers as synthetic receptors for detection of prostate cancer biomarkers, with subsequent integration with a sensing platform to allow for rapid, point of care detection, diagnosis and monitoring. The project was part of a Marie Curie initial training network "PROSENSE".

1.2. Introduction To Prostate Cancer And Relevant Biomarkers

1.2.1. Anatomy of the prostate gland

The prostate gland is a small walnut sized gland located below the bladder and is part of the male reproductive system (Figure 1.1).[6] It is divided into three anatomical zones known as the peripheral, central and transitional zones. The peripheral zone is closest to the rectum, the transitional zone is the middle section of the prostate and the central

zone is in front of the transitional zone and farthest from the rectum. The gland is made up of three different types of cells: gland cells (secrete enzymes), muscle cells (control urine flow) and fibrous cells that support structure of the gland. The physiological role of the prostate is to secrete enzymes for the de-coagulation of semen and to produce citrate, fructose and zinc to facilitate free movement of sperm.[7]

1.2.2. Diseases of the prostate gland

Various conditions affect the prostate such as prostatitis, benign prostatic hyperplasia (BPH) and cancer. Prostatis is the inflammation of the prostate, which is caused by infection and is treated with antibiotics. As men age, the transition zone of prostate gland starts to enlarge till it becomes the largest part of the gland. This condition is termed as BPH and affects virtually all men above the age of 50.[8] BPH also leads to increase in PSA levels in the blood leading to false positives during PCa screening. Prostate cancer arises when a cell in the gland escapes its normal function during cell division and starts dividing abnormally and continuously as a result of mutations in certain genes.[9] This causes the gland to enlarge abnormally as seen in Figure 1.1. Since the prostate gland is well connected to several lymph nodes, PCa metastases are relatively common in aggressive forms of PCa. Although the majority of metastases are found in the bone tissue, the disease is also capable of spreading to the hepatic and respiratory systems.[10]
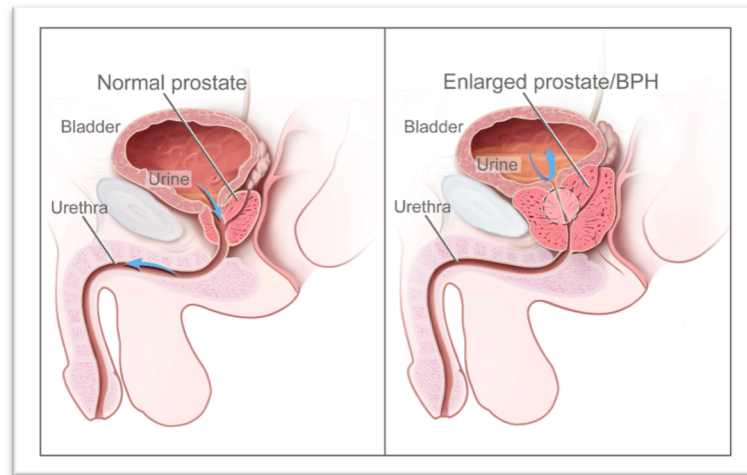
Figure 1. 1: A normal prostate gland versus an enlarged prostate. Prostate enlargement can be because of cancer or benign prostatic hyperplasia (BPH). Source: National Cancer Institute website

1.2.3. Epidemiology of prostate cancer

Prostate cancer is the second most common male cancer, and the fourth most common cancer overall with more than 1,111,000 new cases diagnosed worldwide in 2012.[11] It is also the second most common cancer in the UK, constituting 13 % of all new cancer cases diagnosed in men.[1] In 2013, a total of 46,690 new cases of prostate cancer were reported in the UK, and in 2014 the disease was responsible for 11,287 deaths.[12,13,14] However, only 3 % of men with PCa die as a result of cancer as most men live with the disease and die of old age or other old age related diseases.[15] As there are often no major symptoms of PCa, especially in the early stages of the disease, it mostly goes undetected in men unless it is actively screened for. Early and accurate diagnosis PCa has a relatively high 10-year survival rate (84 %) which currently relies on a combination of different factors such as age, levels of PSA, biopsy and family history.[16] There has been

a steady increase in the incidence rate of prostate cancer in all cancer networks in UK from 1993 to 2010.[12,13,14] This could be partly attributed to wide adoption of PSA testing for screening of prostate cancer in men along with an ageing population. As a result of PSA being a poor diagnostic marker (high false positives), it is highly likely that not all PCa cases were positive which could have also contributed to the increase in the incidence rate.

Prostate cancer is predominant in older men with about 75 % of total cases diagnosed in men above the age of 65 and only 3 % cases being diagnosed in men below the age of 30.[17]. As most old men live with PCa after diagnosis, in 2006, a total of 181,000 men were living with cancer in UK, 10 years since they were first diagnosed, and this number is only set to increase in the coming years (a predicted 12 % increase in the UK between 2014 and 2035).[18] Seeing the trend of incidence rate, the disease burden is only set to rise and increase the pressure on the public health system. There is a significant need for better diagnostic tools to facilitate early and accurate diagnosis of PCa, which the network aims to address. There also exists a need for the development of a platform consisting of a panel of biomarkers that can not only detect PCa but also differentiate between benign and aggressive PCa forms, monitor disease progression and predict the effectiveness of treatment and chances of remission.

1.2.4. Screening and diagnosis of prostate cancer

A variety of physiological examinations are currently used to both screen for and diagnose prostate cancer. Each method of detection has certain shortfalls making it controversial to use any one procedure in isolation for the diagnosis of PCa. Several

clinical studies have tried to study combination of these techniques to increase specificity of diagnosis and reduce overtreatment. [19] These are discussed in turn below.

1.2.4.1. Prostate Specific Antigen (PSA) testing

PSA was first described as a semen biomarker for use in forensic sciences by Hara *et al* in 1971.[20] It was discovered later, in 1981, that PSA could be detected in serum and was elevated in patients with prostate cancer.[21] In 1994, FDA officially approved PSA for the screening of prostate cancer after a study from a multicentre trial concluded that serum PSA could be a useful biomarker for early detection of prostate cancer.[22] Total PSA level in serum, tested by enzyme linked immunosorbent assays, was set with an upper cut-off value of 4 ng/ml for prostate biopsies.[23] The test had very low sensitivity (44 %) but good specificity (92 %).[24] The low sensitivity was a result of elevated PSA levels in serum due to BPH or prostatitis,[25] which resulted in overdiagnosis leading to unnecessary biopsies and radical prostatectomy leaving patients at a high risk of developing serious secondary infections. Additionally, it was discovered that about 20– 50 % of prostate cancers developed in men with PSA levels below 4 ng/ml.[26] This meant that 20 –50 % PCa cases were missed by standard screening process resulting high false negatives. Furthermore, large-scale clinical trials failed to show reduction in disease-specific mortality or increase in survival rates with increased PSA testing making it a highly debated biomarker for PCa screening.[27,28] Surrogate measures such as PSA density, PSA ratio, PSA velocity, age-specific PSA range, PSA isoforms have been used to increase specificity of t-PSA assay for PCa.[23] In May 2012, the US Preventative Services Task Force (USPSTF) recommended against routine PSA blood test for screening of PCa in all men (without symptoms) regardless of age. USPSTF also

emphasised the need for better biomarkers to help patients make informed decision about their treatment options.[29]

1.2.4.2. Digital rectal examination (DRE):

The prostate peripheral zone, where the majority of prostate cancers originate, is located near the rectum, making it straightforward to identify tumour growth via digital rectal examination (DRE).[30] In this procedure, a doctor examines for bumps or swellings in the prostate gland by inserting a gloved finger into the rectum. DRE is an inexpensive method for diagnosis and can detect cancers missed by PSA test. This DRE test is approximately 59 % accurate but has a higher specificity of 83 -94 %.[31] It is regularly used for cancer diagnosis as it has the advantage of detecting cancer in men with normal PSA levels and does not cause much discomfort to patients.

1.2.4.3. Biopsy:

A prostate biopsy is carried out in patients based on (a) the DRE findings, (b) higher PSA levels (greater than 4 ng/ml) and (c) after considering additional factors such as family history, ethnicity, PSA isoform levels and PSA kinetics.[19] In this technique, a small section of the tissue is removed and microscopically examined. Most protocols require a high number of samples to be removed from the peripheral zone of the prostate for PCa detection making it a painful procedure. However, the location and the number of biopsy cores from which the samples need to be retrieved remains controversial, reducing the accuracy of this technique.[32] Apart from being painful, this method has a high risk of severe secondary infection.[33] Gleason score, a grading system based on histologic pattern of cells in H&E-(Hematoxylin and eosin) stained sections, is an

established technique which is used to aid biopsy results for prognosis of PCa.[34] Transrectal ultrasonography (TRUS) is a technique in which an ultrasound probe is used to image the prostate gland by emitting high-energy sound waves.[35] TRUS is used in conjunction with biopsies for guiding needles for the sampling of tissue. It is a beneficial tool for understanding tumour pathology and is well tolerated by patients.[36]

1.2.5. *Prostate cancer biomarkers*

Biomarkers serve as an important diagnostic tool in the early detection and appropriate treatment of prostate cancer.[37] A biomarker is defined as a biological molecule found in blood, urine or other body fluids, or tissues, which indicates the normal or abnormal condition of a body.[38] Measurement of biomarkers can enable: screening of a disease in general population, predicting the outcome of a disease, diagnosis of a disease, predicting the outcome of treatment in patients and for post treatment surveillance of disease. PCa biomarkers that are currently in clinical use, as well as certain upcoming biomarkers, have discussed in the following Sections.

1.2.5.1 Prostate specific antigen (PSA)

PSA is a 30 -32 kDa protein secreted by the glandular epithelial cells in the prostate gland. Androgen hormones regulate the prostatic epithelial cells for expression of PSA at the transcriptional level.[39] Prostatic glandular epithelial cells are surrounded by basal cells and the basement membrane. During the initial stages of PCa there is partial breakdown of the basement membrane, which allows PSA to enter the circulatory system elevating its concentration in blood (Figure 1.3).

PSA is a member of the tissue kallikrein family of proteins, which is a subgroup of serine proteases.[37] There are 15 human kallikrein (hK) proteins synthesised by the kallikrein gene locus (discovered to date), although only three have specific biological function; pancreatic renal kallikrein (hK1), human glandular kallikrein (hK2) and prostate specific antigen (hK3).[40] HK1 is located in the kidney and breaks down a kinnogen substrate brought from blood, hK2 cleaves the precursor form of PSA to yield active PSA[41] and hK3 de-coagulates semen by breaking down proteins (semenogelin I and II) that are responsible for gelation of semen.[42] The discovery of new kallikrein proteins has resulted in studies that indicate their possible role in prostate cancer. Human kallikrein proteins like hK4, hK6, hK10 and hK11 have shown promising results as serum biomarkers for PCa.[43,44]

PSA is 237 amino acid protein which is synthesised in its inactive form, a 244 amino acid protein call pro-PSA.[39] The final protein (active PSA) is a 30 KDa protein with five disulphide bridges and one asparagine-linked oligosaccharide. About 30 % of seminal PSA is enzymatically active while 5 % exists as a complex with protein C.[45] The remaining free PSA in semen is rendered inactive by internal cleavage (enzyme cleaves at the active site) by human kallikrein proteases. In men with prostate cancer, the concentration of these internally cleaved inactive forms may be reduced as a consequence of down-regulation of other kallikrein proteases.[46] Some amount (ng/ml) of active PSA produced by the prostate gland diffuses into circulatory system (serum PSA) where it is inactivated by the protease inhibitor α anti-chymotrypsin to form complexed PSA (Figure 1.3).
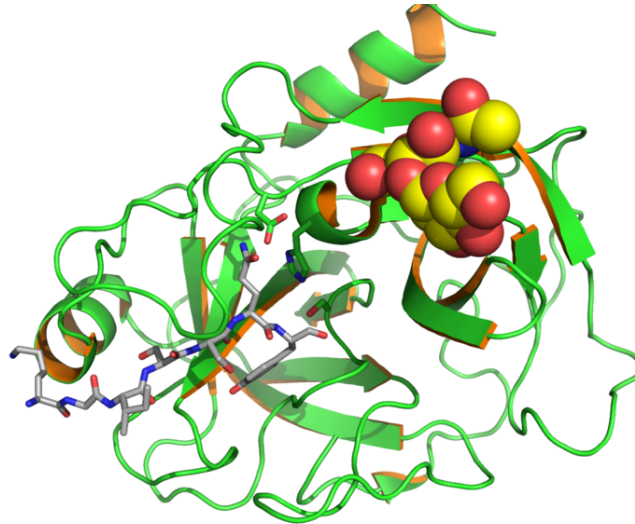
Figure 1. 2: Human prostate specific antigen (PSA/KLK3) with bound substrate from complex with antibody (PDB id: 2ZCK) Obtained from Wikipedia/E A S. A detailed description of crystal structure of PSA and ternary complex formation with anti-chymotrypsin can be found in Ménez, R. (2008).[47]

The majority of serum PSA is found in complexed form with α anti-chymotrypsin. However, other inhibitors such as α 2-macroglobulin and α 1-antitrypsin also form complexes with PSA.[48] Internally cleaved forms of PSA and pro-PSA, with no enzymatic activity, also enter the blood stream but remain uncomplexed and are termed 'free PSA' (fPSA).[49] Most antibody assays recognise free PSA as well as complexed PSA in serum and hence measure total-PSA (t-PSA).[50]
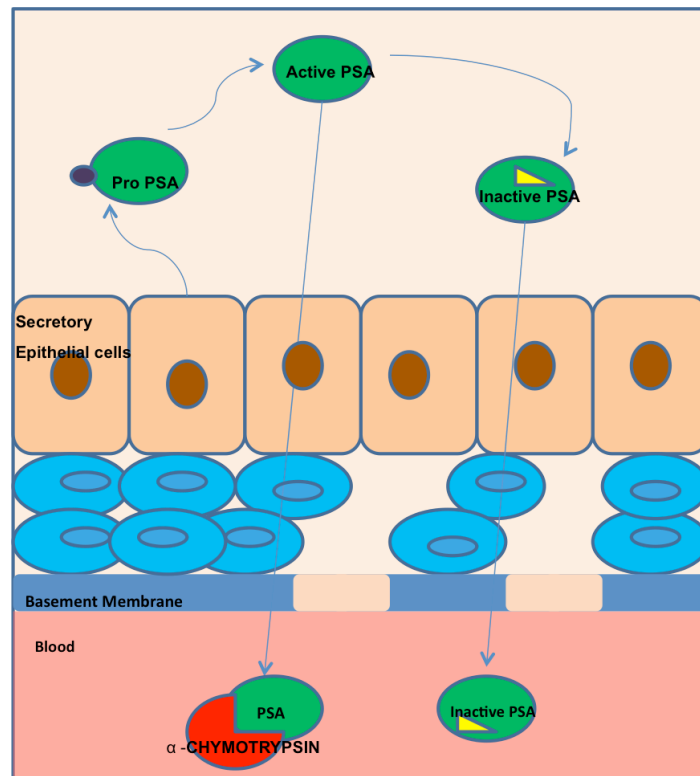
Figure 1. 3: PSA is secreted as pro-PSA by the epithelial cells in the peripheral zone of the prostate gland. Some amount of active PSA escapes into the circulatory system through basement membrane, which is inactivated by α-antichymotrypsin. During the early stages of prostate cancer there is break down of the basement membrane causing more PSA to enter blood elevating the concentration of serum PSA.

1.2.5.2   Free PSA

Free serum PSA (fPSA) is an enzymatically inactive (internally cleaved by various proteases), and non-complexed form of PSA.[39] Free PSA is expressed a percentage of total PSA (% fPSA).[51] Free PSA can be detected in serum using antibodies specifically raised for fPSA. Using the serum fPSA value, a ratio of fPSA to total PSA (complexed and free) can be calculated to give % fPSA. The % fPSA test with a cut of 25 % has a sensitivity of 95 %, and specificity of 13 %.[52] Several studies have reported that % fPSA

test in combination with t-PSA is a better measure of predicting biopsy outcome than t-PSA alone.[53,54] Hence, it was proposed that fPSA could be a better diagnostic marker to increase specificity of the t-PSA test and preventing unnecessary biopsies specifically in men with PSA levels in the diagnostic grey zone of 4 - 10 ng/ml.

1.2.5.3   Pro - PSA

Pro-PSA is an enzymatically inactive precursor form of PSA containing an additional 7 amino acid sequence at its N-terminus.[49] The additional seven amino acid sequence (APLILSR) is cleaved by hK2 enzyme extracellularly to form the enzymatically active form of PSA (active-PSA). Another form of pro-PSA that results from cleavage between the second (serine) and the third (leucine) amino acids is called [- 2] pro-PSA. [-2] pro-PSA is also enzymatically inactive and cannot be cleaved by trypsin or hK2.[49] Various studies have found increased staining of [- 2] pro-PSA in prostate cancer tissue.[55,56] Other forms of truncated pro-PSA [-5], [-7] were also identified and shown to be elevated in prostate cancer.[57] [-2] Pro-PSA was tested in a large multicentre trial to determine its relationship with aggressive form of prostate cancer. The study concluded that [-2] pro-PSA could be a useful biomarker for both the early detection of PCa and determining the aggressiveness of the disease.[58]

1.2.5.4   T-PSA test refinement

T-PSA assay was refined in an attempt to increase the specificity by using surrogate measures such as PSA density, PSA velocity, PSA doubling time and age-specific PSA levels in men.

- PSA density

  PSA density (PSAD) is defined as the ratio of PSA concentration to prostate volume and was first described in a study by Benson *et al*. The study reported that a PSAD value of 0.15 or more indicated towards the development of PCa.[59] Although initial studies using PSAD were able to differentiate between men with PCa and benign hyperplasia, later studies failed to demonstrate an improvement in the specificity of the t-PSA assay. This was likely due to variations in techniques used for determining prostate volume by different physicians, making the technique less accurate.[60] PSAD, however, may be beneficial in understanding tumour pathology and also in the monitoring of disease progression in older men who live with the disease.

- PSA Kinetics

  PSA velocity (PSAV) is termed as the rate of change of serum PSA concentration per year (ng /ml /year). A study by Carter *et al.* demonstrated (using longitudinal ageing data) that men with PSA levels between 4 –10 ng/ml and a PSAV value greater than 0.75 ng/ml/year was indicative of PCa.[61] A PSAV value of 0.75 ng/ml/year or greater had a 90 -100 % specificity in differentiating between BPH and prostate cancer.[62] Another kinetic parameter monitored was the time taken for the serum PSA concentration to double, so-called as the 'PSA doubling time'. PSA doubling time has reportedly been used to predict remission post treatment of PCa and metastasis-free survival.[63,64]

There has been some scepticism regarding the measurement of PSA kinetics with one study concluding that PSAV values fail to predict biopsy results. This could be a result of variation in laboratory protocols, giving rise to differences in sampling and data collection.[65] Standardisation of these protocols could provide better insight into the relationship between PSA kinetics and cancer.

- Age-specific PSA

  Loeb *et al.* studied PSA values for specific age groups to understand their correlation with PCa.[66] Normal geometric mean PSA values were defined as 0.7 ng/ml for men < 60 years and 1.4 ng/ml for men > 60 years.[66] The study also reported that men with PSA concentration greater than the median PSA level for their age group had a higher risk of developing PCa.[66]

- Phi Testing

  A prostate health index called the 'phi index' was introduced by Beckman and Coulter in 2012.[67] The phi index is calculated using a mathematical equation correlating free PSA, total PSA and [-2] pro-PSA. The phi index is calculated using the following equation:

  $$Phi\ (\phi) = \frac{[-2]pro-PSA}{free\ PSA} \times \sqrt{t-PSA} \qquad (1.1)$$

  The phi index has a reported diagnostic accuracy of 70 %[67], which is higher than t-PSA and f-PSA standalone accuracy.[68] In 2012, Beckman Coulter received US FDA clearance for the use of phi test to detect PCa in men with a PSA range of 4 -10 ng/ml.

1.2.5.5   Emerging biomarkers of PCa

Total PSA and refined PSA tests still remain important diagnostic markers for early PCa

detection despite several controversies. The introduction of the Phi index, which

measures combination of isoforms of PSA, has helped in increasing the specificity of t-

PSA assay. However, there is still a clinical need to develop a panel of biomarkers, in

addition to PSA, that can not only detect PCa early but also distinguish between

aggressive and benign forms of the disease. Apart from PSA there are various other

emerging biomarkers, which are being studied for this purpose and are discussed in the

following section.

- Prostate cancer antigen 3 (PCA3) or DD3(PCA3) is a non-coding m-RNA which

  is overexpressed in the prostate tissue in prostate cancer.[69] It is produced by the

  prostate cells and has high specificity (expressed in 95 % prostate cancers) in

  detecting cancer when combined with PSA in a clinical setting.[70]

- Prostate stem cell antigen (PSCA) is cell surface glycoprotein, and its expression

  is upregulated in about 80 % prostate cancer. PSCA is highly expressed in

  aggressive forms of the disease.[71] A correlation between overexpression of

  PSCA and advanced tumour stage has been reported in literature.[75]

- Transmembrane protease, serine 2 (TMPRSS2) - ETS related gene (ERG) gene

  fusion is a transcription factor gene fusion secreted by prostate epithelial cells

  and upregulated in malignant prostate cancer cells.[73] TMPRSS2-ERG is a

  common gene fusion found in almost half of PCa patients. The biomarker has

  37 % sensitivity and 93 % specificity and can be detected in the urine.[74]

- Alpha-methylacyl - CoA racemase (AMACR) is a racemase enzyme expressed in prostate tissue, which can be detected in both blood and urine.[75] AMACR is highly expressed in untreated metastases and castration resistant PCa (88 % cases) making it a highly specific biomarker for PCa. AMACR was shown to have 92.3 % sensitivity and 89.2 % specificity when tested in prostate needle biopsy specimen.[76]

- KLK2 or hK2 is serine protease in prostate gland that converts pro - PSA into active PSA. It has shown to be highly expressed in men with prostate cancer and aids tumourigenesis in an advanced stage of cancer.[37] It has the potential to be a biomarker in combination with t-PSA for differentiating between PCa and BPH.[77]

- Human Prostatic acid phosphatase (hPAP) was the first biomarker discovered for prostate cancer before the use of PSA. Gutmean *et al.* reported higher serum PAP levels in men with PCa and bone metastases.[78] After the discovery of PSA in 1981, PAP was no longer used as a biomarker due to low specificity, however, there has been renewed interest in this marker due to its good prognostic quality.[79]

- Various other biomarkers that are also being evaluated for PCa include circulating tumour cells[80], mi-RNAs[81], PCa 7 gene panel: CTAM, CXCR3, FCRL3, KIAA1143, KLF12, TMEM204, SAMSN1[82] and prostate specific membrane antigen (PSMA).[83]

1.3.   Molecular Imprinting

Molecular recognition is defined as the process of interaction between various biomolecules such as proteins, nucleic acid, carbohydrates and lipids in biological systems.[84] Almost all diagnostic platforms currently rely on this molecular recognition process (with biological elements such as antibodies, enzymes and complimentary DNA/RNA sequences) for detection of disease-associated biomarkers.[85] Biomolecules interact with each other via non-covalent interactions such as hydrogen bonding, hydrophobic and ionic interactions in aqueous systems.[86] Some of these interactions are very strong, for example, the biotin and avidin interaction has a K_d of 10^{-15} M.[87] In spite of such strong interactions, biomolecules like antibodies or DNA are not naturally well-suited to biosensing applications because of their higher costs, poor stability over time and difficulty in engineering them onto various sensing platforms. Taking inspiration from naturally occurring molecular recognition processes, molecular imprinting engineers polymeric molecular recognition units, which are more robust, economical and possess comparable affinity and selectivity towards the template comparable to their biological counterparts.[88] Molecular imprinting is a technique used to engineer synthetic receptors by polymerisation of functional monomers and crosslinkers around a template species. Following removal of the template from the polymer matrix, cavities remain which display both chemical and steric selectivity for the imprinted molecule (Figure 1.4).[89,90] These polymers are termed molecularly imprinted polymers or MIPs.

Molecular imprinting can be classified according to the type of interactions between monomers and template during synthesis, that is, covalent and non-covalent. Wulff and co-workers first reported covalent imprinting where the template molecule was chemically bonded to the monomers during polymerisation and post polymerisation the bond was cleaved for template extraction.[91] Covalent imprinting gives rise to relatively more homogenous binding sites and reduces non-specific binding, giving rise MIPs with better binding characteristics (than non-covalent imprinting).[92] However, the covalent interactions are more stable and therefore require harsh conditions for the removal of the template, which can cause deformation of polymers and loss of binding site affinity. An alternative, non-covalent imprinting approach, was pioneered by Klaus Mosbach and co-workers.[93,94] Non-covalent imprinting relies on the formation of many weaker interactions like hydrogen bonding, hydrophobic and ionic interactions between the template and the monomers to provide overall affinity to the imprinted polymer. These bonds can be easily broken by mild conditions resulting in easier extraction of the template without loss in selectivity. Non-covalent imprinting is more popular due to simplicity of preparation and variety in choice of available monomers. However, the resulting MIPs generally have lower binding affinity than covalent MIPs.[95]

Regardless of the imprinting approach, all MIPs share the same central components (Figure 1.4):

- Template molecule: The template is a molecule, or analogue of a molecule, for which the imprinted polymer is generated. Template species vary from small

molecule, drug-like targets to biomacromolecules such as proteins or even whole cells.

- Functional and/or crosslinking monomers: Functional and crosslinking monomers interact with template molecules to form a pre-polymerisation complex that is subsequently locked in place during polymerisation. Most commonly used functional monomers are methacrylic acid (acidic), vinyl pyridine (basic), acrylamide (hydrogen bonding),[89] while the most common crosslinkers are ethyleneglycol dimethlyacrylate (EGDMA), bisacrylamide and divinylbenzene.[88]

- Porogen: This is the solvent used to dissolve the template molecules and monomers. The choice of solvent should encourage the formation of a pre-polymerisation, solution phase and template – monomer complex. The use of a solvent during the polymerisation process also helps to impart porosity to the final polymer. Certain common solvent for conventional imprinting are acetonitrile, chloroform and toluene.[89]

- Non-imprinted polymers (NIPs) are synthesised in the same manner as MIPs but in the absence of a template species. NIPs allow for the non-specific interactions between the template and polymer to be evaluated.[96]
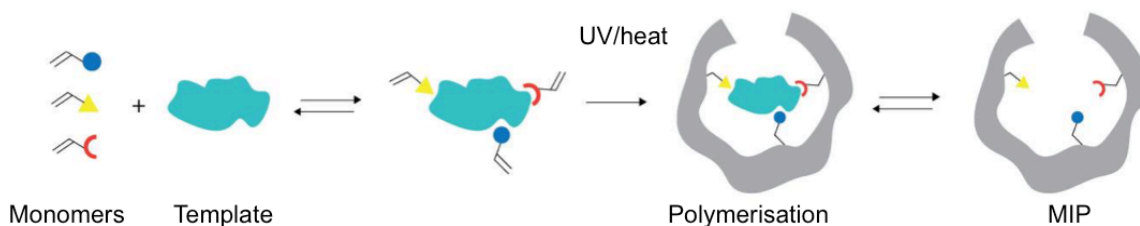
Figure 1. 4: Schematic of the molecular imprinting process: Functional and/or crosslinking monomers interact with a template molecule via non-covalent or covalent interactions. These interactions are locked into place during the polymerisation process, which is initiated by UV or heat. After polymerisation the template is extracted leaving a recognition site in the polymer that displays both chemical and steric selectivity for the template.

Molecular imprinting and its principles mentioned in the section have been extensively reviewed in the literature.[89,97,98] Molecular imprinting has evolved from using small molecules such as amino acids and drug molecules as templates to imprinting large proteins with intelligently designed monomers that demonstrate high affinity towards their template. The ultimate challenge of molecular imprinting has been to synthesise plastic antibodies for complex biomolecules (proteins) with similar affinities to their biological counterparts. The evolution of protein imprinting has been discussed in the following sections to understand the challenges involved.

1.4. Protein Imprinting

1.4.1 Aqueous protein imprinting

Molecular imprinting has been demonstrated to be highly efficient when using small molecule templates, for example, pharmaceutical drugs[99], amino acids[94], peptides[100],

nucleotide bases[101] and sugars.[102] The defined structures of such molecules and good solubility in organic solvents mean that high-affinity binding pockets, capable of selective recognition of the template, can be readily produced during the imprinting process.[89] Macromolecular (e.g. protein) imprinting is however much more challenging; the relatively large size and dynamic structure of such molecules, coupled with their general incompatibility with conventional imprinting solvents, makes the development of well-defined imprinted sites much less likely.[103] The non-polar solvents typically used for small molecule imprinting can cause denaturation/unfolding of proteins meaning that the resultant binding sites are a poor match for the native species. Moreover, as a consequence of their large size, it is often difficult to extract proteins from the imprinted site, with diffusional and mass transfer barriers further impeding re-binding kinetics.[104] Aqueous solvents are generally preferred for protein imprinting to maintain protein conformation and easy solubilisation of the protein. However, in an aqueous imprinting technique, hydrophilic protein has low complementarity to hydrophobic monomers leading to less favourable binding conditions.[105] In the pre-polymerisation mixture, water molecules and functional monomers compete for the same hydrogen bonds, effectively solvating the protein and monomer species, resulting in low chemical selectivity of the final polymer. As a result, to bring about complex formation between monomers and proteins, certain specific non-covalent interactions such as ionic, hydrophobic and/or π-π stacking may be required to build a chemically selective cavity.

In recent years, various research groups have demonstrated efficient imprinting of proteins in aqueous systems with MIPs showing high affinity for template

molecules.[106,107,108,109] Ken Shea's group demonstrated molecular imprinting in an aqueous system using water-soluble monomers by synthesising MIP nanoparticles that were comparable in size to antibodies.[110] Using a rational design of monomers and low crosslinking ratios, the NIP nanoparticles displayed high affinity for its template molecule mellitin (25 amino acid protein). Although, the study demonstrated the potential of MIPs in detection of proteins at clinically relevant concentration, fabrication of MIP-nanoparticles onto sensing platforms can be quite challenging. Piletsky's group have developed a MIP nanoparticle reactor, which can synthesise uniform MIP particles for a surface immobilised template (vancomycin) in aqueous solutions.[111] This technology has the potential for scale-up and large-scale adoption of MIPs with industrial applications. Furthermore, recent progress has demonstrated the integration of specialised functional monomers into these MIP-nanoparticles, which, can be further used for surface immobilisation and sensor fabrication.[111] These studies demonstrate the potential of molecular imprinting in fabricating diagnostic sensors for clinically relevant biomarkers with comparable performance to their biological counterparts.

1.4.2 Bulk imprinting of proteins

Bulk imprinting approach involves entrapping the whole protein to form imprinted cavities into a polymer system similar to small molecule based bulk imprinting. This approach is relatively simpler as the functional monomers, crosslinkers and protein can be solubilised in suitable porogen to form a complex and subsequently subjected to UV/heat for polymerisation. The protein is extracted using multiple washes cycles or enzymatic digestion.[112] Majority of the bulk imprinting work has been carried out using acrylamide gels and its derivatives with proteins templates such as BSA, lysosyme and

hemoglobin.[113,114,115] Hydrogels, which are hydrophilic materials that swell in presence of water, have also shown good recognition properties upon being used in molecular imprinting with acrylamide as monomers.[116,] A major disadvantage of bulk imprinting is inefficient template extraction. The large size of the protein restricts easy extraction of the protein. Complete extraction of template is seldom achieved causing inefficient re-binding and template leaching.[117] Acrylamide imprinted gels are not dense, have poor selectivity, deform under harsh conditions such as strong pH or temperature and lose their recognition properties over time making them ineffective for protein imprinting and sensing.[103]

1.4.3 Surface imprinting

An alternative approach to bulk protein imprinting is immobilising the protein on a surface for partial or complete imprinting. Immobilisation of the protein allows for easier template extraction (than bulk imprinting), better access to the imprinted cavity allowing for faster binding kinetics and greater binding site homogeneity. Surface immobilised template imprinting has been applied to surface of beads (silica beads[118], glass beads[119]), quantum dots[117], nanoparticles (magnetic NPs)[121], nanomaterial (carbon nanotube)[108] and flat surfaces (gold)[122] for imprinting of variety of proteins. A review by Yilmaz *et al* summarising the use of immobilised template for imprinting gives further insight into this field.[123] There are various techniques to immobilise a protein on a surface: passive adsorption, covalent bonding, affinity interactions and metal coordination, which have been discussed in turn below.

1.4.3.1. Protein adsorption on surfaces

In this strategy, the proteins are simply adsorbed onto a surface and subsequently imprinted using radical/electro-polymerisation. One of the first examples of this technique was described Shi *et.al.*[124] Radiolabelled proteins (bovine serum albumin, immunoglobulin G, fibrinogen) were immobilised on a hydrophilic mica surface and coated with disaccharides to prevent denaturation. A thin fluoropolymer film was deposited onto the protein-sugar complex. Post removal of mica and the template protein, small cavities lined with disaccharides were exposed on the polymer, which displayed specific recognition towards the template protein. Some recent examples have used protein stamping and nanopatterning to create imprints in polymers, which has shown varying degrees of success.[125] One major challenge this technique is conserving the natural conformation of the protein, which can change upon adsorption to a surface making the imprinting process less efficient. A refined technique to overcome this problem was demonstrated by Matsunaga *et al* wherein a crystallised protein (lysozyme) was used as the template for surface imprinting.[126] The resulting imprinted polymer exhibited high selectivity towards the template protein.[126] One major drawback of this technique is that it can be only applied to abundantly available proteins that are relatively inexpensive to obtain.

1.4.3.2. Covalent bonding of protein to surface

Covalent bonding of proteins to the surface is another elegant technique to control surface modification pre-polymerisation. Shiomi *et al.* first demonstrated such a technique whereby haemoglobin was covalently immobilised on aldehyde functionalised silica particles *via* imine bonds.[118] The resulting imprinted cavities were found to be

highly selective for haemoglobin when compared to other proteins such trypsin, β-amylase and BSA. Over the years, covalent immobilisation for surface imprinting has been applied to various surfaces such as gold, silica, magnetic nanoparticles, carbon nanotubes utilizing chemistries such as reversible aldehyde chemistry, cleavable crosslinkers and EDC/NHS for protein confinement.[127,128,123] One disadvantage of surface imprinting is partial exposure of the protein for imprinting, which may result in poor selectivity or cross reactivity during the re-binding step.

1.4.3.3. Specific/affinity interaction between protein and polymer

Protein recognition in molecularly imprinted cavities relies heavily on multipoint non-covalent interactions such electrostatic/hydrophobic and hydrogen bonding. Although, good affinity has been reported with polymers based on such interactions, an improvement may be required when measuring clinically relevant biomarkers that are present in very low concentrations (ng/ml or pg/ml). One such approach to overcome the problem is incorporation of affinity-based molecules to the resulting polymer, which, could lend higher specificity, and affinity to the resulting MIP. Some early approaches relied on metal-based affinity for surface imprinting of proteins.[129,130] Mosbach's group first demonstrated metal-affinity based surface imprinting for RNAase protein by exploiting the Cu_2^+ and histidine interaction.[131] Surface imprinting was carried out by methacrylate derivativised silica particles using metal-ligand (Cu_2^+ - histidine) complexes. The chelating monomer N-(4-vinylbenzyl)iminoacetic acid was co-ordinated to histidines on RNAsae by Cu_2^+ ions which incorporated the protein into the surface imprinted polymer. The resulting polymer was reported to selectively recognise RNase over other proteins such BSA (bovine serum albumin), lysozyme, chymotrypsin and

HRP (horseradish peroxidase). Based on a similar concept of metal-ligand interaction a relatively new concept that has emerged in the recent years is that of hybrid imprinting. Hybrid imprinting utilizes bio-receptors (as protein recognition unit) also termed as 'supermonomers' for high affinity based MIP recognition.[132,133] Bowen *et al.* demonstrated this concept for imprinting of LPS template using polymyxin peptide as an affinity receptor for creation of hybrid MIP receptors on the surface of Merrifield resin.[134] This technique has a unique advantage of confining the protein in its preferred conformation during polymerisation permitting homogeneous binding site formation while lending affinity to the polymer. Hybrid imprinting has been discussed in detail in Chapter 4.

1.4.4 *Epitope imprinting*

Epitope imprinting approach is a subset of protein imprinting, which uses small regions peptide sequences that are exposed on the surface of proteins for creating MIPs.[135] The imprinted cavities not only recognise the small epitope sequence but also the larger macromolecule containing the epitope (Figure 1.6). Epitope imprinting has been discussed in further detail in Chapter 2.

1.4.5 *Protein molecular imprinting and sensing*

Molecular imprinting has great potential in diagnostics application for detection of relevant biomolecules and hence their application in biological and chemical sensing has been extensively studied in the literature.[97,130,137] A biochemical sensor consists of few important components such as the analyte (proteins/peptide/DNA/RNA), recognition element (antibody/ DNA/ small molecules), transducer (piezoelectric/ voltammetric/

amperometric/ optical) and the signal processor (potentiostat/ UV spectroscope).[138] In MIP sensors, the imprinted polymer containing complementary cavities is deposited/grown on a sensor surface such as gold, carbon, silica and the binding of protein/biomolecules is observed using an appropriate transducer. Molecular imprinting and sensing have been discussed in further detail in Chapter 3.

1.5 Scope Of Thesis

The overarching aim of this project was to develop an electrochemical platform for detection of prostate cancer biomarkers using synthetic receptors better termed as molecularly imprinted polymers. As part of the Marie Curie ITN, the project aimed to develop synthetic receptors that could be easily adapted to various sensing platforms that were concurrently being developed by project partners in the network. The main objectives of the project could be broadly divided into (a) selection of biomarker, (b) molecular imprinting of the selected biomarker to create MIPs and (c) electrochemical sensing of the biomarker using MIP. As described in Section 1.1 there isn't a single perfect biomarker, which can be treated as a gold standard, for detection of prostate cancer. Although controversial, t-PSA is still one of the most widely used clinical biomarker for initial diagnosis of PCa. From a research perspective, PSA is commercially available, and a MIP sensor developed for PSA could be easily compared to commercially available kits, making it a suitable template for molecular imprinting and sensing. Moreover, since measuring different isoforms of PSA could improve the sensitivity of the test, different isoforms of PSA such as pro-PSA and free-PSA were also explored as templates for the development of molecularly imprinted polymers in the current project. Lastly, the proof of concept study of MIP sensor development for PSA was designed in such a way that it could be easily extended to better biomarkers of PCa in the future.

With regards to molecular imprinting, conventional bulk imprinting is not suitable for imprinting and sensing of a large protein like PSA (due to mass transfer and diffusional

barriers). An alternative/simple technique was to explore epitope imprinting of PSA epitopes using bulk imprinting techniques (Chapter 2). It was hypothesised that the bulk-imprinted polymers could not only recognise small epitopes from PSA but also larger epitopes and subsequently the whole protein, which could be applied for PSA sensing. Epitope imprinting could then be taken a step further to combine with sensing platforms for easy detection of whole PSA protein as seen in Figure 1.5. It was proposed that the epitopes could be modified to get oriented immobilisation on the surface for producing surfaces imprinted polymers with greater homogeneity (Chapter 2). The resulting imprinted polymers could recognise the epitope as well as the whole protein, which could then be detected using electrochemical sensing.
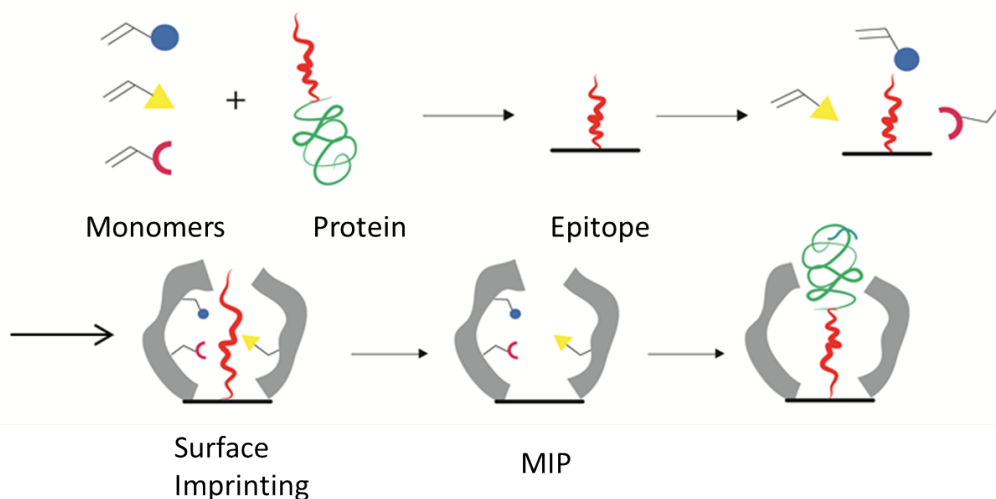
Figure 1. 5: Epitope is immobilised on a surface (i). Monomers interact with epitope (ii). Polymers can be grown around the epitope to create an imprinted site (iii, iv). After extraction of the template the whole protein is introduced for rebinding which can be detected by voltammetric or piezoelectric techniques (v).

Although epitope-imprinting is a simple approach it may lack the sensitivity to detect proteins like PSA, which are found in very low quantities in clinical samples (4 -10 ng/ml). Other bulk imprinting techniques where the polymer's recognition ability relies only on several weak non-covalent interactions acting cumulatively to recognise the whole protein may also not be sensitive enough to detect such low concentration of PSA. Hence a bio-affinity hybrid approach for detection of fPSA (Figure 1.6) was developed as described in Chapter 4 and Chapter 5. A receptor with a well-established affinity towards PSA was used to entrap the protein in its preferred conformation into the polymer. it was hypothesised that post extraction of the protein, the polymeric cavity lined with the bio-receptor would demonstrate greater affinity that the bio-receptor or the polymer alone. It was proposed that the bio-receptor would act synergistically with the polymer to form a superior receptor, which would result in greater affinity for the template. Hybrid imprinting technique could provide the added level of sensitivity required to detect clinically relevant templates like PSA, which are found in extremely low concentration in biological fluids.
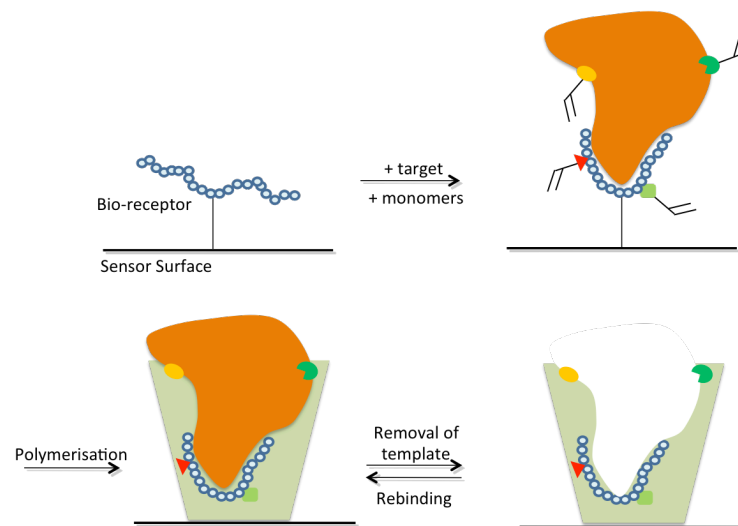
Figure 1. 6: Protein hybrid imprinting technique whereby a receptor holds the protein in its preferred conformation on the surface during polymerisation for the formation of chemically selective cavity. Post removal of protein the cavity lined with the receptor exhibits superior recognition towards the template.

1.6 Objectives

- Chapter 2 studied the epitope imprinting strategy for serum t-PSA (PSA complex with antichymotrypsin and fPSA), by creating bulk molecularly imprinted polymers for small epitopic sequences. The main objectives of Chapter 2 are:

    1. Selection, synthesis and purification of epitopic sequences using standard solid phase peptide synthesis in this case
    2. Characterisation of epitopes/peptides using HPLC - mass spectrometry.
    3. Screening of monomers to select the best functional monomer and further using it to imprint the epitope template.
    4. Rebinding evaluation of epitope imprinted MIPs.

- Chapter 3 investigated the use of pro-PSA peptide (epitope) biomarker as an alternative to t-PSA epitope imprinting. Pro-PSA is a precursor form of PSA containing an additional seven amino acid sequence at the N terminus of the protein and known to be elevated in aggressive forms of cancer. Surface imprinting of epitopes was explored for easy sensing of templates. The main objectives of Chapter 3 are:

    1. Synthesise peptide APLILSR using Fmoc solid phase peptide synthesis.
    2. Modify the peptide with a thiol-linker to enable one-step template immobilisation.
    3. To investigate the electropolymerisation of different electroactive monomers
    4. Optimisation of imprinting methodology for APLILSR peptide using a selected electroactive monomer.
    5. Evaluate MIP sensor performance by undertaking dose response assays with the imprinted peptide and investigating cross-reactivity with control peptides.

- Chapter 4 focussed on the development of the hybrid imprinting strategy for serum fPSA using DNA aptamers. FPSA is an enzymatically inactive form of PSA found in the serum. Free PSA is expressed a percentage of total PSA (% fPSA) and increases sensitivity of t-PSA test for detection of PCa. Main objectives of Chapter 4 are:

  1. To study surface immobilisation strategies of PSA-aptamer complex on electrode surface.
  2. To understand polymerisation strategies for molecular imprinting of aptamer-PSA.
  3. Characterisation of surface post molecular imprinting of aptamer-PSA complex.
  4. Evaluation of apta-MIP sensor performance by performing dose response studies with PSA and performing cross-reactivity studies with homologous proteins as well as serum proteins.

- Chapter 5 extends apta-MIP hybrid sensing on field effect transistor devices (FET). Main objectives of Chapter 5 are:

  1. Evaluation of MOSFET for apta-MIP PSA sensing.
  2. Comparison with aptamer alone MOSFET sensor.
  3. Detection of PSA in human plasma to understand fouling by serum proteins.

1.7 References

1.   Cancer Registration Statistics, England Statistical bulletins - Office for National Statistics. Available at: http://www.ons.gov.uk/peoplepopulationandcommunity/healthandsocialcare/conditionsanddiseases/bulletins/cancerregistrationstatisticsengland/previousReleases. (Accessed: 8th July 2016)

2.   Barry M. J. Early Detection and Aggressive Treatment of Prostate Cancer. *J. Gen. Intern. Med.* **15,** 749–751 (2000).

3.   Kim, E. H. & Andriole, G. L. Prostate-specific antigen-based screening: controversy and guidelines. *BMC Med.* **13,** 61 (2015).

4.   Hayes J. H. & Barry M. J. Screening for prostate cancer with the prostate-specific antigen test: A review of current evidence. *JAMA* **311,** 1143–1149 (2014).

5.   S. P. Balk. Biology of Prostate-Specific Antigen. *J. Clin. Oncol.* **21,** (2003).

6.   Kirby, R. S. *Epidemiology of Prostate Disease* 3–12 (Springer Berlin Heidelberg, 1995).

7.   Lilja, H., Oldbring, J., Rannevik, G. & Laurell, C. B. Seminal vesicle-secreted proteins and their reactions during gelation and liquefaction of human semen. *J. Clin. Invest.* **80,** 281–285 (1987).

8.   Berry S.J., Coffey D.S., Walsh P.C., Ewing L.L. The development of human benign prostatic hyperplasia with age. *J. Urol.* **132,** 474–479 (1984).

9.   Bishop, J. M. The molecular genetics of cancer. *Science* **235,** 305–311 (1987).

10.   Logothetis, C. J. & Lin, S.-H. Osteoblasts in prostate cancer metastasis to bone. *Nat. Rev. Cancer* **5,** 21–28 (2005).

11.   Fact   Sheets   by   Cancer.   Available   at: http://globocan.iarc.fr/Pages/fact_sheets_cancer.aspx. (Accessed: 10th July 2016)

12.   Cancer | Publications | Health Topics | ISD Scotland. Available at: http://www.isdscotland.org/Health-Topics/Cancer/Publications/index.asp.   (Accessed: 10th July 2016)

13.   Unit, W. C. I. and S. Welsh Cancer Intelligence and Surveillance Unit - Cancer in Wales. Available at: http://www.wcisu.wales.nhs.uk/cancer-in-wales-1. (Accessed: 10th July 2016)

14.   Queen's University Belfast | N. Ireland Cancer Registry | Cancer Information. Available   at: http://www.qub.ac.uk/research-centres/nicr/CancerInformation/. (Accessed: 10th July 2016)

15.   Jeffrey J. T., Mufaddal M., Jonathan I. E., Patricia L., Sacha W., Bruce J. T., H. Ballentine C. Intermediate and Longer-Term Outcomes From a Prospective Active-Surveillance Program for Favorable-Risk Prostate Cancer. *J. Clin. Oncol.* **33,** 3379–3385 (2015).

16.   Cancer Survival in England- Adults Diagnosed - Office for National Statistics. Available at:

http://www.ons.gov.uk/peoplepopulationandcommunity/healthandsocialcare/conditionsa

nddiseases/bulletins/cancersurvivalinenglandadultsdiagnosed/2009to2013followedupto2

014. (Accessed: 10th July 2016)

17.   Quinn, M. & Babb, P. Patterns and trends in prostate cancer incidence, survival,

prevalence and mortality. Part I: international comparisons. *BJU Int.* **90,** 162–173

(2002).

18.   Publications. Available at: http://www.ncin.org.uk/publications/. (Accessed: 8th

July 2016)

19.   Simmons, M. N., Berglund, R. K. & Jones, J. S. A practical guide to prostate

cancer diagnosis and management. *Cleve. Clin. J. Med.* **78,** 321–331 (2011).

20.   Hara, M., Koyanagi, Y., Inoue, T. & Fukuyama, T. Some physico-chemical

characteristics of ' -seminoprotein', an antigenic component specific for human seminal

plasma. Forensic immunological study of body fluids and secretion. VII]. *Nihon

Hōigaku Zasshi Jpn. J. Leg. Med.* **25,** 322–324 (1971).

21.   Wang, M. C., Papsidero, L. D., Kuriyama, M., Valenzuela, L. A., Murphy, G. P.

and Chu, T. M. Prostate antigen: A new potential marker for prostatic cancer. *The

Prostate* **2,** 89–96 (1981).

22.   Catalona, W. J., Richie, J. P., Ahmann, F. R., Hudson, M. A., Scardino, P. T.,

Flanigan, R. C., DeKernion, J. B., Ratliff, T. L., Kavoussi, L. R., Dalkin, B. L., Waters,

W. B., MacFarlane, M. T., Southwick, P. C. Comparison of digital rectal examination

and serum prostate specific antigen in the early detection of prostate cancer: results of a

multicenter clinical trial of 6,630 men. *J. Urol.* **151,** 1283–1290 (1994).

23.   Loeb, S. & Catalona, W. J. Prostate-specific antigen in clinical practice. *Cancer Lett.* **249,** 30–39 (2007).

24.   Holmström, B., Johansson, M., Bergh, A., Stenman, U.H., Hallmans, G., Stattin, P. Prostate specific antigen for early detection of prostate cancer: longitudinal study. *BMJ* **339,** b3537 (2009).

25.   Croswell, J. M. *et al.* Cumulative Incidence of False-Positive Results in Repeated, Multimodal Cancer Screening. *Ann. Fam. Med.* **7,** 212–222 (2009).

26.   Schröder, F. H. *et al.* Prostate cancer detection at low prostate specific antigen. *J. Urol.* **163,** 806–812 (2000).

27.   Schröder, F. H. *et al.* Prostate-Cancer Mortality at 11 Years of Follow-up. *N. Engl. J. Med.* **366,** 981–990 (2012).

28.   Andriole, G. L. *et al.* Prostate cancer screening in the randomized Prostate, Lung, Colorectal, and Ovarian Cancer Screening Trial: mortality results after 13 years of follow-up. *J. Natl. Cancer Inst.* **104,** 125–132 (2012).

29.   Final Recommendation Statement: Prostate Cancer: Screening - US Preventive Services Task Force. Available at: http://www.uspreventiveservicestaskforce.org/Page/Document/RecommendationStatem entFinal/prostate-cancer-screening. (Accessed: 10th July 2016)

30.   Schröder, F. H., van der Maas, P., Beemsterboer, P., Kruger, A.B., Hoedemaeker, R., Rietbergen, J., Kranse, R. Evaluation of the Digital Rectal

Examination as a Screening Test for Prostate Cancer. *J Natl Cancer Inst*. 2;90(23):1817-23 (1998).

31.   Flanigan, R.C. *et al.* Accuracy of digital rectal examination and transrectal ultrasonography in localizing prostate cancer. *J. Urol.* **152,** 1506–1509 (1994).

32.   Punnen, S. & Nam, R. K. Indications and timing for prostate biopsy, diagnosis of early stage prostate cancer and its definitive treatment: a clinical conundrum in the PSA era. *Surg. Oncol.* **18,** 192–199 (2009).

33.   Toren, P., Razik, R. & Trachtenberg, J. Catastrophic sepsis and hemorrhage following transrectal ultrasound guided prostate biopsies. *Can. Urol. Assoc. J. J. Assoc. Urol. Can.* **4,** E12-14 (2010).

34.   Humphrey, P. A. Gleason grading and prognostic factors in carcinoma of the prostate. *Mod. Pathol.* **17,** 292–306 (2004).

35.   Palken, M., Cobb O. E., Simons C. E., Warren B.H., Aldape H. C. Prostate cancer: comparison of digital rectal examination and transrectal ultrasound for screening. *J. Urol.* **145,** 86-90–2 (1991).

36.   Joseph, A. S., Peter, T. S., Martin I. R., Alberto, D. H., Steven, C. R. and Marlene, J. E. Transrectal Ultrasound Versus Digital Rectal Examination for the Staging of Carcinoma of the Prostate: Results of a Prospective, Multi-Institutional Trial. *J. Urol.* **157,** 902–906 (1997).

37.   Hong, S. K. Kallikreins as Biomarkers for Prostate Cancer. *BioMed Res. Int.* **2014,** e526341 (2014).

38.   Strimbu, K. & Tavel, J. A. What are Biomarkers? *Curr. Opin. HIV AIDS* **5,** 463–466 (2010).

39.   Balk, S. P., Ko, Y.J. & Bubley, G. J. Biology of prostate-specific antigen. *J. Clin. Oncol. Off. J. Am. Soc. Clin. Oncol.* **21,** 383–391 (2003).

40.   Schedlich, L. J., Bennetts, B. H. & Morris, B. J. Primary structure of a human glandular kallikrein gene. *DNA Mary Ann Liebert Inc* **6,** 429–437 (1987).

41.   Takayama, T. K., Fujikawa, K. & Davie, E. W. Characterization of the precursor of prostate-specific antigen. Activation by trypsin and by human glandular kallikrein. *J. Biol. Chem.* **272,** 21582–21588 (1997).

42.   Lilja, H., Oldbring, J., Rannevik, G. & Laurell, C. B. Seminal vesicle-secreted proteins and their reactions during gelation and liquefaction of human semen. *J. Clin. Invest.* **80,** 281–285 (1987).

43.   Vickers, A., Gupta, A., Savage, C. J., Pettersson, K., Dahlin, A., Bjartell, A. and Lilja, H. A Panel of Kallikrein Marker Predicts Prostate Cancer in a Large, Population-Based Cohort Followed for 15 Years without Screening. *Cancer Epidemiol. Biomarkers Prev.* **20,** 255–261 (2011).

44.   Diamandis, E. P. & Yousef, G. M. Human tissue kallikreins: a family of new cancer biomarkers. *Clin. Chem.* **48,** 1198–1205 (2002).

45.   Christensson, A. & Lilja, H. Complex formation between protein C inhibitor and prostate-specific antigen in vitro and in human semen. *Eur. J. Biochem. FEBS* **220,** 45–53 (1994).

46.   Bostwick, D. G. Prostate-specific antigen. Current role in diagnostic pathology of prostate cancer. *Am. J. Clin. Pathol.* **102,** S31-37 (1994).

47.   Ménez, R., Michel, S., Muller, B.H., Bossus, M., Ducancel, F., Jolivet-Reynaud, C., Stura, E.A., Crystal structure of a ternary complex between human prostate-specific antigen, its substrate acyl intermediate and an activating antibody. *J. Mol. Biol.* **376,** 1021–1033 (2008).

48.   Stenman, U.-H., Leinonen, J., Alfthan, H., Rannikko, S., Tuhkanen, K., and Alfthan, O. A complex between prostate-specific antigen and alpha 1-antichymotrypsin is the major form of prostate-specific antigen in serum of patients with prostatic cancer: assay of the complex improves clinical sensitivity for cancer. *Cancer Res.* **51,** 222–226 (1991).

49.   Mikolajczyk, S. D., Grauer, L. S., Millar, L. S., Hill, T. M., Kumar, A., Rittenhouse, H. G., Wolfert, R. L. and Saedi, M. S. A precursor form of PSA (pPSA) is a component of the free PSA in prostate cancer serum. *Urology* **50,** 710–714 (1997).

50.   Hugo, H., Ackland, M. L., Blick, T., Lawrence, M. G., Clements, J. A., Williams, E. D. and Thompson, E. W. Epithelial—mesenchymal and mesenchymal—epithelial transitions in carcinoma progression. *J. Cell. Physiol.* **213,** 374–383 (2007).

51.   Partin, A.W., Catalona, W. J., Southwick, P. C., Subong, E. N. P., Gasior, G. H. and Chan, D. W. Analysis of percent free prostate-specific antigen (PSA) for prostate cancer detection: Influence of total PSA, prostate volume, and age. *Urology* **48,** 55–61 (1996).

52.   Libermann, S. Can Percent Free Prostate-Specific Antigen Reduce the Need for Prostate Biopsy? *Eff Clin Pract*. 2(6): 266-71 (1999).

53.   Catalona W. J., Partin A. W., Slawin K. M. *et al.* Use of the percentage of free prostate-specific antigen to enhance differentiation of prostate cancer from benign prostatic disease: a prospective multicenter clinical trial. *JAMA* **279,** 1542–1547 (1998).

54.   Roddam, A.W., Duffy, M.J., Hamdy, F.C., Ward, A.M., Patnick, J., Price, C.P., Rimmer, J., Sturgeon, C., White, P., Allen, N.E., Use of prostate-specific antigen (PSA) isoforms for the detection of prostate cancer in men with a PSA level of 2-10 ng/ml: systematic review and meta-analysis. *Eur. Urol.* **48,** 386-399-399 (2005).

55.   Mikolajczyk, S.D., Catalona, W.J., Evans, C.L., Linton, H.J., Millar, L.S., Marker, K.M., Katir, D., Amirkhan, A. and Rittenhouse, H.G. Proenzyme forms of prostate-specific antigen in serum improve the detection of prostate cancer. *Clin. Chem.* **50,** 1017–1025 (2004).

56.   Mikolajczyk, S. D. *et al.* A truncated precursor form of prostate-specific antigen is a more specific serum marker of prostate cancer. *Cancer Res.* **61,** 6958–6963 (2001).

57.   Peyromaure, M., Fulla, Y., Debré, B. & Dinh-Xuan, A. T. Pro PSA : a 'pro cancer' form of PSA? *Med. Hypotheses* **64,** 92–95 (2005).

58.   Heidegger, I., Klocker, H., Steiner, E., Skradski, V., Ladurner, M. *et al.* [-2] proPSA is an early marker for prostate cancer aggressiveness. *Prostate Cancer Prostatic Dis.* **17,** 70–74 (2014).

59.   Benson, M. C. *et al.* Prostate specific antigen density: a means of distinguishing benign prostatic hypertrophy and prostate cancer. *J. Urol.* **147,** 815–816 (1992).

60.   Thon, W. F. *et al.* Prostate-specific antigen density — a reliable parameter for the detection of prostate cancer? *World J. Urol.* **14,** 53–58 (1996).

61.   Carter, H. B. *et al.* Estimation of prostatic growth using serial prostate-specific antigen measurements in men with and without prostate disease. *Cancer Res.* **52,** 3323–3328 (1992).

62.   D'Amico, A. V., Chen, M.-H., Roehl, K. A. & Catalona, W. J. Preoperative PSA Velocity and the Risk of Death from Prostate Cancer after Radical Prostatectomy. *N. Engl. J. Med.* **351,** 125–135 (2004).

63.   Pound, C. R. *et al.* Natural history of progression after PSA elevation following radical prostatectomy. *JAMA* **281,** 1591–1597 (1999).

64.   Spurgeon, S. E. F. *et al.* Assessment of prostate-specific antigen doubling time in prediction of prostate cancer on needle biopsy. *Urology* **69,** 931–935 (2007).

65.   Ross, A. E. *et al.* Prostate-Specific Antigen Kinetics During Follow-Up Are an Unreliable Trigger for Intervention in a Prostate Cancer Surveillance Program. *J. Clin. Oncol.* JCO.2009.25.7311 (2010).

66.   Loeb, S. *et al.* Baseline prostate-specific antigen compared with median prostate-specific antigen for age group as predictor of prostate cancer risk in men younger than 60 years old. *Urology* **67,** 316–320 (2006).

67.   Houlgatte, A. *et al.* [Use of [-2] pro PSA and phi index for early detection of prostate cancer: a prospective of 452 patients]. *Prog. En Urol. J. Assoc. Fr. Urol. Société Fr. Urol.* **22,** 279–283 (2012).

68.   Heijnsdijk, E. A. M., Denham, D. & de Koning, H. J. The Cost-Effectiveness of Prostate Cancer Detection with the Use of Prostate Health Index. *Value Health J. Int. Soc. Pharmacoeconomics Outcomes Res.* **19,** 153–157 (2016).

69.   Bussemakers, M. J. G., van Bokhoven, A., Verhaegh, G. W., Smit, F. P., Karthaus, H. F. M., Schalken, J. A., Debruyne, F. M. J., Ru, N. and Isaacs, W. B. DD3: a new prostate-specific gene, highly overexpressed in prostate cancer. *Cancer Res.* **59,** 5975–5979 (1999).

70.   Marks, L. S. & Bostwick, D. G. Prostate Cancer Specificity of PCA3 Gene Testing: Examples from Clinical Practice. *Rev. Urol.* **10,** 175–181 (2008).

71.   Reiter, R. E., Gu, Z., Watabe, T., Thomas, G., Szigeti, K., Davis, E., Wahl, M., Nisitani, S., Yamashiro, J., Le Beau, M. M., Loda, M. and Witte, O. N., Prostate stem cell antigen: A cell surface marker overexpressed in prostate cancer. *Proc. Natl. Acad. Sci. U. S. A.* **95,** 1735–1740 (1998).

72.   Gu, Z. *et al.* Prostate stem cell antigen (PSCA) expression increases with high gleason score, advanced stage and bone metastasis in prostate cancer. *Oncogene* **19,** 1288–1296 (2000).

73.   Wallrapp, C., Hähnel, S., Müller-Pillasch, F., Burghardt, B., Iwamura, T., Ruthenbürger, M., Lerch, M.M., Adler, G., Gress, T.M.A Novel Transmembrane Serine

Protease (TMPRSS3) Overexpressed in Pancreatic Cancer[1,2.] *Cancer Res.* **60,** 2602–2606 (2000).

74.   Mosquera, J.-M. *et al* Prevalence of TMPRSS2-ERG fusion prostate cancer among men undergoing prostate biopsy in the United States. *Clin. Cancer Res. Off. J. Am. Assoc. Cancer Res.* **15,** 4706–4711 (2009).

75.   Jiang, N., Zhu, S., Chen, J., Niu, Y. & Zhou, L. A-Methylacyl-CoA Racemase (AMACR) and Prostate-Cancer Risk: A Meta-Analysis of 4,385 Participants. *PLOS ONE* **8,** e74386 (2013).

76.   Kumar-Sinha, C. *et al.* Elevated alpha-methylacyl-CoA racemase enzymatic activity in prostate cancer. *Am. J. Pathol.* **164,** 787–793 (2004).

77.   Becker, C., Noldus, J., Diamandis, E. & Lilja, H. The role of molecular forms of prostate-specific antigen (PSA or hK3) and of human glandular kallikrein 2 (hK2) in the diagnosis and monitoring of prostate cancer and in extra-prostatic disease. *Crit. Rev. Clin. Lab. Sci.* **38,** 357–399 (2001).

78.   Gutman, A. B. & Gutman, E. B. An ' acid ' phosphatase occurring in the serum of patients with metastasizing carcinoma of the prostate gland. *J. Clin. Invest.* **17,** 473–478 (1938).

79.   Madu, C. O. & Lu, Y. Novel diagnostic biomarkers for prostate cancer. *J. Cancer* **1,** 150–177 (2010).

80.   Shaffer, D.R., Leversha, M.A., Danila, D.C., Lin, O., Gonzalez-Espinoza, R., Gu, B., Anand, A., Smith, K., Maslak, P., Doyle, G.V., Terstappen, L.W.M.M., Lilja,

H., Heller, G., Fleisher, M. and Scher, H.I. Circulating tumor cell analysis in patients with progressive castration-resistant prostate cancer. *Clin. Cancer Res. Off. J. Am. Assoc. Cancer Res.* **13,** 2023–2029 (2007).

81.   Sun, T., Wang, Q., Balk, S., Brown, M., Lee, G. S. M. and Kantoff, P. The role of microRNA-221 and microRNA-222 in androgen-independent prostate cancer cell lines. *Cancer Res.* **69,** 3356–3363 (2009).

82.   Liong, M. L. *et al.* Blood-based biomarkers of aggressive prostate cancer. *PloS One* **7,** e45802 (2012).

83.   Ghosh, A. & Heston, W. D. W. Tumor target prostate specific membrane antigen (PSMA) and its regulation in prostate cancer. *J. Cell. Biochem.* **91,** 528–539 (2004).

84.   Fersht, A. R. The hydrogen bond in molecular recognition. *Trends Biochem. Sci.* **12,** 301–304 (1987).

85.   Giljohann, D. A. & Mirkin, C. A. Drivers of biodiagnostic development. *Nature* **462,** 461–464 (2009).

86.   McCammon, J. A. Theory of biomolecular recognition. *Curr. Opin. Struct. Biol.* **8,** 245–249 (1998).

87.   Piran, U. & Riordan, W. J. Dissociation rate constant of the biotin-streptavidin complex. *J. Immunol. Methods* **133,** 141–143 (1990).

88.   Mosbach, K. Molecular imprinting. *Trends Biochem. Sci.* **19,** 9–14 (1994).

89.   Whitcombe, M. J., Kirsch, N. and Nicholls, I. A.. Molecular imprinting science and technology: a survey of the literature for the years up to and including 2003. *J. Mol. Recognit.* **19,** 106–180 (2006).

90.   Wulff, G. Molecular Imprinting in Cross-Linked Materials with the Aid of Molecular Templates— A Way towards Artificial Antibodies. *Angew. Chem. Int. Ed. Engl.* **34,** 1812–1832 (1995).

91.   Wulff, G., Sarhan, A. & Zabrocki, K. Enzyme-analogue built polymers and their use for the resolution of racemates. *Tetrahedron Lett.* **14,** 4329–4332 (1973).

92.   Hashim, S. N., Boysen, R. I., Schwarz, L. J., Danylec, B. & Hearn, M. T. comparison of covalent and non-covalent imprinting strategies for the synthesis of stigmasterol imprinted polymers. *J. Chromatogr. A* **1359,** 35–43 (2014).

93.   Andersson, L., Sellergren, B., and Mosbach, K. Imprinting of amino acid derivatives in macroporous polymers. *Tetrahedron Lett.* **25,** 5211–5214 (1984).

94.   Sellergren, B., Ekberg, B., and Mosbach, K. Molecular imprinting of amino acid derivatives in macroporous polymers. *J. Chromatogr. A* **347,** 1–10 (1985).

95.   Lazzoi, M. R., Mergola, L., Mele, G., Sole, R. D., Scardino, A., Scorrano, S., & Vasapollo, G. Molecularly Imprinted Polymers: Present and Future Prospective. *Int. J. Mol. Sci.* **12,** 5908–5945 (2011).

96.   Spivak, D. A. Optimization, evaluation, and characterization of molecularly imprinted polymers. *Adv. Drug Deliv. Rev.* **57,** 1779–1794 (2005).

97.   Blanco-López, M. C., Lobo-Castañón, M. J., Miranda-Ordieres, A. J. & Tuñón-Blanco, P. Electrochemical sensors based on molecularly imprinted polymers. *TrAC Trends Anal. Chem.* **23,** 36–48 (2004).

98.   Chen, L., Wang, X., Lu, W., Wu, X. & Li, J. Molecular imprinting: perspectives and applications. *Chem. Soc. Rev.* **45,** 2137–2211 (2016).

99.   Özcan, L. & Şahin, Y. Determination of paracetamol based on electropolymerized-molecularly imprinted polypyrrole modified pencil graphite electrode. *Sens. Actuators B Chem.* **127,** 362–369 (2007).

100.   Kempe, M. & Mosbach, K. Separation of amino acids, peptides and proteins on molecularly imprinted stationary phases. *J. Chromatogr. A* **691,** 317–323 (1995).

101.   Krstulja, A., De Schutter, C., Favetta, P., Manesiotis, P. & Agrofoglio, L. A. Artificial receptors for the extraction of nucleoside metabolite 7-methylguanosine from aqueous media made by molecular imprinting. *J. Chromatogr. A* **1365,** 12–18 (2014).

102.   Cheng, Z., Wang, E. & Yang, X. Capacitive detection of glucose using molecularly imprinted polymers. *Biosens. Bioelectron.* **16,** 179–185 (2001).

103.   Ge, Y. & Turner, A. P. F. Too large to fit? Recent developments in macromolecular imprinting. *Trends Biotechnol.* **26,** 218–224 (2008).

104.   Turner, N. W., Jeans, C. W., Brain, K. R., Allender, C. J., Hlady, V. and Britt, D. W.. From 3D to 2D: a review of the molecular imprinting of proteins. *Biotechnol. Prog.* **22,** 1474–1489 (2006).

105.   Allender, C. J., Brain, K. R. and Heard, C. M. in *Progress in Medicinal Chemistry* (ed. Oxford, F. D. K. and A. W.) **36,** 235–291 (1999).

106.   Hoshino, Y., Kodama, T., Okahata, Y. & Shea, K. J. Peptide imprinted polymer nanoparticles: a plastic antibody. *J. Am. Chem. Soc.* **130,** 15242–15243 (2008).

107.   Chianella, I., Guerreiro, A., Moczko, E., Caygill, J. S., Piletska, E. V., De Vargas Sansalvador, I. M. P., Whitcombe, M.J., Piletsky, S. A., Direct Replacement of Antibodies with Molecularly Imprinted Polymer Nanoparticles in ELISA— Development of a Novel Assay for Vancomycin. *Anal. Chem.* **85,** 8462–8468 (2013).

108.   Cai, D., Ren, L., Zhao, H., Xu, C., Zhang, L., Yu, Y., Wang, H., Lan, Y., Roberts, M. F., Chuang, J. H., Naughton, M. J., Ren, Z., Chiles, T. C., A molecular-imprint nanosensor for ultrasensitive detection of proteins. *Nat. Nanotechnol.* **5,** 597–601 (2010).

109.   Erdőssy, J., Horváth, V., Yarman, A., Scheller, F. W. & Gyurcsányi, R. E. Electrosynthesized molecularly imprinted polymers for protein recognition. *TrAC Trends Anal. Chem.* **79,** 179–190 (2016).

110.   Hoshino Y., Koide H., Urakami Y., Kanazawa H., Kodama T., Oku N., Shea K. J. Recognition, Neutralization, and Clearance of Target Peptides in the Bloodstream of Living Mice by Molecularly Imprinted Polymer Nanoparticles: A Plastic Antibody. *J. Am. Chem. Soc.* **132,** 6644–6645 (2010).

111.   Moczko, E., Poma, A., Guerreiro, A., Perez de Vargas Sansalvador, I., Caygill, S., Canfarotta, F., Whitcombe, M.J., Piletsky, S., Surface-modified multifunctional MIP nanoparticles. *Nanoscale* **5,** 3733 (2013).

112.   Janiak, D. S. & Kofinas, P. Molecular imprinting of peptides and proteins in aqueous media. *Anal. Bioanal. Chem.* **389,** 399–404 (2007).

113.   Hjertén, S., Liao, J.-L., Nakazato, K., Wang, Y., Zamaratskaia, G., Zhang, H.-X.,. Gels mimicking antibodies in their selective recognition of proteins. *Chromatographia* **44,** 227–234 (1997).

114.   Xia, Y., Guo, T., Song, M., Zhang, B. & Zhang, B. Hemoglobin Recognition by Imprinting in Semi-Interpenetrating Polymer Network Hydrogel Based on Polyacrylamide and Chitosan. *Biomacromolecules* **6,** 2601–2606 (2005).

115.   Hua, Z., Chen, Z., Li, Y. & Zhao, M. Thermosensitive and Salt-Sensitive Molecularly Imprinted Hydrogel for Bovine Serum Albumin. *Langmuir* **24,** 5773–5780 (2008).

116.   Hawkins, D. M., Stevenson, D. & Reddy, S. M. Investigation of protein imprinting in hydrogel-based molecularly imprinted polymers (HydroMIPs). *Anal. Chim. Acta* **542,** 61–65 (2005).

117.   Lorenzo, R. A., Carro, A. M., Alvarez-Lorenzo, C. & Concheiro, A. To Remove or Not to Remove? The Challenge of Extracting the Template to Make the Cavities Available in Molecularly Imprinted Polymers (MIPs). *Int. J. Mol. Sci.* **12,** 4327–4347 (2011).

118.   Shiomi, T., Matsui, M., Mizukami, F., Sakaguchi, K. A method for the molecular imprinting of hemoglobin on silica surfaces using silanes. *Biomaterials* **26,** 5564–5571 (2005).

119.   Ambrosini, S., Beyazit, S., Haupt, K. & Bui, Bernadette Tse Sum. Solid-phase synthesis of molecularly imprinted nanoparticles for protein recognition. *Chem. Commun.* **49,** 6746–6748 (2013).

120.   M. Panagiotopoulou, Y. Salinas, S. Beyazit, S. Kunath, L. Duma, E. Prost, A. G. Mayes, M. Resmini, B. Tse Sum Bui, K. Haupt Molecularly Imprinted Polymer Coated Quantum Dots for Multiplexed Cell Targeting and Imaging. *Angew. Chem. Int. Ed.* **55,** 8244–8248 (2016).

121.   Jia, X., Xu, M., Wang, Y., Ran, D., Yang, S., Zhang, M., Polydopamine-based molecular imprinting on silica-modified magnetic nanoparticles for recognition and separation of bovine hemoglobin. *The Analyst* **138,** 651–658 (2013).

122.   Chun-Hua Lu, Yan Zhang, Shui-Fen Tang, Zhi-Bin Fang, Huang-Hao Yang, Xi Chen, Guo-Nan Chen. Sensing HIV related protein using epitope imprinted hydrophilic polymer coated quartz crystal microbalance. *Biosens. Bioelectron.* **31,** 439–444 (2012).

123.   Yilmaz, E., Haupt, K. & Mosbach, K. The Use of Immobilized Templates—A New Approach in Molecular Imprinting. *Angew. Chem. Int. Ed.* **39,** 2115–2118 (2000).

124.   Shi, H., Tsai, W.-B., Garrison, M. D., Ferrari, S. & Ratner, B. D. Template-imprinted nanostructured surfaces for protein recognition. *Nature* **398,** 593–597 (1999).

125.   Linares, A. V., Falcimaigne-Cordin, A., Gheber, L. A. & Haupt, K. Patterning nanostructured, synthetic, polymeric receptors by simultaneous projection photolithography, nanomolding, and molecular imprinting. *Small Weinh. Bergstr. Ger.* **7,** 2318–2325 (2011).

126.   Matsunaga, T. & Takeuchi, T. Crystallized Protein-imprinted Polymer Chips. *Chem. Lett.* **35,** 1030–1031 (2006).

127.   Bossi, A., Piletsky, S. A., Piletska, E. V., Righetti, P. G. & Turner, A. P. F. Surface-Grafted Molecularly Imprinted Polymers for Protein Recognition. *Anal. Chem.* **73,** 5281–5286 (2001).

128.   Sharma, P. S., Dabrowski, M., D'Souza, F. & Kutner, W. Surface development of molecularly imprinted polymer films to enhance sensing signals. *Trends Anal. Chem.* **51,** 146–157 (2013).

129.   Mallik, S., Johnson, R. D. & Arnold, F. H. Synthetic Bis-Metal Ion Receptors for Bis-Imidazole 'Protein Analogs'. *J. Am. Chem. Soc.* **116,** 8902–8911 (1994).

130.   Hart, B. R. & Shea, K. J. Molecular Imprinting for the Recognition of N-Terminal Histidine Peptides in Aqueous Solution. *Macromolecules* **35,** 6192–6201 (2002).

131.   Kempe, M., Glad, M. & Mosbach, K. An approach towards surface imprinting using the enzyme ribonuclease A. *J. Mol. Recognit.* **8,** 35–39 (1995).

132.   Dechtrirat, D., Gajovic-Eichelmann, N., Bier, F. F. & Scheller, F. W. Hybrid Material for Protein Sensing Based on Electrosynthesized MIP on a Mannose Terminated Self-Assembled Monolayer. *Adv. Funct. Mater.* **24,** 2233–2239 (2014).

133.   Poma, A., Brahmbhatt, H., Pendergraff, H. M., Watts, J. K. & Turner, N. W. Generation of Novel Hybrid Aptamer–Molecularly Imprinted Polymeric Nanoparticles. *Adv. Mater.* **27**: 750–758 (2014).

134.   Kelly, M., Bowen, J., Gumbleton, M. & Allender, C. Molecularly imprinted polymers: macromolecule recognition. *Drug Discov. Today* **15,** 1112 (2010).

135.   Nishino, H., Huang, C.-S. & Shea, K. J. Selective Protein Capture by Epitope Imprinting. *Angew. Chem. Int. Ed.* **45,** 2392–2396 (2006).

136.   Algieri, C., Drioli, E., Guzzo, L. & Donato, L. Bio-Mimetic Sensors Based on Molecularly Imprinted Membranes. *Sensors* **14,** 13863–13912 (2014).

137.   Haupt, K. & Belmont, A.-S. in *Handbook of Biosensors and Biochips* (John Wiley & Sons, Ltd, (2008).

138.   D'Orazio, P. Biosensors in clinical chemistry. *Clin. Chim. Acta* **334,** 41–69 (2003).

2. Chapter: Conventional Bulk Imprinting of PSA Epitopes

2.1. Introduction

2.1.1. General overview

Conventional bulk imprinting has been successfully implemented for recognition of small, biomolecules such as amino acids[1], dipeptides[2], nucleosides[3] and phosphorylated peptides.[4,5] However, the imprinting of larger biomolecules still remains a challenge (Chapter 1, Section 1.4). Epitope imprinting, which utilises small sequences of amino acids exposed on the surface of macro-biomolecules as templates for molecular imprinting, helps circumvent some of the issues associated with macromolecular imprinting.[6] The resulting imprinted polymer not only recognises the smaller epitopes but also, the protein presenting the epitopes. This chapter explores the use of bulk epitope imprinting using conventional imprinting monomers for the recognition of PSA epitopes. To date, epitope imprinting of PSA has not been reported in the literature. It is hypothesised that the imprinted materials will not only recognise the (epitopic) templates but also longer peptide sequences containing the epitope sequence or indeed the native protein. This chapter describes the systematic identification and synthesis of PSA epitopes alongside the screening of monomers for efficient bioimprinting, which could be translated to surface imprinting.

2.1.2. Conventional bulk imprinting

Conventional molecular imprinting has majorly relied on the use of free radical polymerisation to make bulk/plastic polymers.[7,8] Free radical polymerisation consists of three steps initiation, elongation and termination. Initiation consists of the generation of free radical (R^*), formed by decomposition of initiator species, which starts the polymerisation of a relatively unreactive acrylate monomer. Elongation leads to the

successive addition of monomers to grow a chain to form a high molecular weight polymer. This occurs by the attack of free radical species (R*) on the double bond of a monomer, which forms an initiated monomer radical. The initiated monomer radical then further attacks acryl groups monomer leading to chain elongation. Termination step consists of deactivation of reactive species ending the chain elongation process resulting in a stable polymer. There are two types of terminations: recombination (two growing chain form a covalent bond) and disproportionation (transfer of hydrogen from one radical to other to form stable molecules). The most common type initiators are azo-type free radical initiators (Azobisisobutyronitrile (AIBN) is widely used in imprinting) to bring about polymerisation[9]. These initiators upon exposure to heat or UV radiation generate two identical, short-lived cyanopropyl radicals and nitrogen gas (Figure 2.2). AIBN is a popular initiator for molecular imprinting as it can be easily decomposed by heating (60^0 C) or by exposure to UV (366 nm)[10].
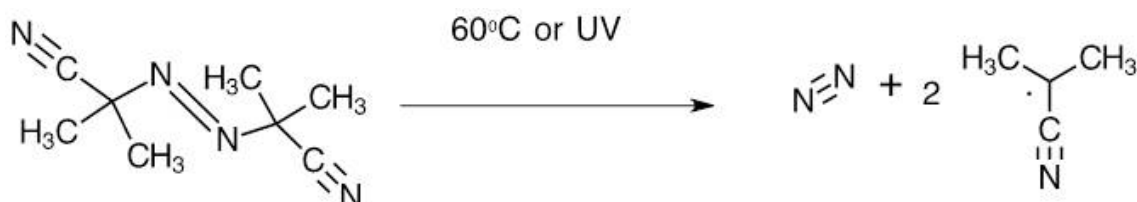
Figure 2. 1: Homogenous cleavage of AIBN to generate two equally reactive radicals, which activate surrounding acrylate monomers. Nitrogen gas is a by-product of the reaction

2.1.3. Epitope imprinting

The large size, dynamic surface and complex conformational structure of proteins, which depends on pH, ionic strength and temperature, makes it challenging to imprint

them with conventional molecular imprinting techniques. Conventional imprinting relies on the use of non-polar solvents to form multiple non-covalent interactions. However, proteins may change their conformation or denature in such conventional solvents preventing the formation of stable non-covalent interactions.[11]

Epitope imprinting, serves as an efficient alternative to the imprinting of the whole protein, enabling the generation of highly specific cavities by exploiting the functionality of the epitopic template (Figure 2.1). It offers the following advantages over whole protein imprinting: the length and design of the epitope can be varied to achieve selectivity for the native protein; non-polar solvents can be used for imprinting due to the small size and non-complex nature of the template; easy and complete extraction of template is possible leading to improved binding characteristics; and finally it allows for modification of epitopes with specific functional groups that can be used for immobilisation onto sensing platforms for surface imprinting.[12] Surface epitope imprinting has been discussed further in Chapter 3. However, one major drawback of this technique is that epitope imprinting can only be adopted for proteins with known protein structure and amino acid sequence. This is in order select a suitable template for epitope imprinting.

Rachkov and Minoura first reported the epitope imprinting approach in 2000, using a four amino acid sequence (YPLG) from the C-terminus of oxytocin as the template they created binding sites capable of recognising the 9-mer neuropeptide (oxytocin).[6,13] Methacrylic acid (MAA) and EGDMA were used as the functional and crosslinker monomers respectively, with binding performance characterised chromatographically. It was demonstrated that the imprinted polymers were capable of retaining not only the

epitope template but also oxytocin when compared to non-imprinted controls. However, to date, most bulk epitope imprinting studies have majorly employed smaller proteins which are < 2000 Da in size. It is anticipated that an epitope from a small protein would lead to a smaller conformation change of the epitope when separated from the native protein due to the absence of tertiary and quaternary structures. On the other hand, epitopes separated from a larger protein like PSA may not maintain the same conformation as the native protein. An epitope may lose its native conformation or adopt different conformations in different imprinting solvents upon being isolated from the whole protein. Using conventional imprinting approaches to epitope imprint larger proteins (greater than 10 kDa) could cause conformational restriction to rebinding of epitopes on native protein. This can lead to the formation of epitope-imprinted sites, which rebinds to the native protein less efficiently than the epitope itself. Hence selecting appropriate solvents for bulk epitope imprinting could be key in maintaining the native conformation of the epitopes (from larger proteins) during polymerisation for efficient rebinding to the native protein.

Ken Shea's group presented an alternative approach, whereby peptide epitope sequences from proteins (> 30 kDa) were confined to the surface and subsequently imprinted using surface imprinting technique.[14] The surface imprinted films were able to recognise the epitopes as well the native protein. Bossi *et al.* developed an alternative approach to epitope imprinting where unique peptide sequences (epitopes) were identified using bioinformatics tools to generate bulk MIPs, which could detect the epitopes from partially digested proteins.[15] This approach was unique because it did not rely on surface presented epitopes but identified unique epitopes, which may be buried inside the

protein. Although the technique requires an additional protein digestion step, this approach could be useful for large proteins that don't have their epitopes mapped and where maintaining native conformation of the epitope is a challenge. These studies suggested that epitope imprinting could be successfully employed for protein imprinting and sensing.
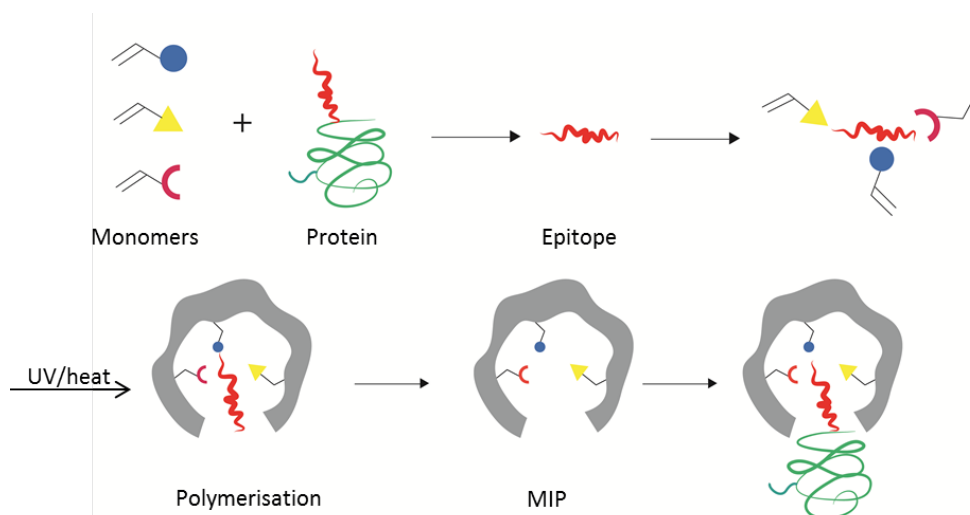
Figure 2. 2: A schematic illustrating the epitope imprinting process. A small portion of the protein that is exposed on the protein surface is used as the template. Functional monomers form a complex with the epitope which is subsequently locked in place during the polymerisation process (initiated by the application of UV radiation or heat). Extraction of the epitopic molecule leaves a cavity capable of recognising both the template and the native protein that displays the epitope on its surface.

2.1.4. Epitope selection

Epitopes are short sequences of amino acids presented on the surface of the protein, which can be easily recognised by antibodies.[16] There are two types of epitopes that participate in antibody recognition: linear and conformational. Linear epitopes are made of consecutive amino acids in the protein while conformational epitopes are amino acids

sequences that brought together due to the folding of the protein.[17] From an imprinting perspective, it is logical to choose a linear epitope due to ease of synthesis and conservation of natural conformation. However, taking into consideration the mechanism of antibody binding (the two arms binding to different parts of the protein), the majority of epitopes are conformational making the process of choosing epitopes quite challenging. The length of the epitope sequence is also critical to maintain selectivity towards the native protein. Epitopes with less than nine amino acids could lead to cross-reactivity between proteins from the same family due to sequence homology. An epitope length of 9 -12 amino acids is often specific for a particular protein.[16] This uniqueness and can be checked using sequence alignment bioinformatics software such as BLAST (Basic local alignment search tool) which is freely available on Uniprot website (http://www.uniprot.org/).[18,19] A protein can possess more than one surface epitope and choosing the best target sequence can be a challenge. An alternative way of identifying an appropriate epitopic sequence is to map protein-surface antibody binding epitopes. A study by Lu *et al.* utilised epitope mapping of HIV protein to chose the epitopic template for imprinting and sensing.[20] However, since not all proteins have their epitopes mapped, this technique would be limited to certain proteins only.

2.1.5. Peptide synthesis

As epitopes are small peptide sequences, they can be synthesised chemically using standard peptide synthesis reactions. Peptide synthesis in simple terms involves a repetitive amidation reaction between an α amino group of one amino acid and an α carboxyl group of another amino acid to form an amide or peptide bond.[21] Various synthetic strategies have been described, which could be broadly categorised as either

solution phase or solid phase synthesis approaches.[22] Bruce Merrifield pioneered the field of solid phase peptide synthesis (SPSS), developing an insoluble resin that facilitates the controlled synthesis of peptides from its surface with a single cleavage step required to release the peptide.[23] Development of SPSS led to the much-needed simplification of the peptide synthesis process, reducing the tedious purification steps involved in solution phase synthesis. Synthesising peptides on a solid support has further advantages; firstly the entire process can be carried out in one vessel with excess reagents driving reaction equilibrium thus increasing efficiency, secondly it permits draining off any excess unreacted reagents while preserving the peptide on the solid support and thirdly it bypasses the multiple purification steps required by solution phase synthesis.[24] Moreover, the SPPS strategy facilitated automation of the process, enabling integration of robotic instrumentation which permits rapid and large-scale synthesis of multiple peptide sequences.[25]

Solid phase synthesis usually employs an amine-functionalised polystyrene bead, to which an amino acid (α NH_2 protected) is attached via its carboxyl functionality to form the C-terminus of the peptide. The NH_2-protecting group of the immobilised amino acid is then removed (usually base labile) to expose the free amine group to which the following amino acid can be coupled. This deprotection/coupling process is repeated until all the amino acids are sequentially attached to yield the desired peptide (Figure 2.3).

The side chain functional groups are shielded using protecting groups, which are stable under the coupling reaction conditions but can be removed during the final cleavage process. In general two protecting strategies are employed: N^{α}-tert-butyloxycarbonyl

(Boc)/(Benzyl)Bzl[26] and 9-fluoromethoxycarbonyl (Fmoc)/Boc.[27] The Boc/Bzl strategy relies on the difference in the acid lability of the two groups; the Boc group (NH_2 protecting) is deprotected with neat TFA while Bzl, the side chain protecting groups, are only deprotected post-cleavage by treating with hydrofluoric (HF) acid.[26] The use of strong acids, particularly HF that is highly toxic, prevented the widespread adoption of this strategy, meaning that it is often reserved for the synthesis of long (>25 amino acids) peptides and proteins.[28] Fmoc/Boc uses an orthogonal protecting group strategy where base labile Fmoc protects the amino group, while the side chain protecting groups (Boc) are acid labile.[27] This approach permits selective deprotection of Fmoc groups for peptide elongation while masking the side chain functional group until the final cleavage. It also allows for the use of milder acid for peptide cleavage from the resin making it more practical than the Boc/Bzl strategy.
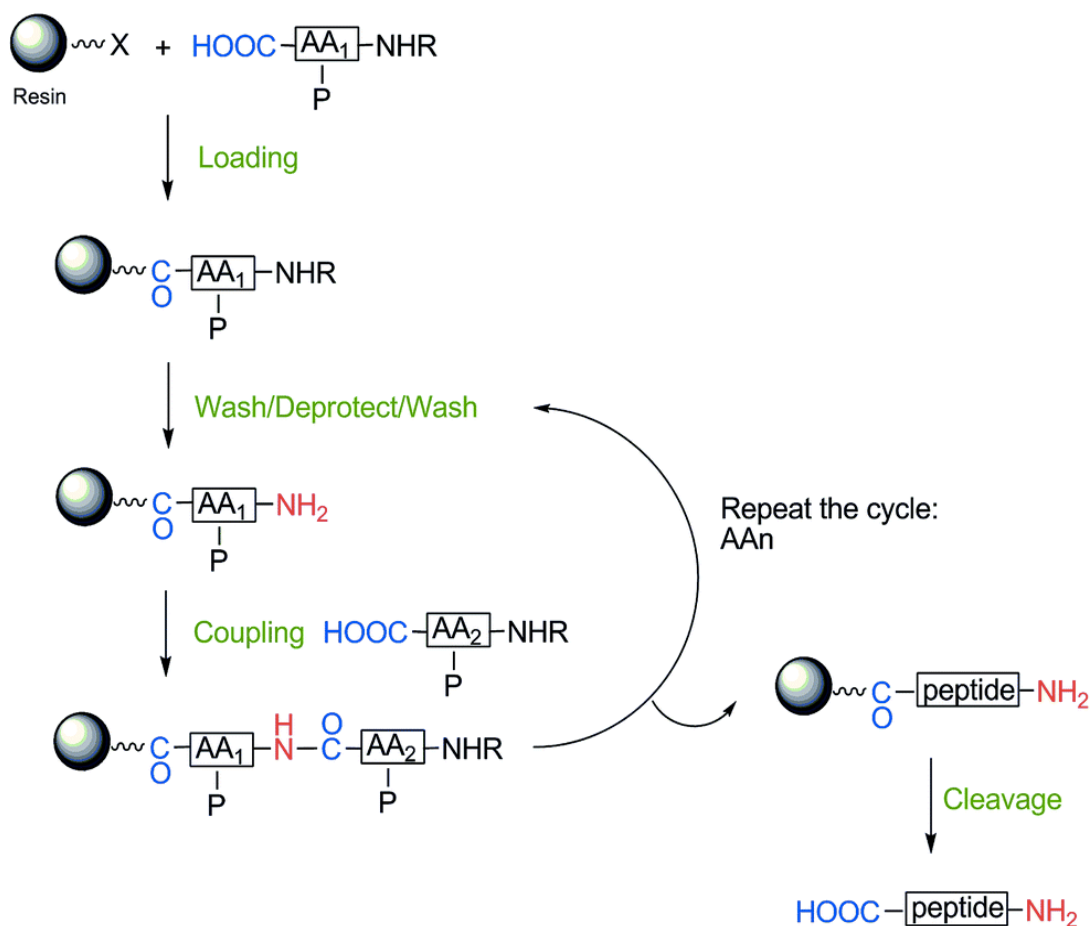
Figure 2. 3: General schematic of solid-phase peptide synthesis.[21] The strategy highlights the orthogonal protection scheme where the amine protecting group (R) is deprotected using a base to expose the primary amine to facilitate attachment of a carboxyl-activated amino acid (coupling). The side chain groups are protected by an acid labile group (P). The process is repeated until the peptide sequence is complete, with cleavage from the resin being achieved using a strong acid. Reproduced from Jose M. Palomo et al. (2014),[21] with permission from The Royal Society of Chemistry.

2.1.6. General scheme of peptide synthesis

Although, the overall SPPS strategy is relatively straightforward, various issues such as resin swelling, loading, nature of linker groups, protecting groups as well as the solvents

used in the synthesis need to be carefully considered and selected for synthesis of any peptide.[26] A general scheme of peptide synthesis has been discussed here, however slight changes were made depending on the sequence to be synthesised, which have been discussed in the respective sections.

2.1.6.1.   Peptide Synthesis resin

Polystyrene is the most common core resin used in SPSS containing 1-2 % diacrylatebenzene as a crosslinking agent to ensure the stability of the resins in common synthesis solvents.[29] Rink amide resins are popular with Fmoc protection strategy to generate peptide amides (Figure *2.4*).[30] For generation of peptide acids (COOH terminated) containing proline and asparagine (as with the current template), 2-cholorotitryl resin (Figure 2.5) was found to be the preferred choice to prevent isomerisation and avoid diketopiperization reaction.[31]
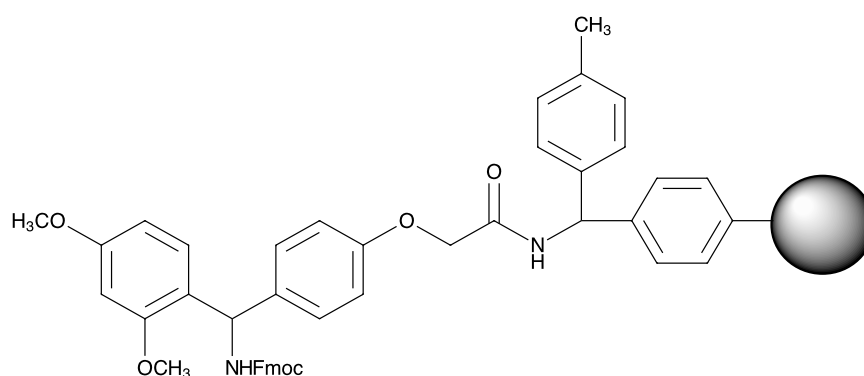
Figure 2. 4: MBHA rink amide resins are popular for peptide amide synthesis. The amine is always protected with a Fmoc group and requires deprotection before the first coupling.
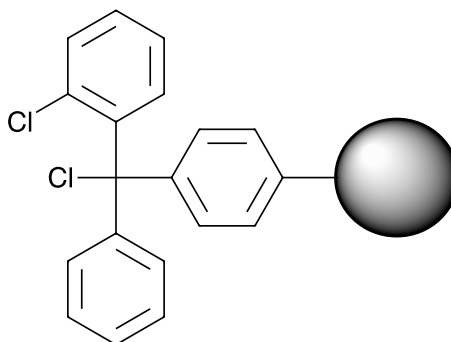
Figure 2. 5: 2-cholorotitryl chloride resins are typically used for those peptide sequences that contain proline as the first amino acid to help prevent diketopiperization reaction and also reduce racemisation[32].

2.1.6.2.   Fmoc protection and deprotection

The Fmoc (9-fluoromethoxycarbonyl) group is used as a protecting group for primary α-amines on amino acids to prevent self-polymerisation of the amino acids (*Figure 2.6*).
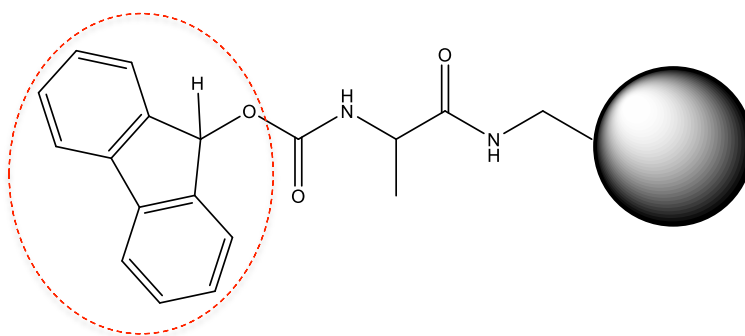
Figure 2. 6: Fmoc protection scheme on amino acids

During the deprotection step, piperidine attacks the relatively acidic proton in the fluorenyl ring of Fmoc, which leads to hydrogen elimination and formation of dibenzofulvene, which is further scavenged by piperidine, producing CO_2 as a by-

product.[27] Most peptide synthesis protocols in the literature use piperidine for Fmoc deprotection[33], however, as a consequence of piperidine being used in drug manufacturing, methyl piperidine was used as an alternative deprotecting solution, which has been shown to be equally effective as piperidine (*Figure* 2.7).[32] Scheme of Fmoc deprotection has been elaborated in Figure 2.7.

Fmoc protected AA
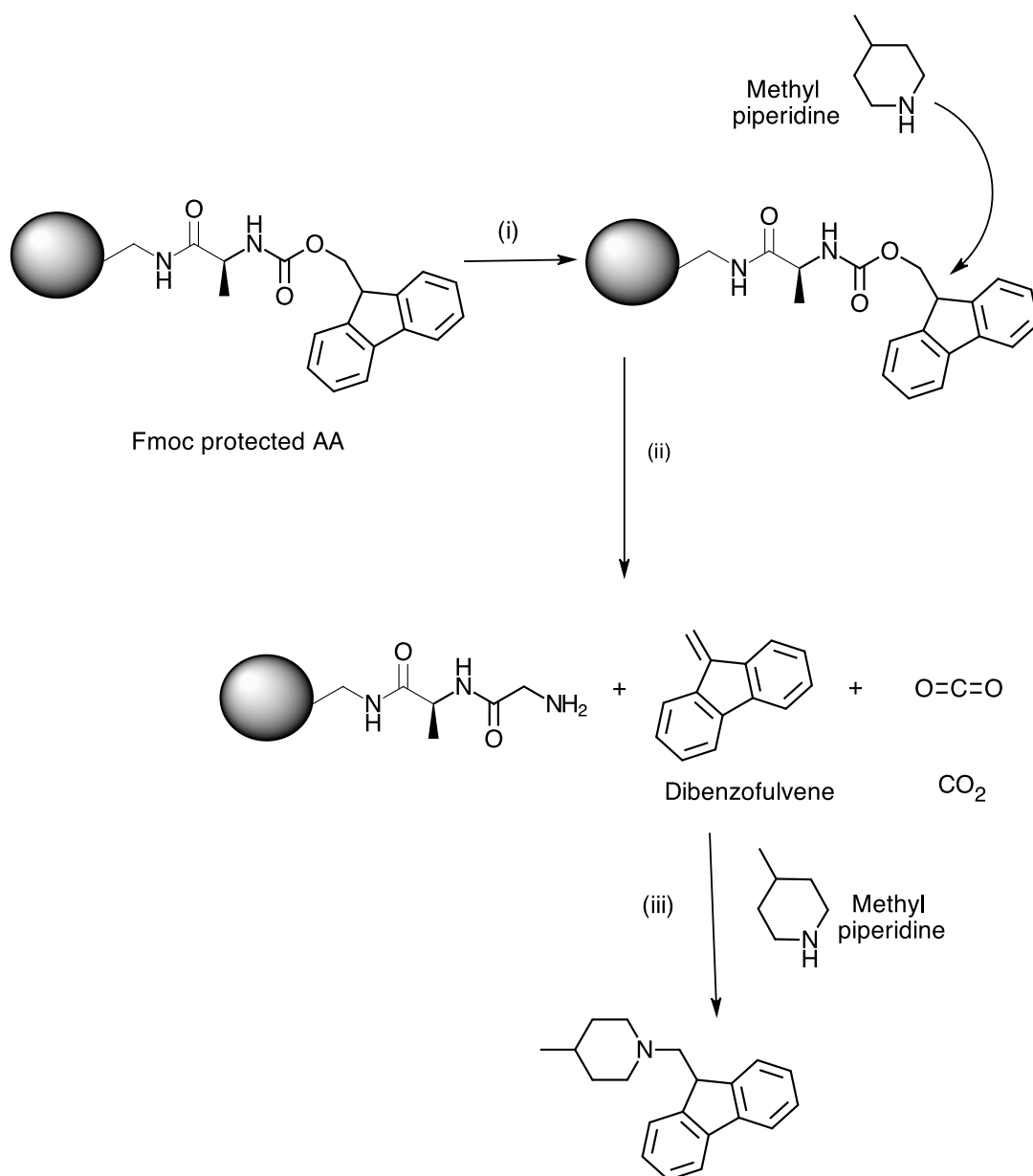
Figure 2. 7: Fmoc deprotection. Methyl piperidine attacks the proton in the fluorenyl ring (i) eliminating hydrogen and releasing dibenzofulvene and carbon dioxide (ii). Dibenzofulvene is scavenged my methyl piperidine to prevent it from further reacting with the α-amine of the amino acid (iii).

2.1.6.3. Monitoring of peptide synthesis

Kaiser test is a sensitive test for detecting primary amines by the formation of an intense blue colour, which is helpful in monitoring the coupling and deprotection of amino acids during synthesis.[35] The presence of an intense blue colour post deprotection indicates the presence of free amines, while a yellow solution with clear beads indicates completion of coupling or absence of free amines. The mechanism of the Kaiser test is provided in Figure 2.8.
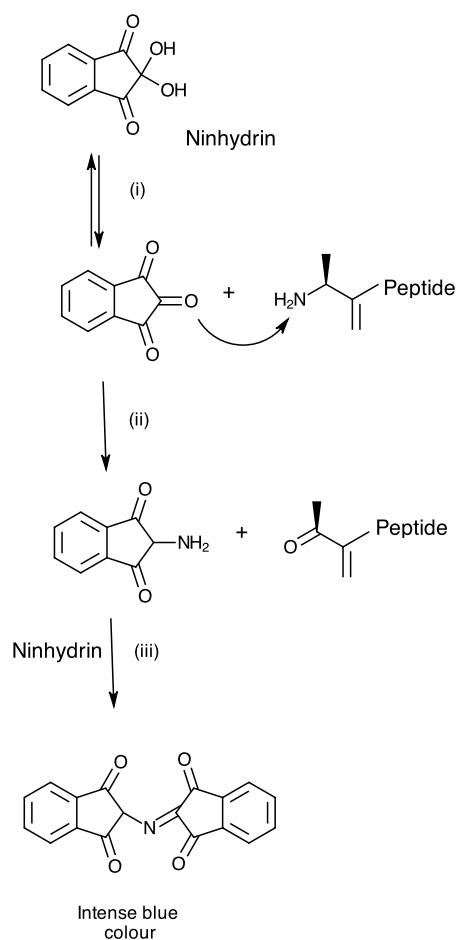
Figure 2. 8: The Kaiser test is based on a ninhydrin test. 1,2,3 tricarbonyl carbon in ninhydrin (i) is a strong electrophile and readily attacks the free amine on the amino acid to form a stable compound which is a Schiff's base (ii). The base further reacts with another ninhydrin molecule to give a strong chromophore: 2-(1,3-dioxoindan-2-yl)iminoindane-1,3-dione which forms an intense blue colour(iii).[36] The Kaiser test is only positive for primary amines.

2.1.6.4. Coupling reaction of amino acids

Coupling agents are required to activate the α-carboxyl group on the amino acid for the formation of amide bond and an extensive list can be found in the review by Alvericio *et al.*[37] One of the most popular activating agents in peptide synthesis is HBTU (O-

(Benzotriazol-1-yl)-N, N, N', N'- tetramethyluronium hexafluorophosphate) due to its high coupling efficiency (< 6 mins) and minimum racemisation.[38] HBTU is also added in lower amounts than the amino acid (0.9:1) as excess uronium salt can directly react with the amine of the peptide causing chain termination.[38] The structure of HBTU and HOBt is shown in Figure 2.9. The mechanism of amino acid activation has been depicted in Figure 2.10, and the formation of amide bond has been depicted in Figure 2.10.
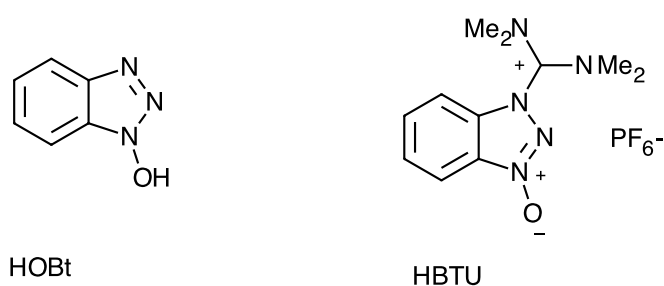
Figure 2. 9: Coupling agents HOBt and HBTU
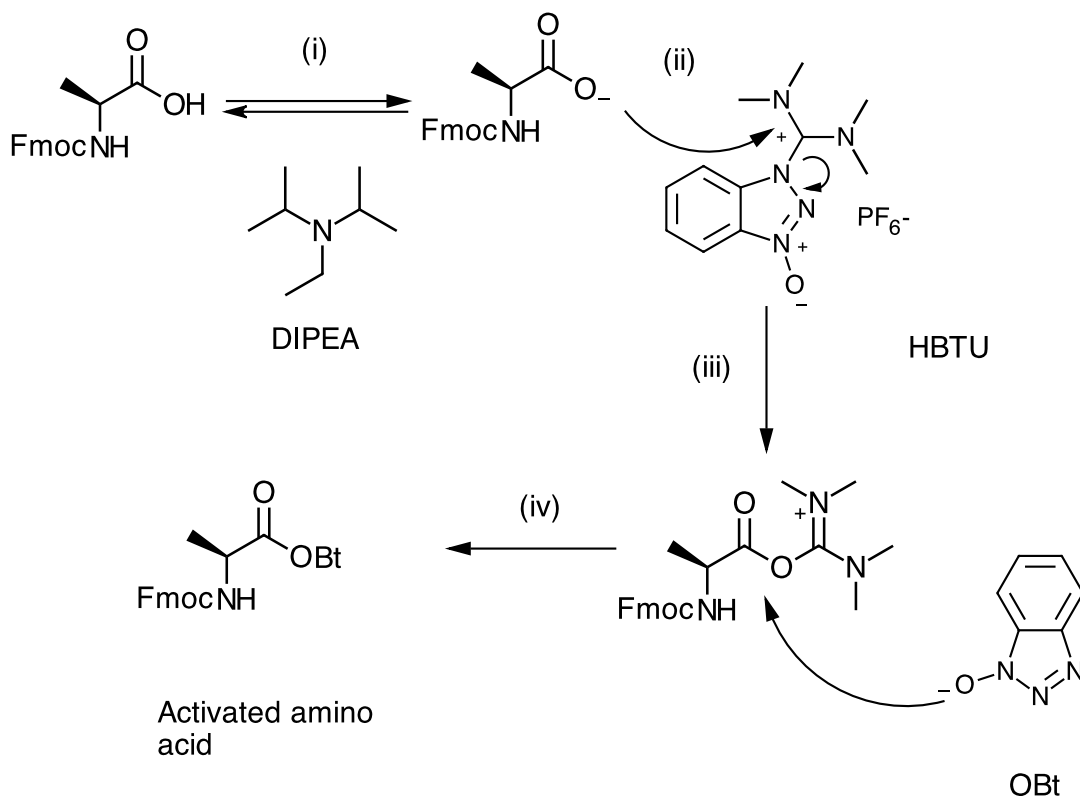
Figure 2. 10: Mechanism of amino acid activation can be divided into three steps: The base (DIPEA) deprotonates the amino acid first (i). Post deprotonation the resulting carboxylate ion attacks the electron deficient carbon atom of HBTU (ii),(iii). The newly formed HBTU – amino acid intermediate reacts with the HOBt anion to form an OBt activated ester (iv).
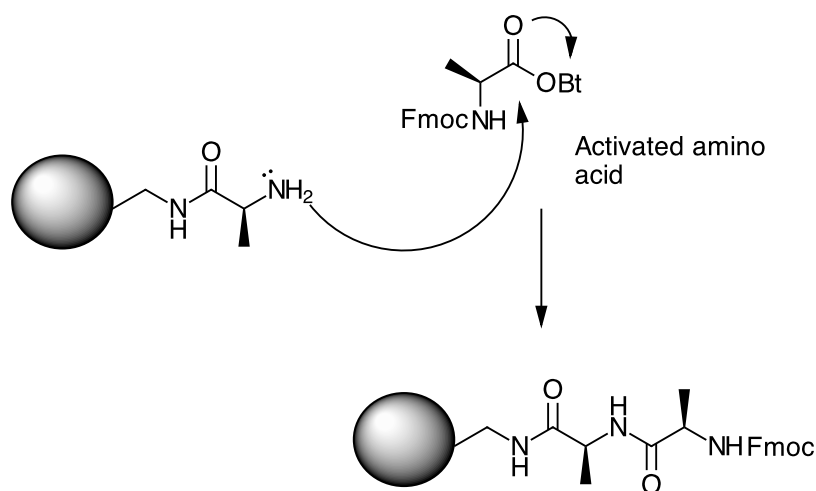
Figure 2. 11: The OBt activated ester attacks the electron rich free amine on the resin to form the amide bond.

2.1.6.5.   Cleavage of peptide

Post addition of all amino acids, the penultimate Fmoc group is deprotected, and the peptide is cleaved from the resin. Cleavage cocktail is made of strong acid called trifluoroacetic acid (TFA), which is efficient in cleaving most Fmoc based resins.[39] The side chain protecting groups are also acid labile and get cleaved during the cleavage step. Scavengers like TIPS/ thioanisole/ phenol are added to scavenge the secondary protecting groups, which may attack certain amino acids such as tryptophan, histidine and cysteine.[29]

2.1.7. PSA epitope synthesis and conventional imprinting

In the current study, PSA epitopes were identified and synthesised by standard Fmoc solid phase synthesis using available literature methods outlined in Section 2.1.6. Post-purification and characterisation of the epitopes, conventional monomers (MAA, AAm, 2-VP) were utilised for bulk imprinting of the epitopic templates. The aim was to

identify monomers that are suitable to imprint the PSA epitopes (peptides) to synthesise MIPs with maximum binding efficiency. It was hypothesised that using the conventional bulk imprinting methods, monomers/crosslinker/template ratios could be identified to efficiently imprint the PSA epitopes. This could then be easily translated to a surface imprinting strategy for incorporating into sensing platforms.

2.2.   Aims And Objective

The overarching aim of this chapter is to rationally design an epitope imprinting strategy

for the recognition of PSA.

Objectives:

1. Selection, synthesis and purification of epitopic sequences using standard solid

    phase peptide synthesis in this case

2. Characterisation of epitopes/peptides using HPLC - mass spectrometry.

3. Screening of monomers to select the best functional monomer and further using

    it to imprint the epitope template.

4. Rebinding evaluation of epitope imprinted MIPs.

2.3. Material And Methods

2.3.1. Reagents

All Fmoc amino acids and rink amide 4-methylbenzhydrylamine (MBHA) resin were purchased from Sigma Aldrich, UK and stored at -20°C. 2-Chlorotrityl chloride resin was obtained from Novabiochem, UK. All reagents for peptide synthesis were of synthesis grade and were also purchased from Sigma Aldrich, UK. DMF and DCM used for synthesis were analytical grade and purchased from Fisher Scientific, UK. Methacrylic acid (MAA), Vinyl pyridine (VP), acrylamide (AAm) and ethyleneglycoldimethycrylate (EGDMA) were purchased from Sigma Aldrich UK. HPLC grade acetonitrile and methanol were purchased from Fisher Scientific, UK.

2.3.2. Apparatus

A peptide synthesis vessel with medium sized frit was acquired from Sigma Aldrich, UK. UV absorbance experiments were carried out on Cary 60 UV-Vis, Agilent, UK. Reverse phase HPLC analysis was performed using a Thermo Scientific HPLC automated system (SpectraSystem), UK. The peptides were analysed by reverse-phase HPLC using a C18 RP Kromasil C18, 5 μm, 250 mm × 4.6 mm using a gradient mobile phase (Table 2.1) where solvent A was (99 % water, 1 % acetonitrile (MeCN), 0.1 % TFA) and solvent B (1 % water, 99 % acetonitrile, 0.1 % TFA), UV detection at 260 nm, 20 μl injection volume and a flow rate of 1 ml/min. Peak areas were analysed using Chromquest software.

Time (minute)	Solvent A (v/v)	Solvent B (v/v)	Flow rate
0	99 %	1 %	1 ml/min
30	1 %	99 %	1 ml/min
40	99 %	1 %	1 ml/min

Table 2. 1: Gradient run conditions for elution of peptide.

The peptides were freeze dried using an Alpha 1-2 LD plus freeze drier (Martin Christ, Germany). Mass spectrometry analysis (LC-MS) was conducted using a Thermo Finnigan Navigator system (Paisley, UK), with a Thermo Separation HPLC (Paisley, UK),

2.3.3. Peptide synthesis of Fmoc-vanp

The peptide synthesis protocol was developed based on published protocols.[21,29,33] Peptides were synthesised on a 0.25 mmol scale using a peptide synthesis glass vessel fitted with a medium sized frit. The peptide synthesis protocol has been described for Valine-Alanine-Asparagine-Proline (Val-Ala-Asn-Pro) (VANP) peptide in the following section. However, the same protocol was also used for the synthesis of other peptides throughout the project. Based on the C terminus functional group, two resins were used in peptide synthesis:

2.3.3.1.   Swelling

Rink amide MBHA resin was used to synthesise amide-terminated peptide (VANP)-CONH. 2-chlorotitryl chloride resin was used to synthesise carboxyl terminated peptide

VANP(COOH). 250 mg of resin with a loading factor of ~1 mmol/g was added to 20 mL dry dichloromethane (DCM) and allowed to swell for 30 minutes in a peptide synthesis vessel (Sigma Aldrich, UK) before the first deprotection step.

2.3.3.2.   Deprotection

Rink amide resins are Fmoc protected and therefore required deprotecting before addition of the first amino acid. After swelling the resin, DCM was drained from the peptide synthesis vessel with a stream of nitrogen. Approximately, 10 ml of deprotecting solution containing 25 % (v/v) methyl piperidine in dimethylformamide (DMF) was added to the swelled resin. After two minutes, the deprotecting solution was drained using nitrogen and the resin was washed once with 2 ml of DMF to remove traces of methyl piperidine. Thereafter, a second deprotection step was carried out for 10 minutes to remove any remaining Fmoc protecting molecules on the resin. Following deprotection the resin was washed with 2 ml DMF (2X) and 2 ml DCM (2X). The vessel was drained under a stream of nitrogen to remove any residual DCM before conducting the Kaiser test. 2-cholorotitryl resins did not require an initial Fmoc deprotection step prior to addition of the first amino acid (see Section 2.3.3.4).

2.3.3.3.   Monitoring deprotection and coupling

Fmoc deprotection was monitored by observing the presence of free amine group post-deprotection using the Kaiser test.[40] The three solutions require were prepared and stored in dark dropper bottles:

- Solution A: 5 g ninhydrin dissolved in 100 ml ethanol

- Solution B: 80 g liquefied phenol dissolved in 20 ml ethanol

- Solution C: 2 ml of 0.001 M potassium cyanide (KCN) plus 98 ml pyridine

To test for free amine post deprotection of Fmoc group, two drops of solution A, and one drop of solution B and C solution were added to few beads of resin in a glass tube and placed in a sand bath at 120^0 C. Presence of dark blue colour on the beads indicated presence of free amines and completion of the Fmoc deprotection step.

2.3.3.4. Addition of the first amino acid:

When using Rink amide resins, the first amino acid was coupled using the method described in Section 2.3.3.5.

For 2-Chlorotrityl chloride, 250 mg (0.25 mmol) of resin was swelled in dry DCM (10 mL) for 5 minutes in the peptide synthesis vessel. Upon draining the vessel with a stream of N2, a coupling solution containing 126.51 mg (0.375 mmol) of Fmoc-proline-OH and 175 μl of DIEA (N,N- Diisopropylethylamine) (1mmol) dissolved in 6 mL of DCM was added to the resin. The reaction was carried out for 3-4 hours at room temperature. The resin was then twice washed with 2 mL DCM and treated with 5 mL of DCM/ MeOH/ DIEA (80: 15: 5) v/v for 10 minutes. The resin was again washed with DMF and the reaction completion was checked using the Kaiser test (Section 2.3.3.3).

2.3.3.5. Coupling reaction

A coupling cocktail was prepared to activate Fmoc-proline-OH for attachment to the rink amide resin. All calculations were done on the bases of loading factor of resin (0.25mmol). (4X resin) Fmoc-proline amino acid (1mmol, 333 mg), 169 mg of HBTU (2-(1H-benzotriazol-1-yl)-1,1,3,3-tetramethyluronium hexafluorophosphate) (0.95 mmol) was weighed out in screw cap vial and the mixture was dissolved in 2 mL DMF. Thereafter, N, N - diisoproylethylamine (DIPEA) (1.5 mmol, 300 μL) was added the

amino acid/HBTU solution to activate the Fmoc-proline-OH. The coupling cocktail solution was incubated for 5 minutes until the solution turned light yellow (demonstrates activation of amino acid). Following a positive Kaiser test after deprotecting step, the activated amino acid coupling solution was added to the resin. The coupling reaction was then carried out in the peptide synthesis vessel for 2 - 3 hours. Thereafter, the resin was washed with 2 ml DMF (3X) and 2 ml DCM (2X) and dried under a stream of NO_2. A Kaiser test was conducted to check for completion of reaction as elaborated in Section 2.3.3.3. The presence of transparent beads indicated completion of coupling reaction. Post coupling, steps 2.2.3.2 - 2.2.3.4 were repeated until Asparagine-Alanine-Valine amino acids were attached.

2.3.3.6. Cleavage

After coupling all the amino acids to the resin a cleavage cocktail of 90 % trifluoroacetic acid (TFA), 5 % water, 5 % tri-isopropylsilane (TIPS) was prepared fresh. Cleavage solution (5 ml or roughly double the volume of the resin) was added to the resin and placed on the shaker for two hours. The cleavage cocktail solution containing the peptide was then collected in a round bottom flask from the peptide synthesis vessel. The resin was further washed twice with 5 ml DCM to remove any residual TFA. The solution was then rota vaporised (Buchi, UK) to reduce TFA in cleavage solution before the precipitation step.

2.3.3.7. Precipitation

The cleavage solution (roughly 5-6 ml) was then added drop wise to 50 ml of ice-cold ether to precipitate the peptide. The precipitated solution was poured into a 15 mL centrifuge tubes and spun down at 3000 RPM in (Sigma 2-16 Centrifuge, UK) for 5

minutes in centrifuge tubes. The precipitate, obtained after discarding the supernatant, was washed with 10 ml ice-cold ether twice to remove any residual scavengers and TFA.

2.3.3.8. Purification

The crude peptide was analysed and purified by reversed phase HPLC fitted with a Luna, 5μm, C18, 250 mm x 10 mm silica column (Phenomenex, UK). The peptide was purified by injecting 2 mg of crude peptide per injection (injection volume 2 ml) and eluting the peptide using a gradient run mentioned Table 2.1 at a flow rate of 2 ml/min. Peptides were collected manually and analysed using LC-MS(company). The samples containing the correct peptide was pooled together and roto-vaporised to remove any acetonitrile or solvent. The aqeous peptide solution was then poured in a centrifuge tube and freeze dried in liquid nitrogen for 10 minutes. Thereafter, the frozen peptide in the centrifuge tube was left in a freeze drier overnight to obtain the dry peptide.

2.3.4. Peptide characterisation by UV

Fmoc protected peptides were analysed by UV spectroscopy (Cary 60 UV-Vis Agilent Technologies, UK). Aliquots (1 ml) of various peptide concentrations (25 - 400 μg/mL) were added to 1 cm pathlength quartz cuvettes (Sigma Aldrich, UK) and a UV scan over 200 - 500 nm obtained.

2.3.5. Non-Imprinted polymers for monomer screening

Using a 1:4:20 (template: monomer: crosslinker) ratio, a series of non-imprinted polymers were produced. Methacrylic acid (MAA), acrylamide (AAm) and 2-vinylpyridine (2-VP) were employed as functional monomers with ethylene glycol dimethacrylate serving as the crosslinker. Monomer (400 μmol; MAA - 33.8, μl, AAm -

56.9 mg, 2-VP - 86 μl) and EGDMA 2000 μmol (754.4 μl) were added to 850 μl

acetonitrile (1.5 times of the total volume of monomer and crosslinker) in 20 mL

polymerization vials. 1,1'-azobis cyclohexanecarbonitrile (ABCN, 1 % w/w, 4.1 mg)

was added as the initiator. The vials were crimp sealed and sonicated for 5 minutes,

before being cooled for another 5 minutes in the refrigerator. Subsequently the solution

was degassed with nitrogen for 10 minutes. The vials were then placed on an ice pack

and irradiated with UV light (100 mw/cm^2, 325 nm at a distance of 8 inches) for 2

hours. The polymers were dried overnight in under vacuum at 40^0C, then ground using

a mortar and pestle before washing with methanol and acetic acid (6:1) for 4 hours. The

polymer was subsequently washed with methanol and acetonitrile to removal residual

acid and dried overnight under vacuum. For binding evaluation, 20 mg of polymer was

incubated with 1ml of 200 μM Fmoc-VANP-COOH peptide in 10 ml polymerization

vials. The vials were placed on the shaker overnight. Following centrifugation (3200

rpm, 5 minutes), the supernatant was passed through a 0.45 μm nylon syringe filter

(Kinesis, UK) to remove any polymer residue. The UV absorbance of the final solutions

were analysed at 260 nm and 301 nm.

2.3.6. Molecular Imprinting with MAA

Due to the scarcity of the template material a shift in MIP synthesis strategy was

undertaken. Instead of synthesising conventional bulk polymers, MIPs were synthesised

in HPLC vials with 30 μl pre-polymerisation mixtures. The resulting MIPs were

obtained as solid polymer pellets which were 1-2 mm in size. This prevented the need to

grind and sieve the polymers, helped the judicious use of the template and facilitated

easy diffusion and mass transfer of template. The binding studies were carried out in the

HPLC vials containing the mini-MIPs. The method of synthesising mini-MIPs was developed by Sellegren *et al* to produce a large number of MIPs for monomer screening studies.[41]

2.3.6.1 Synthesis of MAA-MIP with ratio of 1:4:40 (T:M:C)

10 mg of (freeze dried) peptide (16 μmol) was solubilised in 20 μl of DMSO. The solution was heated in a water bath at 50^0 C to encourage dissolution. A nitrogen-purged solution of 170 μl of acetonitrile (2X of monomers) with 75 μL of EGDMA (640 μmol) with 4.5 μL MAA (64 μmol) was added dropwise to the peptide solution with 1 mg (1 % w/w) AIBN initiator. The resultant polymerisation solution (under nitrogen) was pipetted in HPLC vials (30 μL polymerisation solution per vial) and irradiated with UV for two hours and then left in the water bath at 60^0 C overnight. Post polymerisation, polymers were subjected to repetitive washes of methanol and acetic acid (6:1) until the template was undetectable in the wash solution. The wash solutions were analysed using analytical HPLC to check for any residual peptide (Section 2.3.2.). Non-imprinted polymers (NIPs) were prepared in the same fashion but in the absence of the peptide template.

2.3.6.2 Peptide kinetic binding assay

The study was conducted to understand the saturation time for binding of the template to the MIPs. Polymers were incubated with 1000 μL (200 μg/mL) of peptide solution. Aliquots (50 μl) were removed from the incubating solution at the following time points: 2, 5, 10, 15, 30, 60, 120, 180 minutes. The 50 μl peptide solution (incubated with

the polymer) was diluted with 350 µl water and analysed by RP-HPLC (as described in Section 2.3.2).

2.3.6.3 Synthesis of MAA-MIP with ratio of 1:4:80 (T:M:C)

5 mg of (freeze dried) peptide (8 µmol) was dissolved in 10 µL of DMSO to solubilise the peptide. The solution was kept warm by placing in a water bath at 50^0 C to prevent peptide from precipitating on addition of acetonitrile. A nitrogen-purged solution of 259.2 µl acetonitrile with 126.9 µL of EGDMA (640 µmol) and 2.8 µL MAA (32 µmol) and 1.34 mg (1 % w/w) AIBN initiator was added to the peptide solution drop-wise. The resultant polymerisation solution was placed in HPLC vials (30 µL polymerisation solution per vial) and irradiated with UV for two hours and then left in water bath at 60^0C overnight to form mini-MIPs. Post polymerisation polymers were subjected to repetitive washes of methanol and acetic acid (6:1) until the template was undetectable in the wash solution.

2.3.7. Molecular Imprinting with AAm

2.3.7.1 Synthesis of AAm-MIP with ratio 1:4:40 (T:M:C)

10 mg of (freeze dried) peptide (16 µmol) was dissolved in 20 µL of DMSO to solubilise the peptide. The solution was heated in a water bath at 50^0 C and a nitrogen-purged solution of 180 µl of acetonitrile (1.5X of monomers) containing 75 µL of EGDMA (640 µmol), 4.54 mg AAm (64 µmol) added to the solution with 1 mg (1 % w/w) AIBN initiator. The solution was placed in HPLC vials (30 µL polymerisation solution per vial), irradiated with UV for two hours and then left in the water bath at 60^0 C overnight to form mini-MIPs. Post-polymerisation, polymers were subjected to

82

repetitive washes of methanol and acetic acid (6:1) until the template was undetectable in the wash solution.

2.3.8. Molecular Imprinting with urea monomer

Dr. Panagiotis Manesiotis at Belfast University provided the monomer: 1-(4-acrylatephenyl)-3-(3-trifluoromethylphenyl) urea (urea monomer) for the study as a kind gift.

2.3.8.1 Formation of TBA peptide

Equimolar concentrations of Fmoc-VANP-COOH (12 μmol) and tetrabutylammonium hydroxide (TBA) (12 μmol) was dissolved in 1ml dry methanol and incubated for an hour at room temperature. TBA-peptide was obtained by rota-vaporising the sample to remove the methanol with further drying at 40^0 C for an hour under vacuum.

2.3.8.2 Synthesis of urea-MIP with ratio 1:1:4:20 (T:M1:M2:C):

8 mg TBA-peptide (12 μmol) was mixed with 4.80 mg urea monomer (12 μmol), 3.7 μl AAm (48 μmol) and 38.80 μl EGDMA (240 μmol). AIBN (1 % w/v, 4.5 mg) and 100 μL acetonitrile was added to the monomer solution. DMSO (5 μl) was added to solubilise the peptide that was poorly soluble in acetonitrile. A similar polymer was prepared using DMF as a porogen.

All solutions were purged with nitrogen and transferred into HPLC vials (30 μL polymerisation solution per vial) prior to irradiation with UV (2 hours). Subsequently, the vials were transferred to a 60^0 C water bath for 18 hours. Post-polymerisation, polymers were subjected to repetitive washes of methanol and acetic acid (6:1) until the template was undetectable

2.3.8.3 Peptide kinetic binding assay:

The study was conducted to understand the time taken to reach binding equilibrium of the template to the MIPs. Polymers were incubated with 1000 µL (100 µg/mL) of peptide solution. Aliquots (50 µl) were removed from the incubating solution at the following time points: 2, 5, 10, 15, 30, 60, 120, 180 minutes. The 50 µl peptide solution (incubated with the polymer) was diluted with 350 µl water and analysed by RP-HPLC as described in Section 2.3.2.

2.3.9. Peptide binding assay for MAA/AAm/urea monomer MIPS/NIPS:

The batch binding assay was conducted to understand binding affinities of MIPs. Conventionally, 1mg of the polymer is weighed in to different vials and incubated with varying concentrations of target analyte. In the min-MIP format the polymer yield was typically < 50 mg thus insufficient for a conventional systematic equilibrium-binding assay. In order to make the most efficient use of the MIPs equilibrium binding was performed by sequential addition. Initially, 0.5 ml of a 1 µg/ml peptide solution (in MeCN) and 30 mg of MIP or NIP were measured into glass vials containing the mini-MIP monolith. After incubation at room temperature for one hour 250 µl of MeCN was removed for analysis and was replaced with an aliquot of a 200 µg/ml peptide stock solution and an additional volume of MeCN to return the overall volume to 0.5 ml. This was repeated hourly to generate a range of incubation concentration as described in Table 2.2 moved hourly and an additional amount of a stock peptide the same polymer was incubated sequentially with increasing concentrations of peptide after every hour. The MIPs were incubated with 500 µl peptide (10 - 200 µg/mL) added sequentially for

one hour according to the Table 3.1 250 µL of the concentration was removed and diluted with 250 µL water in a HPLC vial and analysed by RP HPLC.

Concentration (µg/ml) (total volume 500 µl)	Amount removed after 1 hour (µl)	Volume added of 200 µg/ml peptide solution	Volume of MeCn added (µl)
1	250	-	
2	250	1.5	248.5
5	250	3.75	246.25
10	250	7.5	242.5
15	250	11.25	238.75
20	250	15	235
40	250	30	220
60	250	45	205
80	250	60	190
100	250	75	175
120	250	90	160
150	250	111.25	138.75

200	250	150	100

Table 2. 2 Concentration of peptide added to each mini-MIP vial using sequential addition of peptide with stock concentration of 200-µg/ml peptide solutions. Additonal MeCN was added to the vials to get the total volume of the solution to 500 µl.

2.4. Results And Discussion

2.4.1. Selection of epitope

PSA is a 30 kDa serine protease containing 237 amino acid residues.[42] Despite the controversy surrounding PSA testing, it was chosen as a biomarker for this proof of concept study due to its ease of availability and known crystal structure. A literature search was conducted to select an appropriate template for PSA epitope imprinting. Michel *et al* have previously demonstrated the involvement of a C-terminal peptide of total-PSA in antibody recognition with peptide phage display libraries.[43] The C terminal peptide was shown to be surface localised (as seen in the crystal structure in Figure 2.12), which made it a potential target for epitope imprinting. Furthermore, this particular sequence of amino acids is known to be non – glycosylated, making it less complex and a better defined template for imprinting due to the absence of sugar moieties on the amino acids.[44] A nine amino acid sequence (IKDTIVANP) from the C-terminus of PSA was chosen as a template for molecular imprinting as it would be highly selective for PSA and would help in recognition of the whole protein. The protein BLAST (Basic Local Alignment Search Tool) search query for the sequence IKDTIVANP returned a 100% hit (http://www.uniprot.org/) for PSA demonstrating the uniqueness of the sequence (Figure 2.13). [45]

Historically, very few literature studies have reported a rationalised approach to choosing an appropriate template/epitope for epitope imprinting. Nishino *et al's* article on surface epitope imprinting for selective protein capture used a unique epitope sequence from each of the template proteins however, they were all C terminus sequences.[14] This approach cannot be applied to all proteins, as the C terminus

sequences may not be the best target for epitope imprinting in each case. Epitope

mapping by phage display libraries is a more suitable technique that allows one to

choose surface localised epitopes that are suitable for epitope imprinting. However, one

drawback of this technique is that availability of epitope mapping data is limited to

certain proteins.
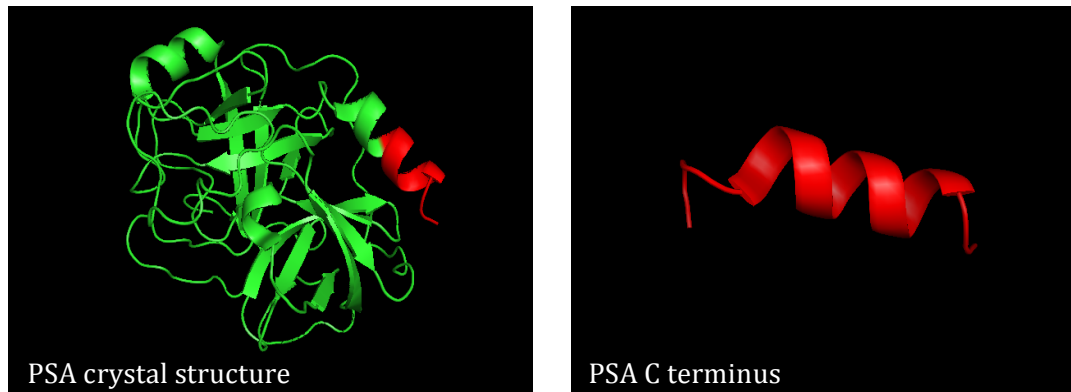
Figure 2. 12: PSA crystal structure showing the C-terminus portion of the protein highlighted in red. The C terminus peptide formed an alpha helix structure [44].

Figure 2. 13: Protein Blast results for the C terminus sequence IKDTIVANP showing a 100 % match to PSA (KLK3)

The peptide sequences were designed with truncated sequences of 4 mer, 6 mer and 9 mer to design molecularly imprinted polymers and to perform competitive binding assays. Initially, the synthesis, characterisation and imprinting of the 4 mer sequence (VANP) was the focus.

2.4.2. Optimisation of peptide synthesis protocol

2.4.2.1. Purification and characterisation Fmoc-VANP(CONH):

The 4 mer (Fmoc-VANP) was initially synthesised by Fmoc solid phase synthesis on MBHA rink amide resin to obtain a peptide amide. The crude peptide was analysed by RP-HPLC with MeCN/water (66/34) mobile phase, eluting as a single peak at 5 minutes with $\approx$ 95 % purity (Figure 2.15). The peptide was not purified further and was used as synthesised, post lyophilisation. As there was no site for positive ionization on the peptide, the mass spectrometry (MS) data did not show the exact mass of the peptide (622 g/mol), however, the sodium adduct of the peptide (+22) was observed (643.3 g/mol) (Figure 2.16). The exact mass of the peptide could not be determined using MALDI due to the low molecular weight of the peptide.
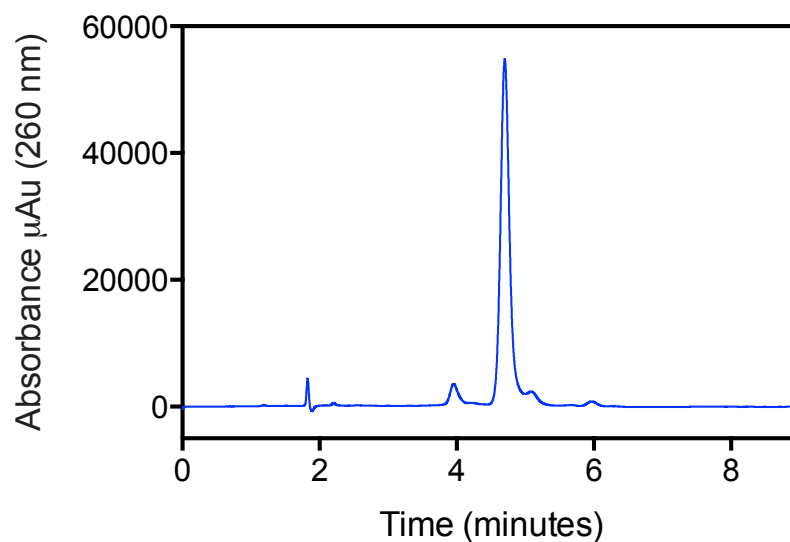
Figure 2. 14: HPLC chromatogram of the as-synthesised 4-mer peptide (Fmoc-VANP) showing one major peak.
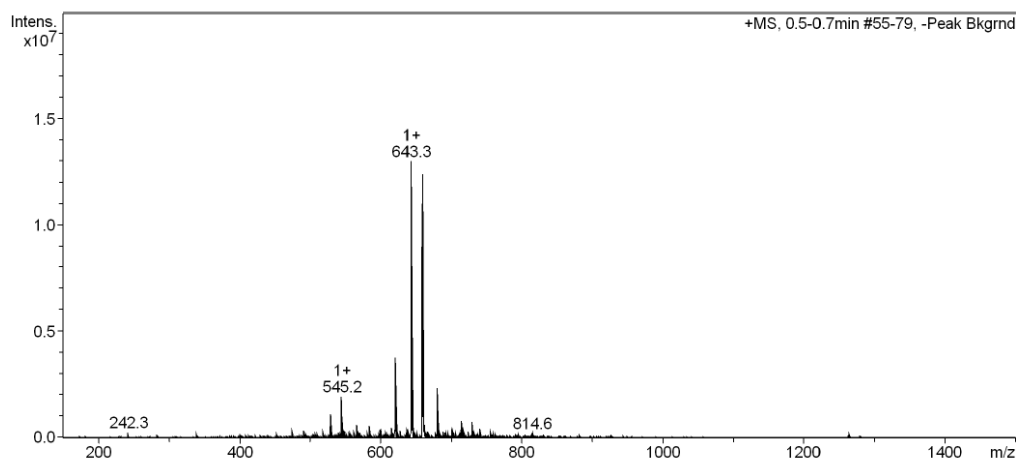
Figure 2. 15: Mass spectrometry of VANP 4mer peptide showing the sodium adduct of the peptide (+22) with a mass of 643.3 g/mol. This is common in chemical species, which do not contain a positive site for ionisation.

The calculated theoretical yield of the peptide using Fmoc solid phase synthesis (based on 0.25 mmol scale) should be roughly 96 % or 150 mg. This is based on the fact that

there is a loss of 1 % in coupling efficiency after the addition of each amino acid.[33]

However, the actual peptide yield obtained from the Fmoc-VANP(CONH) synthesis

was only 14.5 mg. The peptide synthesis produced the desired peptide, however the

yield was $\approx$ 10 % of the theoretical yield. The low yield could be attributed to an

unfavourable side reaction called 'diketopiperisation' reaction (Figure 2.14). This

reaction is observed in Fmoc synthesis when using resins with benzyl ester-peptide

linkages (rink amide resins) with certain amino acids (proline, glycine) as the first amino

acid. In this reaction, when piperidine deprotects the Fmoc group of the penultimate

amino acid, the free amino group cleaves the resin ester peptide linkage forming a

cleaved dipeptide product called piperazinedione.[46] This reaction is accelerated when

proline followed by asparagine are the first two amino acids in the sequence. This is a

consequence of improved accessibility to the ester bond on the resin and the presence of

the cis-amide bond on proline.[32] This side reaction may lead to partial or complete loss

of the peptide.

To disfavour this reaction, deprotection of asparagine was carried out with a reduced

base concentration (20 % piperidine in DMF) in the deprotection solution with longer

deprotection reaction time (20 minutes). However, this approach increased the yield of

the peptide by only 5 %. Given that at least 100 - 200 mg of the template would be

required in the preparation the molecular imprints and subsequent rebinding assays, an

alternative and potentially higher-yielding approach was explored based on a difference

resin (Section 2.4.3).
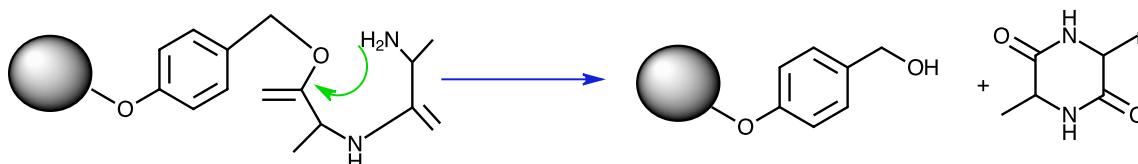
Figure 2. 16: Diketopiperization reaction: the free amine group of asparagine attacks the ester linkage on the resin to form a diketopierazine product.

Another point to note during the synthesis was the change in colour of resin from yellow to bright orange after the addition of proline and asparagine residues, and the colour change made it challenging to check for free amines using the Kaiser test (following deprotection and coupling steps). The change in colour has not been described in the literature and it is suspected that the change could be the result of a side chain protecting group reacting with the resin.

2.4.2.2. Purification and Characterisation of Fmoc-VANP(COOH)

The 4 mer Fmoc-VANP(COOH was synthesised by Fmoc solid phase synthesis on 2-chlorotrityl resin to obtain a peptide acid. The peptide was purified with RP-HPLC with MeCN/water as mobile phase using a gradient run (Section 2.3.2) by isolating the largest peak at 22 minutes (Figure 2.17). The fraction at 22 minutes was analysed by mass spectrometry, which showed the correct mass of the peptide with two sodium adducts (666.25 g/mol) (Figure 2.18). The peptide obtained from 2-cholotitryl resin synthesis was less pure (70%) than that obtained from Rink amide resin. Incomplete coupling of the first amino acid to 2-cholorotitryl resin or degradation of resin due to moisture could explain lower purity of the peptide. Furthermore, coupling efficiency of rink amide resins for first amino acid is higher than other resins leading to purer yields.[33]
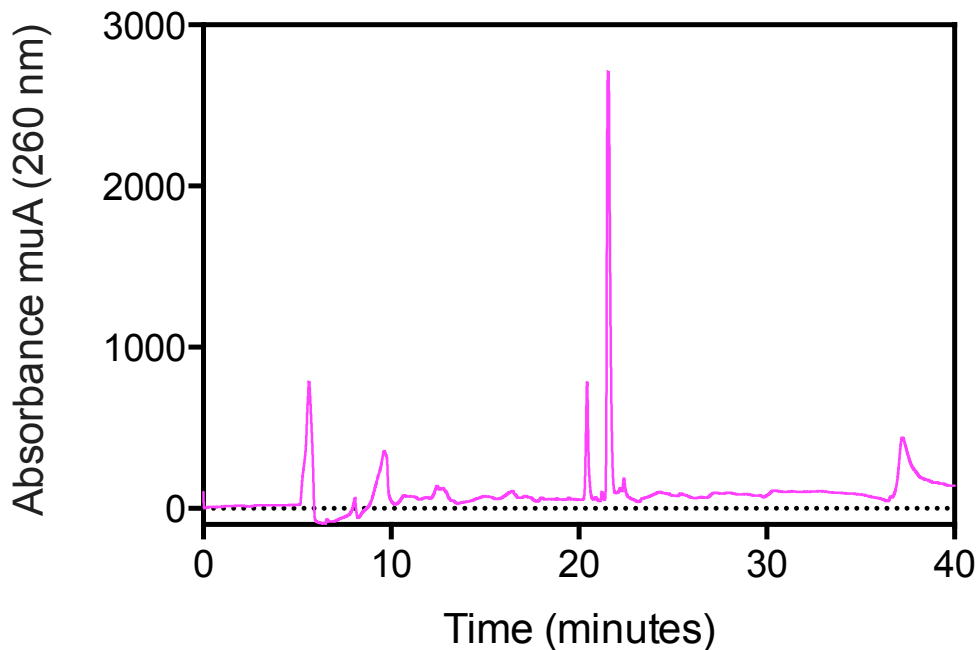
Figure 2. 17: Chromatogram of Fmoc-VANP(COOH) using gradient elution showed two peaks

with the peptide eluting at 22 minutes.
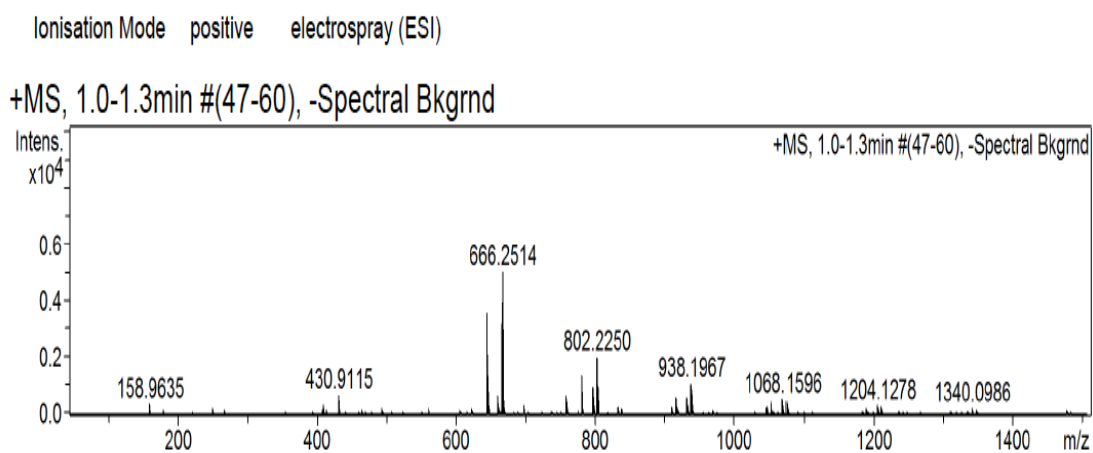
Figure 2. 18: Mass spectrometry analysis of the peptide showed the mass of the peptide with two

sodium adducts (666.25 g/mol). This is due to the absence of any site for positive ionisation in

the MS.

After discovering the occurrence of an undesired side reaction with rink amide resins and proline in the synthesis, a literature search for alternate resins was conducted to obtain higher yields of the peptide. Wang resins and 2-cholorotitry resins are popular resin for obtaining carboxyl-terminated peptides. Peptide synthesis of VANP peptide using Wang resins failed to produce a significant yield of the peptide (~ 0.1 % of theoretical yield), however, the use of 2-cholorotitryl resin, which has been reported to suppress the diketopiperisation reaction[31], resulted in good yields. It is known from literature that the rigidity of the linker and absence of ester group in 2-chlorotitryl resin prevented cyclisation and early cleavage of the peptide via the diketopiperisation reaction.[31] The resin is also reported to suppresse racemisation of the first amino acid which results in the higher purity of the final peptide.[31] Hence, 2-cholorotitryl was used further for the synthesis of Fmco-VANP-COOH peptide in the study. The peptide was obtained at much higher yields with the 2-cholorotitryl resin when compared to the rink amide resin; ~ 50 mg (33 %) of theoretical yield compared to 10 %.

2.4.3. *UV characterisation of Fmoc-VANP(COOH) peptide:*

The UV scans of the Fmoc-peptide showed three characteristic absorption peaks at 265, 288 and 300 nm, which was characteristic of, n - π* and π - π* electronic transitions (Figure 2.19).[47] The addition of Fmoc group lead to a stronger π - π* absorption spectrum at 265 nm as a result of low valence p electrons (present in fluorenyl ring) and weaker n - π* interaction at 285 and 301 nm as shown in Figure 2.19. Electronic transitions for organic molecules in the visible spectrum mostly involve p, n, s electrons and the most common transitions for organic molecules involve π to π* or n to π* electronic transitions which fall in the visible range 200-700 nm.[48] The π - π* absorption

spectrum in peptides (without aromatic amino acids) comes from the amide bonds (CONH) which occurs at 190 nm (strong transition) and n - $\pi*$ transition which occurs at 220 nm (weak transition).[49] The absorption wavelength of 210 - 220 nm however, is not ideal for analysing peptides as there are various other organic molecules that absorb in this region making discrimination of peptides difficult. The chosen epitope template VANP did not contain an aromatic residue therefore the Fmoc protecting group on the valine residue was left to enable detection using UV.
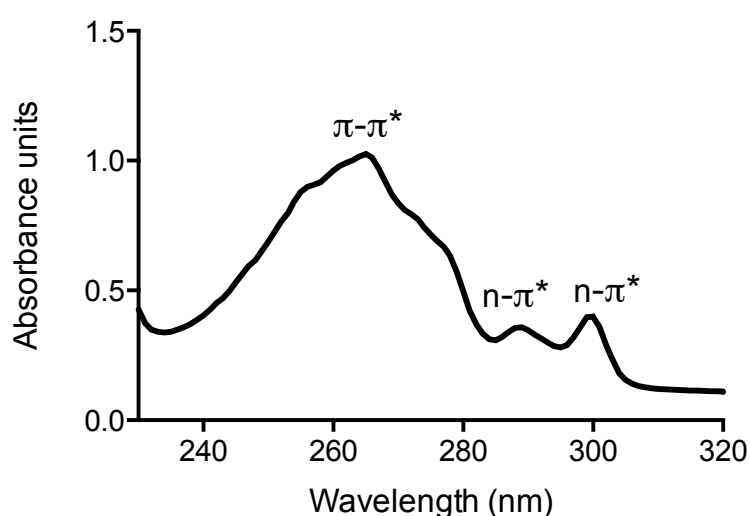
Figure 2. 19: UV spectrum of FMOC-VANP(COOH) peptide scanned from 220-320 nm. The peptide showed characteristic peaks at 265 nm, 285 nm and 301 nm.

Recording the absorbance maxima at 265 nm and 301 nm allowed the generation of a calibration curve (Figure 2.20). The peptide calibration at 265 nm was used for assays with the lower concentration of peptide while 301 nm was used for higher concentration of peptide. The peptide calibration curve was linear from 25 μg/ml- 200 μg/ml at 265 nm wavelength and linear from 25 μg/ml to 400 μg/ml at 301nm wavelength. The

calibration curves were used to calculate the amount of peptide bound to the polymers in

the monomer screening assays.
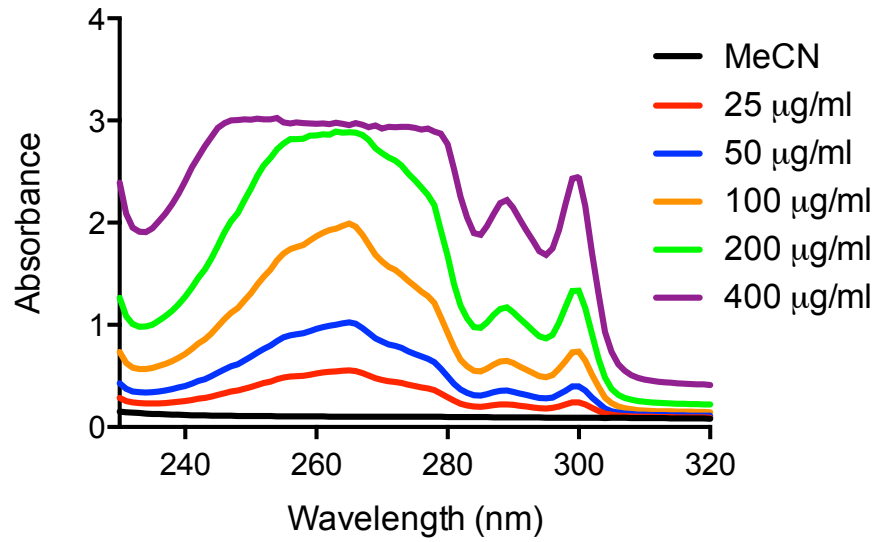
Figure 2. 20: Peptide calibration curve for Fmoc-VANP(COOH) peptide. The peptide demonstrated a linear detection range up to 400 ug/ml at 301 nm, while the calibration curve at 265 nm was only linear unto 200 ug/ml.

The plot shows:
- y = 5.420*x
- R^2= 0.995
- Y-axis: Absorbance units at 300 nm (0.0 to 1.5)
- X-axis: Peptide concentration mg/ml (0.00 to 0.25)
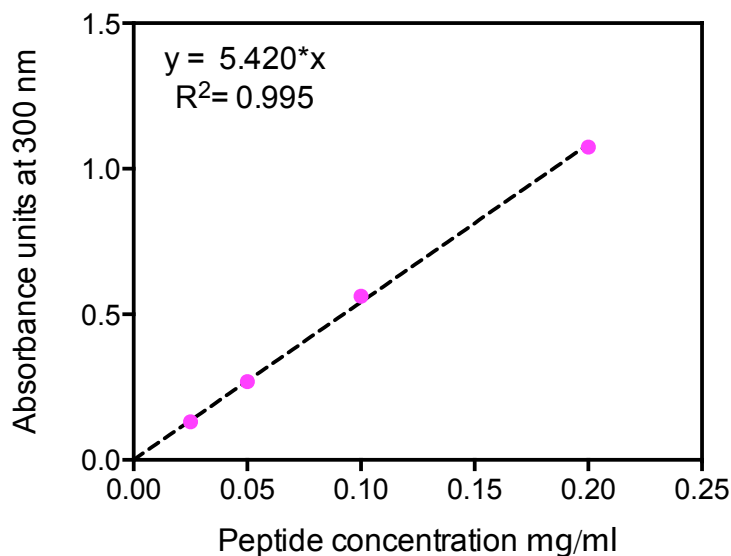
Figure 2. 21: Calibration curve for Fmoc-VANP(COOH) at 300 nm wavelength as obtained by UV spectroscopy

2.4.4.   Monomer screening study with Fmoc-VANP(COOH):

As a control, non-imprinted polymers, synthesised with different monomers, were incubated with the peptide to understand and evaluate interaction of the peptide with the non-imprinted polymers. The polymers were initially incubated with acetonitrile to check for any unreacted monomer leaching. Upon incubation of polymers in acetonitrile (no peptide) overnight, the UV spectrum in Figure 2.22 suggested that there was no leaching of unreacted monomer (if any) at 300 nm (wavelength for analysing the peptide). The high absorbance below 300 nm was an artefact produced by polystyrene cuvettes. This suggested minimal (< 2 %) interference from any monomers (if present) in the incubating solution.
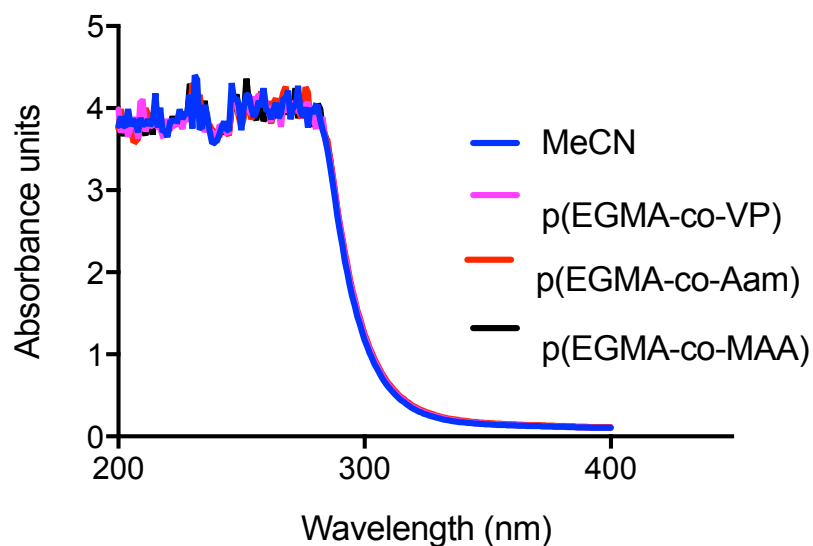
Figure 2. 22: NIPs incubated overnight in acetonitrile did not show a peak for peptide indicating any unreacted monomer did not interfere with peptide absorption peak.

The Figure 2.23 demonstrates that the p(EGMA-co-MAA) polymer displayed the highest non-specific binding to the peptide, binding 13.35 nmol of peptide per mg of polymer while p(EGMA-co-AAm) and p(EGMA-co-VP) bound 6.37 nmol/mg and 0.7 nmol/mg respectively.
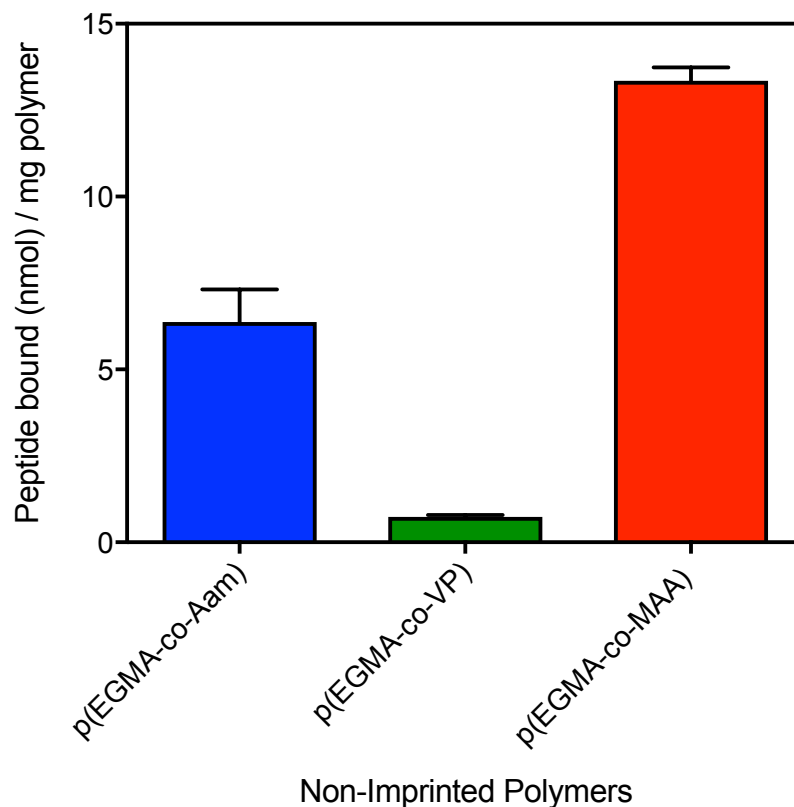
Figure 2. 23: NIP screening study showing the amount of peptide non-specifically bound to different non-imprinted polymers: p(EGMA-co-MAA), p(EGMA-co-AAm), p(EGMA-co-VP).

Due to the scarcity of pure peptide it was not possible to perform NMR titration experiments to identify suitable candidate functional monomers for the imprinting of Fmoc-VANP(COOH). Therefore, as an alternative, studies were undertaken to evaluate the non-specific interaction of the peptide with a number of non-imprinted polymer (NIP) systems.   Monomers for the polymer system were chosen based on their functionality and on previously reported applications in the area of peptide/amino acid imprinting.[5] Three monomers were chosen for creating NIPs with different properties to evaluate non-specific interactions of the peptide (Fmoc-VANP(COOH)): methacrylic acid (MAA) as an acidic monomer, 2-vinyl pyridine (2-VP) as a basic monomer and

acrylamide (AAm) as a monomer that interacts via hydrogen bonding. EGDMA was chosen as crosslinker initially as it produces polymers with mechanical and thermal stability, demonstrating good wettability in most imprinting solvents and good recognition properties.[7] Acetonitrile was chosen as the porogen due to its ability to form polymers with higher porosity and better ability to solubilise amino acids and dipeptides than non-polar solvents such as chloroform and toluene.[7] In a co-polymerisation system containing one or various monomers, cross linker/ moles of monomer ratio and the volume of porogen are the two parameters that govern the physical nature of the polymers. Peter Cormack's review titled 'Molecularly imprinted polymers: synthesis and characterisation' presented a pseudo-phase diagram, which could be used to predict the physical nature of the polymer based on volume of porogen and cross-link ratio.[10] Based on the pseudo-phase diagram, it can be observed pre-polymerisation mixtures containing higher cross-link ratio and/or in presence of high volume of solvent gave rise to macroporous polymers. These types of polymers contain permanently porous structures (even in dry state) and have mechanical strength which are ideal characteristics preferred for a MIP (allows for easy diffusion of template to binding site).[10] Polymers containing very high solvent or very low cross linker lead to the formation of gel-like powder or microgel polymer both of which are not preferred characteristics for MIPs. As a starting point the ratio of 1:5 monomer: crosslinker (EGMA) along with 1.5X of solvent to total monomer content, which has been traditionally used for creating molecularly imprinted polymers, was used for synthesising the NIPs.[10,50,51] This was a suitable approach in the absence of NMR titration study to understand peptide binding to polymers with different functional monomer content. It is proposed that the higher

non-specific binding for p(EGMA-co-MAA), p(EGMA-co-AAm) could be attributed to hydrogen bonding and good porosity of the resulting polymer. On the other hand, absence of any amine group in p(EGMA-co-VP) and lack of any π-π interaction could be attributed to low non-specific binding with Fmoc-VANP(COOH).[52] As the p(EGMA-co-MAA), p(EGMA-co-AAm) based NIPs displayed higher interaction with the Fmoc-VANP(COOH) peptide, they were studied further for imprinting of the peptide.

2.4.5. *Solubility study with Fmoc-VANP(COOH) peptide*

A solubility study with the Fmoc-VANP(COOH) peptide also was undertaken simultaneously with the NIP screening study to select an appropriate solvent for imprinting. As observed in literature the peptide was found to insoluble in non-polar solvents like DCM, chloroform, toluene at a concentration of 1 mg/mL. The peptide was sparingly soluble in acetonitrile at 1 mg/mL but became soluble at lower concentrations of 200 μg/mL. The peptide was found to be highly soluble in DMSO and DMF (aprotic solvents) at a concentration of 1 mg/mL. The solubility of the peptide in the choice of porogen is important due to its influence on the type of interactions taking place between the monomers and the peptide.[50] The choice of porogen is also important as it brings all the component of the pre-polymerisation mixture in one phase and is responsible for creating well defined pores and high specific surface area in the final polymer which aid in the rebinding capacity and efficiency MIP.[10] Polar and hydrogen bonding interactions are more favourable in non-polar solvents, however, peptides, in general, have very low solubility in such solvents.[53] Use of polar solvents is generally not preferred, as they compete with the peptide for hydrogen bonding lowering the overall binding efficiency of the imprinted system. Certain groups have demonstrated

imprinting of peptides in aprotic solvents such as DMF[15] and DMSO[54] using monomers that interact strongly with complementary functional groups to form good MIP recognition systems. Acetonitrile although slightly more polar than chloroform and toluene, has been demonstrated to be a good choice of solvent in imprinting peptides and amino acids as a result of increased porosity of MIPs.[55] Hence, to keep the pre-polymerisation mixture as non-polar as possible, acetonitrile was chosen as a solvent for imprinting and as a compromise, DMSO was added to improve the solubility of the peptide. It was hypothesised that DMSO would help solubilise the peptide while acetonitrile would encourage hydrogen bonding in the pre-polymerisation complex. The amount of DMSO was kept below 10 % of total solvent encourage these interactions.

2.4.6. Molecular imprinting with MAA as a functional monomer:

2.4.6.1. Synthesis of MAA-MIPS

Based on the NIP study, p(EGMA-co-MAA) and p(EGMA-co-AAm) demonstrated higher interaction with the template. As a consequence these polymers were studied further for imprinting of the VANP template. Although, it is ideal to have equal number of monomer molecules to functional sites on the template to maximise complexation and increase imprinting efficiency, conventional molecular imprinting ideally uses excess monomers (1:4) (T:M) for preparation of MIPs to encourage formation of template and functional monomer assemblies. The template Fmoc-VANP(COOH) contained various hydrogen bonding sites for template interaction, however initial studies with higher (T:M) ratios did not result in a positive imprinting effect. This could be due to various reasons from non-optimised crosslinker ratio to the choice and amount of porogen (acetonitrile).

Hence, the ratio of (1:4:20) (T:M:C), which has been widely used in the literature, was adopted for preparing the MIPs to start understanding the effect of T:M ratio on imprinting effect. Post the NIP screening study, the ideal experiment would have been to synthesise MIPs with the same monomer to cross linker ratio (M:C 1:5) with the peptide template (Fmoc-VANP(COOH)) (1:4:20) (T:M:C). It was hypothesised that the peptide although insoluble in acetonitrile, would be soluble in the pre-polymerisation mixture due to presence of acidic monomer and the interaction of MAA with peptide. However, the peptide was found to be insoluble in the given pre-polymerisation mixture of 1:4:20 (T:M:C) ratio. However this was not case which was suggestive of weak interaction of the peptide with the monomer. As a result, MIPs with two different ratios were synthesised and tested: 1:4:40 and 1:4:80 (T:M:C). This was done in order to increase the volume of pre-polymerisation mixture to better solubilise the peptide. Wulff *et al*. demonstrated for covalent molecular imprinting, enantioselectivity of MIPs increased with maximization of crosslinker.[56] In the study, the polymer was prepared with a template, a non-crosslinking monomer and varying concentration of EGDMA. An increase in enantioselectivity was observed for MIPs upon increasing the crosslinker from 50 % to 70 %, after which enantioselectivity increased slowly to a maximum for 95 % crosslinker. Furthermore, Shoravi *et al*. demonstrated that EGDMA contributed to template complexation via hydrogen bonding and hence contributed in the development of a highly selective cavity.[57] As a result, it was hypothesised that doubling the crosslinker from 5 times of monomer to 10 times of monomer in the current study should not significantly affect the polymer's recognition ability and selectivity.

The resulting mini-MIPs were washed exhaustively with methanol and acetic acid to break the hydrogen bonds between the template and the polymer to facilitate the removal of the template. Acetic acid causes a change in pH while methanol alters the porosity of the polymer encouraging solubilisation and removal of the peptide in the extraction solution.[58] MIPs treated with multiple rounds of wash solution were incubated in acetonitrile overnight. The supernatant analysed by HPLC (Section 2.3.2) on the following day demonstrated an absence of peptide peak at 22 minutes indicating successful template extraction. Due to optimisation of various steps involved, total peptide extracted was not calculated as the aim was to determine an imprnitng effect and evaluate the performace of the MIPs in the intial study.

2.4.6.2. Kinetic binding assay

A binding study was undertaken to study the binding kinetics of the MAA mini-MIP. The amount of peptide bound to the MIP was calculated by analysing free peptide by RP-HPLC and concentrations were calculated using the calibration curve in Figure 2.24.

The plot shows Peak area (y-axis, from 0.0 to 2.0×10^6) versus Peptide concentration µg/ml (x-axis, from 0 to 140) with the equation:

$$Y = 13982*X$$
$$R^2 = 0.998$$
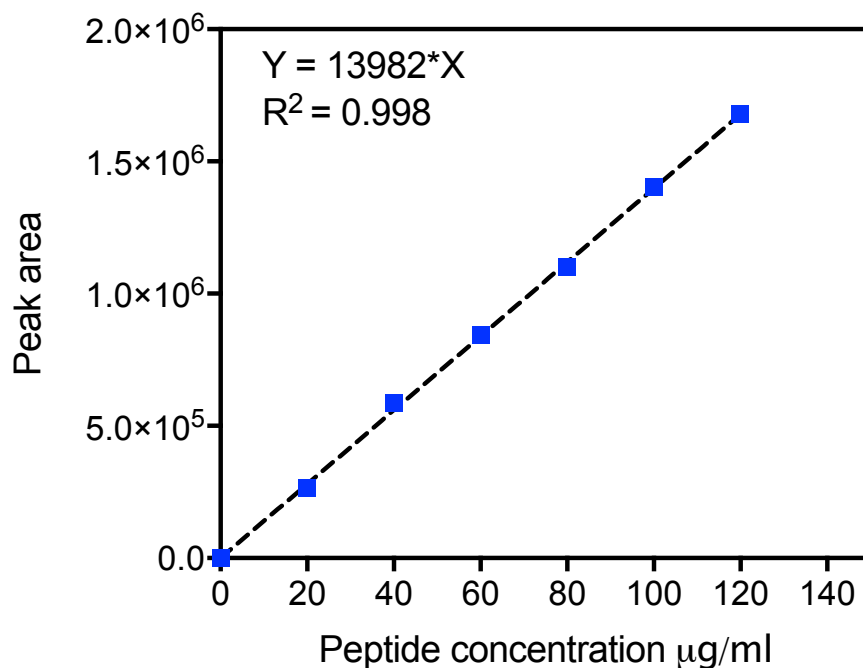
Figure 2. 24: Peptide calibration curve for Fmoc-VANP(COOH) peptide analysed by RP-HPLC

It can be observed from the binding isotherm (Figure 2.25) that maximum binding (60 %) was achieved within 10 minutes of incubation while complete saturation occurred within 1 hour of peptide incubation. Beyond one hour, a second curve or further binding was observed with the template. A possible explanation for the two curves could be faster binding kinetics for surface imprnited cavities follwoed by slow diffusion of the template to the binding cavities present in the inner core polymer leading to slower binding kinetics. As close to 75% binding was observed in one hour (Figure 2.25), MIP binding studies with Fmoc-VANP(COOH) peptide were conducted with 1 hour incubation periods to obtain binding isotherms.
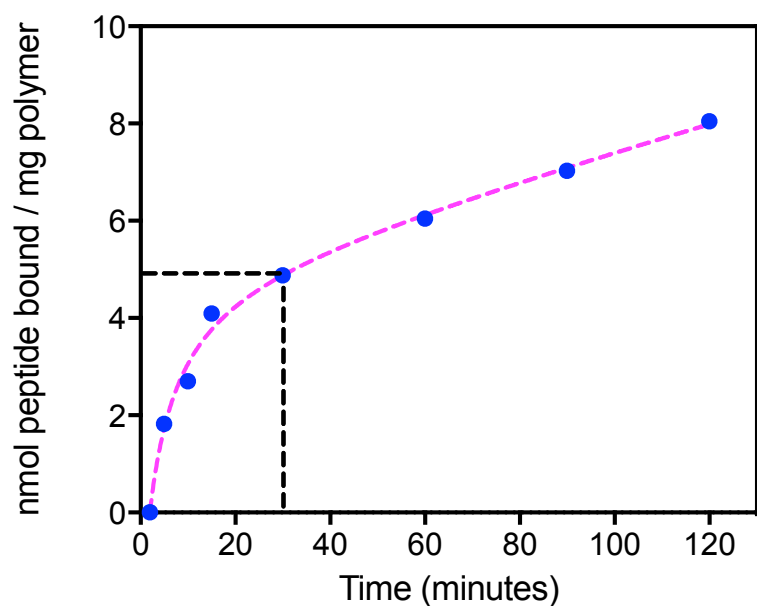
Figure 2. 25: Equilibrium binding kinetics for Fmoc-VANP(COOH) peptide (100 μg/ml) demonstrating faster binding kinetic till 30 minutes and slower binding kinetics beyond 30 minutes.

2.4.6.3. Peptide binding assay with MAA MIPs (1:4:40)

Studies were undertaken to understand the binding efficiency between MAA MIPs and NIPs. The binding data of the peptide for MAA (1:4:40) MIP and NIP has been depicted in Figure 2.27. NIPs displayed some level of non-specific binding to the peptide, which was expected given the non-specific binding observed in NIP screening study in Figure 2.23. However, the NIP response was considerably lower than MIPs suggesting an imprinting effect.

It is reasonable to assume that a number of non-covalent interactions (dipole, hydrogen, ionic) between monomer and template lead to the formation of a selective cavity capable of recognising the template. However, these non-covalent interactions are majorly dominated by hydrogen bonding between MAA and Fmoc-VANP(COOH) peptide as

shown in Figure 2.26. MAA has multiple points of hydrogen bond interactions with the amide backbone of the peptide, which could lend specificity to the MIP cavity (Figure 2.26). The R groups on the amino acid residues mainly consist of methyl groups (valine, alanine and asparagine) with the exception of an additional amide group on asparagine, which suggests that the dominant interaction was hydrogen bonding. It is known from various published studies that ionic interactions lead to more stable and specific interactions leading to higher to imprinting factors.[59,60] As the Fmoc group protected the amine group on N-terminus of VANP, it was hypothesised that the imprinting factor and binding affinity could be lower than what could have theoretically been achieved if the peptide was not protected. However, due to the limitation of the detection technique (UV) used for analysing the peptide, Fmoc protection was necessary for the study.
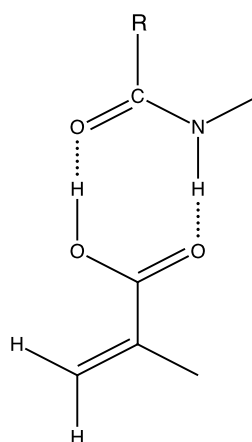
Figure 2. 26: MAA hydrogen bonding with amide bond in the peptide backbone
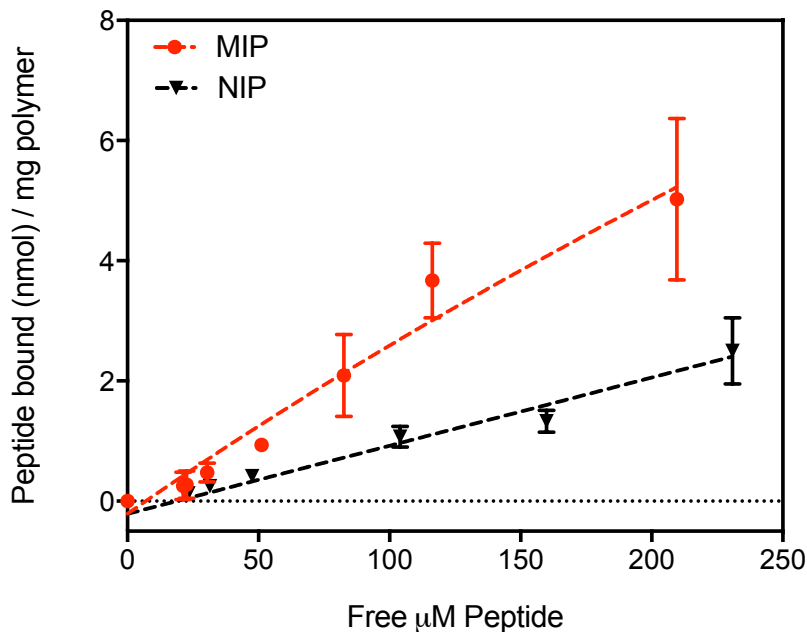
Figure 2. 27: Binding data of MAA MIPs and NIPs with Fmoc-VANP(COOH) peptide in acetonitrile. (N = 8 +/- SD). Langmuir adsorption isotherm fitted data for MAA imprinted polymers

To further understand and characterise the binding properties of the MIP, the binding data was fitted to Langmuir adsorption isotherm (Figure 2.27).

$$B = \frac{Bmax \times [X]}{[X]+Kd} \quad (2.1)$$

A Bmax 4.622 nmol/mg polymer and Kd of 222 μM was obtained for MAA MIPs using Langmuir adsorption isotherm binding model. The R^2 value of 0.915 was obtained for fitting the MIP binding data to the model. A usable Scatchard plot of the data could not be obtained due to an absence of experimental data points at higher concentrations of peptide. The reason for this was the low solubility of the peptide in acetonitrile, with

200 μg/ml being the upper end of its solubility. The linear regression of the data indicated poor fit with a Kd > 1100 μM.

The Langmuir adsorption isotherm with the limiting slopes analysis of Scatchard plots has been applied to various MIP systems for evaluation of binding affinities.[61,62,63] However, an important assumption made for fitting Langmuir adsorption isotherm is the binding site homogeneity. Theoretically, to build a MIP system where all binding sites have the same affinity towards the template molecule would require every monomer-template interactions to take place in the same manner, with the same affinity, every time during the polymerisation. In practice, this is extremely difficult to achieve because the interactions between template and monomer are not consistent but vary from batch-batch and time-to-time. Furthermore, in a pre-polymerisation mixture, various complexes exist at the same time, and their capture during various stages of polymerisation leads to further heterogeneity within a polymer.[61] Moreover, the monomers do not interact with all of the template interaction sites with the same binding affinity, which could lead to the formation of MIPs with two to infinite binding site models preventing accurate representation of binding model with Langmuir adsorption isotherm.

The degree of variation is also dependent on the rigidity of the template and type of functional groups on the template in non-covalent imprinting. Rigid templates have historically shown the highest imprinting efficiency with non-covalent imprinting possibly due to the stability of the interactions in the pre-polymerisation mixtures.[64] Peptides on the other hand are not rigid molecules, they rotate around the amide backbone, which further disrupts the formation of stable interactions between monomer

and template in the pre-polymerisation mixture.[65] Langmuir model can approximate heterogeneity to a certain extent by grouping the heterogeneous data into two binding groups: low and high affinity, which can be observed from a Scatchard plot (bound vs free) with varying slopes. However, the plot only demonstrates heterogeneity in the system and cannot be used for estimating binding affinities. An example of Scatchard plots illustrating such grouping of low and high binding affinities can be seen in Figure 2.35. Freundlich isotherm has also been applied for modelling the MIP binding data as it seemed a better fit to experimental binding data obtained with heterogeneous MIPs.[66] However, Freundlich isotherm also suffers from certain drawbacks such as problems in modelling saturation behaviour and validity over a large set of concentrations.

As a result, a different model was used for modelling the heterogeneous MIP binding data. Langmuir-Freundlich isotherm also termed as Sips equation, first described by Umpbley *et al* [67], describes the relationship between the equilibrium concentrations of bound analyte and free analyte with three constants Bmax, a and m, whereby Bmax is the total number of binding sites, a is related to median binding affinity and m represents the heterogeneity index.[67] Heterogeneity index m, indicates the heterogeneity of the system and varies from 0 to 1. A system which is completely homogenous has m = 1 which translates the equation into Langmuir adsorption isotherm. Freundlich-Langmuir adsorption (FHL) model was shown to be a better fit to the MAA-MIP binding affinity data as it accounted for binding site heterogeneity in its model.

$$B = \frac{Bmax\ a\ X^m}{1 + aX^m}\ \ (2.2)$$
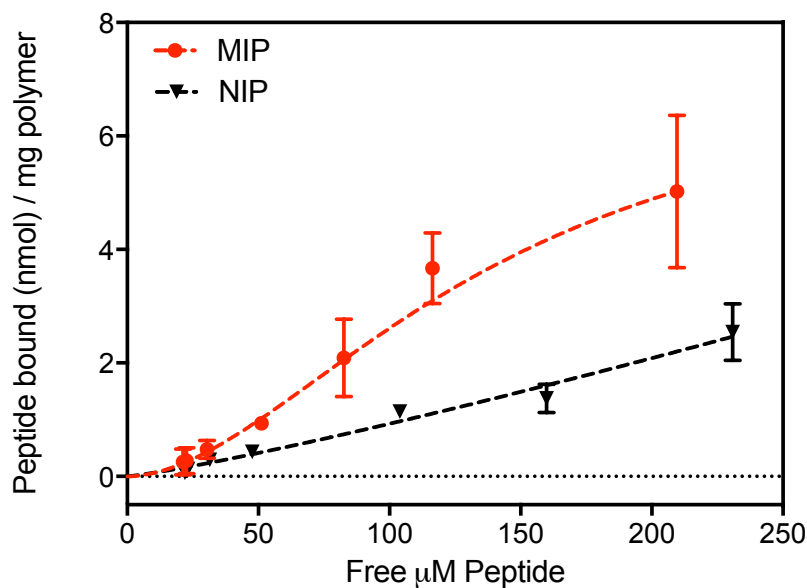
Figure 2. 28: Binding isotherm fitted with Freundlich-Langmuir adsorption isotherm

FHL model demonstrated better fit to the MAA-MIP binding data with an R^2 value of 0.994 with a Bmax of 6.019 nmol/mg polymer and apparent Kd of 102.1 µM (Figure 2.28). This further establishes that MIP binding cavities for complex molecules like peptides are not made of similar binding sites that promote equal interaction with the template. An imprinting factor of the 2.07 was obtained for MAA MIP polymers. An imprinting factor > 1 suggests imprinting effect in the system and preference for the template. However, it is important to note that imprinting factor is meaningful for understanding binding efficiency between MIP and NIP at saturation concentrations (Bmax).[7] Imprinting factors calculated below the saturation concentration can result in skewed IF values, which may not truly reflect the binding performance of MIPs. In the current study, IF could not be calculated at saturation conditions due to solubility issues with template. Hence, understanding of the MAA MIP systems was limited due to absence of Bmax data. With the available data, although a reasonable imprinting factor

was obtained with MAA MIP, the binding capacity and affinity was lower than that observed with conventional MIP systems for small molecules in literature.[68,69,70]

The maximum (1:4:40) MAA MIP response was 2.4 times lower that the response of p(MAA-co-EGDMA) in the NIP screening study in Section 2.4.4. A possible explanation for this could be the change in porosity and rigidity of the polymer due to the addition of DMSO[71] and the use of higher amount of crosslinker in synthesis of the imprints.[72] It was also hypothesised that DMSO interacted with the peptide competing with MAA for hydrogen bonding, preventing formation of cavity with superior recognition properties. Furthermore, the use of mini-MIPs, which is larger in size than traditionally ground and sieved MIPs, could limit easy diffusion of the peptide to the imprinted cavities in the polymer. It was proposed that all these factors could have an overall effect on the binding kinetics and mass transfer of the peptide from/to the binding site in the polymer lowering its binding capacity and affinity.

2.4.6.4.   Peptide binding assay with MAA MIP (1:4:80)

To understand the effect of cross linker on MIP imprinting efficiency another MIP system was synthesised with a ratio of 1:4:80 (T:M:C). The system demonstrated a reverse effect with NIPs displaying more binding than MIPs (Figure 2.29). This could be explained by inefficient removal of template leading to loss in imprinting effect in the polymer. It is proposed that an increase in crosslinker in the polymer reduces its porosity making the polymer more rigid, which could further prevent easy diffusion of the template during extraction/binding. Furthermore, increase in crosslinker leads to dilution of the template, which causes less binding sites per gram of polymer further reducing

the binding properties of the MIP. As a consequence higher crosslinker to monomer ratios were not investigated further for imprinting of Fmoc-VANP(COOH) peptide.
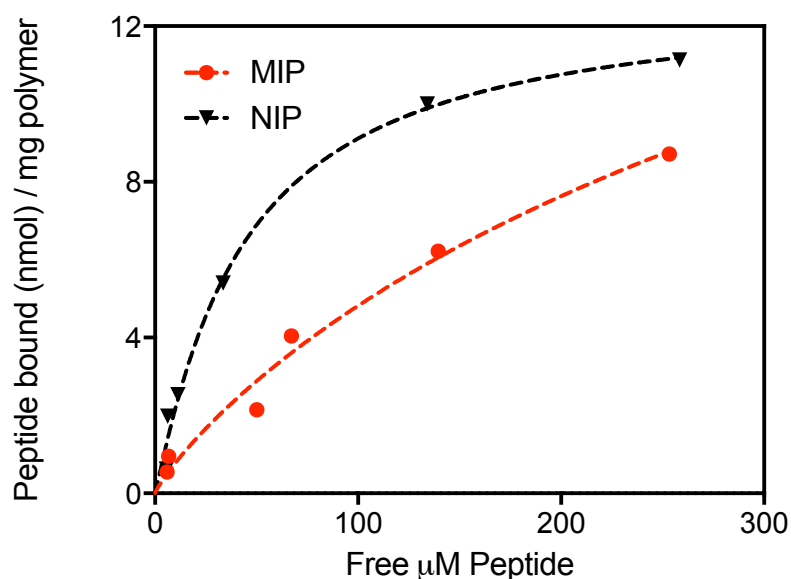
Figure 2. 29: Binding Isotherm of MAA MIP (1:4:80) demonstrating loss of imprinting effect between MIP/NIPs for peptide.

2.4.7.   Molecular imprinting with AAm as a functional monomer:

A comparison study was conducted with AAm as a monomer to understand the influence of monomer on the MIP system. Although AAm would still be heavily dependent on hydrogen bonding to form interactions with Fmoc-VANP(COOH) peptide, it was proposed that a higher imprinting efficiency could be achieved as a result of low non-specific binding of peptide to the NIPs as observed in NIP screening study (Figure 2.22). AAm monomers are strong hydrogen donors, as seen in Figure 2.30, and can interact with the peptide backbone and have been used for imprinting various proteins and peptides in the literature.[5,14,73,74]
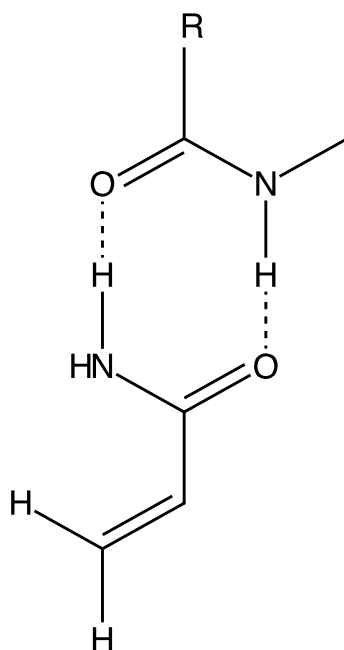
Figure 2. 30: Hydrogen bonding of peptide backbone 'CONH bond' with acrylamide monomer

Upon conducting binding studies with Fmoc-VANP(COOH) peptide, AAm MIPs displayed recognition towards Fmoc-VANP(COOH) peptide when compared to NIP as seen Figure 2.31. The imprinting efficiency or factor (IF) of 2.04 was comparable to MAA MIP, which further suggested that the dominant interaction between monomers and template was hydrogen bonding. Surprisingly, AAm MIPs demonstrated slightly higher binding capacity than MAA MIPs, possibly owning to more monomer molecules being available for interacting with the template (lack of self-association as observed with MAA). Bmax 23.57 nmol/mg and an apparent Kd of 254.3 μM were obtained by fitting the Freundlich Langmuir adsorption isotherm model to the data (R^2 - 0.995). An imprinting factor of 2.04 was obtained using AAm MIP polymers.
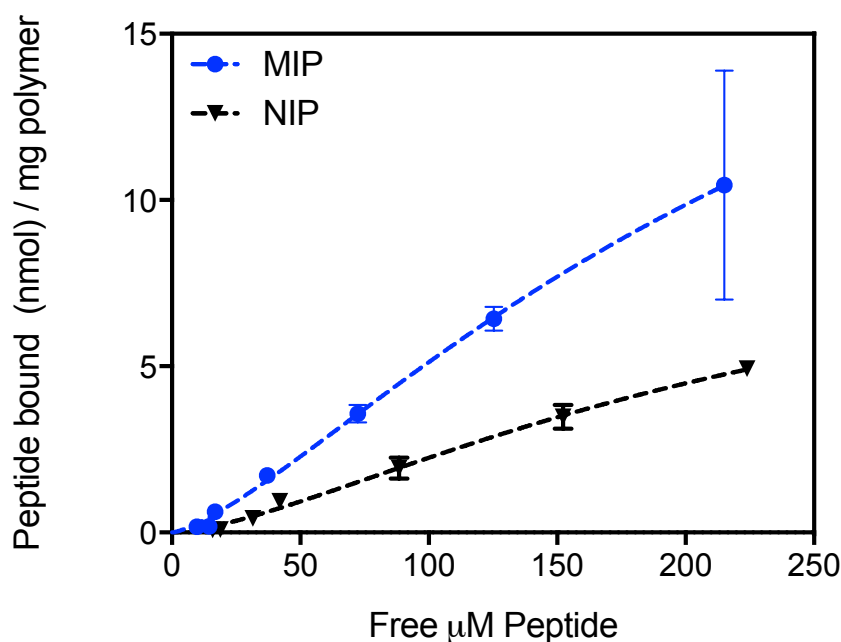
Figure 2. 31: Binding isotherms for AAm/MAA MIPs and NIPs fitted with Langmuir-Freundlich isotherm (N = 8 +/- SD).

MAA and AAm MIPs both demonstrated reasonable recognition and affinities towards the Fmoc-VANP(COOH) template over NIP with an IF ≈2. However, considering the clinical concentration of PSA in the blood which is 4-10 ng/ml [42], much higher affinities, close to few pM, would be required to detect the peptides in this clinical range. Such high affinities have been reported by Nishino *et al.* for mellitin MIP nanoparticles where the apparent dissociation constant was reported to be in the range of 7.3-25 pM.[75] However, to obtain such high affinities with conventional bulk polymers is quite challenging. The lower imprinting efficiency of the mini-MIPs could be a result of non-specific nature of interaction that is mostly dominated by hydrogen bonding used to build the polymeric cavities. To better utilise the peptide functionality, the template's carboxylate group (COOH) was targeted using a specialised urea monomer for

imprinting the peptide. It was proposed that if slightly higher affinity (than MAA/Aam MIPs) could be obtained with the specialised urea monomer then the polymers could be transferred to a surface imprinted system to achieve higher sensitivity.

2.4.8. Molecular imprinting with urea monomer as a functional monomer:

Various groups have reported the use of specialised monomers to form strong interactions with certain function groups on peptides and amino acids for obtaining highly selective MIP cavities. For example, Ken Shea's group utilised the strong interaction between Ni and histidine to form polymeric cavities that could discriminate between histidine containing dipeptide sequences in aqueous solution.[76] Sellegren's group targeted the phosphorylated tyrosine (pTyr) residue by using urea based host monomers to form strong interactions with the pTyr dianion in pre-polymerisation solution leading to highly specific binding cavities.[77]

Based on a similar concept, Fmoc-VANP's carboxyl functional group was targeted for using urea monomers to form strong interaction in pre-polymerisation mixtures. Urea monomers associate strongly with carboxylate ion to form ionic interactions[78] (Figure 2.32). Furthermore, to increase the specificity of the polymer towards the peptide, a secondary monomer was introduced to improve the binding affinity of the MIPs. AAm was chosen as a secondary monomer to provide hydrogen bonding for the amide backbone of the peptide during polymerisation. Although MAA MIPs displayed a slightly higher affinity for the peptide than Aam MIP, it was not used as a secondary monomer to prevent interaction between MAA's carboxyl group with the urea monomer. A strong base: tertrabutylammmonium hyrodoxide (TBA) was used for deprotonating the carboxyl group to allow it to freely interact with the urea monomer. Two different

progens DMF and acetonitrile were used for imprinting the peptide to understand the effect porogen on monomer template interactions.
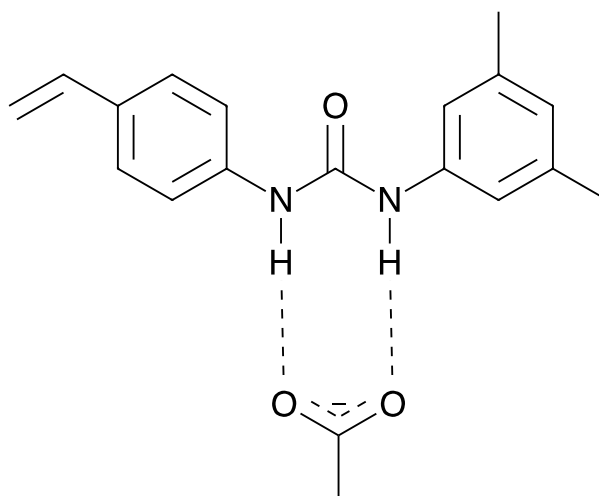
Figure 2. 32: Ionic interaction of urea monomer with carboxylate ion of the peptide.

2.4.8.1.   Peptide equilibrium binding assay

Binding saturation of Fmoc-VANP(COOH) peptide reached within 60 minutes of incubation for urea imprinted MIPs (Figure 2.33) .
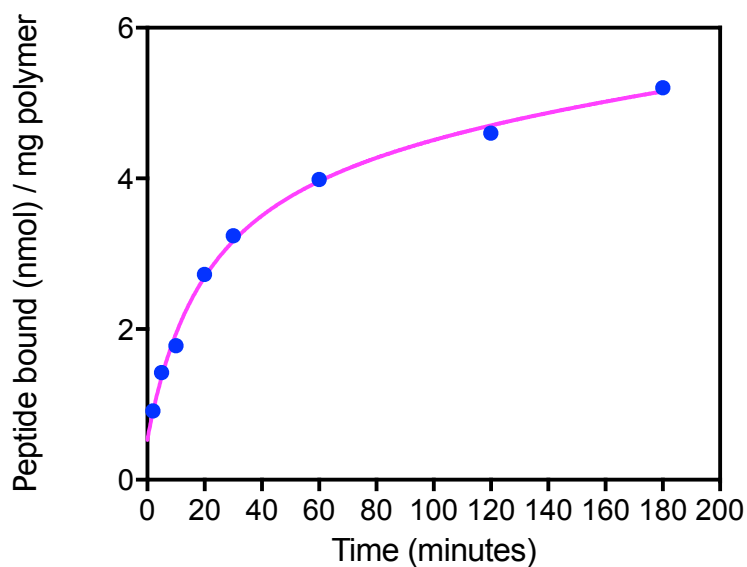
Figure 2. 33: Equilibrium binding kinetics for acetonitrile imprinted urea monomer polymers.

2.4.8.2.   Peptide binding assay with Urea Monomer MIPs

Binding studies of the Urea MIP polymer demonstrated certain recognition over NIPs

(Figure 2.34), however the resulting imprinting efficiency/factor (1.42) was not greater

than AAm and MAA MIPs. The binding capacity of the polymers (23.1 nmol/mg

polymer) was however, slightly higher than that of AAm and MAA polymers. It is

proposed that this could be a result of slightly stronger interaction with the template than

MAA/AAm leading to more template incorporation into the polymer. Bmax of 23.1

nmol/mg and apparent Kd of 194 μM was obtained using Langmuir Freundlich

adsorption isotherm (R^2 - 0.978). An imprinting factor of 1.42 was obtained for the

MIPs. On comparing the Scatchard plot in Figure 2.35, two distinct slopes could be

obtained indicating heterogeneous binding sites. The heterogeneous binding sites could

arise from two different monomer producing binding sites with varying affinities in the

polymer. The low imprinting effect could be explained by urea monomers non-specifically interacting with the carboxylate group in the peptide in NIPs.
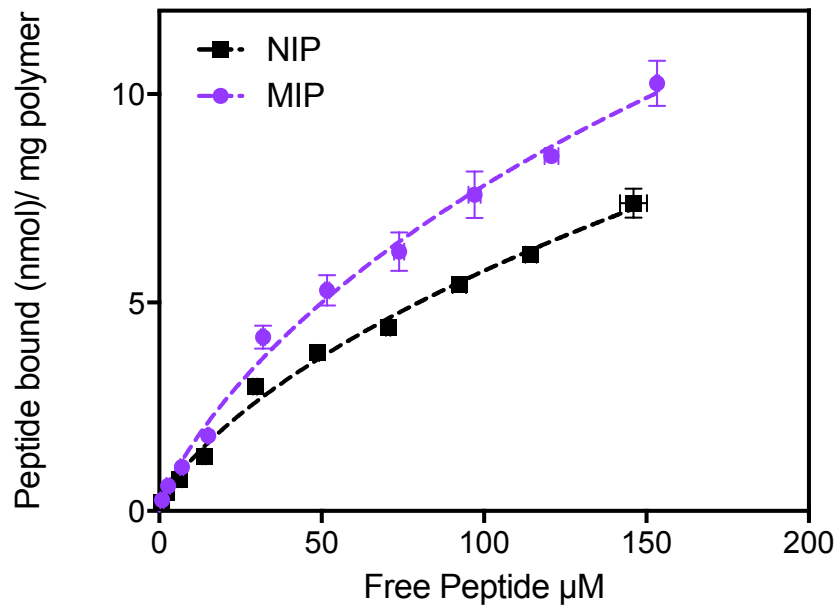
Figure 2. 34: Binding isotherm for acetonitrile imprinted urea monomer polymers. MIPs demonstrated higher binding than NIPS (N = 8 +/- SD).
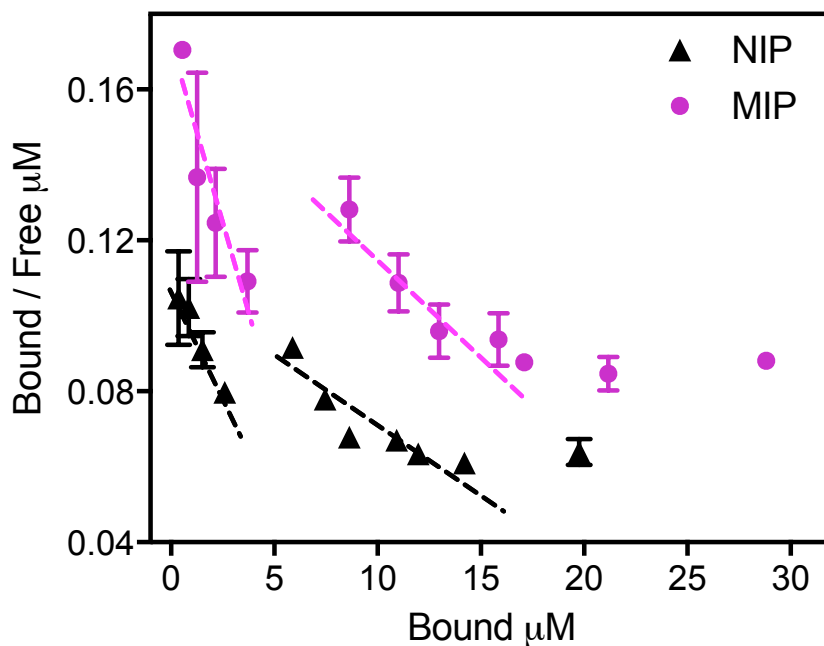
Figure 2. 35: Scatchard plot analysis showed more than one slope for the data indicating binding site heterogeneity. This could be a result of AAm and urea monomers playing a role in formation of binding sites with different binding affinities.

The urea monomer MIPs were also prepared using DMF as a porogen to understand the effect of solvent on binding affinities (Figure 2.36). The DMF based MIPs showed lower imprinting efficiency than acetonitrile imprinted MIPs indicating DMF was a poor solvent for imprinting. Bmax value of 11.07 nmol/mg was obtained with an apparent Kd of 96.20 μM. The imprinting factor was 1.29 was obtained for the DMF imprinted system. It is proposed that the slightly lower binding capacity of DMF imprinted urea MIP could a result of DMF inhibiting hydrogen bonding between AAm and peptide in the pre-polymerisation mixture. Slightly higher non-specific binding indicated that the urea monomer itself was participating in non-specific binding of the peptide suggesting

use of special monomers may not necessarily provide greater imprinting efficiency in molecular imprinting of biomolecules such as peptides.
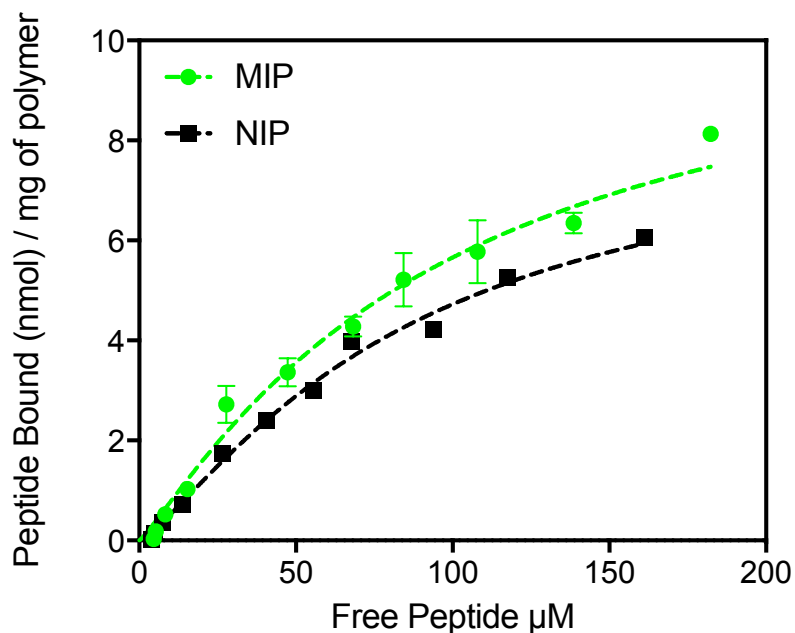
Figure 2. 36: Binding isotherm for the peptide with urea monomers imprinted in DMF porogen. (N = 8 +/- SD).

2.5. Challenges Associated With Mini-MIPS:

The study adopted the use of mini-MIPs to judiciously use the Fmoc-VANP(COOH) templates, which is hard to synthesise and limited in quantity. Mini-MIPs allowed for the formation solid polymeric particles, which were about a few mm in size with low initial volume of the polymerisation mixture. This technique also helped skip the grinding and sieving step preventing loss of precious material. Although mini-MIPs offered certain advantages, there were several drawbacks to the method such as; they were difficult to handle and weigh due to their small size, they had to be re-used for

binding assays, and multiple rounds of washes with methanol and acetic acid were required to regenerate the MIPs.

Additionally, the mini-MIP format prevented the traditional equilibrium batch binding assays for generating the standard bound versus free isotherms for calculating affinity constants for imprinted polymers. As a consequence, a different approach had to be adopted whereby sequential addition of peptide was carried to understand the binding capacity, affinity and efficiency of MIPs. This type of experiment, whereby each peptide concentration was sequentially added to the same polymer mass, created new equilibrium conditions at each concentration. The time take to reach this new equilibrium for each peptide concentration could be different, but changing the incubation time was limited by the experimental conditions where 1 hour incubation per peptide concentration was kept constant conduct the experiments. This could cause errors in the binding data. Moreover, an error introduced in one peptide concentration addition could propagate to the following peptide additions preventing accurate representation of the binding data. Although, precautions were taken by creating stock peptide solutions before conducting the experiments, errros while pipetting and evaporation of solvent could cause unintended errors in data collection.

Ideally, mini-MIPs would be a great tool to experimentally evaluate template binding to MIPs with monomers that have been screened computationally for a particular template, however, the template should be abundantly available for such experiments.

In summary three polymer systems were evaluated for their binding characteristics, which have been summarised in the Table 2.3 below:

MIP	Crosslinker	I.F	Bmax (nmol/mg polymer)	Apparent Kd (μM)
MAA	EGDMA	2.62	7.42	102.4
AAm	EGDMA	2.02	15.83	154.3
Urea	EGDMA	1.42	23	194

Table 2. 3: Summary of bulk polymers and their binding affinities and imprinting factors.

From Table 2.3 it can be concluded that MAA polymers demonstrated the highest affinity however the lowest binding capacity per mg of polymer while urea monomers demonstrated higher binding capacity but lower affinity for the peptide.

Conventional epitope imprinting although a great alternative for whole imprinting has particular challenges associated with it such as; selection of epitopic template, lack of functionality of amino acids in the sequence, conformational restrictions for longer epitopes and low binding affinities. The study indicates that molecular imprinting of larger biomolecules such as peptides/proteins is quite challenging in a conventional bulk imprinting setting and perhaps surface imprinting would be a more feasible approach to efficiently imprint such biomolecules to overcome the drawbacks of bulk imprinting. Furthermore, regardless of the length of the sequence, each epitope template requires careful consideration regarding monomer, cross-linker, and porogen for successful imprinting. The study allowed for the identification of individual monomers that could

be used in a surface imprinting strategy for imprinting of the PSA C-terminus template, which has been further examined in Chapter 3. Further work with 6 mer and 9 mer templates was not conducted due to lack of promising results with 4 mer template.

2.6. Conclusion

In conclusion, a strategy was developed for the synthesis C-terminus (epitope) peptide sequences of PSA (Fmoc-VANP(COOH) peptide) with high purity and good yields. Three polymers with different monomer compositions were prepared and evaluated for binding with the Fmoc-VANP(COOH) template. In the binding study, MAA MIPs demonstrated the highest affinity (apparent Kd) (102.4 µM) and imprinting factor (2.62) for Fmoc-VANP(COOH) peptide. The study suggests that MAA/EGDMA MIP system is a good monomer/ crosslinker combination when moving to surface imprinting of PSA epitopes. Although conventional bulk imprinting may not be suitable for imprinting of epitopes from large macromolecules it gives us an insight into monomer template interactions for smaller peptide templates.

2.7. References

1.   Andersson, L., Sellergren, B. & Mosbach, K. Imprinting of amino acid derivatives in macroporous polymers. *Tetrahedron Lett.* **25,** 5211–5214 (1984).

2.   Titirici, M. M., Hall, A. J. & Sellergren, B. Hierarchical Imprinting Using Crude Solid Phase Peptide Synthesis Products as Templates. *Chem. Mater.* **15,** 822–824 (2003).

3.   Krstulja, A., De Schutter, C., Favetta, P., Manesiotis, P. & Agrofoglio, L. A. Artificial receptors for the extraction of nucleoside metabolite 7-methylguanosine from aqueous media made by molecular imprinting. *J. Chromatogr. A* **1365,** 12–18 (2014).

4.   Emgenbroich, M., Borrelli, C., Shinde, S., Lazraq, I., Vilela, F., Hall, Andrew J., Oxelbark, J., De Lorenzi, E., Courtois, J., Simanova, A., Verhage, J., Irgum, K., Karim, K. and Sellergren, B. A phosphotyrosine-imprinted polymer receptor for the recognition of tyrosine phosphorylated peptides. *Chem. Weinh. Bergstr. Ger.* **14,** 9516–9529 (2008).

5.   Janiak, D. S. & Kofinas, P. Molecular imprinting of peptides and proteins in aqueous media. *Anal. Bioanal. Chem.* **389,** 399–404 (2007).

6.   Rachkov, A. & Minoura, N. Recognition of oxytocin and oxytocin-related peptides in aqueous media using a molecularly imprinted polymer synthesized by the epitope approach. *J. Chromatogr. A* **889,** 111–118 (2000).

7.   Yan, M. *Molecularly Imprinted Materials: Science and Technology*. (CRC Press, 2004).

8.   Mosbach, K. Molecular imprinting. *Trends Biochem. Sci.* **19,** 9–14 (1994).

9.   Husseman, M., Malmström, E.E., McNamara, M., Mate, M., Mecerreyes, D., Benoit, D.G., Hedrick, J.L., Mansky, P., Huang, E., Russell, T.P., Hawker, C.J. Controlled Synthesis of Polymer Brushes by 'Living' Free Radical Polymerization Techniques. *Macromolecules* **32,** 1424–1431 (1999).

10.   Cormack, P. A. G. & Elorza, A. Z. Molecularly imprinted polymers: synthesis and characterisation. *J. Chromatogr. B* **804,** 173–182 (2004).

11.   Turner, N.W., Jeans, C.W., Brain, K.R., Allender, C.J., Hlady, V. and Britt, D.W., From 3D to 2D: a review of the molecular imprinting of proteins. *Biotechnol. Prog.* **22,** 1474–1489 (2006).

12.   Whitcombe, M.J., Chianella, I., Larcombe, L., Piletsky, S.A., Noble, J., Porter, R., Horgan, A., The rational development of molecularly imprinted polymer-based sensors for protein detection. *Chem. Soc. Rev.* **40,** 1547–1571 (2011).

13.   Rachkov, A. & Minoura, N. Towards molecularly imprinted polymers selective to peptides and proteins. The epitope approach. *Biochim. Biophys. Acta BBA - Protein Struct. Mol. Enzymol.* **1544,** 255–266 (2001).

14.   Nishino, H., Huang, C.-S. & Shea, K. J. Selective Protein Capture by Epitope Imprinting. *Angew. Chem. Int. Ed.* **45,** 2392–2396 (2006).

15.   Bossi, A.M., Sharma, P.S., Montana, L., Zoccatelli, G., Laub, O., Levi, R. Fingerprint-Imprinted Polymer: Rational Selection of Peptide Epitope Templates for the Determination of Proteins by Molecularly Imprinted Polymers. *Anal. Chem.* **84,** 4036–4041 (2012).

16.   Geysen, H. M., Rodda, S. J., Mason, T. J., Tribbick, G. & Schoofs, P. G. Strategies for epitope analysis using peptide synthesis. *J. Immunol. Methods* **102,** 259–274 (1987).

17.   Luštrek, M., Lorenz, P., Kreutzer, M., Qian, Z., Steinbeck, F., Wu, D., Born, N., Ziems, B., Hecker, M., Blank, M., Shoenfeld, Y., Cao, Z., Glocker, M.O., Li, Y., Fuellen, G., Thiesen, H.-J. Epitope Predictions Indicate the Presence of Two Distinct Types of Epitope-Antibody-Reactivities Determined by Epitope Profiling of Intravenous Immunoglobulins. *PLOS ONE* **8,** e78605 (2013).

18.   Camacho, C. *et al.* BLAST+: architecture and applications. *BMC Bioinformatics* **10,** 421 (2009).

19.   Protein BLAST: search protein databases using a protein query. Available at: http://blast.ncbi.nlm.nih.gov/Blast.cgi?PAGE=Proteins. (Accessed: 25th March 2016)

20.   Lu, C.-H. *et al.* Sensing HIV related protein using epitope imprinted hydrophilic polymer coated quartz crystal microbalance. *Biosens. Bioelectron.* **31,** 439–444 (2012).

21.   Palomo, J. M. Solid-phase peptide synthesis: an overview focused on the preparation of biologically relevant peptides. *RSC Adv.* **4,** 32658–32672 (2014).

22.   Bodanszky, M. *Principles of Peptide Synthesis*. (Springer Science & Business Media, 2012).

23.   Merrifield, R. B. Solid Phase Peptide Synthesis. I. The Synthesis of a Tetrapeptide. *J. Am. Chem. Soc.* **85,** 2149–2154 (1963).

24.   Grant, G. A. *Synthetic Peptides: A User's Guide*. (Oxford University Press, 2002).

25.   Merrifield, R. B. Automated Synthesis of Peptides. *Science* **150,** 178–185 (1965).

26.   Merrifield, B. Solid phase synthesis. *Science* **232,** 341–347 (1986).

27.   Carpino, L. A. & Han, G. Y. 9-Fluorenylmethoxycarbonyl function, a new base-sensitive amino-protecting group. *J. Am. Chem. Soc.* **92,** 5748–5749 (1970).

28.   Carpino, L. A. *et al.* Rapid, Continuous Solution-Phase Peptide Synthesis: Application to Peptides of Pharmaceutical Interest. *Org. Process Res. Dev.* **7,** 28–37 (2003).

29.   Amblard, M., Fehrentz, J.-A., Martinez, J. & Subra, G. Methods and protocols of modern solid phase Peptide synthesis. *Mol. Biotechnol.* **33,** 239–254 (2006).

30.   Albericio, F. Developments in peptide and amide synthesis. *Curr. Opin. Chem. Biol.* **8,** 211–221 (2004).

31.   Barlos, K. *et al.* Application of 2-chlorotrityl resin in solid phase synthesis of (Leu15)-gastrin I and unsulfated cholecystokinin octapeptide. *Int. J. Pept. Protein Res.* **38,** 555–561 (1991).

32.   Chiva, C., Vilaseca, M., Giralt, E. & Albericio, F. An HPLC-ESMS study on the solid-phase assembly of C-terminal proline peptides. *J. Pept. Sci.* **5,** 131–140 (1999).

33.   Hansen, P. & Oddo, A. in *Peptide Antibodies* (ed. Houen, G.) 33–50 (Springer New York, 2015). doi:10.1007/978-1-4939-2999-3_5

34.   Hachmann, J. & Lebl, M. Alternative to Piperidine in Fmoc Solid-Phase Synthesis. *J. Comb. Chem.* **8,** 149–149 (2006).

35.   Sarin, V. K., Kent, S. B., Tam, J. P. & Merrifield, R. B. Quantitative monitoring of solid-phase peptide synthesis by the ninhydrin reaction. *Anal. Biochem.* **117,** 147–157 (1981).

36.   Kaiser, E., Colescott, R. L., Bossinger, C. D. & Cook, P. I. Color test for detection of free terminal amino groups in the solid-phase synthesis of peptides. *Anal. Biochem.* **34,** 595–598 (1970).

37.   El-Faham, A. & Albericio, F. Peptide Coupling Reagents, More than a Letter Soup. *Chem. Rev.* **111,** 6557–6602 (2011).

38.   Carpino, L. A. 1-Hydroxy-7-azabenzotriazole. An efficient peptide coupling additive. *J. Am. Chem. Soc.* **115,** 4397–4398 (1993).

39.   Guy, C. A. & Fields, G. B. in (ed. Enzymology, B.-M. in) **289,** 67–83 (Academic Press, 1997).

40.   Coin, I., Beyermann, M. & Bienert, M. Monitoring solid phase peptide synthesis. *Protoc. Exch.* (2007). doi:10.1038/nprot.2007.461

41.   Lanza, F. & Sellergren, B. Method for Synthesis and Screening of Large Groups of Molecularly Imprinted Polymers. *Anal. Chem.* **71,** 2092–2096 (1999).

42.   Balk, S. P., Ko, Y.-J. & Bubley, G. J. Biology of prostate-specific antigen. *J. Clin. Oncol. Off. J. Am. Soc. Clin. Oncol.* **21,** 383–391 (2003).

43.   Michel, S. *et al.* Involvement of the C-terminal end of the prostrate-specific antigen in a conformational epitope: characterization by proteolytic degradation of monoclonal antibody-bound antigen and mass spectrometry. *J. Mol. Recognit.* **14,** 406–413 (2001).

44.   Stura, E. A. *et al.* Crystal structure of human prostate-specific antigen in a sandwich antibody complex. *J. Mol. Biol.* **414,** 530–544 (2011).

45.   BLASTp results [completed]. Available at: http://www.uniprot.org/blast/uniprot/B201603259CMAUV8W9L. (Accessed: 25th March 2016)

46.   Bodanszky, P. D. M. in *Principles of Peptide Synthesis* 169–214 (Springer Berlin Heidelberg, (1993)

47.   Patil, A. J., Kumar, R. K., Barron, N. J. & Mann, S. Cerium oxide nanoparticle-mediated self-assembly of hybrid supramolecular hydrogels. *Chem. Commun.* **48,** 7934–7936 (2012).

48.   Suzuki, H. *Electronic absorption spectra and geometry of organic molecules: An application of molecular orbital theory*. (Elsevier, 2012)

49.   Aitken, A. & Learmonth, M. in *The Protein Protocols Handbook* (ed. Walker, J.) 3–6 (Humana Press, 2002).

50.   Alexander, C. *et al.* Molecular imprinting science and technology: a survey of the literature for the years up to and including 2003. *J. Mol. Recognit.* **19,** 106–180 (2006).

51.   Andersson, L. I., Nicholls, I. A. & Mosbach, K. in *Advances in Molecular and Cell Biology* (ed. E. Edward Bittar, B. D. and L. B.) **15,** 651–670 (Elsevier, 1996).

52.   Scorrano, S., Mergola, L., Del Sole, R. & Vasapollo, G. Synthesis of Molecularly Imprinted Polymers for Amino Acid Derivates by Using Different Functional Monomers. *Int. J. Mol. Sci.* **12,** 1735–1743 (2011).

53.   Stevenson, C. L. Characterization of Protein and Peptide Stability and Solubility in Non-Aqueous Solvents. *Curr. Pharm. Biotechnol.* **1,** 165–182 (2000).

54.   Asanuma, H., Akiyama, T., Kajiya, K., Hishiya, T. & Komiyama, M. Molecular imprinting of cyclodextrin in water for the recognition of nanometer-scaled guests. *Anal. Chim. Acta* **435,** 25–33 (2001).

55.   Sellergren, B. & Shea, K. J. Influence of polymer morphology on the ability of imprinted network polymers to resolve enantiomers. *J. Chromatogr. A* **635,** 31–49 (1993).

56.   Wulff, G., Kemmerer, R., Vietmeier, J. & Poll, H. Chirality of Vinyl-Polymers - the Preparation of Chiral Cavities in Synthetic-Polymers. *Nouv. J. Chim.-New J. Chem.* **6,** 681–687 (1982).

57.   Shoravi, S., Olsson, G. D., Karlsson, B. C. G. & Nicholls, I. A. On the influence of crosslinker on template complexation in molecularly imprinted polymers: a computational study of prepolymerization mixture events with correlations to template-polymer recognition behavior and NMR spectroscopic studies. *Int. J. Mol. Sci.* **15,** 10622–10634 (2014).

58.   Lorenzo, R. A., Carro, A. M., Alvarez-Lorenzo, C. & Concheiro, A. To Remove or Not to Remove? The Challenge of Extracting the Template to Make the Cavities Available in Molecularly Imprinted Polymers (MIPs). *Int. J. Mol. Sci.* **12,** 4327–4347 (2011).

59.   O'Mahony, J., Molinelli, A., Nolan, K., Smyth, M. R. & Mizaikoff, B. Towards the rational development of molecularly imprinted polymers: 1H NMR studies on

hydrophobicity and ion-pair interactions as driving forces for selectivity. *Biosens. Bioelectron.* **20,** 1884–1893 (2005).

60.   Karim, K. *et al.* How to find effective functional monomers for effective molecularly imprinted polymers? *Adv. Drug Deliv. Rev.* **57,** 1795–1808 (2005).

61.   García-Calzón, J. A. & Díaz-García, M. E. Characterization of binding sites in molecularly imprinted polymers. *Sens. Actuators B Chem.* **123,** 1180–1194 (2007).

62.   Vlatakis, G., Andersson, L.I., Müller, R. and Mosbach, K. Drug assay using antibody mimics made by molecular imprinting. *Nature* 361, 645–647 (1993).

63.   Andersson, L. I., Müller, R., Vlatakis, G. & Mosbach, K. Mimics of the binding sites of opioid receptors obtained by molecular imprinting of enkephalin and morphine. *Proc. Natl. Acad. Sci.* **92,** 4788–4792 (1995).

64.   Sellergren, B. Polymer- and template-related factors influencing the efficiency in molecularly imprinted solid-phase extractions. *TrAC Trends Anal. Chem.* **18,** 164–174 (1999).

65.   Corey, R. B. & Pauling, L. Fundamental Dimensions of Polypeptide Chains. *Proc. R. Soc. Lond. B Biol. Sci.* **141,** 10–20 (1953).

66.   Rushton, G. T., Karns, C. L. & Shimizu, K. D. A critical examination of the use of the Freundlich isotherm in characterizing molecularly imprinted polymers (MIPs). *Anal. Chim. Acta* **528,** 107–113 (2005).

67.   Umpleby, R. J., Baxter, S. C., Chen, Y., Shah, R. N. & Shimizu, K. D. Characterization of molecularly imprinted polymers with the Langmuir-Freundlich isotherm. *Anal. Chem.* **73,** 4584–4591 (2001).

68.   Brüggemann, O., Haupt, K., Ye, L., Yilmaz, E. & Mosbach, K. New configurations and applications of molecularly imprinted polymers. *J. Chromatogr. A* **889,** 15–24 (2000).

69.   Yoshikawa, M., Fujisawa, T., Izumi, J., Kitao, T. & Sakamoto, S. Molecularly imprinted polymeric membranes involving tetrapeptide EQKL derivatives as chiral-recognition sites toward amino acids. *Anal. Chim. Acta* **365,** 59–67 (1998).

70.   Ansell, R. J., Ramström, O. & Mosbach, K. Towards artificial antibodies prepared by molecular imprinting. *Clin. Chem.* **42,** 1506–1512 (1996).

71.   Deepthi, K. P. & Mathew, B. Effect of Porogen on the Catalytic Activity of Molecular Imprinted Polymers. *Asian J. Chem.* **25,** 1985–1990 (2013).

72.   Iturralde, I., Paulis, M. & Leiza, J. R. The effect of the crosslinking agent on the performance of propranolol imprinted polymers. *Eur. Polym. J.* **53,** 282–291 (2014).

73.   Zhang, W., Qin, L., He, X.-W., Li, W.-Y. & Zhang, Y.-K. Novel surface modified molecularly imprinted polymer using acryloyl-β-cyclodextrin and acrylamide as monomers for selective recognition of lysozyme in aqueous solution. *J. Chromatogr. A* **1216,** 4560–4567 (2009).

74.   Fu, G., Zhao, J., Yu, H., Liu, L. & He, B. Bovine serum albumin-imprinted polymer gels prepared by graft copolymerization of acrylamide on chitosan. *React. Funct. Polym.* **67,** 442–450 (2007).

75.   Hoshino, Y., Kodama, T., Okahata, Y. & Shea, K. J. Peptide Imprinted Polymer Nanoparticles: A Plastic Antibody. *J. Am. Chem. Soc.* **130,** 15242–15243 (2008).

76.   Hart, B. R. & Shea, K. J. Molecular Imprinting for the Recognition of N-Terminal Histidine Peptides in Aqueous Solution. *Macromolecules* **35,** 6192–6201 (2002).

77.   Emgenbroich, M. *et al.* A phosphotyrosine-imprinted polymer receptor for the recognition of tyrosine phosphorylated peptides. *Chem. Weinh. Bergstr. Ger.* **14,** 9516–9529 (2008).

78.   Hall, A. J. *et al.* Urea Host Monomers for Stoichiometric Molecular Imprinting of Oxyanions. *J. Org. Chem.* **70,** 1732–1736 (2005).

3. Chapter: Surface Imprinting of Pro-PSA Activation Sequence

3.1. Introduction

3.1.1. General overview

Chapter 2 demonstrated that conventional bulk imprinting of peptide (epitopes) remains a challenge due to their low solubility in conventional imprinting solvents and poorer binding performance in polar aqueous solutions. Bulk polymers are not very useful for sensing applications, as they are difficult to integrate with sensing platforms. This is due to their physical nature, meaning that MIP particles cannot be easily bound to the transduction platform for efficient signal transduction/amplification. Furthermore, the characterisation of MIP performance often relies on batch rebinding studies in which binding parameters are evaluated by determining the concentration of analyte left free in solution. For MIPs to be a useful recognition system in sensing of biomolecules, this disconnect between binding and 'read-out' needs to be addressed, that is, the MIP must interface directly with a transduction platform. This disconnect has been partly addressed by surface imprinting and in particular the area of electrochemical sensing which has shown great promise in direct sensing of both small and macromolecular templates.[1,2] Various research papers have successfully demonstrated the use of electrochemical (E)-MIPs as sensitive recognition elements[3,4] and a summary has been provided in Table 3.1. As a result, to overcome some of the challenges of bulk imprinting, the current chapter extends the concept of epitope imprinting explored in Chapter 1 to surface imprinting and electrochemical sensing of PSA epitopes.

3.1.2. Surface imprinting

Surface imprinting (Figure 3.1) refers to the growth of a polymer in the presence of a template to create an imprinted cavity on a suitable substrate/electrode. There are two

approaches for template presentation in surface imprinting; complete entrapment of the template (without surface immobilisation) during polymer growth and surface immobilisation of the template. The later approach confers several significant advantages:

1. The template molecule can be presented homogenously and oriented on the surface, ultimately leading to higher quality, more equitable binding sites in the polymer.[5,6]

2. Once immobilised, solubility of template in the imprinting solvent is less of an issue (assuming template is stable / not denatured under such conditions).[7]

3. By carefully controlling the growth of the polymer around the template, the thickness of the polymer can be modulated to get maximum imprinting effect. Integration of the polymerisation and the sensing process, as in the case of electropolymerisation and electrochemical sensing, also enables the removal of template to be monitored.[8]

4. Surface imprinting with thin polymers means rebinding is more efficient, with improved mass transfer and binding kinetics and overall greater sensitivity than conventional MIP systems.[9,10]
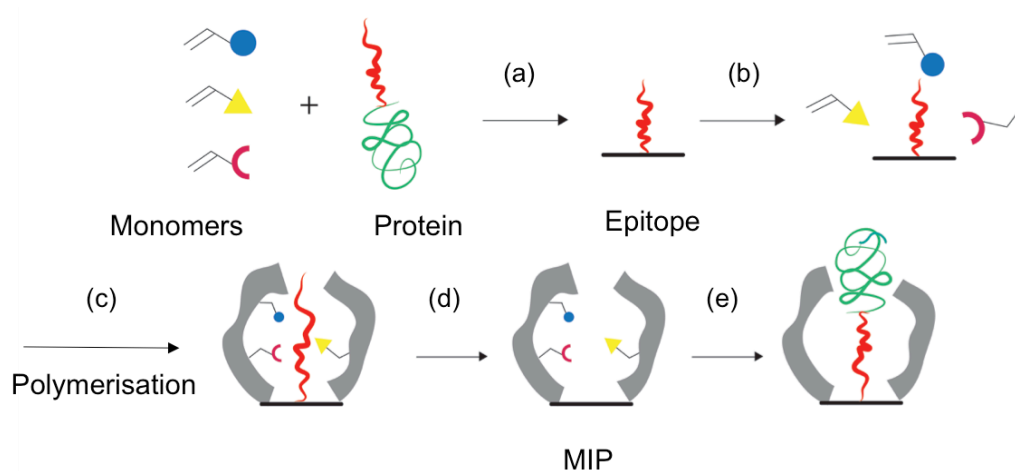
Figure 3. 1: The schematic illustrates a general surface imprinting approach. An epitope from a protein is immobilised on the surface. Functional monomers are introduced that interact with the epitope. These interactions are locked into place by polymerisation of the monomers. Post removal of the template/epitope cavity remains, which now has recognition properties for the epitope and the protein displaying the epitope.

The Allender group has previously explored surface imprinting strategies for the detection of bio-macromolecules, employing Merrifield resin as a solid support. The resin was used for the surface imprinting of LPS using a co-immobilised template (polymyxin) and iniferter groups.[11] However, poor control over the growth of polymer layers on the surface of the Merrifield resin and its inherent hydrophobicity limited the success and further implementation of this work. Electropolymerisation of monomers reportedly allows fine control over polymer growth on an electrode[1] while at the same time enabling direct detection of template molecules via electrochemical sensing.[12] As a result, the polymerisation of a variety of electroactive monomers for use in surface imprinting of a PSA epitope was explored in the current chapter. Various electrochemical techniques, used for surface characterisation and assessment of MIP binding performance, were also investigated in the current study.

3.1.3. *Surface imprinting using electropolymers:*

Conventional imprinting involves free-radical polymerisation of vinyl/acrylate monomers, which leads to the formation of a solid bulk polymer. These bulk polymers can then be ground into a fine powder and sieved and sedimented to yield polymer particles. These particles, due to their physical nature, cannot be easily immobilised onto sensor surfaces such that close and intimate contact between the polymer and transducer is maintained. This leads to poor signal transduction, which in turn gives rise to sensor insensitivity.[12] Various methods have been used to facilitate direct immobilisation of MIPs on transducer surfaces including drop-coating of a polymer solution[13], covalent immobilisation of MIPs[14], *in-situ* polymerisation and spin coating of MIPs[15], preparing a composite membrane using a conducting material[16] (carbon nanotubes, graphite or carbon black) and electropolymerisation of electroactive monomers.[17,10,18]

Of these methods, MIP films resulting from electropolymerisation have demonstrated superior properties when compared to conventional MIPs in terms of stable attachment to the transducer surface, ease of preparation in aqueous/non-aqueous solutions and easy pathway to conduction of electrons through electrodes.[12] Furthermore, it is possible to control the rate and extent of polymer growth and polymer properties by optimising electrochemical parameters.[19] For example, control over polymer film thickness can be achieved by controlling the total amount of charge passed through the electrode, and polymer morphology can be defined by the electrolyte / solvent employed during polymerisation.[19] Electropolymerisation of electroactive monomers can be performed under galvanostatic (constant current), potentiostatic (constant potential) or potentiodynamic (variable potential) conditions.[20] In electropolymerised MIP, just as in

conventional MIPs, monomers are spatially positioned around the template to form a stable complex in the pre-polymerisation solution, which gets locked in during the polymerisation process. The resulting cavity has good structural rigidity and stability ensuring that its shape and functionality is maintained when the polymer is washed and the template removed. Furthermore, the electroactive monomers possess various functional groups that participate in π-π interaction, hydrogen bonding, ionic interactions and hydrophobic interaction promoting chemical selectivity of the imprinted cavity similar to conventional imprinting monomers.[21] Various electroactive monomers such as pyrrole, aniline, aminophenol, thiophene, aminophenoboronic acid, phenol, aminothiophenol, aminobenzoic acid, phenylenediamine, dopamine have found application in electrochemical sensing of amino acids, small molecules, proteins and nucleotides with E-MIPs.[21,17] (Table 3.1)

A general protocol for the synthesis of an E-MIP system involves preparing a combined solution of electroactive monomer and template (surface immobilised or in solution). This is then subjected to a specific voltage range that causes the oxidation/reduction of electroactive monomer at the surface of the electrode leading to polymer growth.[17] The template becomes entrapped during this process, which results in the formation of imprinted cavities. The morphology of the polymer (porosity and rigidity) is governed by choice of solvent, the rate at which the charge is transferred to the monomers (voltage scan rate of oxidation/reduction) and the amount of charge transferred during electropolymerisation (dependent upon the properties of the electrode surface).[19] A brief overview of some electroactive monomers and their application in electrochemical sensing of various templates has been provided in Table 3.1.

Electro-monomer	Conductivity	Templates
Pyrrole	Conducting	Adenosine/ inosine/ATP[22], caffeine[23], paracetomol[24], tryptophan[25]
Thiophene	Conducting	Histamine[26], dopamine[27], avidin[28]
Aminophenolboronic acid	Conducting	Nucleotide and monosaccherides[29], lysosome, cytochrome C[30]
4-Aminobenzoic acid	Conducting	Melamine[31]
Dopamine	Non-conducting	Nicotine[4], HIV-epitope[32], IgG[5]
Aminophenol	Non-conducting	2,4-dichlorophenoxyacetic acid, dopamine[33] Myoglobin[34]
Scoloptien	Non-conducting	Conclavin-A[35], cytochrome C nonapeptide[8]
Phenol	Non-conducting	Phenylalanine[1], ferritin[36], theophylline[37], D-glucose[38]
1,2 phenyldiamine	Non-conducting	Glucose[39], sorbitol[40], troponin[41]

Table 3. 1: Summary of electroactive monomers and templates imprinted using e-MIPs

3.1.4. *Electrochemical techniques for molecular imprinting:*

A general overview of some of the electrochemical techniques used in the fabrication and evaluation of electrochemical (E)-MIPs in the current work has been detailed in the section below.

3.1.4.1. Electrochemical MIP biosensors

Electrochemical biosensors are devices capable of converting and measuring a chemical/biochemical signal, arising from a biomolecule interacting with an analyte, into an electrical signal.[42] In the case of molecular imprinting, the biomolecular layer consists of an imprinted polymer with a memory for the template as seen in Figure 3.2. A typical biosensor consists of an electrode surface, which has been modified with a bio-layer with certain recognition properties, a transducer surface that converts the binding events into an electrical signal and a signal processing system which quantifies and amplifies the signal (Figure 3.2).[42] The electrochemical properties of an electrode change upon interaction of a template with the bio-layer. These changes convert into quantifiable changes in either the current (amperometric), potential (potentiometric and field effect devices), impedance (impedometric) or conductivity (conductometric) of the system.[43]
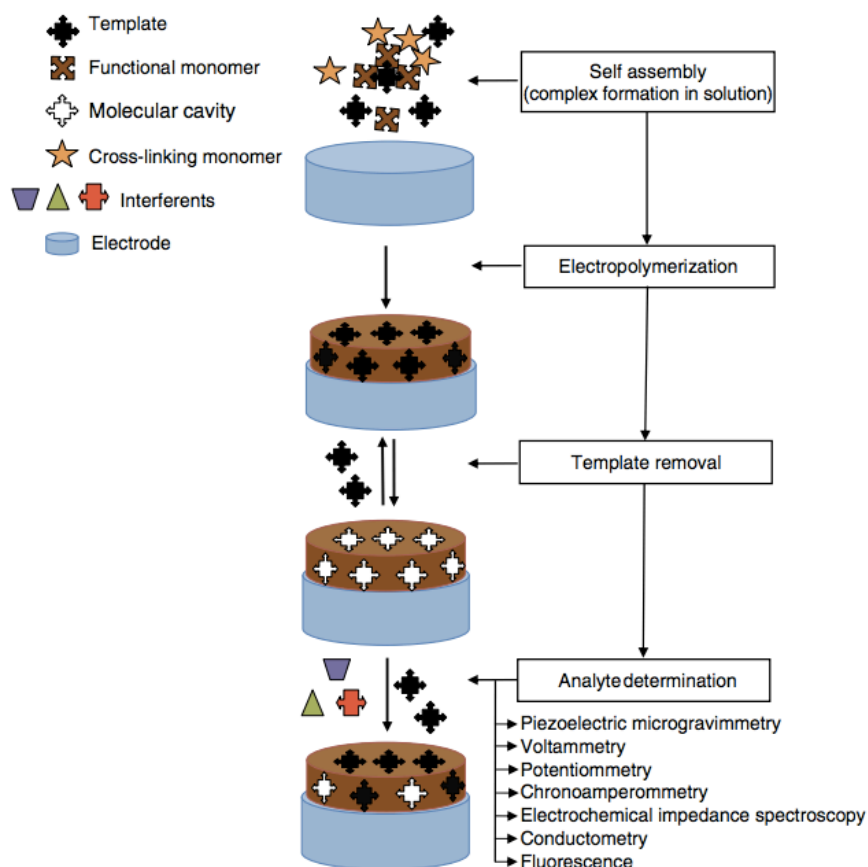
Figure 3. 2: General schematic of the construction of E-MIP sensor has been depicted. A pre-polymerisation mixture allows for interactions between the template and the functional monomer. The template is then entrapped into the polymer upon electropolymerisation locking the interactions in place. The template is washed away to expose the imprinted cavities. Rebinding of the template is measured via different electroanalytical techniques. The schematic has been reproduced from Sharma et al., 2012.[12]

3.1.4.2. Electrochemical configuration in MIP electrochemical biosensors

The simplest electrochemical set up consists of two electrodes: a working electrode (WE) and a counter electrode (CE) whereby current flows from the WE to the CE. The working electrode is the electrode where a biolayer/polymer is immobilised, with any changes due to binding of analyte producing a change in the electrical signal. The

counter electrode completes the circuit and provides a reference potential for measuring the change in electrical signal occurring at the working electrode.[44] Although, this may seem a simple set-up, practically it is difficult to implement due to challenges in keeping the counter electrode at a constant potential during electrochemical measurements. As a result, a 3-electrode setup is preferred consisting of a reference electrode (RE) in addition to the working and counter electrodes as shown in Figure 3.3.[44] The WE and RE form a half-cell and maintain a constant potential allowing measurement of the flow of current through the CE. The RE simply provides a reference potential and does not participate in the flow of electrons between the working and counter electrodes. The internationally accepted primary reference electrode is a standard hydrogen electrode (SHE), which has unit potential.[45] Potentials are usually quoted with reference to SHE because it is not experimentally convenient to use SHE in the laboratories (difficult to set up apparatus and maintain hydrogen gas pressure at 1 bar).[45] The most common reference electrode applied in electrochemistry measurement is a silver-silver chloride (Ag/AgCl) electrode dipped in a saturated potassium chloride solution, which has a potential of 0.197 V with reference to SHE.[45]
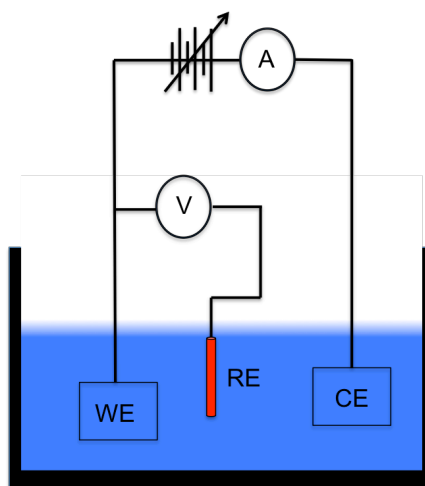
Figure 3. 3: Schematic of 3-electrode setup showing the working electrode (WE), reference electrode (RE) and a counter electrode (CE) connected to an external potentiostat.

3.1.4.3.   Faradaic and non-Faradaic processes:

There are two type of processes that occur at the electrode surface: Faradaic processes and non-Faradaic processes.[46] Faradaic processes occur when there is transfer of charges (electrons) from the electrode to the metal-electrolyte interface, which is governed by Faraday's law hence termed Faradaic processes.[46] There are also secondary processes that occur at the surface of the electrode as a result of adsorption and desorption of charged molecules which are termed non-Faradaic processes.[46] Both, Faradaic and non-Faradaic processes occur simultaneously during an electrochemical reaction.

- Non-Faradaic process

Non-Faradaic processes occur due to adsorption/desorption of charged molecules on the metal-electrolyte interface. A metal (electrode) surface consists of either an excess or deficiency of electrons that are present in close proximity to the surface (< 0.01 nm). The electrolyte solution in contact with the metal surface mostly contains an excess of

anions and cations.[47] When the metal surface comes in contact with the electrolyte solution, the charge distribution at the electrode-electrolyte interface depends on the potential difference between the electrode and the electrolyte. This potential difference is characterised by a double layer capacitance also termed as the electrochemical double layer (EDL). [47]

The structure of EDL, in solution, is made up of various layers as depicted in Figure 3.4. The innermost layer is present at the electrode surface and comprises of specifically adsorbed solvent molecules and ions and is termed as the inner Helmholtz plane (IHP).[48] The IHP molecules and ions are de-solvated and are chemically bound to the electrode surface. The layer that sits on top of the IHP is known as the as outer Helmholtz plane (OHP), which comprises of solvated ions which are non-specifically adsorbed to the surface and are attracted to the charged electrode by long-range electrostatic forces.[48] The OHP extends from the IHP to the electrical centers of the nearest solvated ions. Beyond the OHP is the diffuse layer where the ions are distributed as a result of thermal motion. The thickness of the diffuse layer depends on the total ionic concentration of the electrolyte.[48] The structure of the EDL can affect the rate of electrochemical reactions/ Faradaic processes. The effect of EDL becomes significant when electro-active species are present in low concentrations, and hence it must be taken into account with Faradaic processes when calculating change in electrochemical signal.
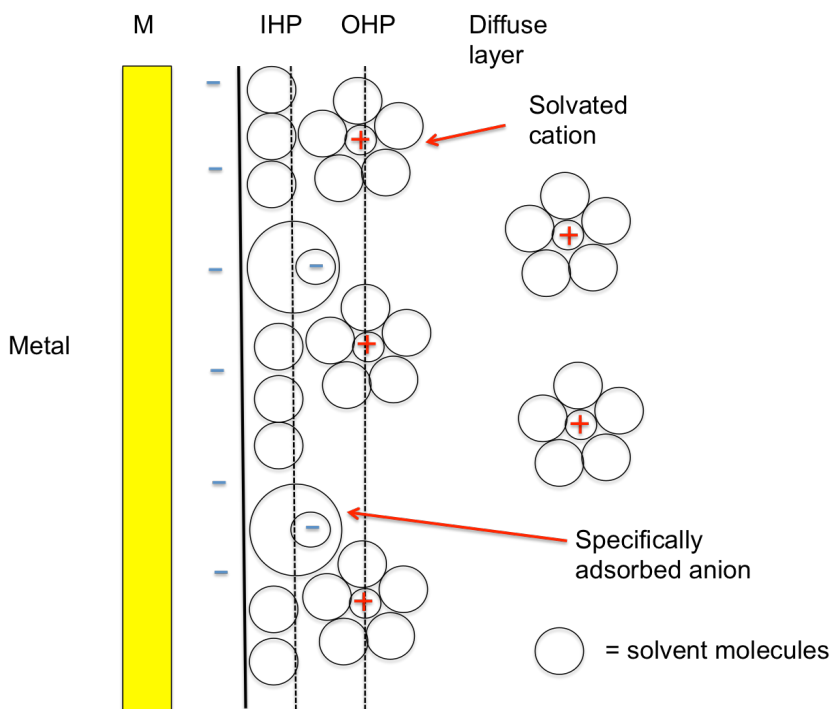
Figure 3. 4: Structure of electrochemical double layer: The inner Helmholtz plane (IHP) is closest to the metal surface containing specifically adsorbed species, the outer Helmholtz plane (OHP) consists of solvated ions non-specifically attracted towards the IHP and the diffuse layer consists of ions that are attracted by long distance forces.

- Faradaic processes:

Faradaic processes obey Faraday's law, which states that the total chemical deposition occurring at the electrode surface due to the flow of current is directly proportional to the amount of charge (coulombs) passed through the electrode.[46] In the case of biosensors, Faradaic currents are of most interest as they are directly proportional to the binding event between an analyte and receptor. There are two types of chemical reactions that occur in an electrochemical cell: oxidation and reduction. If the electrode is driven to a more negative potential by connecting it to an external power supply, the electrons of ions in solution gain energy and transfer into a vacancy in the valence shell

of the ion.[46] The current flows from metal to solution (cathodic) and the ion in the solution which gains an electron is reduced. This reaction can be written as:

$$O + ne^- \leftrightarrow R$$
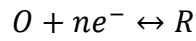
Where n is the charge, O is oxidised species and R its reduced form.

If the electron transfer occurs in the opposite direction, from solution to metal, the current is anodic, and the metal atom loses an electron and thus is oxidised. The electrochemical reactions (oxidation/reduction) occurring in an electrochemical cell are governed by Faraday's law. When investigating the electrochemical behaviour of an electrochemical cell, certain conditions are kept constant to allow changes in variables such as current, potential, or concentration to be observed. According to Faraday's law the reduction and oxidation current are directly proportional the concentration of the reduced/oxidised species [46]:

$$i_R = -\eta FAK_R c'_O$$

$$i_O = \eta FAK_O c'_R$$

Where i_R is the reduction current, η is overpotential, which is departure of the electrode potential from equilibrium value upon passage of current (E -E$_{eq}$), A is the area of the electrode, K_R and K_o are the reaction constant and c'_O and c'_r are the concentration of the oxidised and the reduced species. If an electrochemical reaction is considered, it consists of various steps that cause the conversion of the dissolved oxidised species to its reduced state R, in solution. The rate of the electrode reaction is governed by:

1. Movement of electrons through a solid electrode (generally very fast),

2. Mass transfer through the bulk solution to the interface (consisting of migration, convection and diffusion of charges).

3. Chemical reactions following the electron transfer process such as protonation, dimerization, and catalytic decomposition on the electrode surface.

4. Surface reactions such as adsorption, desorption or crystallization.

All the above factors are taken into account when calculating the electrochemical rate of reaction in a cell.[44]

3.1.4.4.   Cyclic voltammetry:

In amperometric biosensors, the reduction / oxidation current between the CE and WE is measured by applying a set voltage to the WE with respect to the reference electrode. In cyclic voltammetry (CV), the set potential of an electrode is varied with respect to time and the resulting current is measured.[46] The potential applied to the WE can be termed an "excitation signal", which is swept between two set potential values also termed as switching potentials.[46] The linear potential scan can be represented as a triangular waveform as shown in Figure 3.5(a). The resulting current can be termed as a "response signal". Qualitative and quantitative information about an electrochemical reaction can be obtained from observing the oxidation/reduction peaks of cyclic voltammogram (CV) (graphical representation) as shown in Figure 3.5 (b).[46] A detailed description on theory of CV can be found in 'Understanding Voltammetry ' by Richard G. Compton *et al*.[49] A brief overview has been provided in the following section.

In a typical CV experiment, the potential of the working electrode (vs reference) is swept linearly with respect to time from an initial potential (E0) to a switching potential (E1), and once again after which the direction of the linear sweep is reversed until the

initial potential (E0) is reached (see Figure 3.5 (b)).[45] The potential voltage limits are

chosen such that the oxidation and reduction potential of the electroactive species under

investigation lies within the potential window. The forward scan (change in potential in

the positive direction) produces an anodic current for an analyte that is being oxidised

within the scanned potential range. The oxidation causes the concentration of the analyte

to decrease at the surface of electrode, which leads to an increase in current.[49] As the

potential increases, more and more analyte is oxidised until it becomes completely

depleted from the electrode surface. At this point mass transfer reaches its maximum

value and a peak current (ip) is observed.[49] The potential at this point is termed as E_{pa}

(anodic potential). Further increase in potential leads to a zone of depletion (mass

transfer slows down) and hence the current starts to decrease. When the potential is

switched (reverse scan), reduction of the analyte occurs causing a cathodic current to

flow through the electrode. If the electrochemical reaction is reversible, the oxidised

species will be reduced to its original state after reaching the switching potential on the

reverse scan.[49] In reversible electrochemical reactions, the cathodic current produced by

the reduction of the analyte has a similar shape as that of the anodic current. In

irreversible electrochemical reactions, the cathodic current may show different peaks as

a result of different reactions occurring at the electrode surface.[50] The result of the

experiment is plotted as a cyclic voltammogram from which information about the

electrochemical reactions of the system can be obtained. Faradaic currents can be

generated either through redox activity of a chemical species in the solution at the

electrode surface ($Fe[CN]_6^{-3/-4}$), a redox mediator (ferrocene) that interacts with the

analyte of interest or by oxidation/reduction of electroactive molecules in the case of

electropolymerisation.[50] The residual current in the absence of any electroactive species

is a direct result of non-Faradaic processes.[50]

(a)   (b)
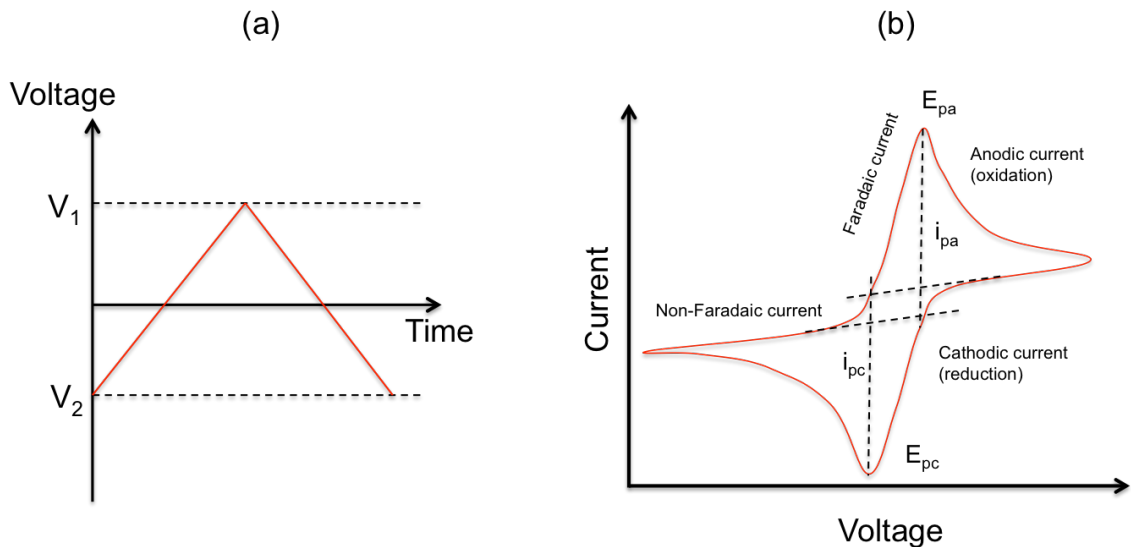
Figure 3. 5 Cyclic voltammetry (a) demonstrates the variation of voltage versus time. In cyclic voltammetry the voltage is switched from one potential to another over time and resulting current is recorded to obtain a graph as show in 3.5 (b). This graph of current versus voltage in cyclic voltammmetry is termed as cyclic voltammogram. In figure 3.5 (b) cyclic voltammogram of a reversible oxidised species is depicted. The graph shows peak similarity in both forward and reverse scan. An increase in potential (voltage) leads to oxidation of species, which causes an increase in anodic current (faradaic current) shown by the sharp increase in the curve. When all the species on the surface of the electrode are oxidised the anodic current reaches its peak (i_{pa}) at anodic potential (E_{pa}), Thereafter, further increase in potential leads to decrease in current shown by the drop in curve. When the potential is reversed, the oxidised species on the surface is reduced leading to an increase in cathodic current in the opposite direction. As the species can be reversibly oxidised and reduced a similar peak (i_{pc}) is obtained in the reverse scan at cathodic potential (E_{pc}). Any residual current not obtained from oxidation of species is termed as non-faradaic current.

3.1.4.5.   Electrochemical impedance spectroscopy:

While cyclic voltammetry is a useful technique to understand what electrochemical reactions are occurring at an electrode surface, it is not sufficiently sensitive to allow for the detection of biomolecular interaction. Alternative techniques such as electrochemical impedance spectroscopy (EIS) have therefore been increasingly applied as a label-free electrochemical technique in biosensing.[51]. In EIS, a small (~5 mV) *perturbing* potential (cyclic voltage) is applied across an electrode. The perturbing potential applied varies in a cyclic sinusoidal manner such that the time-averaged overpotential is zero (a steady state situation occurs).[51] As the voltage changes in a cyclical manner, the current also alternates producing an alternating current (AC). When a constant voltage, V, is applied across an electrochemical cell with a resistance, R, it induces a constant current, I, according to Ohm's law:

$$V = IR \quad (3.1)$$

Similarly, if a sinusoidal varying potential is applied to an electrochemical cell it induces an alternating current, as shown in Figure 3.6

$$\bar{V} = \bar{I}Z \quad (3.2)$$

Where Z is the impedance (vector form of resistance) of the circuit, and $\bar{V}$ and $\bar{I}$ are time dependent voltage and current respectively. Therefore, simply speaking, impedance is a resistance that varies in a cyclical manner and has the unit of ohms (Ω).[52]
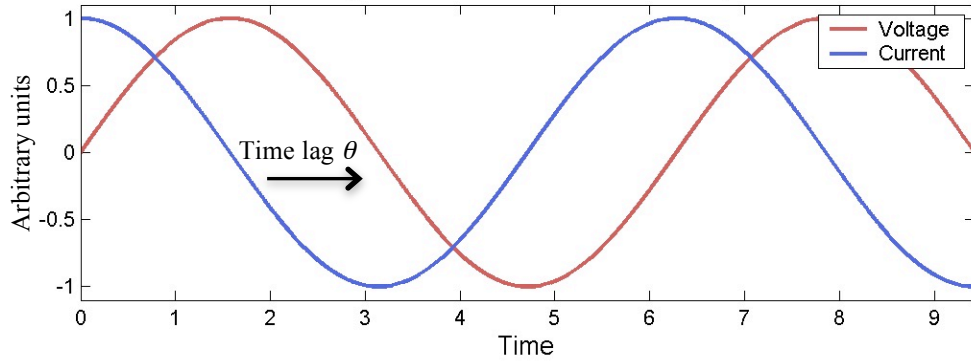
Figure 3. 6: A sinusoidally varying potential is applied to a sample and the time dependent current is measured as a function of frequency. It can be seen from the image that the current induced is out of phase with the potential by a time lag θ.[53]

The perturbation signal or excitation signal (V) can also be expressed with the following equation[52]:

$$V_t = V_0 \sin(\omega t) \quad (3.3)$$

Where, V_t is the potential at time t, V_0 is the total perturbation signal applied or the amplitude of the signal, ω is the radian frequency (radians/sec) expressed as 2πf.

The resulting response signal or current to the excitation signal is not equal to the total voltage applied and is shifted in phased by φ[52]:

$$I_t = I_0 \sin(\omega t + \phi) \quad (3.4)$$

As impedance is defined as the ratio of voltage to current, it can be now expressed by the following equation[52]:

$$Z = \frac{V_t}{I_t} = \frac{V_0 \sin(\omega t)}{I_0 \sin(\omega t + \phi)} = Z_0 \frac{\sin(\omega t)}{\sin(\omega t + \phi)} \quad (3.5)$$

Hence, total impedance at a specific time point is defined in terms of magnitude Z_0 and phase shift of ϕ.[52]

If one plots the applied sinusoidal perturbation signal V_t on the X-axis and the resulting sinusoidal current response signal I_t on the Y axis of a graph, an oval shape is obtained on the graph which is termed as 'Lissajous Figure'[52] (Figure 3.7) This figure was analysed for impedance measurement before the arrival of EIS instruments such as potentiostat.
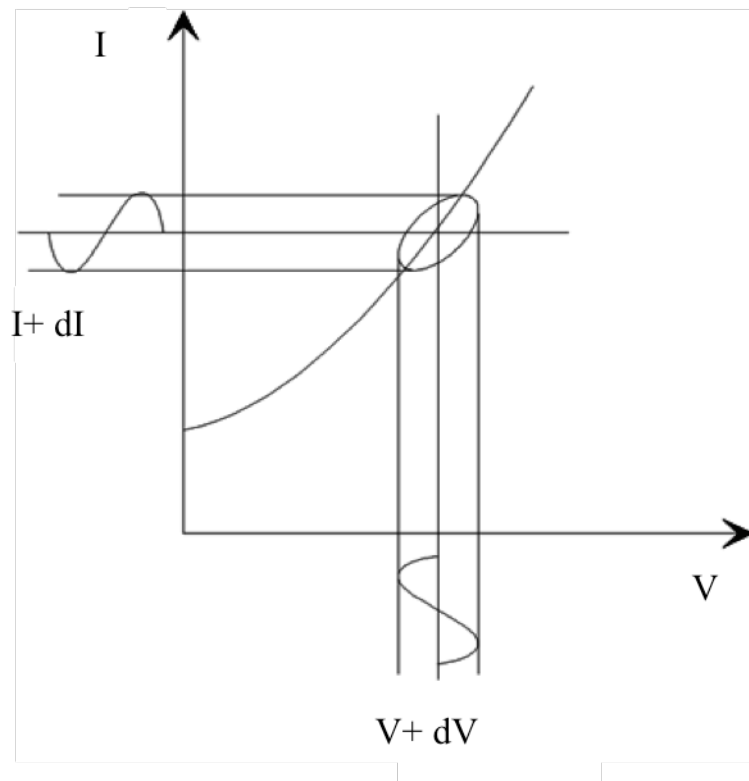
Figure 3. 7: If one plots the applied sinusoidal perturbation signal V_t on the X-axis and the resulting sinusoidal current response signal I_t on the Y axis of a graph, an oval shape is obtained on the graph which is termed as 'Lissajous Figure'. The Lissajous figureis used to calculate impedance.

The potentiostat measures the impedance by applying the sinusoidal voltage and measuring the resulting sinusoidal current and calculates the resulting impedance for each specified frequency which is then plotted as a Nyquist plot as shown (Figure 3.8)[52]:

With Eulers relationship (a mathematical function): $\exp(j\phi) = cos\phi + jsin\phi$ (3.6), where j is an imaginary number, impedance can be expressed as a complex function:

$$Z(\omega) = \frac{V}{I} = Z_0 \exp(j\phi) = Z_0(cos\phi + jsin\phi) = Z_0(cos\phi) + Z_0 j(sin\phi) \ (3.7)$$

$$Z(\omega) = Zreal + Zimg \ (3.8)$$

Hence, complete impedance Z(ω), is comprised of two components - real (Z') and imaginary impedance (Z'') which are related by the equation[52]:

$$Z(\omega) = Z' + jZ'' \qquad (3.9)$$

Where $j = \sqrt{-1}$, is an imaginary number and hence the term complex impedance.

The modulus of impedance can be calculated as:

$$|Z| = \sqrt{(Z' + Z'')} \quad (3.10)$$

If the real part (Z') is plotted on the X axis and the imaginary part (Z'') on the Y axis of a chart, it forms the Nyquist plot or an impedance plot as shown in Figure 3.8.

In an EIS experiment, the frequency dependent resistance, Z^*, is measured over a wide frequency range (0.1Hz to 10^6 Hz). The potentiostat or frequency analyser applies a tiny voltage (sinusoidally modulated) to the electrode and measures the respective time dependent current, calculating Z^* and the time lag ϕ. The potentiostat then alters the frequency at which the voltage oscillates and repeats the measurement until Z^* at all

frequencies are calculated. From all the values of Z(ω) and ϕ, the components Z' and

Z" are obtained which is then plotted in the form of a Nyquist plot (Figure 3.8).[52]
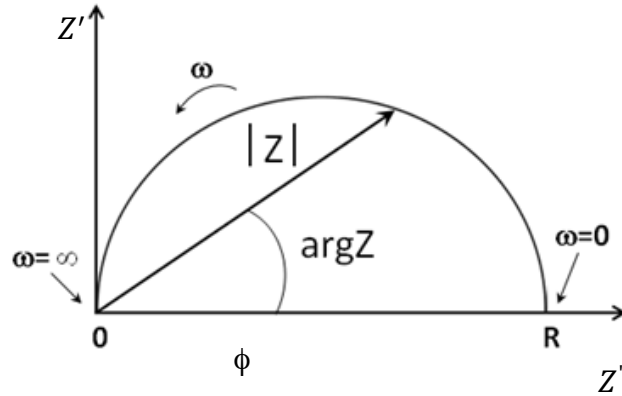
Figure 3. 8: The figure represents the Nyquist plot on which the impedance can be represented

as a vector of length |Z|. The angle between the vector and the X axis is referred to as phase

angle f(=argZ). Impedance is represented as a complex number with the following

equation: $Z(\omega) = \frac{E}{I} = Z_0 \exp(j\phi) = Z_0(cos\phi + jsin\phi)$ *where Z is impedance, ω is radians which*

is related to frequency by $2\pi f$, E potential, I current and j is an imaginary number. Hence, from

the equation Z(ω) is composed of *Z' (real)* (Z_0 cosφ) plotted on the X axis and *Z'' (imaginary)*

component (Z_0 j sinφ) on Nyquist plot.

To analyse impedance data a critical concept is that of 'equivalent circuits'. It is

assumed that any electrochemical cell or electrode modified with biomolecules can be

approximately explained by an array of electrical components. Any electrical

component has three inherent properties: resistance (R), capacitance (C) and inductance

(L), oxidised the first two components mostly dominate in an electrical circuit.[54] The

electrochemical cell is theoretically modelled based on an array of resistors and

capacitors such that the behaviour in Nyquist plot can be reproduced exactly. It is

further assumed that the components exhibit 'pure; behaviour such that a 'pure' resistor has nothing to do with capacitance and a 'pure' capacitor has nothing to do with resistance. The impedance of a purely resistive circuit is characterised by zero time lag that is the current is in phase with the potential. Hence R is described by

$$Z^*(R) = Z' = R \quad (3.11)$$

Capacitance is defined as the ability to store charge. For a pure capacitor the time lag of current by voltage is -90^0. A pure capacitor has a resistive component hence the real impedance or Z' is zero. The impedance of a capacitor is given by the following equation:

$$Z^*(C) = Z'' = -\frac{1}{j\omega C} \quad (3.12)$$

The impedance of a capacitor is a function of frequency, hence the impedance of a capacitor is infinite when a DC voltage is applied ($\omega = 0$) and the impedance approaches zero at very high frequencies.

In general, when considering real electrical components we can assume that real impedance behaves largely like a resistor and imaginary impedance behaves largely like a capacitor. For many electrochemical systems, the most common employed equivalent circuit is the Randle's equivalent circuit.[46] In the Randle's equivalent circuit Rs describes the solution resistance, Rct is the charge transfer resistance and CDL the double layer capacitance as shown in Figure 3.9.[46] Modelling the electrochemical system with the Randle's equivalent circuit can help in understanding the theory behind the phenomena occurring in the cell when some techniques are used for investigation. However, in reality, electrochemical diffusion processes affect experimental Faradaic currents. Diffusion processes can be modelled in an equivalent circuit by using a

distributed element, in series with the charge transfer resistance (Rct), called a Warburg element (W).[54] The Warburg impedance, W, depends on the concentration of the redox markers and, is frequency-dependent.[55] Since the Warburg element takes into account the mass transfer processes, it is more predominant at low frequencies.
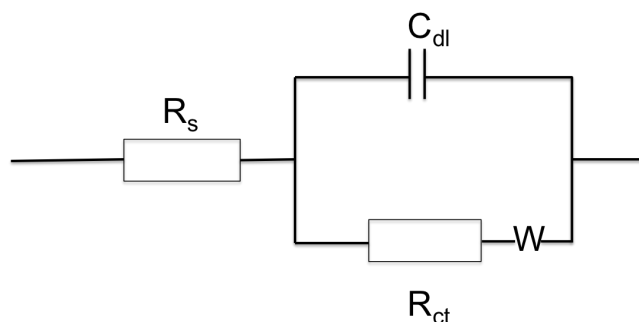
Figure 3. 9: A typical Randle's equivalent circuit for EIS circuits. Rs is the solution resistance which remains more or less constant. Rs is in series with charge transfer resistance (Rct) and double layer capacitance (Cdl). Rct is the charge transfer resistance of the biolayer immobilised on the surface. Cdl is defined as the capacitance exhibited by the two parallel layers of charge surrounding the electrode. W is defined as the Warburg's element, which models the diffusion process in the system.

All of the above techniques have been used in this work for electrode characterisation and evaluation binding characteristics of the MIP sensor in the current work.

3.1.5. PSA activation peptide sequences as a biomarker

Pro - PSA is an enzymatically inactive precursor form of PSA containing an additional 7 amino-acid sequence at its N-terminus (Figure 3.10).[56] The seven amino acid sequence, APLILSR (Figure 3.11), is cleaved by the hK2/hK4 enzyme extracellularly to produce the enzymatically active form of PSA.[57] [- 2] pro - PSA is cleaved between the third (leucine) and the second (serine) amino acids leaving two amino acids attached to PSA,

which is not cleaved further. [-2] Pro-PSA has been found in elevated levels in serum samples of patients with prostate cancer in several preclinical studies[58,59,60], with immunohistochemical tests also reporting an increased staining of [-2] pro-PSA in cancer tissue.[58]
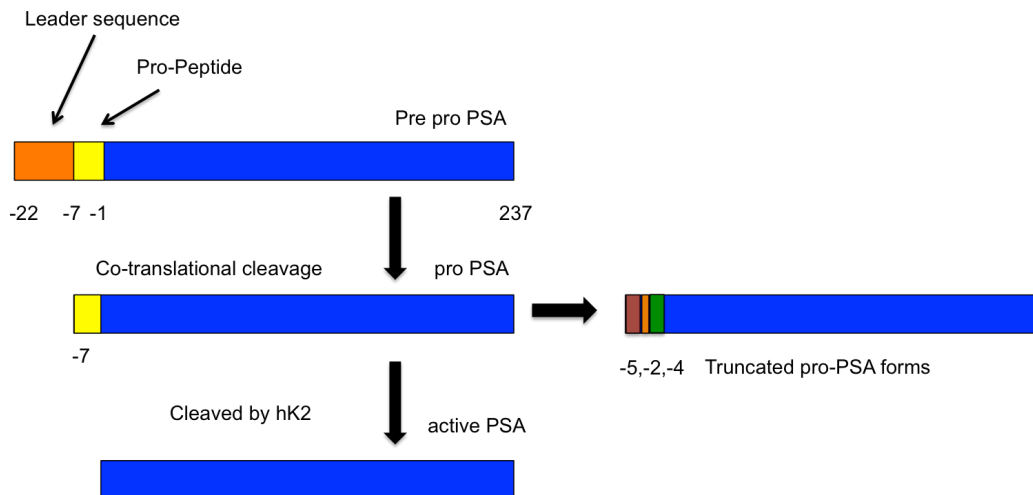
Figure 3. 10: Formation of active PSA and pro-PSA forms distinguished by the amino acid sequence and the site of truncation. PSA is a 237 amino acid protein with 7 amino acid activation sequence in the pro-form which is cleaved by hK2 extracellulary to give active PSA.[61]
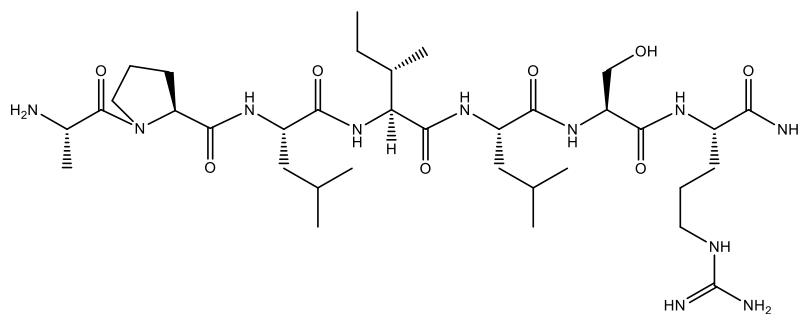
Figure 3. 11: Structure of pro-PSA peptide, APLILSR, showing alanine-proline-leucine-isoleucine-leucine-serine-arginine in the chemical structure.

A study by Engleheart and co-workers reported increased levels of PSA activation peptide sequence (APLILSR) in urine samples of patients with PCa.[62] Furthermore, higher peptide concentrations in patients correlated with a more aggressive form of prostate cancer, which potentially makes the peptide an important diagnostic and prognostic biomarker for the disease. The study reported high concentrations of the activation sequence in both the kidney and bladder, in line with renal clearance of the peptide. The activation peptide was detected using antibodies, which were raised for the activation sequence, via an immunoblotting technique. The level of peptide in urine samples was found to be greater than 10 ng/ml. The high concentration of peptide could be a result of elevated PSA levels in patients with the aggressive forms of PCa.[63] The study also proposed that the antibodies which were specific to a small part of the peptide, could also capture truncated sequences of the peptide (APLIL), which could be correlated to [-2] pro-PSA, making them highly specific for measuring aggressive PCa. Hence, an alternative method of detecting PSA/ [-2] pro-PSA would be the detection of the 7 and 5 amino acid activation sequences that are cleaved from PSA before entering the blood stream due to their co-relation with aggressiveness of the disease. This test would also lend specificity to t-PSA test for PCa detection.

3.1.6. *Pro-peptide imprinting and electrochemical sensing:*

The PROSENSE network aimed at exploring alternative biomarkers that could improve the specificity of the t-PSA test for PCa detection. Pro-PSA activation peptide was not only shown to be a diagnostic marker for PCa but also a discriminatory marker for benign and aggressive forms of cancer. As a result, we chose to study pro-PSA peptide for creating a surface imprinted MIP biosensor that would lend further specificity to t-

PSA test alone. Furthermore, pro-PSA activation sequence, due to low molecular weight, could be easily synthesised with modifications to enable efficient and reliable surface immobilisation ahead of imprinting. The use of the peptide sequences offered advantages in terms of the peptide stability, ease of template synthesis and flexibility to engineer on to different sensing platforms, which was more efficient than using whole pro-PSA protein which is an expensive template.

Figure 3.12 depicts the general scheme for the imprinting of the pro-PSA activation sequence. The pro-PSA peptide was modified with a thiol linker to facilitate direct attachment of the sequence to the electrode via thiol-gold interaction. The peptide was trapped on the surface using electropolymerised monomer, following which the peptide was extracted by selectively cleaving the thiol linkage of the peptide (subjecting to a specific voltage) and washing exhaustively with water to expose the imprinted cavities. Rebinding to the MIP modified electrodes was then evaluated using EIS. The use a linker / spacer thiol molecule was also hypothesised to help preserve the conformation of the template (mostly linear but not rigid as is the case with small molecules), while also leading to the uniform and oriented assembly of the peptide on the surface through a self-assembled monolayer (SAM), such that more homogenous binding sites should form upon polymerisation. As the activation peptide sequence relates to the aggressiveness of PCa and can be found in urine, the sensor could be potentially used as a non-invasive diagnostic and prognostic tool for early detection and monitoring progression of PCa. Furthermore, it was hypothesised that the results could be translated to epitope sequences from t-PSA selected in Chapter 1.
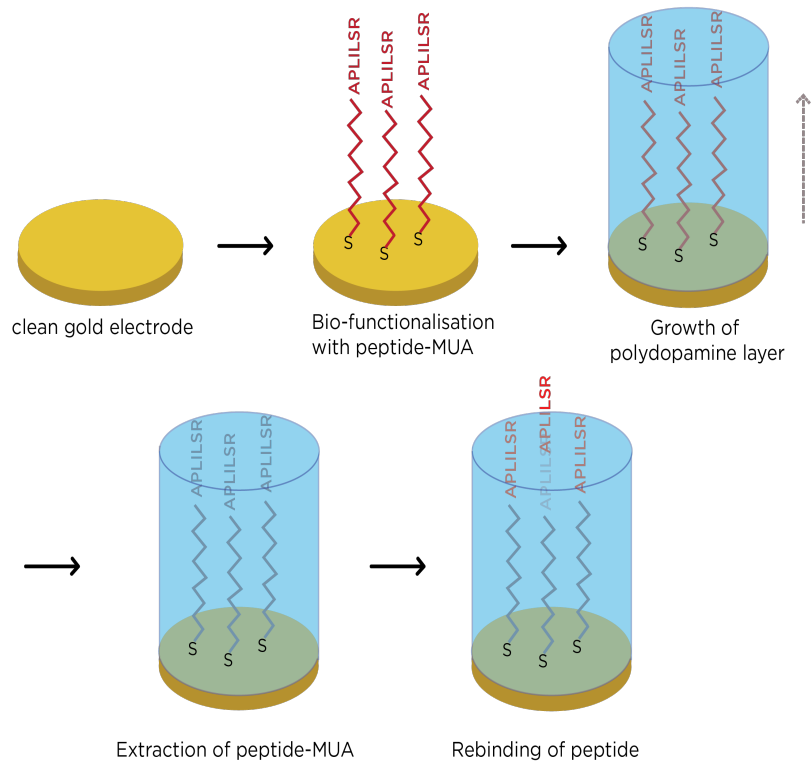
Figure 3. 12 Schematic of the Pro-PSA peptide imprinting process. (a) A gold bare electrode was first cleaned electrochemically and chemically (b) Thiolated-pro-PSA peptide was immobilised on the electrode (c) Immobilised electrode was trapped into a polymer via electropolymerisation (d) The peptide was removed to expose imprinted cavities (e) pro-PSA peptide was reintroduced to study binding characteristics using electrochemical techniques.

3.2.   Aims And Objectives Of Chapter 3

The overall aim of this chapter is to construct a surface imprinted MIP sensor for the sensitive and selective detection of pro-PSA activation peptide sequence (APLILSR).

Key objectives of this chapter are:

1. Synthesise the peptide APLILSR using Fmoc solid phase peptide synthesis.

2. Modify the peptide with a thiol-linker to enable one-step template immobilisation.

3. To investigate the electropolymerisation of different electroactive monomers

4. Optimisation of imprinting methodology for APLILSR peptide using a selected electroactive monomer.

5. Evaluate MIP sensor performance by undertaking dose response assays with the imprinted peptide and investigating cross-reactivity with control peptides.

3.3. Materials And Methods

3.3.1. Reagents

Dopamine hydrochloride, aniline aminophenol, aminobenzoic acid, trisma base, concentrated sulphuric acid, potassium phosphate monobasic solution (1 M), potassium phosphate dibasic solution (1 M), potassium hexacyanoferrate (III), potassium hexacyanoferrate (II) trihydrate, hexaammineruthenium (III) chloride, Tween 20, potassium chloride and magnesium chloride were all purchased from Sigma–Aldrich, UK. Ethyl acetate, DCM, DMF, acetic acid and acetonitrile were purchased from Fisher, UK. All aqueous solutions were prepared using ultra-pure water $18.2\,\mathrm{M\Omega\,cm}$ from a Milli Q system with Pyrogard filter (Millipore, UK). Gold working electrodes were obtained from CH Instruments, USA and mechanical electrode polishing kit from Buehler, UK.

3.3.2. Electrochemical apparatus

Electrochemical measurements were performed using a PARSTAT 2273 potentiostat (Princeton Applied Research, USA) with a three-electrode configuration comprising a Ag/AgCl reference electrode (BASi, USA), connected via a salt bridge filled with 10 mM phosphate buffer saline (PBS) pH 7.4 containing 150 mM NaCl and 10 mM KCl, and a platinum (Pt) counter electrode (ALS, Japan). The electrochemical impedance spectra were measured in 10 mM PBS (pH 7.4) measurement buffer containing 10 mM ferro/ferricyanide $[Fe(CN)_6]^{3-/4-}$ over the frequency range of 100 kHz to 100 mHz, with a 10 mV a.c. voltage superimposed on a bias D.C Voltage of 0.2 V vs Ag/AgCl reference electrode (corresponding to the formal potential of the redox couple). All

measurements were performed at room temperature in 10 mL glass beakers as shown in Figure 3.13.
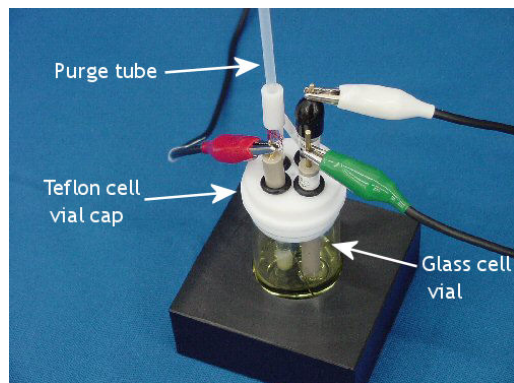
Figure 3. 13: Three-electrode setup with working (green), counter (white) and reference (red) electrodes. The set up is connected to a potentiostat that records electrochemical measurements.

3.3.3. Synthesis of triphenylmethyl protected mercaptoundecanoic acid (MUA):

Tritylchloride/ Chlorotriphenylmethane, (3.1 g, 2.28 mmol) and MUA (500 mg, 2.28 mmol) were dissolved in 7.5 mL of dry DCM in a round bottom flask and left stirring overnight on a magnetic stirrer at room temperature. Crude product MUA and tritylchloride was individually run on silica gel thin layer chromatography (TLC) plates (Merck KGAa, Germany) with ethyl acetate (EtOAc) / petroleum ether (v/v 20:80) as the eluent for 30 seconds. The silica TLC plate was dipped in concentrated H_2SO_4 for 10 seconds and subsequently heated using a heat-gun. The presence of the product was confirmed by the formation of a bright yellow color arising from the fluorescence of triphenyl group. The solution containing the crude product was evaporated using a vacuum rotary evaporator (Buchi, Rotovapour, R-200). Thereafter, the dried crude product was dissolved in DCM (15 mL) and water (12.5 mL) and phase separated using

a separating funnel. The aqueous phase was removed and the organic phase containing the product was washed with water (2 × 15 mL) and then dried with MgSO$_4$ (500 mg). The product was then filtered (Whatman filter paper, Grade 1) and vacuum dried to yield crude MUA-(Trt). The crude compound (dissolved in 5 ml DCM) was loaded onto a silica gel column (Sigma Aldrich, UK) and eluted using EtOAc/petroleum ether (20:80) mobile phase. Fractions (5 mL X 30) were collected and analyzed by TLC (eluent 50/50 EtOAc) /petroleum ether) to detect MUA-(Trt) in the fractions. The fractions containing the MUA-(Trt), as confirmed by TLC, were pooled together and vacuum rotary evaporated with further drying under vacuum overnight (at room temperature). Purified MUA-(trt) was dissolved in deuterated chloroform (3 mg in 1 mL CdCl$_3$) and tested for purity by NMR (Bruker BioSpin GmbH, Germany).

3.3.4. Peptide synthesis

The APLILSR peptide was synthesised using standard Fmoc solid phase synthesis strategy using 250 mg (0.15mmol) MBHA rink amide resin (Novabiochem, 200-400 mesh, 0.60 mmol/g loading) and an automated synthesiser (Activo P11, Activotec, UK) fitted with a reactor-heating jacket. After swelling the resin in DMF (5 mL, 10 min) the Fmoc protecting group was deprotected using 20 % piperidine/DMF (v/v) (10 mL, 2 min and then 10 min). The first amino acid was coupled manually using 4 eq of amino acid (Fmoc-Arginine (PMC-OH)) (0.6 mmol, 397.4 mg) activated with 4 eq DIC (0.6 mmol, 93.9 μL) and 4eq HOBt (0.6 mmol, 81 mg) for 1 hour in 2 mL DMF. This was followed by an acetylation step (Acetic acid/DIPEA/DMF = 1/1/8 (v/v/v), 10 mL, 1 x 10 min). The success of the coupling was confirmed by confirming absence of residual free amines using the Kaiser test. The resin was then loaded on to the Activo P11 automated

synthesiser fitted with a reactor heating jacket for the addition of the remaining six amino acids. Subsequent Fmoc deprotecting steps were performed using 20 % piperidine/DMF (v/v) as above, with the chain elongation steps being performed at 60°C using 3 eq. (0.45 mmol) of Fmoc-protected amino acid (Fmoc-Alanine-OH (140 mg), Fmoc-Proline(Trt)-OH (151.7 mg), Fmoc-Leucine(Boc)-OH (159 mg), or Fmoc-Isoleucine-OH (159 mg), Fmoc-Serine (tbu)-OH (172.4 mg)) 3 eq. of PyBOP (234.2 mg), and 6 eq. of DIPEA(157 µL) in 10 mL of DMF (1 x 25 min).

3.3.5. Addition of MUA thiol linker to pro-PSA peptide

After completion of coupling of all amino acids, the resin was weighed out and 50 % (by wt) of the resin was subsequently modified with MUA. Following Fmoc deprotection purified MUA-(Trt) was coupled to the peptide using 6 eq of MUA-(Trt) (100 mg), 5.9 eq of HATU (336.44 mg) and 6 eq of DIPEA (157 µL) in DMF (2 mL) for 2 hrs followed by an acetylation step (Acetic acid/DIPEA/DMF = 1/1/8, 10 mL, 1 x 10 min). The cleavage was performed with TFA: TIPS: water (v/v) (95/25/25) (3 mL) for 2 hours and the peptide was obtained by precipitating in diethyl ether (10 mL) and centrifuging (3900 rpm, 2 mins) to separate the peptide.

3.3.6. Purification and characterisation of pro-PSA peptide

Analytical RP-HPLC to evaluate the purity of the synthesised sequence was performed using a Dionex Ultimate 3000 system (Thermo Scientific, UK), with a VWD-3400 (Thermo Scientific, UK) variable wavelength detector, and a RF-2000 fluorescence detector (Thermo Scientific, UK). The analysis was performed at 35 ± 0.1 °C on a Gemini 5 µ C18 110A column, (150 x 4.6 mm - Phenomenex, UK), equipped with a SecurityGuard C18 (ODS) 4 x 3.0 mm ID guard column (Phenomenex, UK), at a flow

rate of 1 mL/min. A gradient elution comprising mobile phase A (0.1% aq TFA) and mobile phase B (0.1 % TFA in MeCN) was employed. (Method: 0.0 –10.0 min 0-95 % B, 10.0 –15.0 min 95 % B, 15.0–15.1 min at 95-5 % B, 15.1–18.0 min 5 % B.). Semi-preparative RP-HPLC was performed on a Dionex HPLC with a Gemini 5 μ C18 110A column, (250 x 10 mm - Phenomenex, UK) and equipped with a SecurityGuard C18 (ODS) 10 x 10 mm ID guard column (Phenomenex, UK), at a flow rate of 2.5 ml/min.

3.3.7. Fabrication of MIP sensors

3.3.7.1. Cleaning of electrodes

Gold disk working electrodes with a radius of 1.0 mm (CH Instruments, Austin, TX, USA) were mechanically polished for 5 min with 50 nm alumina slurry (Buehler, Lake Bluff, IL, USA) on a polishing pad (Buehler) and then sonicated for 5 min in ethanol and 10 min in ultra-pure water to remove any remaining alumina particles. Electrodes were then treated with piranha solution (three parts concentrated sulphuric acid to one part hydrogen peroxide) for 5 minutes. Thereafter, electrodes were rinsed thoroughly with ultra-pure water to remove any residual acid. Subsequently, the electrodes were electrochemically cleaned in 0.5 M H_2SO_4 by scanning the potential between the oxidation and reduction of gold, − 0.05 V and + 1.1 V vs Hg/Hg_2SO_4, for 50 cycles until no further change in the voltammogram was observed. Finally, the electrodes were washed with ultra-pure water and dried under nitrogen.

3.3.7.2. Screening of electropolymers

Cyclic voltammetry was used to bring about the electropolymerisation of different electroactive monomers. Clean gold electrodes were set in a three-electrode configuration with monomer solution (see Table 3.2 for details) and the potential

applied with reference to Ag/AgCl (3 M KCl) reference electrode with a platinum wire as a counter electrode. All monomer solutions were degassed with nitrogen for 10 minutes prior to polymerisation.

Monomer	Voltage range (vs Ag/AgCl)	Scan rate	Buffer (10mL)
Aminophenol (50 mM, 5.45 mg/ml)	-0.2 to + 0.8 V	50 mV/sec	Acetate buffer pH 4.6
Aminobenzoic acid (50 mM, 6.857 mg/ml)	-0.2 to + 0.9 V	50 mV/sec	500 mM Sulphuric acid
Dopamine (5 mM, 0.948 mg/ml)	-0.5 to + 0.5 V	20 mV/sec	PBS pH 7.4

Table 3. 2: Polymerisation conditions for electroactive monomers for NIP screening study.

Post polymerisation the electrodes were washed with water and incubated with 1mL of 10 mM ferro/ferricyanide $[Fe(CN)_6]^{3-/4-}$ solution in 10mM PBS pH 7.4 for half an hour. Three impedance measurements of the WE were taken to measure the stability of the electropolymers. Post stability measurements, the electrodes were incubated with 1 µg/mL PSA for 20 minutes. Thereafter, the electrodes were washed with water and the response was recorded using EIS measurements as mentioned in section 3.4.2.

3.3.7.3. Peptide immobilisation

A stock of 1mM pro-PSA peptide-(MUA) was prepared by dissolving 0.968 mg peptide in 1ml 50/50 (v/v) EtOH: water. The stock was used to further prepare lower

concentrations of the peptide. The electrochemically-cleaned gold electrodes were washed with water, dried under nitrogen and immediately incubated in various concentrations (10 μM, 5μM, 1μM, 0.1 μM) of the peptide in 50/50 (v/v) EtOH: water for one hour. The functionalised electrodes were subjected to scanning voltage from -0.2 V to 0.4 V vs Ag/AgCl at a scan rate of 50 mV/sec in 10 mM ferro/ferricyanide $[Fe(CN)_6]^{3-/4-}$ in 10 mM PBS pH 7.4 solution to characterise the surface coverage of the peptide.

3.3.7.4.   Removal of the peptide

To evaluate the peptide desorption from the gold electrodes, 1 mM pro-PSA peptide-MUA solution (50:50 EtOH: water) was incubated with the clean gold electrodes for 1 hour. The functionalised electrodes were subjected to negative potential sweep 0 to -1.5 V vs Ag/AgCL in 50 mM NaOH. To evaluate desorption, the functionalised electrodes were subjected to scanning voltage from -0.2 V to 0.4 V (50 mV/sec) vs Ag/AgCL in 10 mM ferro/ferricyanide $[Fe(CN)_6]^{3-/4-}$ solution before and after the desorption process.

Pro-PSA peptide-(MUA) was extracted from MIP electrodes by subjecting the electrodes to an optimised step voltage (-1.2 V) for a short period of time (30 seconds) in 50 mM degassed NaOH solution using the three electrode setup. The electrodes were immediately rinsed with excess water and left overnight in washing solution (0.1 % v/v sulphuric acid and 0.1 % w/v TWEEN 20 in water) with stirring to remove any template embedded in the polymer.

3.3.7.5.   Molecular Imprinting of the peptide with polydopamine

Clean gold electrodes were incubated with MUA-peptide (500 nM, 100μL water: EtOH (50:50)) for 1 hour. Post incubation the electrodes were washed with ethanol and water

mixture twice followed by multiple washes with water to remove any non-specifically bound thiols. The molecular imprinting step was performed by electropolymerising dopamine on to the peptide-modified electrode. Briefly, 10ml of 10 mM PBS buffer (pH 7.4) containing 5 mM dopamine was degassed with nitrogen (10 min) and electrodeposited using cyclic voltammetry (3/6/9 cycles, -0.5 V to 0.5 V *vs* Ag/AgCl, scan rate of 20 mV/s). Optimised number of polymerisation cycles based on this study was used for fabricating MIPs for pro-PSA peptide. A non-imprinted 'control' electrode (NIPs) was prepared in the same way but in the absence of the pro-PSA peptide.

3.3.8. MIP sensor evaluation with the peptide

To evaluate the peptide rebinding, the electrodes were rinsed with water before being allowed to stabilise in the measurement buffer (10 mM PBS (pH 7.4) containing 10 mM $Fe(CN)_6^{3-/4-}$ and 0.05 % v/v TWEEN 20). To evaluate sensor performance, the electrodes were mounted in a three-electrode configuration with the apta-MIP or apta-NIP as the working electrode. Following baseline stabilisation, the electrodes were exposed to 100 µl of a range of peptide (APLILSR) solutions (1, 2, 5, 10, 20, 50, 100 µg/ml) in 10 mM PBS buffer pH 7.4 containing 10 mM $Fe(CN)_6^{3-/4-}$ and 0.05 % v/v TWEEN 20 for 20 minutes. The electrodes were washed with 10 mM PBS buffer pH 7.4 containing 10 mM $Fe(CN)_6^{3-/4-}$ and 0.05 % v/v TWEEN 20 and electrochemical impedance spectroscopy (EIS) was used to measure capacitive changes at the electrode/electrolyte interface resulting from the peptide re-binding. The binding data was fitted with one site total binding isotherm using Prism 7, Graphpad Software, (CA, USA).

3.3.9. MIP sensor evaluation with test and cross-reactant peptides

Binding specificity was evaluated by challenging the MIP systems with the test peptide: TIVANP (Threonine-Isoleucine-Valine-Alanine-Aspargine-Proline) and cross-reactive peptide: VPLIQSR (Valine-Proline-Leucine-Isoleucine-Glutamine-Serine-Arginine (Severn Biotech, UK) under the same conditions in a non-competitive assay. Briefly 1, 10, 100 μg/ml of control peptide in 10 mM PBS buffer pH 7.4 containing 10 mM $Fe(CN)_6^{3-/4-}$ and 0.05 % v/v TWEEN 20 was incubated with MIP electrodes for 20 minutes. The electrodes were washed as described in 3.3.6 and then measured using EIS.

3.3.10. Preparation of conventional MIP capacitive sensors

For the preparation of a conventional capacitive MIP sensor i.e. without prior immobilisation of the template at the surface of the electrode, APLILSR peptide (5 mM) was solubilised with 5 mM dopamine in PBS buffer pH 7.4. The solution was degassed for 10 minutes with N_2. The solution was then subjected to electropolymerisation by cyclic voltammetry (15 cycles) from - 0.5 V to 0.5 V at a scan rate of 20 mV/sec vs Ag/AgCl as reference electrode. The electrodes were washed with 100 mM H_2SO_4 and 0.1 % TWEEN 20 solution for removal of the peptide, washed with water overnight. Slightly higher acidic conditions were used to remove the peptide efficiently from the polymer due to absence of an electrochemical stimulus as seen with the surface (immobilised template) imprinted sensor (3.3.7.4). The rebinding of the pro-PSA peptide was evaluated as described in section 3.3.8. The imprinting protocol was adapted from molecular imprinting of nicotine in electropolymerised polydopamine by Liu *et al.*, 2006.[4]

3.4. Results And Discussion

3.4.1. Synthesis of triphenylmethyl protected mercaptoundecanoic acid (MUA):

Mercaptoundecanoic acid was coupled to the pro-PSA activation peptide sequence during Fmoc-peptide synthesis to provide a mechanism (gold – thiol) for directly conjugating the template to the electrode surface. MUA is 11-carbon alkane thiol which is widely used for immobilising biomolecules on the gold surface using EDC/NHS chemistry.[18] Various groups have studied the formation of SAM layers by MUA on gold, reporting compact packing of the molecule in a well-ordered manner on surfaces.[64,65] It was therefore hypothesised that MUA-tagged peptide would also create a well-organised SAM on the surface allowing for homogenous binding site creation during the imprinting process.

During the synthesis reaction of MUA coupling to the peptide (on the resin), it was important that the thiol group on MUA was protected to prevent oxidation and unwanted side reactions from occurring.[66] The triphenylmethyl (Trt) group was used to protect the thiol on MUA; Triphenylmethyl (Trt) is a popular protecting group for Fmoc-cysteine since it is be readily deprotected with strong acid during the final cleavage step.[67] The synthesis was performed as described in section 3.3.3. Upon running a silica TLC of the reactants and crude product, different retention factors were obtained: Trt-Cl (0.8), MUA (0.44) and product (0.52). Upon exposing the TLC silica plate to sulphuric acid, a strong-yellow colour was obtained from the crude product and Trt-Cl (but not MUA) which was strongly suggestive of formation of MUA-(Trt) (Figure 3.14). When deprotonated the MUA thiol functional group is a good nucleophile and attacks the tertiary carbon of Trt-Cl to form 10 - triphenylthiodecanoic acid, releasing hydrochloric

acid in the process (Figure 3.14).[68] The triphenyl group on MUA is acid-labile, and the

addition of a strong acid such as sulphuric acid cleaves the protecting group from MUA.
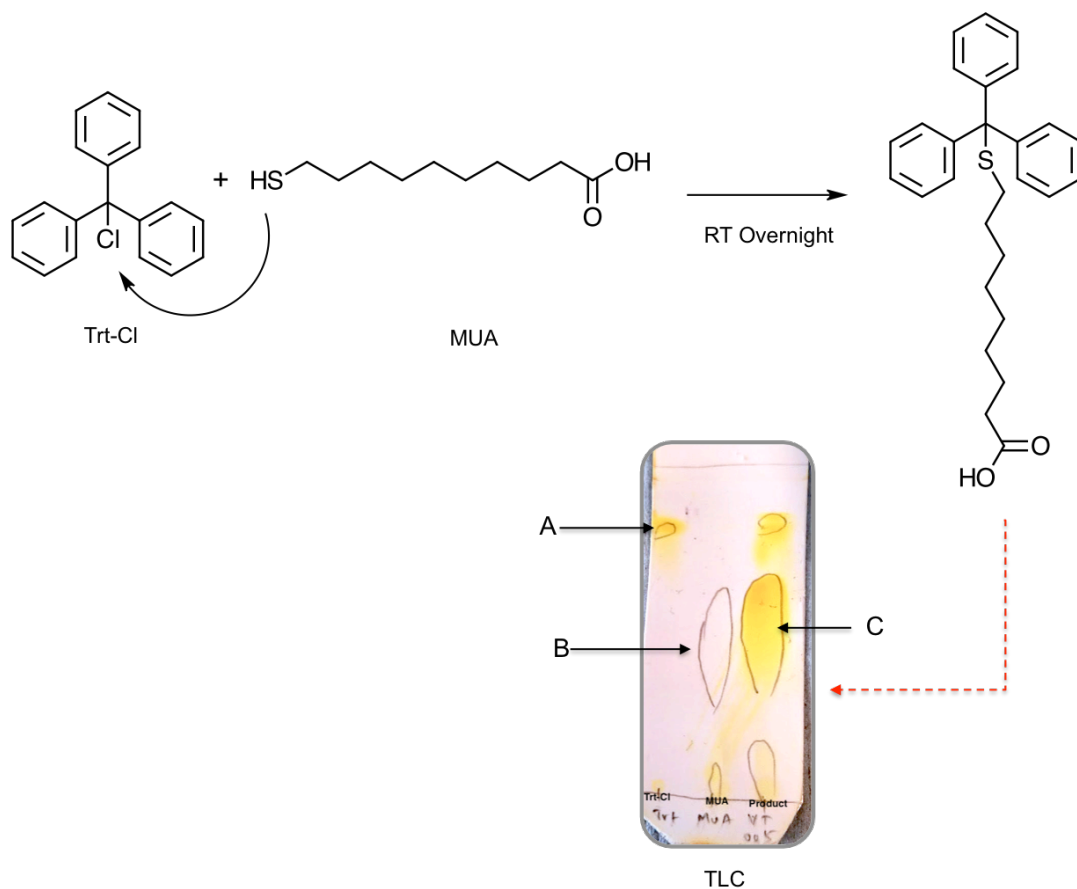
Figure 3. 14: Synthesis process of MUA-(Trt) whereby equimolar (2.28 mmol) concentration of

Trt-Cl and MUA dissolved in 7.5 ml dry DCM and stirred overnight at room temperature. The

TLC shows the retention of Trt-Cl (A), MUA (B) and the product (C), which forms a bright

yellow colour upon exposing to sulphuric acid, with a different retention time than Trt-Cl.

The structure of MUA (Trt) has been represented in Figure 3.15. The total yield of the

product was 110 mg (22 % yield). The purity of the molecule was tested using NMR

(Figure 3.16). 1H NMR (500MHz, Choloroform-d8) δ 7.10-7.35 (9H, m), δ 7.35-7.55

(6H, m), δ 1.10-1.45 (6H, m), δ1.6 (4H, s), δ 2.1(4H, m), δ 2.33 (4H, t)]. Figure 3.16

shows the 1H NMR of the final product. The NMR signal from 7.15 to 7.55 ppm represents the aromatic protons (no. 20 - 34), while the shifts from 1 to 1.7 ppm (no. 6 - 15) represent the alkane chain protons. The NMR shifts for MUA-(Trt) were similar to that reported by Stathopoulos *et al.*[69]

10-(Triphenylthio)decanoic acid
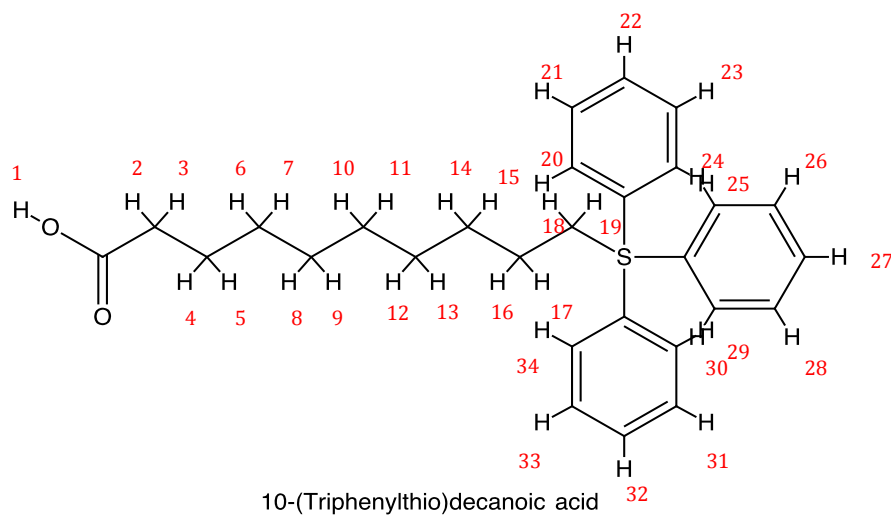
Figure 3. 15: Structure 10-(triphylthio) decanoic acid (MUA-(Trt))
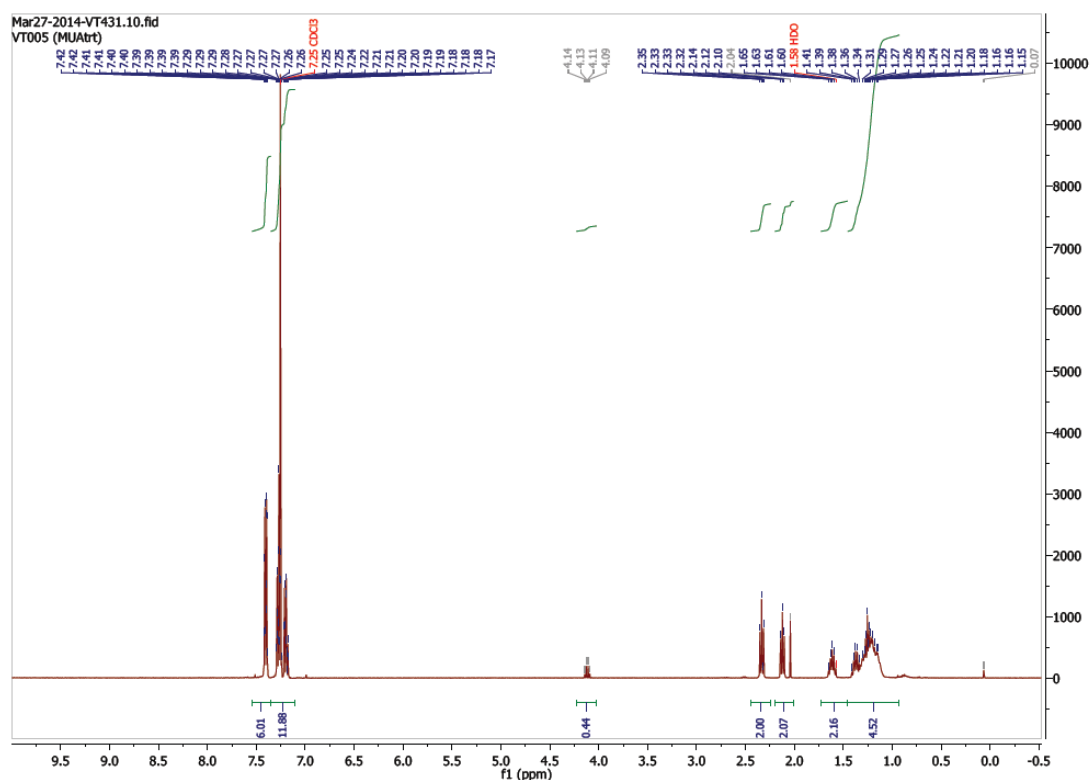
Figure 3. 16: 1H NMR of 10-trypheynlthiodecanoic acid showing respective shifts for hydrogen molecules.

In surface macromolecular imprinting the conformation and orientation of the template has a great influence on overall imprinting efficiency.[70] Specifically in the case of epitope imprinting where the ultimate goal is to rebind the 'whole protein', the orientation of the template will influence interaction with the native protein, increasing sensitivity and speeding-up binding kinetics.[8] Various covalent and non-covalent strategies have been employed for immobilisation of template molecules. For the peptide and protein imprinting, immobilisation strategies have used EDC / NHS chemistry[10], reversible crosslinkers[71], passive adsorption of protein,[72] metal-coordination chemistry[73], and modification of the biomolecule with cysteine to confer thiol functionality[74] allowing direct immobilisation to gold surfaces. EDC/NHS and

cross-linker approaches are often non-specific as they can involve multiple amino acid residues (lysine/ arginine), moreover, they also add complexity given an additional synthetic step is required to prepare the E-MIP. The use of cysteine terminated peptide as reported by Dietrich and co-workers[8] is an easy one step process, however, it can restrict or alter peptide conformation as a consequence of the molecule being immobilised in close proximity to a hydrophobic gold surface.[75] Metal co-ordination chemistry has shown favourable results. However, the template requires presence or addition of histidines to form the metal co-ordination. Giving due consideration to the peptide template in this study was therefore modified with mercaptoundecanoic acid (MUA) to facilitate direct immobilisation via thiol chemistry while providing an 11 carbon 'spacer' between the peptide and the electrode surface.

3.4.2. *Peptide synthesis*

Pro-PSA peptide and pro-PSA peptide-(MUA) were synthesised using standard Fmoc solid phase synthesis resulting in a good yield of the peptide (95%). The peptide was synthesised on Rink amide (MBHA) resin to obtain the amide-terminated peptide, as the activation sequence is part of the whole protein sequence and would therefore not contain a typical carboxyl terminated C terminus. There were no significant issues observed in the coupling of any of the amino acids, and the synthesis was completed with the crude peptide showing 97 % purity (peak area of the peptide/peak area of all peaks) as calculated from the analytical HPLC chromatogram in Figure 3.17. The peptide was further purified using semi-preparative HPLC with mass spectrometry confirming the correct mass – 768.51 g/mol (Figure 3.18).
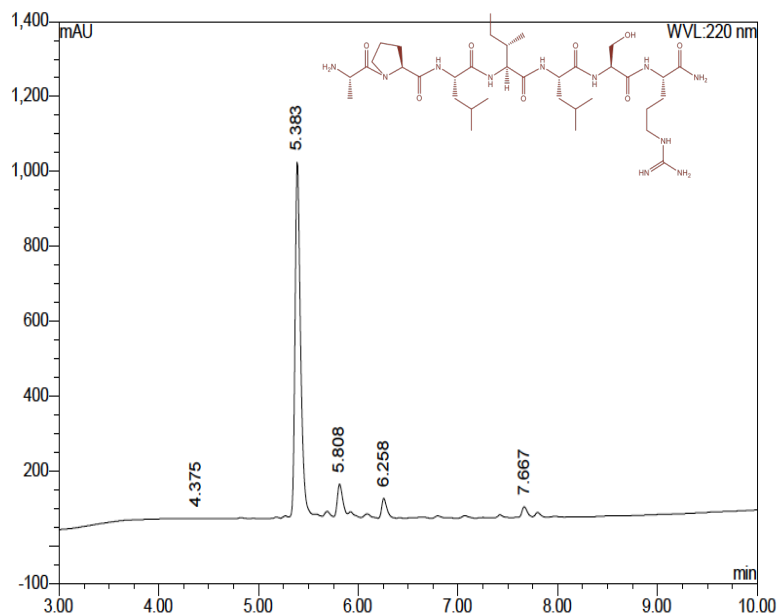
Figure 3. 17: Chromatographic evaluation of pro-PSA activation peptide containing one major or the dominant peak at 5.38 minutes.
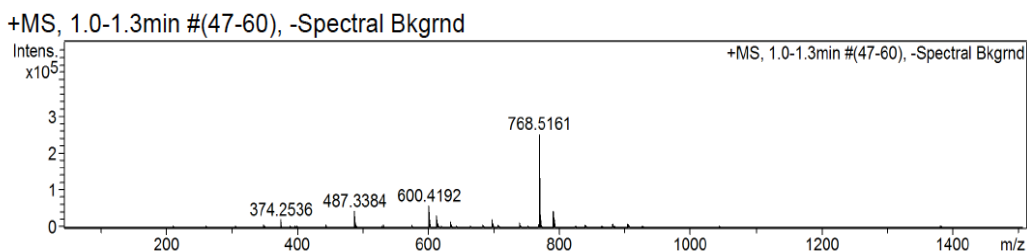
Figure 3. 18: Mass spectrometry of pro-PSA activation peptide (APLILSR) showing the correct mass of 768 g/mol.

Similarly, Figure 3.19 shows the chromatogram for pro-PSA peptide-(MUA) with mass spectrum again confirming the correct mass (968.1 g/mol) (Figure 3.20) The HPLC analysis for pro-PSA peptide-(MUA) was conducted at a higher wavelength to ensure residual protected MUA-(Trt) from the synthesis was not present in the crude peptide sample. MUA-(Trt) would ideally show a strong adsorption at 254 nm due presence of aromatic groups and could be easily isolated from the peptide-(MUA) peak during the

chromatographic run. Pro-PSA peptide tagged with MUA showed a slightly higher

retention time (5.7 minutes) than pro-PSA peptide further indicating that the

modification was successful.
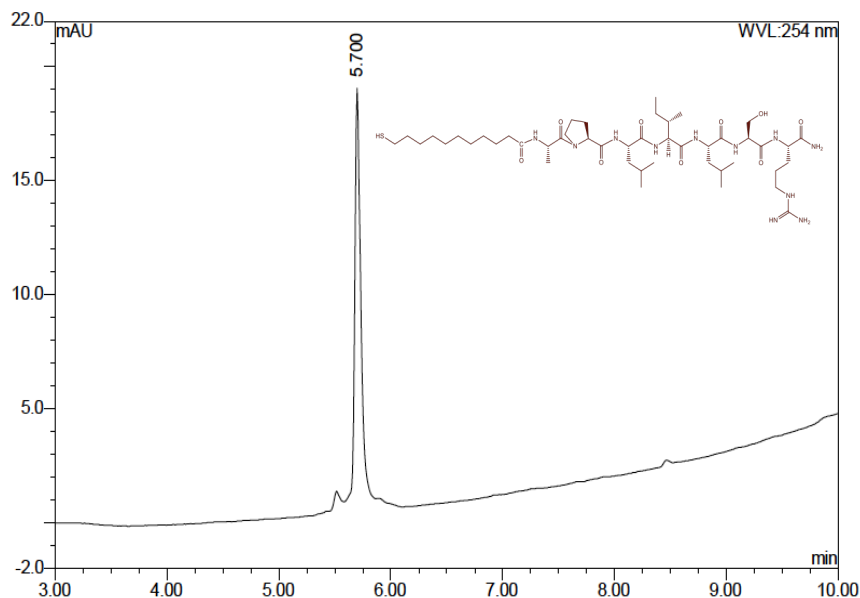
Figure 3. 19: Chromatography of MUA tagged pro-PSA activation peptide showing slightly longer retention time than the pro-PSA peptide. A drift in baseline during the analytical run was obtained which could be a result of residual solvents in the HPLC gradient run.
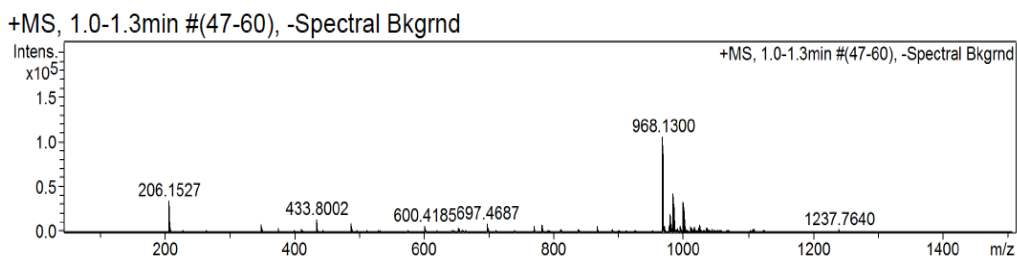
Figure 3. 20: Mass spectrometry of MUA tagged pro-PSA peptide showing the correct mass of 968 g/mol.

3.4.3. MIP electrode fabrication and optimisation:

3.4.3.1.   Electropolymer Screening study

Three electroactive monomers –aminophenol, aminobenzoic acid and polydopamine - were investigated in this screening study. The screening study was conducted simultaneously for the apta-MIP work in Chapter 4, which used PSA as the template. It was hypothesised that PSA would be better template to understand non-specific binding (due to various epitopes presented on its surface for interaction with the polymer) than a small peptide. The monomers were chosen based on the functional groups available for interaction with PSA. Polydopamine is predominantly a hydrogen donor and takes part in π-π stacking[76] while polyaminophenol and polyaminobenzoic acid provide opportunities for ionic interactions in addition to hydrogen bonding and π-π stacking.[77,31] Aniline, which produces a conducting polymer,[78] was also evaluated as a monomer in screening study. However, initial experiments showed high instability over time meaning that interaction with PSA could not be measured. This was likely a result of degradation of polymer at pH 7.4 as has been previously reported in the literature.[79] Polyaminophenol, poly-3-ABA and polydopamine modified electrodes were taken forward into binding assays to evaluate the non-specific interaction between each polymer surface and PSA.

- Polydopamine (PDA):

The cyclic voltammogram (CV) of dopamine polymerisation showed a reduction in current with consecutive cycles of polymerisation (Figure 3.21). The distinct oxidation and reduction peaks represent oxidised and reduced species respectively of dopamine during the polymerisation process. The peak at 0.32 V in the oxidation cycle represents

dopamine orthoquinone (DAQ), while the reduction cycle shows peaks at 0.09 V, which represents leucodopaminechrome (LDAC), and -0.32 V represents dopaminechrome (DAC). In the second cycle an oxidation peak occurs at -0.18 V which represents 5,6-dihydroxyindole which further undergoes polymerisation (Please refer to Figure 3.22).

Aqueous electrochemical oxidation of dopamine is proposed to occur via an ECE mechanism (Figure 3.22) where E stands for electrochemical and C stands for a chemical reaction.[80,81] The first step is the electrochemical (E) oxidation of dopamine into (DAQ), which proceeds to form LDAC. LDAC is an aminechrome formed by intra-molecular cyclisation of DAQ; the chemical-step in the process (C). LDAC further oxidises via a two-electron transfer to give dopaminechrome (E), which spontaneously rearranges itself to form 5,6-dihydroxyindole, the last electrochemical step for polymerisation. 5,6-dihydroxyindole further undergoes polymerisation reactions to form melanin-like polymer layers on the gold surface as shown in Figure 3.22, which decreases electron transfer reactions at the surface i.e. it is an insulating, rather than conducting, polymer layer.[82]
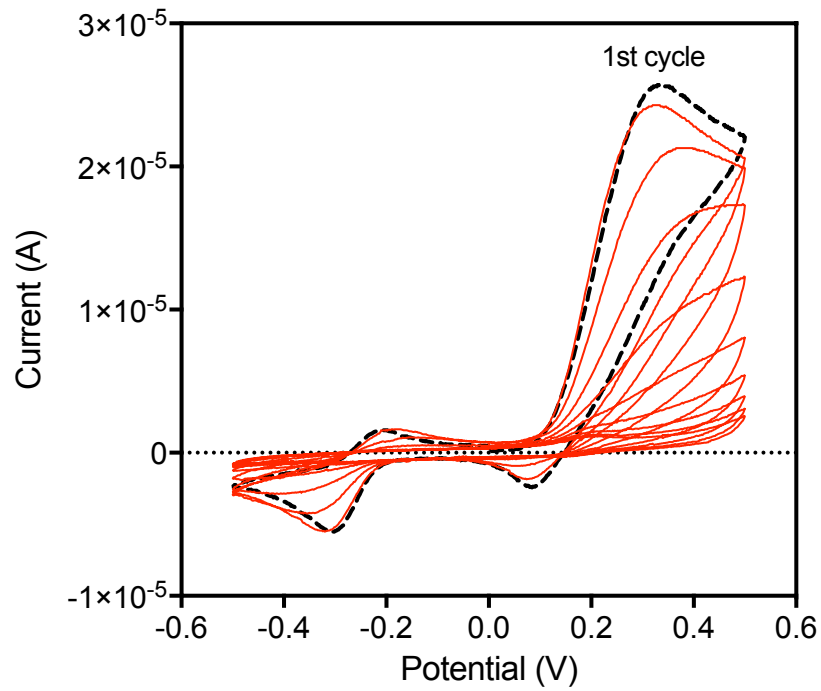
Figure 3. 21 Cyclic voltammogram of electropolymerisation of dopamine. The polymerisation of dopamine leads to reduction in peak current at 3.9 V with increasing number of cycles indicating deposition of a non-conducting polymer.
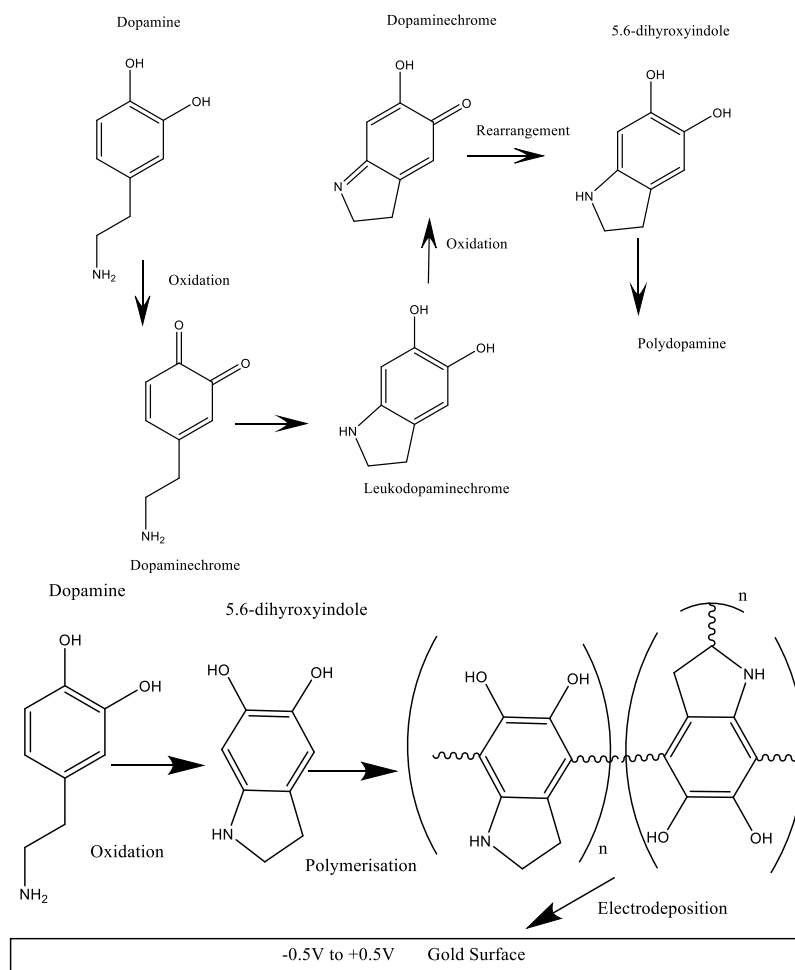
Figure 3. 22: Polymerisation of dopamine is proposed to occur via an ECE mechanism. The first step involves the electrochemical oxidation to dopamine orthoquinone (DAQ), which proceeds to form leucodopaminechrome (LDAC). LDAC further oxidises to dopaminechrome, which rearranges itself to 5,6-dihydroxyindole, which further polymerises on the gold surface.

• Polyaminophenol (PAP):

The electrochemical oxidation of ortho-aminophenol by cyclic voltammetry is shown in Figure 3.23. Oxidation of o-aminophenol is recorded as a distinct, irreversible peak at 0.52 V, which possibly corresponds to the formation of O-AP $^{.+}$ radical.[83] The absence of any complementary peaks in the reverse sweeps indicates chemical certain follow-up

reactions. The CV showed a reduction in the current oxidation peak of O-AP (0.52 V) with consecutive cycles, indicating the formation of a non-conducting polymer. The highest current was obtained with the first cycle, with the subsequent large decrease in peak current observed between the 1st and 2nd cycle suggesting that almost maximum coverage of polymer was obtained after the first cycle.[84]
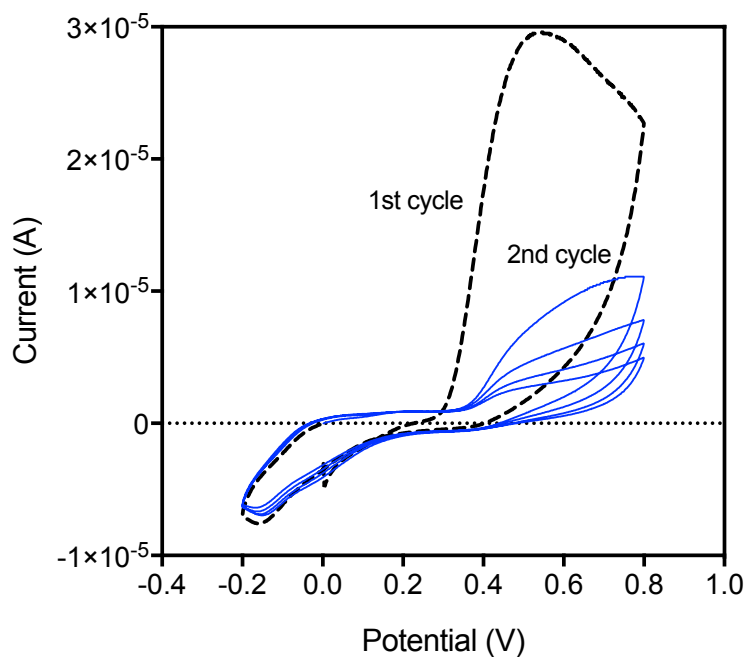
Figure 3. 23 Cyclic voltammogram of electropolymerisation of aminophenol, which depicts a large decrease in current after 1st cycle of polymerisation indicating maximum polymer coverage after the 1st cycle. A decrease in current also indicates the deposition of a non-conducting polymer.

Although the structure of poly-(OAP) is quiet simple, mainly consisting of phenoxazine ring like units, the mechanism of O-AP electropolymerisation in acidic medium is complex and poorly understood.[83] A general overview of OAP oxidation involves the formation of aromatic amine cation radicals, O-AP$^{+\cdot}$, which form dimers, that

chemisorb on to the metal surface, followed by an anodic oxidation and polymerization reactions (addition of dimers) to form linear chain or ring chain polymers (Figure 3.24).[85] In this process, the polymerization sequesters the –OH groups in O-AP monomer through the formation of C–O–C bonds.

O-AP   O-AP
                       radical
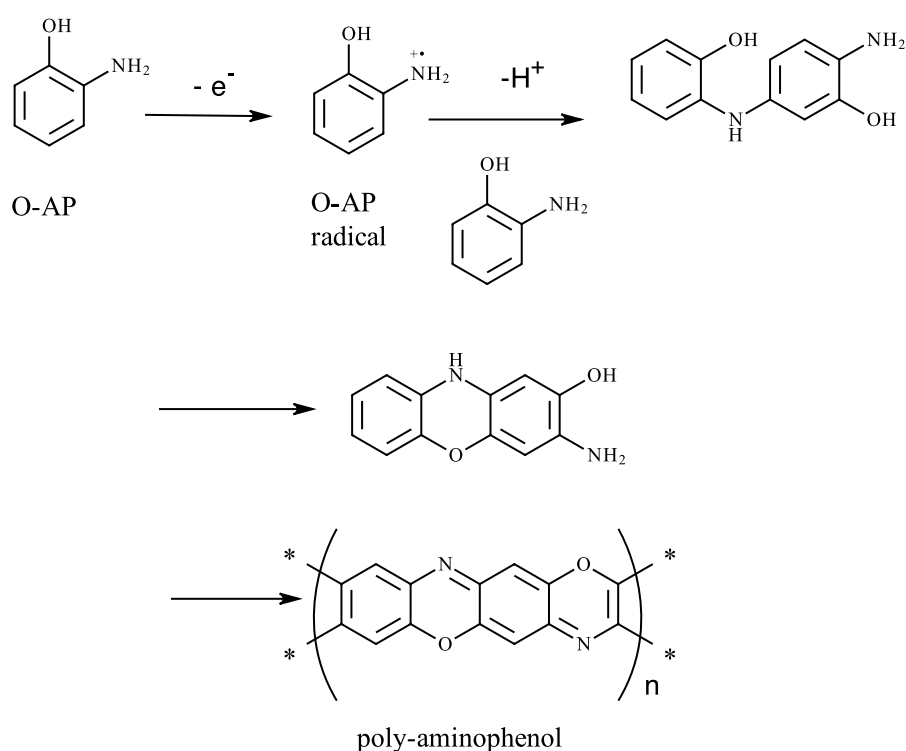
poly-aminophenol

Figure 3. 24: Electropolymerisation mechanism of polyaminophenol. The O-AP$^{+ \cdot}$ radical forms a dimer, which is subsequently oxidised to form polyaminophenol.

• Poly- 3-aminobenzoic acid (3-ABA):

The electropolymerisation of 3-aminobenzoic acid (3-ABA) by cyclic voltammetry is shown in Figure 3.25. The CV shows one large oxidation peak at 0.9 V, which

significantly reduces after the first cycle (Figure 3.25). The redox peaks correspond to the peaks associated with the electropolymerisation of 3-aminobenzoic acid.[31]
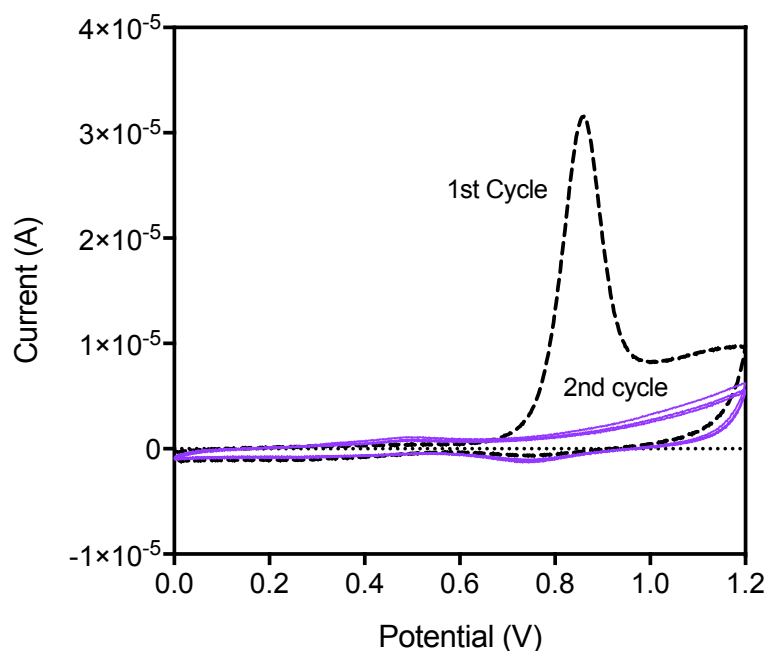
Figure 3. 25 Cyclic voltammogram of electropolymerisation of poly 3-aminobenzoic acid. The CV shows one large oxidation peak at 0.9 V, which significantly reduces after the first cycle indicating deposition of a non-conducting polymer.

Although the exact mechanism of 3-aminobenzoic acid electropolymerisation has not been elucidated, as it is a substituted aniline monomer it would be anticipated that it follows a similar mechanism to the that of the electropolymerisation of aniline.[86] Electrochemical polymerization of aniline occurs through a generally accepted mechanism which involves formation of anilinium radical cation by anodic oxidation on the electrode (rate determining step for polymerisation).[78] This electrochemical reaction for aniline polymerisation is generally carried out in an acidic environment. The

anilinium radicals couple together to form polyaniline as shown in Figure 3.26. However, the redox peak for 3-ABA (0.9 V) differs from that of aniline (0.2 V)[78], as observed in the literature, suggesting that the mechanism of 3-ABA polymerisation may be different than aniline. Furthermore, 3-aminobenzoic acid produces a non-conducting polymer as opposed to conducting polymers formed by other substituted anilines.[87]

Aniline Anodic oxidation
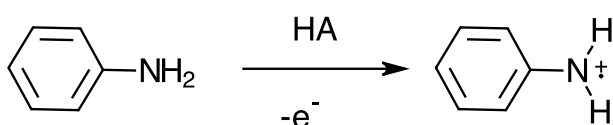
Coupling of Radicals
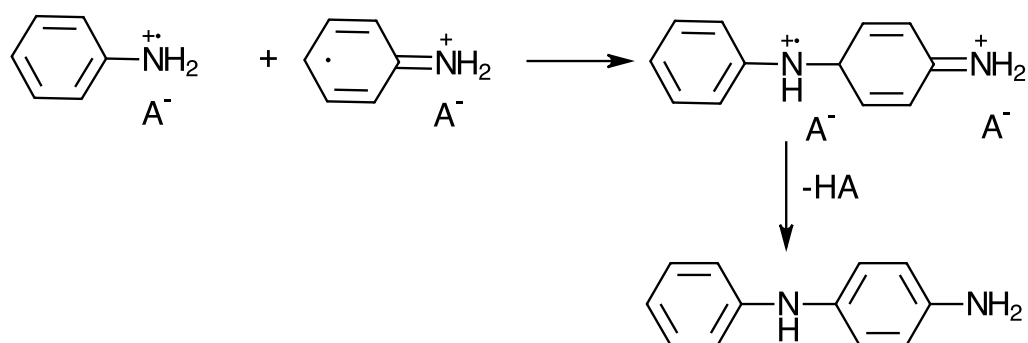
Figure 3. 26: The first step of the polymerization process of aniline is the formation of aniline cation radicals by anodic oxidation on the electrode surface. Following the formation of the cations, coupling of the anilinium radicals occurs, which is then followed by elimination of two protons and re-aromatization leading to formation of dimer.[78] The dimers is further oxidised leading to the formation of polyaniline on the electrode surface.

Electrochemical impedance spectroscopy (EIS), considered as an ideal electrochemistry technique to characterise interfacial phenomena,[52] was used to measure the impedance

of the system to quantify any PSA binding with the polymeric layer. Nyquist plots

obtained as result of EIS, provide information on the nature polymer layers attached on

the surface. Typically, Niqust plot can be divided into two parts: the semi-circular plot,

which represents the fast charge transfer process, and the straight line called Warburg

diffusion element which represents the slow diffusion controlled process. Due to the

non-conducting nature of the polymers, very high impedances ($\sim10^5 - 10^6$ ohms) were

observed in the Nyquist plots. The Nyquist curves with high impedance indicate that the

behaviour of the PAP and PDA films was dominantly diffusion controlled as opposed to

charge transfer controlled, with the absence of any well-defined semi-circular plots

(Figure 3.27).[33]
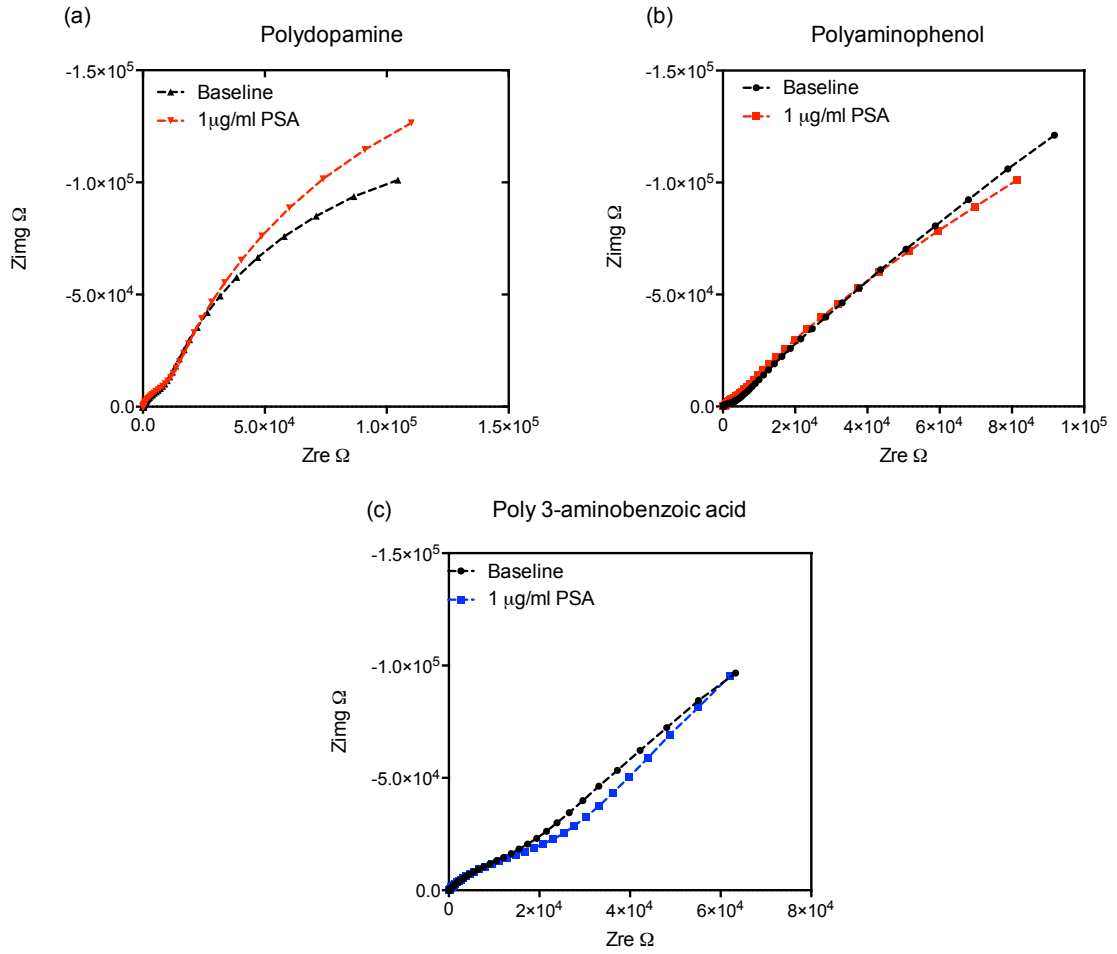
Figure 3. 27: EIS response of electropolymers to 1μg/mL PSA (a) polydopamine (PDA) (b) polyaminophenol (PAP) (c) polyaminobenzoic acid (ABA)

As a consequence of the non-conducting nature of films, the polymer behaves more like a capacitor than a resistor, and therefore it is more meaningful to look at the capacitive behaviour of such films.[88] This is due to the fact that small electrochemical changes as a result of protein binding can better observed through capacitance than impedance. Capacitance has an inverse relationship to impedance and can be calculated using equation 3.6 :

$$Z''(C) = C'' = -\frac{1}{2\pi f(Z_{img})} \qquad (3.7)$$

184

Where, C is the capacitance, f is the AC frequency (Hz), and Zimg is the imaginary part of impedance. In Bode plots the impedance is plotted with log frequency on the x-axis and both the absolute value of the impedance $(|Z| = Z_0)$ and phase-shift on the y-axis.[52] Functionalized/modified electrodes have been shown to behave like an ideal capacitor when the phase is close to 90^0.[88] Capacitance was calculated at 100 Hz as the phase was close to 90^0 between 10 - 100 Hz (as observed from Bode plots).

As is evident from Figure 3.28, polydopamine (PDA) showed a slightly higher change in capacitance (0.36 µF), which is indicative of greater binding to PSA, than polyaminophenol (PAP) and polyaminobenzoic acid (PABA), which displayed a change of 0.095 µF and 0.171 µF respectively. The higher response observed with polydopamine could be a result of its relative hydrophilicity with hydroxyl groups on the surface interacting with PSA.[89] The hydrophilic nature of polydopamine films has been used to enable direct immobilisation of proteins through non-specific adsorption which explains the enhanced interaction between the polymer and PSA.[90] Polyaminophenol on the other hand forms a semi-permeable membrane, which excludes certain molecules such as uric acid.[85] Given the size of PSA it is highly likely that the molecule is unable to diffuse into the polymer layer. Furthermore, when aminophenol is polymerised it is possible that the surface availability of free amino groups on the resulting polymer layer may be low,[85] effectively lowering the number of points available for interaction with PSA (Figure 3.24). On the other hand, polyaminobenzoic acid demonstrated higher interaction with PSA that PDA. This could be due to an increased number of free carboxylic acid and amino groups available for interaction

with PSA. Polyaminobenzoic acid has been utilised to immobilise antibodies on surfaces by activating the carboxylic group which is supportive of the hypothesis that functional groups remain available to interact with PSA following polymerisation.[32]
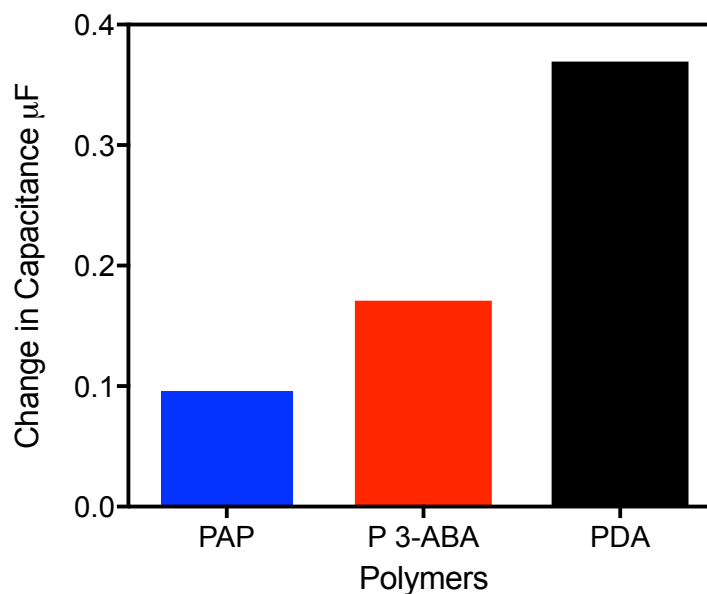
Figure 3. 28 Capacitance responses of electropolymers upon incubation with 1µg/mL PSA. Polydopamine (PDA) showed the maximum change in capacitance when compared to polyaminophenol (PAP) and polyaminobenzoic acid (P 3-ABA) (n=2).

The higher interaction (0.36 µF) observed between PDA and PSA (as seen in Figure 3.28) meant that it was selected as the monomer to take forward into the imprinting studies for pro-PSA peptide and hybrid PSA imprinting (Chapter 4) for initial research. Other than higher interaction with PSA, dopamine also possesses low oxidation/reduction potential that would also allow for polymerisation to be performed in the presence of the surface immobilised peptide without fear of oxidising the thiol linkage that holds it to the surface. Moreover, due to the presence of hydroxyl and amide functional groups in dopamine, it was anticipated that these functional groups would

form multiple non-covalent interactions with the peptide, as has been demonstrated in the literature with various templates[4,5], thus contributing to the formation of a chemically and sterically selective imprinted site. As a result, dopamine was studied for further polymerisation studies for imprinting of pro-PSA (MUA) peptide.

3.4.3.2.   Peptide Immobilisation study

The second step of the electrode fabrication process was focused on the optimisation of the template immobilisation on to the electrode surface. To characterise the fabrication of different layers of the sensor, cyclic voltammetry was used in the presence of a redox couple, 5 mM $Fe(CN)_6^{3-/4-}$ solution in PBS (pH 7.4). The redox couple allowed for sensitive measurement of current and resistance on the electrode surface. Initial experiments used a high concentration peptide-(MUA) (1mM) to ensure maximum coverage of the electrode surface with the template. The CV of the peptide functionalised electrodes showed close to 100 % reduction in peak current as seen in Figure 3.29 suggesting very high resistance to the flow current through the electrode. Modification of the gold electrodes by a resistive layer such as alkanethiols, or in this case peptide molecules, results in passivation of the surface, which leads to lower oxidation/reduction currents when compared to a bare gold electrode.[91] MUA is known to form well-packed SAMs that behave like a capacitive layer[91], which would explain the low peak current observed with pro-PSA peptide-MUA immobilised electrodes.
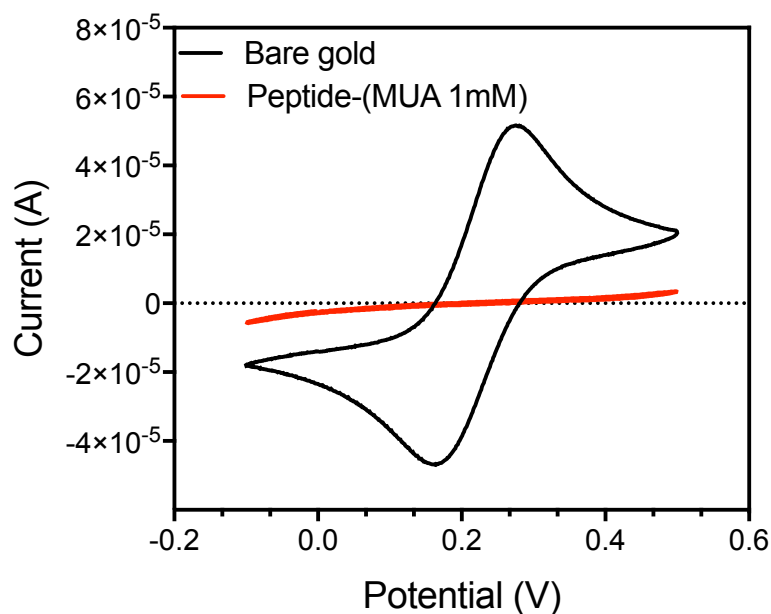
Figure 3. 29: Compares the CV of bare golf with gold modified with 1mM peptide-MUA. CV of a bare gold (black) showing well-defined oxidation and reduction peaks. CV post pro-PSA-(MUA) peptide modification on the electrode (red) shows (~ 100 %) loss in peak current.

Polydopamine was subsequently polymerised on the pro-PSA peptide functionalised electrodes, however, as observed from Figure 3.30 the electropolymerisation CV did not show the major oxidation and reduction peaks typically associated with dopamine polymerisation. Furthermore, the peak at 0.39 V had shifted to 0.5 V, with very little reduction in current observed with consecutive polymerisation cycles. Upon measuring the impedance of the peptide functionalised electrodes surface pre- and post-modification with polymer, negligible change impedance or R_{ct} (~10-20 %) was observed. This suggested that there was little growth of polydopamine on the surface; as a very large change in impedance / current would be expected following the formation of a non-conducting polymer layer.[92] It is likely that the well-packed peptide-MUA SAM, which may have minimum pinhole defects, inhibited the diffusion of dopamine

monomers to the electrode surface thus preventing polymerisation. A similar behaviour

has also been reported by Spegel *et al.* where the SAM modified electrodes were used to

improve the resistance of the electrode surface to dopamine polymerisation.[93] The study

concluded that charged SAM layers (such as MUA) more effectively prevented

dopamine polymerisation than uncharged SAMs.
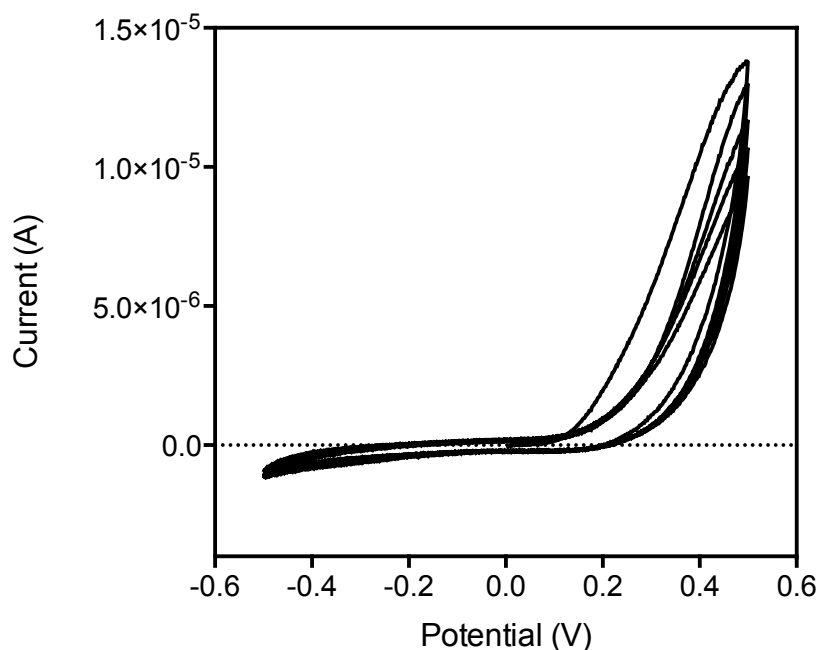
Figure 3. 30: Polydopamine polymerisation on the MUA/Peptide functionalised electrodes

In order to explore the influence of the template (pro-PSA peptide-(MUA)) layer on the

subsequent electropolymerisation of dopamine, the electrodes were incubated with

varying concentrations of the template in an effort to prepare a less densely pack surface

layers. It was proposed that a lower concentration of the peptide immobilised on the

surface would provide more opportunity for dopamine molecules to diffuse to the

surface and polymerise on the electrode surface. Figure 3.31 shows that as the template

concentration was increased a proportional decrease in oxidation and reduction peak

current was observed. The bare gold electrode showing well-defined peak potential at

0.23 V, which is a higher peak current than was observed for any of the bio-

functionalised electrodes.[94]
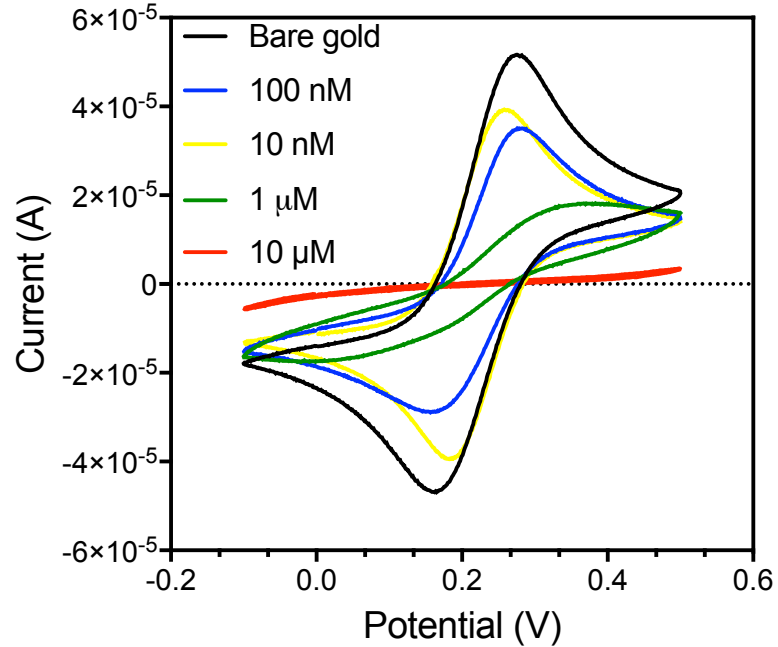
Figure 3. 31: Cyclic voltammograms of the bare gold electrode (black) showing well defined

peaks at 0.23V corresponding to oxidation of gold in K_3/K_4. A subsequent reduction in peak

current was observed with increasing concentrations of peptide (100 nM to 10 μM) due to

presence of a resistive peptide layer on the surface.

The observed decrease in peak current allows for estimation of fractional monolayer

surface coverage, termed θ^i_{CV}. The peak current is directly proportion to SAM surface

coverage according to equation 3.7. [95]

$$I_a = \left(\frac{n^2 F^2}{4RT}\right) \Gamma A \upsilon \qquad (3.8)$$

where I_a is peak current, Γ is surface coverage, A is the surface area, v is the sweep rate,

T is the temperature, R is the universal gas constant, F is the Faraday's constant, n is

total number of moles/electrons transferred.   Fractional coverage of monolayer,

assuming diffusion in uncovered parts is linear and is given by equation 3.8. [91]

$$\theta_{CV}^{Q} = 1 - \left(\frac{I_a^{SAM}}{I_a^{AuE}}\right) \qquad (3.9)$$

Where, I_a^{AuE} is the peak current of bare electrode and I_a^{SAM} is the peak current of the

modified electrode. The electrode coverage was calculated for each of the incubation

concentrations (10 nM, 100 nM, 1 µM, 10 µM pro-PSA peptide). The predictive surface

of the electrode that was exposed to 10 µM peptide was close to 100 %, while 10 nM

peptide showed 40 % coverage following a one-hour incubation with the peptide

solution. From Figure 3.32 it can be observed that the surface coverage reaches it's

maximum at a peptide concentration of 100 nM. Concentrations > 100 µM, were also

investigated to explore the limits of this approach as a predictive tool for surface

coverage and although surface coverage of > 80 % were observed it seemed likely that

this was the result of secondary events such as peptide stacking and secondary SAM

layer formation influencing the result.
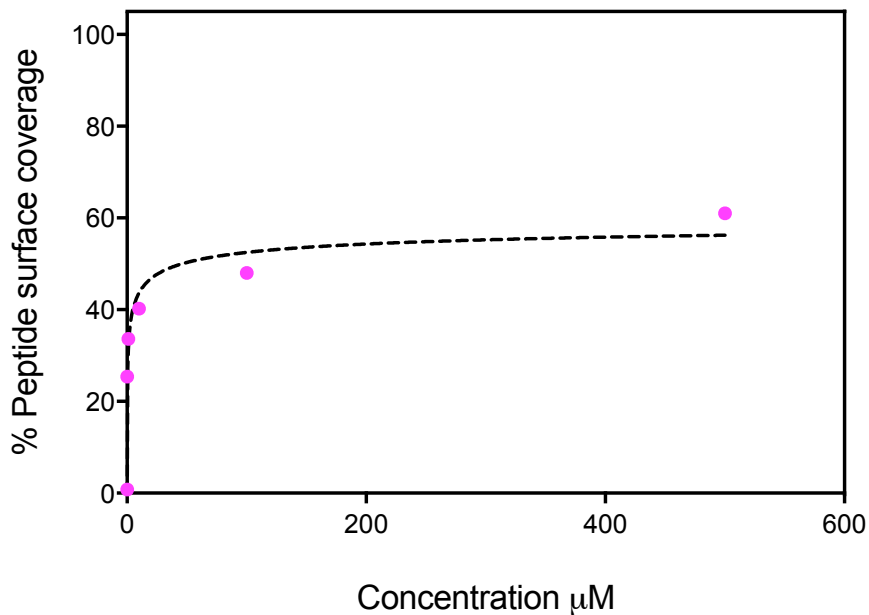
Figure 3. 32: Pro-PSA-MUA peptide approximate surface coverage on the bare gold electrodes measured at different concentrations of the peptide.

It was feared that concentrations lower than 100 nM would provide very low initial concentration of the template on the surface with less than 40 % coverage. Dietrich *et al*. for a similar surface imprinted study using cysteine-modified peptide used 60 % surface coverage of the peptide on the electrode surface for electropolymerisation. As a result, initial experiments were carried out with 500 nM peptide concentrations. Electropolymerisation of dopamine with 500 nM peptide demonstrated electropolymerisation of dopamine with similar oxidation and reduction peaks to polydopamine electropolymerisation on the bare electrode.

Since the peptide concentration of 500 nM was calculated to have a slightly higher approximate surface coverage of the peptide (60 %) than 100 nM or 10 nM on the electrode surface, it was taken forward into initial polymerisation studies. Cyclic voltammogram of dopamine polymerisation on the pro-PSA MUA functionalised

electrode is plotted in Figure 3.33 showing reduction in current with consecutive cycles. The distinct oxidation and reduction peaks represent oxidised species of dopamine during the polymerisation process. The peak at 0.36 V in the oxidation cycle represents DAQ, while the reduction cycle shows peaks at 1.2 V which represents LDAC and -0.28 V represents DAC. In the second cycle an oxidation peak occurs at -0.18 V which represents 5,6- dihydroxyindole which further undergoes polymerisation. No new peaks were observed during polymerisation demonstrating that no conducting analogues were being produced during electropolymerisation. The polymer growth is self-limiting as the insulating polymer being deposited prevents electron transfer reactions for further oxidation of dopamine.
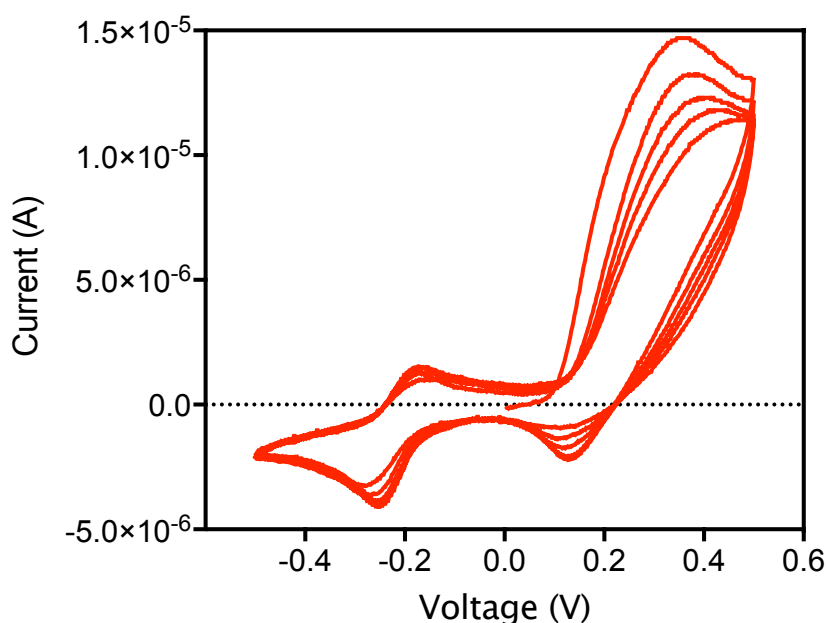
Figure 3. 33: Polydopamine polymerisation on the electrodes pre-incubated with 500 nM peptide with 5 cycles of electropolymerisation. The CV shows distinct oxidation and reduction peaks indicative of successful dopamine polymerisation.

In Figure 3.34 the CV peak currents for the bare gold electrode decreased from 52.4 µA to 9.2 µA with an associated shift in peak voltage from 0.25 V to 0.45 V, following polymerisation with dopamine. These results also provide further evidence of polymer growth on the peptide functionalised electrodes.
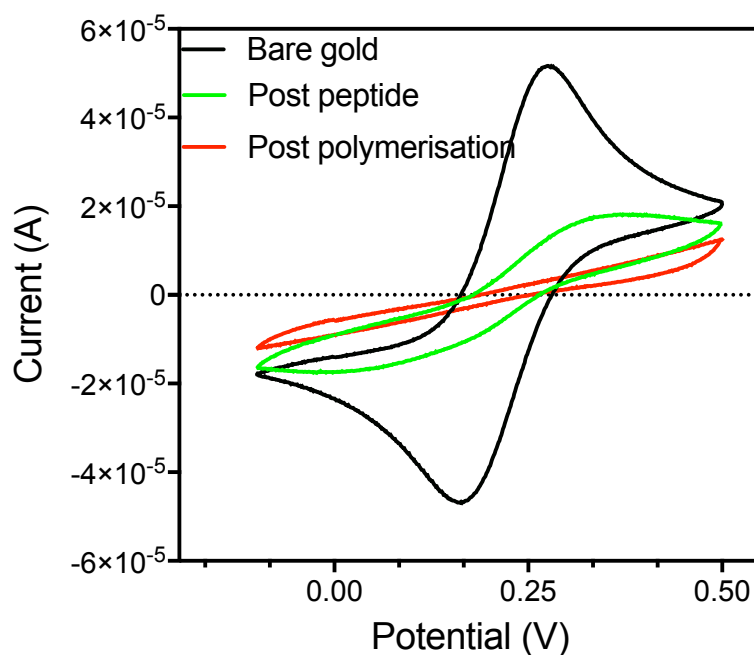
Figure 3. 34 Cyclic voltammogram of the peptide modified electrode post electropolymerisation. A further decrease in current was observed following 5 cycles of polymerisation.

From these experiments, a concentration of 500 nM peptide was chosen for the functionalization of electrodes pre-electropolymerisation of dopamine.

3.4.3.3. Removal of the peptide:

Further studies were undertaken to optimise the peptide removal from the polymer to expose the imprinted a great number of imprinted cavities. As the peptide was covalently bound to the gold surface, changes in potential were applied to break the thiol bond between the template and the surface in order to maximise the peptide removal. It

is accepted that the properties of SAM immobilised on the gold electrodes undergo significant change upon application of various potentials.[96,97] A study by Imabayashi *et al.* exploited this effect, selectively removing specific alkanethiols from an immobilised mixed SAM on the gold electrodes by applying slightly different desorption (stripping) voltages.[98] The study demonstrated that the length of the carbon chain of the alkanethiol influences the voltage required to effectively strip the SAM molecules from the electrode surface. As a result, it was hypothesised that polydopamine (being a polymer) would posses slightly different stripping potential than the pro-PSA-MUA. Hence, selective desorption of the peptide from the polydopamine (MIP) layer could be achieved.

The reductive desorption voltage of MUA has been reported to be -1.0 V in the literature.[96] To understand the stripping voltage of the pro-PSA-(MUA), the peptide functionalised electrodes were subjected to a negative potential sweep (via CV) as mentioned in Section 3.3.5.4. The reductive desorption CV of pro-PSA-MUA functionalised electrode did not demonstrate any sharp peaks at -1.0 V as has been observed with the MUA functionalised electrodes in the literature.[96] However, a broad peak was observed from -1.0 to -1.1 V which could be attributed to pro-PSA-MUA desorption peak (Figure 3.35). It is anticipated that this peak would be absent in the reductive desorption CV of bare gold electrode or pre-immobilisation of SAM. This is because the gold electrodes were electrochemically and chemically cleaned and hence are not expected to have any molecules covalently bound to the surface. Furthermore in the second scan (post desorption of SAM), it is anticipated that the peak observed in Figure 3.35 would reduce in area due to desorption/removal of some SAM molecules. It

is not expected that the peak would completely disappear as the scanning voltage ranges from 0 to -1.5 V and the resulting electrochemical signal would not be strong enough to remove all SAM molecules.[98,99] Hence, some SAM molecules will remain bound to the electrode after the first scan, which will result in a smaller peak in the second scan. However, it is hypothesised that with subsequent scans, the peak would eventually disappear leaving only an activated gold electrode surface.
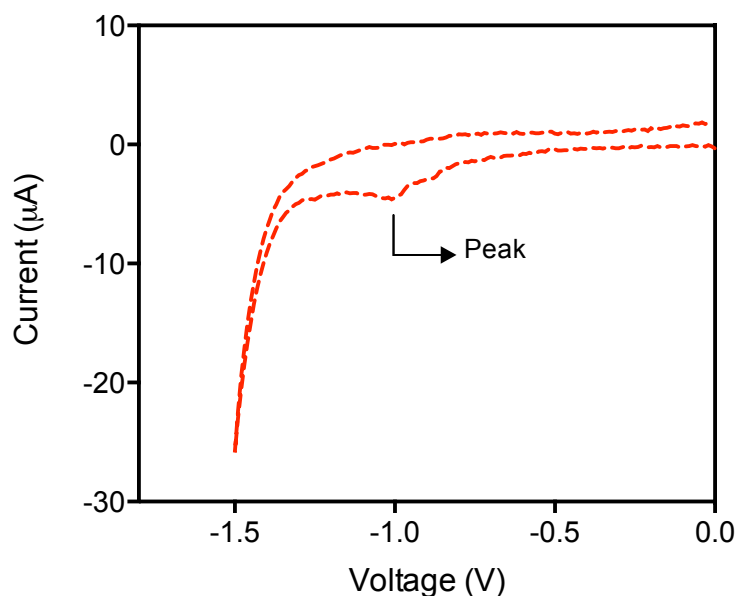
Figure 3. 35: Reductive desorption of pro-PSA peptide from the bare gold electrode in 50 mM NaOH shows a peak at -1.0 V which is assumed to be corresponding to the pro-PSA-MUA peptide.

The CV of the peptide functionalised electrodes was measured pre and post desorption in presence of $Fe(CN)_6^{3-/4-}$ to understand the change in electrochemical properties of the electrodes. This is because the redox couple are more sensitive to electrochemical changes on the electrode surface. Following the reductive desorption CV scan, a 20 % increase in current (0.55 μA) was observed, suggesting the successful removal of at least

some of the pro-PSA-MUA peptide (Figure 3.36). However, the MIPs subjected to this protocol for the peptide removal, did not subsequently show efficient rebinding of the peptide template (data not shown). Hence, further optimisation studies were undertaken to successfully remove pro-PSA template from the imprinted cavity.
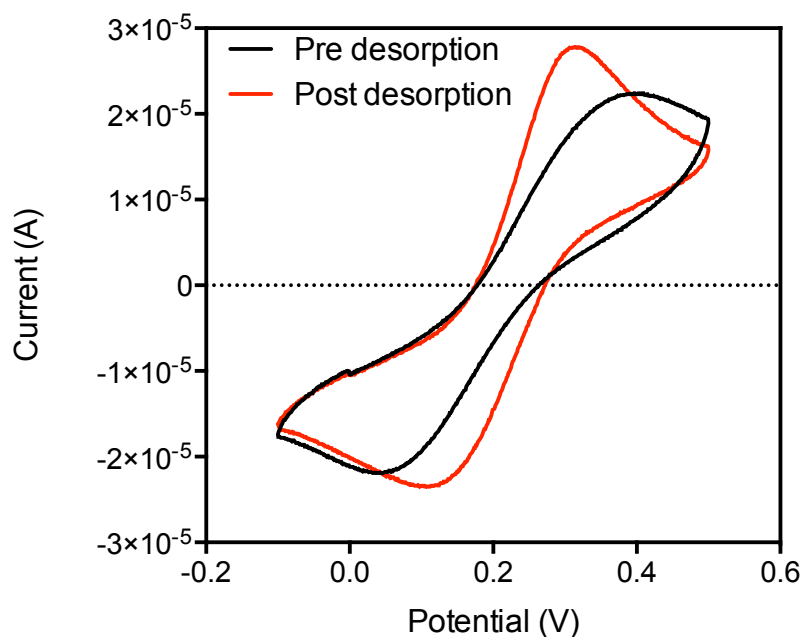
Figure 3. 36 CV of pro-PSA peptide immobilised electrodes pre and post reductive desorption. An increase in current and a shift in voltage was observed post desorption of peptide by subjecting electrodes.

A study by Balasubramanian *et al.* used step voltage for reductive desorption of proteins covalently attached to MUA from the gold electrodes.[99] In the step voltage process, the functionalised electrodes are subjected to a constant voltage for a specific amount of time. In the Balasubramanian *et al.* study complete removal of protein from the surface was observed by SPR after subjecting the electrodes to a step voltage of -1.2 V for 30 seconds. It was proposed that since the pro-PSA-MUA was embedded into the polymer

a slightly higher step potential (- 1.2 V than -1.0 V) would help facilitate its removal from the polymer. An alternative (non-electrochemical) way of understanding successful removal of peptide/protein from the polydopamine coated electrode would be to fluorescently tag the pro-PSA peptide and monitor the changes in the fluorescent signal to understand removal of peptide using reductive desorption protocol. Loss of fluorescent signal could be directly correlated to the percentage of peptide removed from the MIP sensor.

As a result, the MIPs were subjected to a step potential of -1.2 V for 30 seconds for removal of the template. Following this desorption step an increase of 26.31 μA from 2.6 μA was observed suggesting increased permeability of the polydopamine to the redox couple potentially resulting from the template desorption (Figure 3.37) (The CV scan of the electrode was conducted from -0.2 to 0.8 V. As $Fe(CN)_6^{3-/4-}$ oxidised between -0.2 V and 0.4 V only the relevant voltage has been depicted in the Figure 3.37)

Dechtrirat *et al.* also used a similar protocol to desorb surface immobilised the peptide from an imprinted polymer whereby the peptide entrapped within the polymer was subjected to oxidative desorption at 1.5 V for 30 seconds (the removal of the fluorescently labelled template peptide was monitored by measuring changes in fluorescence)[8] In the absence of a fluorescent tag in our study, pro-PSA template removal could only be predicted by changes in the electrode current post desorption. Post reductive desorption, the MIP modified electrodes were further washed with water and wash solution, to encourage removal of any trapped pro-PSA peptide.
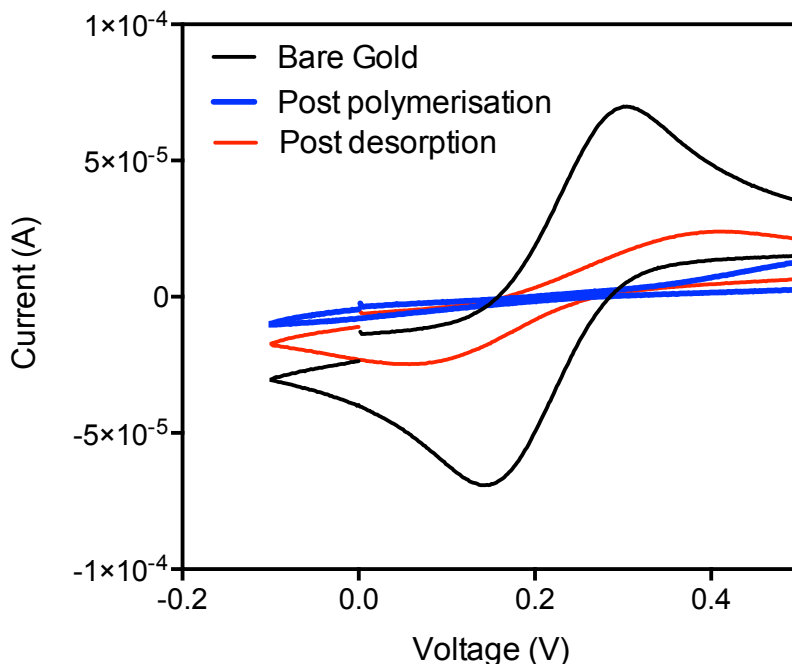
Figure 3. 37: CV of the electrodes showing change in peak current. There is a decrease in peak current post polymerisation of polydopmaine (blue) at 0.22V. Post desorption of the peptide, the peak current is observed to increase (red line) which is likely due to removal of the peptide and increased permeability of polydopamine.

Surprisingly, on the following day (after overnight washing of the electrodes) a further decrease in peak current (27.1 µA) was observed upon measuring the CV of the electrodes. The high impedance/low current obtained from MIP modified electrode following treatment was suggestive of a non-conducting polymer present on the electrode surface. It was expected that the peak current would change relatively little following desorption, however, the decrease in peak current post overnight incubation suggest further passivation (non-conductive) of the surface. A bare electrode incubated in TWEEN 20 solution did not show any change in current suggesting that TWEEN was

not responsible for this passivation. Another, theory could be reattachment of the polymer trapped pro-peptide to the electrode surface, however, in that case very little peptide binding should be observed in the re-binding step (Section 3.3.4) which was not the case. One possible explanation could be the oxidation/reduction of dopamine monomers on the surface leading to secondary reactions post-desorption process causing decreased permeability of the polymer. Over-oxidation of dopamine monomer post polymerisation has been reported by Łuczak, 2008.[80] Łuczak et al. reported that post oxidation of polydopamine film in NaOH led to considerable change in morphology of the polymer, which was also observed in the SEM images, whereby the uniform structure of the film was destroyed replacing it with granular-like structures. The study also reported that films adhered to gold more strongly suggesting passivation of the surface due to changes in the polymer characteristics, which is likely due to oxidation/reduction of certain monomeric species.

3.4.3.4. Molecular Imprinting and optimisation of polymerisation cycles

The assumption underlying this work is that electropolymerisation of dopamine on a peptide functionalised electrode, following the template removal, will result in a polymer layer containing cavities that are complimentary in shape and functionality to the template. To achieve this, the dopamine polymer must be able to interact with all the available interaction sites on the template and that these interactions must be maintained during electropolymerisation process. The most likely interaction between dopamine and pro-PSA peptide is proposed to be via hydrogen bonding which lends chemical selectivity to the cavity (Figure 3.30). In addition to these interactions, template removal should be possible post-polymerisation without damaging the imprinted cavities and fast

binding kinetics and mass transfer should occur during the template rebinding process. A key variable influencing these processes is the polymer layer thickness. If the polymer layer is insufficiently thick (too thin) and does not entrap the peptide then minimal imprinting effect is anticipated leading to inefficient rebinding.[9] On the other hand, if the polymer layer is considerably thicker than the total length of the immobilised peptide then there is the possibility of imprinted sites being 'buried' deep within the polymer layer leading to inefficient template removal and rebinding. Additionally, with a thicker polymer layer, complete removal of the template would be difficult to achieve with possible permanent entrapment of the template. [9] Hence, it was important to study the optimum polymer thickness for obtaining maximum imprinting efficiency for the MIP sensor. To understand the effect of polymer thickness on the pro-PSA activation peptide imprinting efficiency different numbers of cycles of electropolymerisation were evaluated. Different cycles of polymerisation correlate to different thickness of polymer layer. The imprinting efficiency was calculated by comparing the sensor response of MIP and NIP coated electrodes when re-challenged with the peptide. Polydopamine thickness can be controlled by adjusting the total amount of charge passed through the electrode, i.e. by changing the number of polymerisation cycles.[4]

Stöckle *et al.* studied the precise control of polydopamine thickness via electropolymerisation and found that the polymer thickness was linearly proportional electropolymerisation cycles up to 15 cycles, after which the growth becomes non-linear (due to the non-conducting nature of the polymer).[92] Stöckle *et al.* also reported that 5 cycles of polymerisation on the bare gold electrodes resulted in a polymer that was approximately 9 nm (estimated by XPS) - 19 nm (estimated AFM) thick. Based on the

Stöckle *et al.* study a fair assumption could be made that electropolymerisation of polydopamine on the pro-PSA functionalised electrodes (up to 5 cycles) would lead to deposition of a very thin polymer layer which is likely between 10 - 20 nm. During the apta-MIP construction (in chapter four) it was observed that 13 cycles of polymerisation on the bio-functionalised electrodes produced polymers of ~ 9 – 10 nm thick.[100] The length of MUA modified peptide sequence was calculated to be ≈ 4 nm (MUA - 1.2 nm and peptide - 3 nm) and therefore using 13 cycles would likely result in significant overgrowth of the peptide. Consequently three different polymerisation cycles (3, 6 and 9) were investigated. It was anticipated that 6/7 cycles of polymerisation would result in a polymer layer thickness not dissimilar to the length of the MUA-peptide template. MIP and NIP surfaces were produced for each of the polymerisation cycle studies to allow imprinting factors (IF) to be calculated.

Figure 3.38 illustrates how sensor signals for both MIPs and NIPs varied for the three different polymerisation regimes. Assuming sensor signal was proportional to the amount of the peptide rebinding to the electrode then for the NIPs binding varied in the order 9 > 3 > 6 and for the MIPs 6 > 3 > 9. Interestingly the variation in binding across the 3 systems was greater for the NIPs than it was for the MIPs. This suggests that polymer thickness influences the peptide rebinding significantly. The imprinting factors for each of the polymerisation regimes (3, 6, 9) were 2.2, 14.1 and 0.6 respectively for 100 μM of the peptide template.

Three cycles of polymerisation demonstrated an imprinting effect but there was a relatively small difference between the rebinding to the MIP and NIP (IF of 2.2) suggesting that the polymer was only interacting with part of the peptide molecule

(Figure 3.38). Nine cycles of polymerisation led to more peptide binding to the NIP compared to the MIP, which suggests a high degree of non-specific binding and possible entrapment of the template within the polymer structure prevents further peptide binding to the MIP electrode. The most efficient imprinting demonstration was achieved with 6 cycles of polymerisation, giving rise to an imprinting factor of 14. Further increasing the number of cycles to 7 resulted in the imprinting factor reducing to 10 suggesting that 6 cycles of polymerisation were optimal for the imprinting of the pro-PSA activation peptide sequence. It was hypothesised that 6 cycles of polymerisation resulted in thickness closest to the peptide length allowing for efficient imprinting and rebinding. A similar observation was made in a study investigating the imprinting of IgG using electropolymerised dopamine.[5] The study reported that the MIP with a thickness closest to the length of IgG displayed maximum binding efficiency when compared to NIPs, as a result of improved binding kinetics and easy accessibility of the template to the binding cavity. The study also reported that NIP/MIP thickness varies for the same cycles of electropolymerisation due to lesser surface area available in the functionalised electrodes (used for fabricating MIPs) which could also give rise to slightly different binding characteristics in resulting MIPs and NIPs.
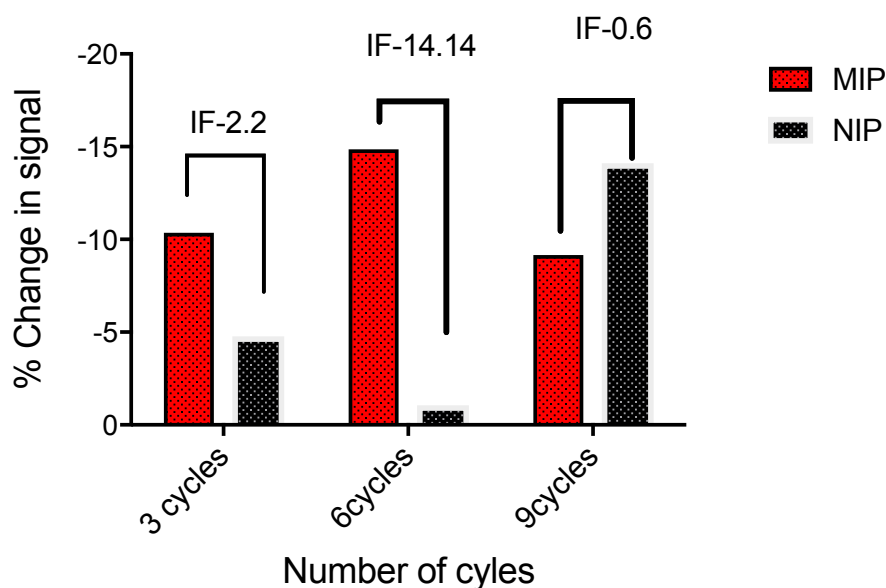
Figure 3. 38 MIPs with different cycles (3,6,9) of polymerisation when challenged with 100 μM peptide showed different imprinting factors. MIPs with 3 cycles showed a lower imprinting factor than 6 cycles, which could be due insufficient coverage of the peptide during polymerisation. 9 cycles of polymerisation showed a reverse effect suggesting certain entrapment of the peptide into the polymer.

3.4.4. MIP sensor evaluation with the peptide

Electrochemical impedance spectroscopy (EIS) was used in this study to measure capacitive changes at the electrode/electrolyte interface resulting from pro-PSA peptide re-binding as cyclic voltammetry is not sensitive enough to measure small changes in template binding. It was anticipated that upon binding of the peptide to the polymer layer, the surface properties of the electrode would change which could be monitored using changes in impedance using EIS.

The imprinted sensor was mounted in a three-electrode configuration as the working electrode and stabilized in measurement buffer (10 mM PBS (pH 7.4) containing 10 mM

$Fe(CN)_6^{3-/4-}$ and 0.05 % v/v TWEEN 20 for 1 hour before measuring the impedance. The Niquist data was modelled using ZSimWin software (Solarton Analytical, USA). The Niquist data could be best fitted with a variation of Randle's equivalent circuit: Rs (Q1//R1(Q2//R2))) (Figure 3.39, data plotted in Figure 3.40) which comprised two R1//C1and R2//C2 (resistance in parallel with capacitance) circuits. One circuit was in series with Rs also termed as solution resistance, while the other was in series with R1, which represents the resistance of the polymer layer. R2 resistance element could originate from the residual peptide molecules embedded in the polymer layer. Q1 and Q2 are constant phase elements (CPE) with impedance $Z_{CPE} \equiv 1/Q_{CPE}(j\omega)^n$, which accounts for a suitable fitting of the data. The two curves in the Niquist plot are likely to be associated with the electrochemical double layer and the polymer itself. For the blank measurement of the sample shown in Fig. 3.34 (a) with a 1.0 mm radius, the fitted values are R1 125.3 Ω, R2 13.08 KΩ, Q1 44.1 μF, Q2 7.754 μF, R3 0.159 KΩ. Measurement errors in impedance data = < 2.67 pct. The high value of charge transfer resistance (R2 13.08 KΩ), indicate the presence of an insulating layer (polydopamine) on the surface of the electrode.
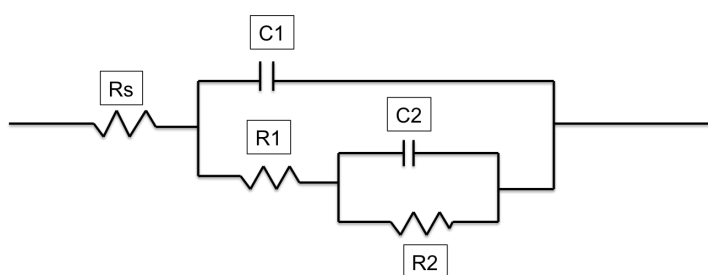
Figure 3. 39: RC circuit fro modelling the impedance curves obtained for the polydopamine modified electrodes.

However, polydopamine being a non-conducting polymer behaves more like a capacitor than resistor, and hence, it is more meaningful to look at capacitance than impedance. Given the high impedance values of the polydopamine-coated electrode, which has certain pinhole defects, the impedance data evaluated with traditional circuit elements yields large errors.[101] As a result a better evaluation of the capacitance was obtained by defining a complex capacitance in equation 3.10.[102,101]

$$C^* = C' + jC'' \equiv \frac{1}{j\omega Z} = -\frac{Z''}{\omega |Z|^2} - j\frac{Z'}{\omega |Z|^2} \quad (3.10)$$

The capacitance was calculated as $C = -1/j\omega Z''$ for the plotting dose response with the MIP and NIP sensors based on the frequency which showed maximum changes. A frequency of 1 Hz was chosen for calculating capacitance as maximum changes were observed at this frequency. The EIS Niquist plots for pro-PSA polydopamine imprinted sensor were similar to the apta-MIP sensor response, as seen in Chapter 4.[100]
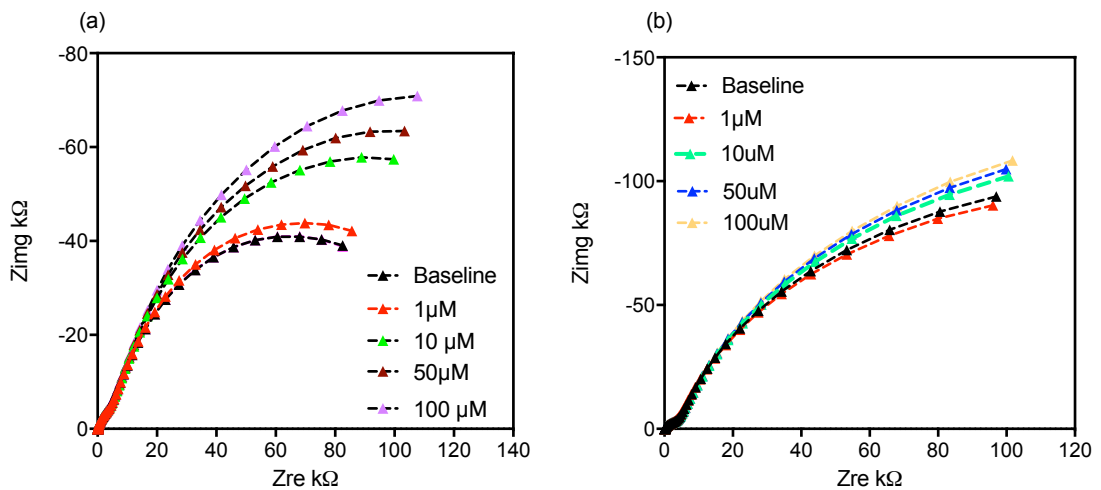
Figure 3. 40 Impedance cole-cole plots of MIP (a) and NIP (b) response to the pro-PSA peptide. It can be seen from the graphs that MIP response to the pro-PSA peptide was significantly higher that the NIP electrodes.

It can be observed from Figure 3.40 that the MIP sensor showed a decrease in capacitance with increasing concentration of peptide. A decrease in capacitance is related to an increase in impedance, which could be explained by the blocking effect of the peptide to easy diffusion of the redox couple $Fe(CN)_6^{3-/4-}$ to the sensor surface. Increased impedance in MIP based sensors has been reported in the literature whereby non-electroactive templates upon binding to the polymeric cavity change it's properties making them more resistive to the easy flow of charge.[39] A change of 4.01 % was observed at 1 μM peptide concentration while a change 16.11 % was seen at 100 μM. Non-imprinted polymers on the other hand showed negligible change (< 5 %) in impedance even at 100 μM peptide concentration. The slight initial increase in capacitance with the NIP electrodes (decrease in impedance) could be a result of the sensor establishing equilibrium with the redox couple, which takes time to diffuse through the polymer to the surface of the electrode. However, as the concentration of the peptide was increased a decrease in capacitance was observed which suggested non-specific interaction of the polymer with the peptide. Modelling the pro-PSA binding data with a Langmuir adsorption isotherm (total binding fit) gave an apparent K_d of 2.90 μM, B_{max} of 9.019 μM with an R^2 value 0.87 (Prism 7, Graphpad Software). The limit of detection (calculated based on discrimination from baseline signal of NIPs) was found to be 1 μM peptide (Figure 3.41).
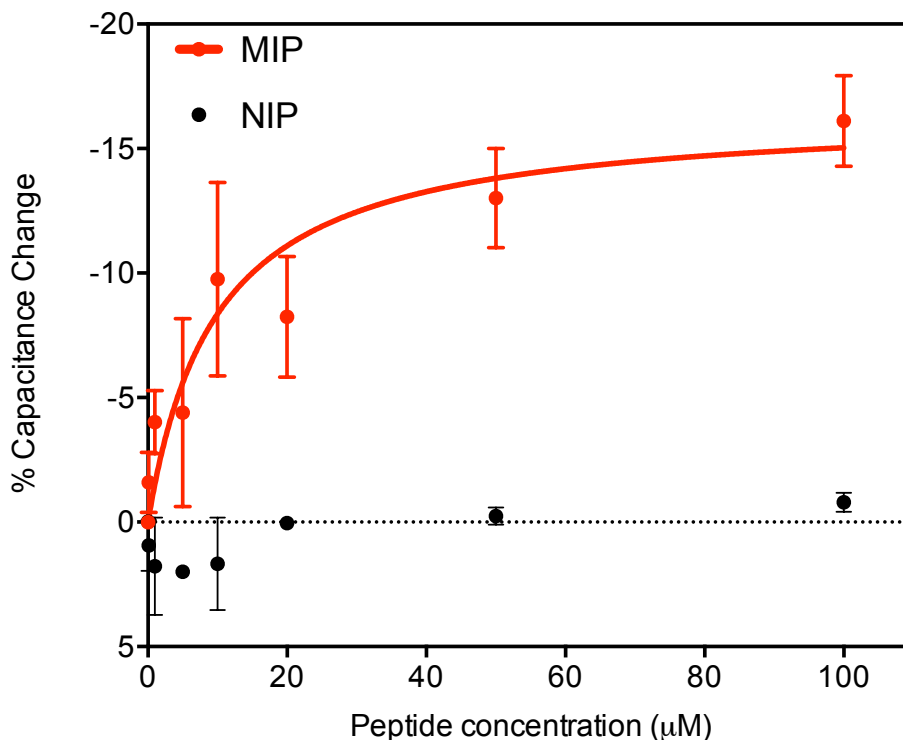
Figure 3. 41 Relative changes in capacitance of MIP and NIP electrode to different concentration of the pro-PSA peptide (APLILSR). MIP electrodes demonstrated a higher response when compared to NIP electrodes at the same concentration, which was indicative of an imprinting effect. (Data represents n=6 and error bars represent standard deviation.)

Although a good imprinting factor was observed with the MIP electrode, variation in response between electrodes led to large errors in aggregate data. The macro electrodes used for fabricating the MIPs are not uniform and the surface roughness varies depending on the level of polishing and cleaning.[103] It is hypothesised that the variations observed in the data could be a result of variations in the number of peptide molecules binding to the uneven gold surface, ultimately causing a change in the amount of polymer deposited as well as contributing to changes in the overall density of imprinted sites. It is anticipated that moving the fabrication process to a less-rough gold surface,

such as gold evaporated on to mica, would reduce variability between electrodes. Work was initiated with thin film electrodes from MicruX technologies (Spain), however, due to low stability of the electrodes post-polymerisation, further progress could not be reported. It should be noted that the NIP sensor was fabricated with only polydopmaine and subjected to similar template extraction conditions as MIP sensor. However, it is understood that the thickness of the polymer can vary depending on the SAM present on the surface of the electrode as discussed in section 2.4.3.2. As a result, the polymer thickness between MIP and NIP in this study could vary leading to an imperfect control. A closer control NIP sensor that could provide better understanding of MIP/NIP binding would be a NIP sensor made with MUA SAM layer only. However, achieving similar peptide-MUA versus MUA surface coverage could prove to be a challenge.

When compared to the bulk-imprinted mini-MIPs described in Chapter 2 for Fmoc-VANP epitope, an improvement in K_d and LOD was observed for surface imprinted the pro-PSA peptide MIPs (although the template are slightly different the backbone of the template remains the same). This suggests that surface imprinting is slightly more efficient that bulk imprinting technique for peptide imprinting. Although, an improvement in Kd and LOD was achieved, the LOD of the sensor meant that it would not be possible to use the system to detect the presence of the pro-PSA sequences in clinical samples where typical concentrations range from 1 to 10 ng/mL (1.42 - 14.2 nM).[56] The binding characteristics of the current system are similar to the peptide imprinted sensor produced by Dietrich *et al.* where the LOD and K_d were ~ 1 μM , 8.5 μM respectively.[8] Dietrich's sensor also showed early saturation at 12 μM, similar to the pro-PSA peptide MIP sensor.[8] This suggests that there could be an inherent limitation to

achieving higher affinities with peptide-imprinted sensors created with electropolymerised monomers. It is proposed that this could be due to the relatively limited functionality of electroactive monomers meaning that interactions between the template and monomer are heavily dependent on hydrogen bonding. Furthermore, it is hypothesised that the peptide molecules cannot form as strong π-π interactions with electroactive monomers as small aromatic molecules, suggesting that better designed electroactive monomers may be required to specifically target certain peptide functionality to achieve higher affinities.[23,29] Moving forward it would be better to use multifunctional electroactive monomers or employ a copolymerisation strategy to increase binding interactions to encourage the formation of high affinity imprinted sites.

3.4.5. *Sensor response with test peptide and cross-reactant peptide:*

To understand the selectivity of the sensor, a test-peptide was introduced in the system in a non-competitive assay. The test-peptide was made with a random amino acid sequence (TIVANP) containing 3 amino acids (I,A,P) matching the pro-PSA activation peptide sequence (APLILSR). Upon performing the binding study, the test peptide (TIVANP) showed an opposite behaviour to the pro-PSA peptide with the MIP electrode, that is a decrease in impedance upon binding was observed. The sensor displayed a 2 % change in capacitance when challenged with 1 μM test-peptide, while a maximum signal of 5 % was reported at 100 μM test-peptide. However, the response was lower and discriminatory than the signal change for 100 μM pro-PSA peptide (15 %) (Seen in Figure 3.42). The test peptide has an overall positive charge, which could potentially increase the ionic interaction between the polymer surface and the negatively charged redox couple ($Fe(CN)_6^{3-/4-}$) hence, decreasing the impedance of the sensor. It

was hypothesised that the decrease in impedance (increase in capacitance) could be due to a combination of the charge effect of the peptide as it non-specifically interacts with the surface of the polymer rather than the imprinted site and equilibration of the redox couple with the MIP surface.

To further challenge the selectivity of the sensor a potential cross-reactant peptide (VPLIQSR) was used in the selectivity study (non-competitive assay). The VPLIQSR peptide is the activation sequence from pro-hK2 (similar clearing mechanism as the pro-PSA activation sequence), which has only two amino acid mismatches with the pro-PSA peptide.[57] The peptide would be a potential cross-reactant in the clinical setting when measuring the pro-PSA peptide. The sensor showed a response of 6.32 % and 19 % when challenged with 1 μM and 100 μM pro-hK2 peptide respectively (Figure 3.42), which was slightly higher than the response observed with the template pro-PSA peptide sequence. This is not surprising given the close homology of the two sequences; the difference between valine and alanine is only one methyl group, making the sequence almost identical. It is hypothesised that the actual binding of pro-Hk2 peptide and the pro-PSA peptide to the imprinted sensor is fairly similar and the difference could be attributed to the low n value for the experiments.

Additional control study for understand the selectivity of the MIP sensor could be to fabricate a control MIP sensor with a test/cross-reactive peptide and challenging it with the template peptide to understand robustness of the fabricating technique and establishing selectivity of the sensor. However, this study was not conducted during the work.
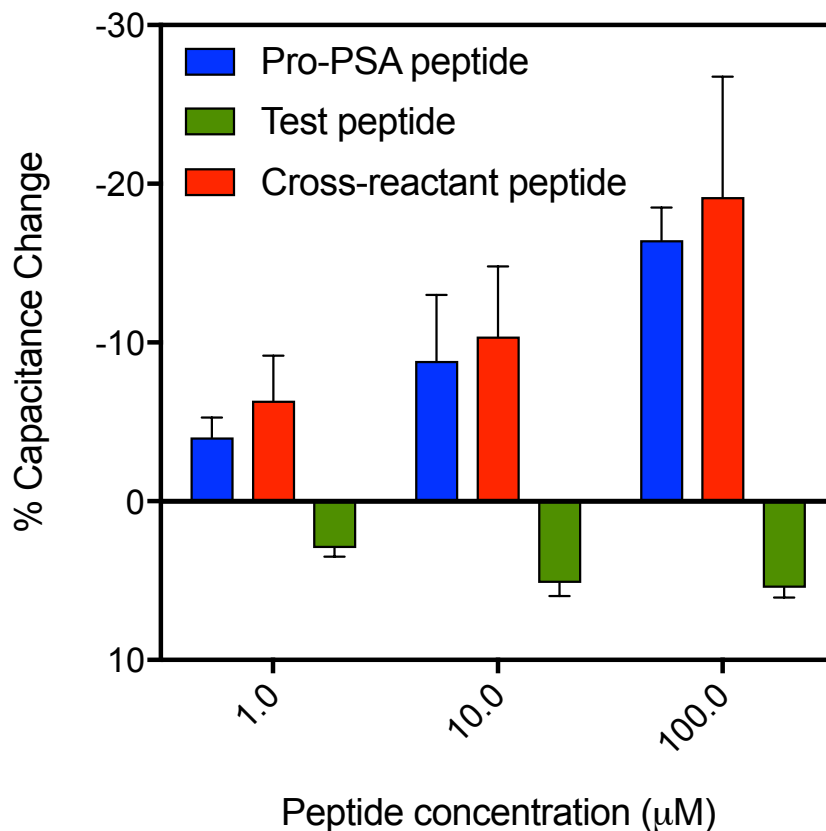
Figure 3. 42 The pro-PSA MIP sensor responses to test peptide and cross-reactant peptide in a non-competitive assay. The test peptide contained a random amino acid sequence (Threonine-Isoleucine-Valine-Alanine-Aspargine-Proline), which would demonstrate very low shape and chemical similarity to the pro-PSA activation peptide. Hence, it was expected that the MIP sensor would not recognise the test peptide. The sensor displayed some response towards the test peptide however it was a non –specific binding response. The MIP electrode failed to distinguish between cross-reactant (pro-hK2) peptide and the pro-PSA activation sequence which had greater than 90% sequence similarity. Data represents n=4 and error bars represent standard deviation.

3.4.6. Conventional MIP performance (non-surface immobilised template)

The purpose of this study was to understand whether confining the peptide to the surface using MUA tag offered any significant advantage over conventional imprinting protocols where the template is simply entrapped and randomly incorporated within the polymer (no surface confinement). The majority of surface imprinted technique in literature have not utilised immobilised or orientated template for fabrication of imprinted sensors. Hence, it was important to understand the difference in the two techniques. The protocol for the conventional imprinting of the pro-PSA peptide was adopted from literature studies for direct comparison. An equimolar concentration of the template and monomer was used in an attempt to maximise the amount of the template ultimately entrapped within the polymer during polymerisation. The number cycles were restricted to 15 so as to encourage the template entrapment while producing a relatively thin layer of polymer to maximise signal transduction. As is evident from Figure 3.43, the limit of detection for the conventionally imprinted system was 10 μM pro-PSA peptide compared to 1μM for the surface immobilised imprinted MIP. It is likely that despite the higher template concentrations being used during the imprinting process and a greater number of polymerisation a cycle, fewer peptide molecules become entrapped into the polymer. Furthermore, it is proposed that the peptide molecules are entrapped randomly throughout polymer layers meaning that binding sites are distributed throughout, thus providing an additional diffusional barrier in the rebinding process. This suggests that surface immobilisation of the template provides the advantage of carefully controlling the polymer thickness while hopefully encouraging localisation of binding sites at the surface, thus providing improved access for the template on

rebinding. Additionally, the resistance of conventional NIP to the peptide indicates the

low non-specific binding (2 % for 100 µM peptide) of polydopamine to the peptide.
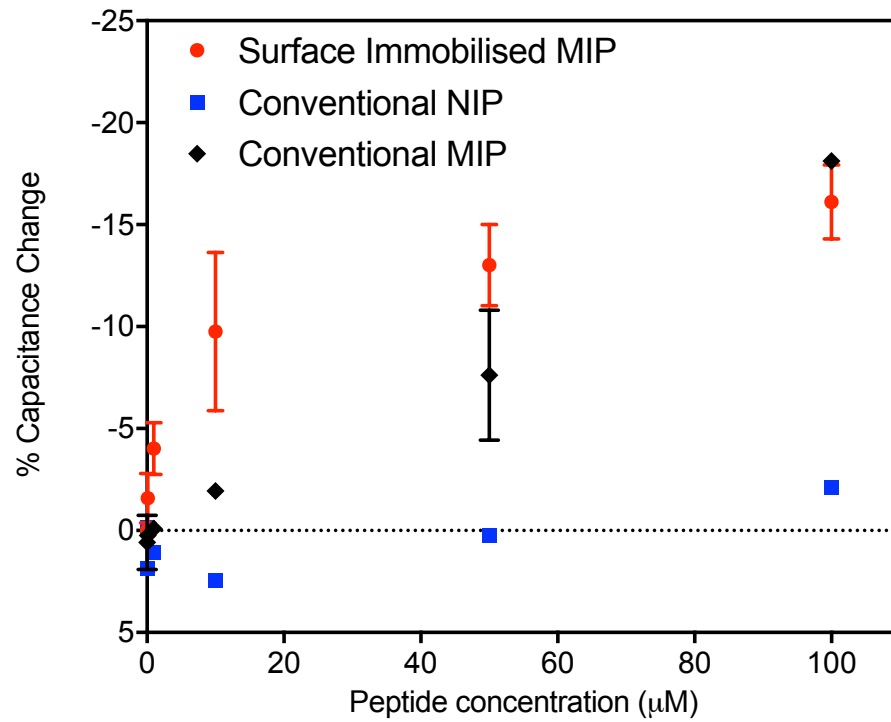
Figure 3. 43 Response of conventionally prepared pro-peptide MIP/NIP sensors. Data

represents n=3 and error bars represent standard deviation.

214

3.5. Conclusion:

In conclusion, a pro-PSA activation sequence imprinted sensor was fabricated with an LOD of 1 μM and Kd of 9.2 μM. The sensor showed a good imprinting factor (IF = 14) when compared to its non-imprinted counterpart and could also discriminate a random peptide sequence possessing 50 % sequence homology. When comparing with a conventional MIP sensor the oriented template MIP sensor had 10 times higher sensitivity. This suggests that using an oriented, the surface-confined template during the imprinting process helps to improve the overall sensitivity of the sensor. Despite not being sensitive enough to detect clinically relevant concentrations of the peptide, this technique could be extended to other peptides/ small molecule biomarkers, which are typically present at higher concentrations (μg/ml - mg/ml) in clinical samples.

3.6. References

1.   Panasyuk, T. L., Mirsky, V. M., Piletsky, S. A. & Wolfbeis, O. S. Electropolymerized Molecularly Imprinted Polymers as Receptor Layers in Capacitive Chemical Sensors. *Anal. Chem.* **71,** 4609–4613 (1999).

2.   Blanco-López, M. C., Lobo-Castañón, M. J., Miranda-Ordieres, A. J. & Tuñón-Blanco, P. Electrochemical sensors based on molecularly imprinted polymers. *TrAC Trends Anal. Chem.* **23,** 36–48 (2004).

3.   Özcan, L. & Şahin, Y. Determination of paracetamol based on electropolymerized-molecularly imprinted polypyrrole modified pencil graphite electrode. *Sens. Actuators B Chem.* **127,** 362–369 (2007).

4.   Liu, K., Wei, W.-Z., Zeng, J.-X., Liu, X.-Y. & Gao, Y.-P. Application of a novel electrosynthesized polydopamine-imprinted film to the capacitive sensing of nicotine. *Anal. Bioanal. Chem.* **385,** 724–729 (2006).

5.   Tretjakov, A. *et al.* Surface molecularly imprinted polydopamine films for recognition of immunoglobulin G. *Microchim. Acta* **180,** 1433–1442 (2013).

6.   Yilmaz, null, Haupt, null & Mosbach, null. The Use of Immobilized Templates-A New Approach in Molecular Imprinting. *Angew. Chem. Int. Ed Engl.* **39,** 2115–2118 (2000).

7.   Nishino, H., Huang, C.-S. & Shea, K. J. Selective protein capture by epitope imprinting. *Angew. Chem. Int. Ed Engl.* **45,** 2392–2396 (2006).

8.   Dechtrirat, D., Jetzschmann, K. J., Stöcklein, W. F. M., Scheller, F. W. & Gajovic-Eichelmann, N. Protein Rebinding to a Surface-Confined Imprint. *Adv. Funct. Mater.* **22,** 5231–5237 (2012).

9.   Turner, N. W. *et al.* From 3D to 2D: a review of the molecular imprinting of proteins. *Biotechnol. Prog.* **22,** 1474–1489 (2006).

10.   Bossi, A., Piletsky, S. A., Piletska, E. V., Righetti, P. G. & Turner, A. P. F. Surface-Grafted Molecularly Imprinted Polymers for Protein Recognition. *Anal. Chem.* **73,** 5281–5286 (2001).

11.   Bowen, J. L., Kelly, M. A., Gumbleton, M., Davies, P. R. & Allender, C. J. A simple zero length surface-modification approach for preparing novel bifunctional supports for co-immobilisation studies. *Tetrahedron Lett.* **53,** 3727–3730 (2012).

12.   Sharma, P. S., Pietrzyk-Le, A., D'Souza, F. & Kutner, W. Electrochemically synthesized polymers in molecular imprinting for chemical sensing. *Anal. Bioanal. Chem.* **402,** 3177–3204 (2012).

13.   Piletsky, S. A. *et al.* Atrazine sensing by molecularly imprinted membranes. *Biosens. Bioelectron.* **10,** 959–964 (1995).

14.   Hedborg, E., Winquist, F., Lundström, I., Andersson, L. I. & Mosbach, K. Some studies of molecularly-imprinted polymer membranes in combination with field-effect devices. *Sens. Actuators Phys.* **37,** 796–799 (1993).

15.   Blanco-López, M. C., Lobo-Castañón, M. J., Miranda-Ordieres, A. J. & Tuñón-Blanco, P. Voltammetric sensor for vanillylmandelic acid based on molecularly imprinted polymer-modified electrodes. *Biosens. Bioelectron.* **18,** 353–362 (2003).

16.   Andrea, P., Miroslav, S., Silvia, S. & Stanislav, M. A solid binding matrix/molecularly imprinted polymer-based sensor system for the determination of clenbuterol in bovine liver using differential-pulse voltammetry. *Sens. Actuators B Chem.* **76,** 286–294 (2001).

17.   Malitesta, C., Losito, I. & Zambonin, P. G. Molecularly Imprinted Electrosynthesized Polymers: New Materials for Biomimetic Sensors. *Anal. Chem.* **71,** 1366–1370 (1999).

18.   Putzbach, W. & Ronkainen, N. J. Immobilization Techniques in the Fabrication of Nanomaterial-Based Electrochemical Biosensors: A Review. *Sensors* **13,** 4811–4840 (2013).

19.   Bidan, G. in *Electropolymerization* (eds. Cosnier, S. & Karyakin, A.) 1–26 (Wiley-VCH Verlag GmbH & Co. KGaA, 2010).

20.   Sarac, A. S. in *Encyclopedia of Polymer Science and Technology* (John Wiley & Sons, Inc., 2002).

21.   Haupt, K. & Mosbach, K. Molecularly Imprinted Polymers and Their Use in Biomimetic Sensors. *Chem. Rev.* **100,** 2495–2504 (2000).

22.   Spurlock, L. D., Jaramillo, A., Praserthdam, A., Lewis, J. & Brajter-Toth, A. Selectivity and sensitivity of ultrathin purine-templated overoxidized polypyrrole film electrodes. *Anal. Chim. Acta* **336,** 37–46 (1996).

23.   Ebarvia, B. S., Cabanilla, S. & Sevilla III, F. Biomimetic properties and surface studies of a piezoelectric caffeine sensor based on electrosynthesized polypyrrole. *Talanta* **66,** 145–152 (2005).

24.   Choong, C.-L. & Milne, W. I. Dynamic modulation of detection window in conducting polymer based biosensors. *Biosens. Bioelectron.* **25,** 2384–2388 (2010).

25.   Molecularly imprinted polypyrrole prepared by electrodeposition for the selective recognition of tryptophan enantiomers - Kong - 2009 - Journal of Applied Polymer Science - Wiley Online Library. (Accessed: 27th July 2016)

26.   Pietrzyk, A., Suriyanarayanan, S., Kutner, W., Chitta, R. & D'Souza, F. Selective Histamine Piezoelectric Chemosensor Using a Recognition Film of the Molecularly Imprinted Polymer of Bis(bithiophene) Derivatives. *Anal. Chem.* **81,** 2633–2643 (2009).

27.   Pietrzyk, A. *et al.* Molecularly imprinted poly[bis(2,2′-bithienyl)methane] film with built-in molecular recognition sites for a piezoelectric microgravimetry chemosensor for selective determination of dopamine. *Bioelectrochemistry* **80,** 62–72 (2010).

28.   Menaker, A. *et al.* Electrosynthesized Surface-Imprinted Conducting Polymer Microrods for Selective Protein Recognition. *Adv. Mater.* **21,** 2271–2275 (2009).

29.   Sallacan, N., Zayats, M., Bourenko, T., Kharitonov, A. B. & Willner, I. Imprinting of Nucleotide and Monosaccharide Recognition Sites in Acrylamidephenylboronic Acid−Acrylamide Copolymer Membranes Associated with Electronic Transducers. *Anal. Chem.* **74,** 702–712 (2002).

30.   Rick, J. & Chou, T.-C. Using protein templates to direct the formation of thin-film polymer surfaces. *Biosens. Bioelectron.* **22,** 544–549 (2006).

31.   Liu, Y. T. *et al.* Electrochemical sensor based on a poly(para-aminobenzoic acid) film modified glassy carbon electrode for the determination of melamine in milk. *Electrochimica Acta* **56,** 4595–4602 (2011).

32.   Lu, C.-H. *et al.* Sensing HIV related protein using epitope imprinted hydrophilic polymer coated quartz crystal microbalance. *Biosens. Bioelectron.* **31,** 439–444 (2012).

33.   Li, J., Zhao, J. & Wei, X. A sensitive and selective sensor for dopamine determination based on a molecularly imprinted electropolymer of o-aminophenol. *Sens. Actuators B Chem.* **140,** 663–669 (2009).

34.   Moreira, F. T. C. *et al.* Protein-responsive polymers for point-of-care detection of cardiac biomarker. *Sens. Actuators B Chem.* **196,** 123–132 (2014).

35.   Dechtrirat, D., Gajovic-Eichelmann, N., Bier, F. F. & Scheller, F. W. Hybrid Material for Protein Sensing Based on Electrosynthesized MIP on a Mannose Terminated Self-Assembled Monolayer. *Adv. Funct. Mater.* **24,** 2233–2239 (2014).

36.   Cai, D. *et al.* A molecular imprint nanosensor for ultrasensitive detection of proteins. *Nat. Nanotechnol.* **5,** 597–601 (2010).

37.   Wang, Z., Kang, J., Liu, X. & Ma, Y. Capacitive Detection of Theophylline Based on Electropolymerized Molecularly Imprinted Polymer. *Int. J. Polym. Anal. Charact.* **12,** 131–142 (2007).

38.   Granot, E., Tel-Vered, R., Lioubashevski, O. & Willner, I. Stereoselective and Enantioselective Electrochemical Sensing of Monosaccharides Using Imprinted Boronic Acid-Functionalized Polyphenol Films. *Adv. Funct. Mater.* **18,** 478–484 (2008).

39.   Cheng, Z., Wang, E. & Yang, X. Capacitive detection of glucose using molecularly imprinted polymers. *Biosens. Bioelectron.* **16,** 179–185 (2001).

40.   Feng, L., Liu, Y., Tan, Y. & Hu, J. Biosensor for the determination of sorbitol based on molecularly imprinted electrosynthesized polymers. *Biosens. Bioelectron.* **19,** 1513–1519 (2004).

41.   Karimian, N. *et al.* An ultrasensitive molecularly-imprinted human cardiac troponin sensor. *Biosens. Bioelectron.* **50,** 492–498 (2013).

42.   Balasubramania, S. G. Development of Smart Functional Surfaces for Biosensor Applications. (2008).

43.   Thévenot, D. R., Toth, K., Durst, R. A. & Wilson, G. S. Electrochemical biosensors: recommended definitions and classification1. *Biosens. Bioelectron.* **16,** 121–131 (2001).

44.   Calvo, E. J. in *Comprehensive Chemical Kinetics* (ed. Compton, C. H. B. and R. G.) **26,** 1–78 (Elsevier, 1986).

45.   Kissinger, P. & Heineman, W. R. *Laboratory Techniques in Electroanalytical Chemistry, Second Edition, Revised and Expanded*. (CRC Press, 1996).

46.   Bard, Allen J. *Wiley: Electrochemical Methods: Fundamentals and Applications, 2nd Edition - Allen J. Bard, Larry R. Faulkner*. (John Wiley & Sons, Ltd, 1980).

47.   Morrison, S. R. Electrochemistry at semiconductor and oxidized metal electrodes. (1980).

48.   Stojek, Z. in *Electroanalytical Methods* (eds. Scholz, P. D. F. et al.) 3–9 (Springer Berlin Heidelberg, 2010). doi:10.1007/978-3-642-02915-8_1

49.   *Understanding Voltammetry* i–xv (IMPERIAL COLLEGE PRESS, 2011).

50.   Heinze, J. Cyclic Voltammetry—'Electrochemical Spectroscopy'. New Analytical Methods (25). *Angew. Chem. Int. Ed. Engl.* **23,** 831–847 (1984).

51.   Lisdat, F. & Schäfer, D. The use of electrochemical impedance spectroscopy for biosensing. *Anal. Bioanal. Chem.* **391,** 1555–1567 (2008).

52.   Orazem, M. E. & Tribollet, B. *Electrochemical Impedance Spectroscopy.* (John Wiley & Sons, 2011).

53.   ErtuğruL, H. D. & Uygun, Z. O. Impedimetric Biosensors for Label-Free and Enzymless Detection. (2013).

54.   Krause, S. in *Encyclopedia of Electrochemistry* (Wiley-VCH Verlag GmbH & Co. KGaA, 2007).

55.   Jorcin, J.-B., Orazem, M. E., Pébère, N. & Tribollet, B. CPE analysis by local electrochemical impedance spectroscopy. *Electrochimica Acta* **51,** 1473–1479 (2006).

56.   Mikolajczyk, S. D. *et al.* A precursor form of PSA (pPSA) is a component of the free PSA in prostate cancer serum. *Urology* **50,** 710–714 (1997).

57.   Denmeade, S. R., Lövgren, J., Khan, S. R., Lilja, H. & Isaacs, J. T. Activation of latent protease function of pro-hK2, but not pro-PSA, involves autoprocessing. *The Prostate* **48,** 122–126 (2001).

58.   Heidegger, I. *et al.* [-2]proPSA is an early marker for prostate cancer aggressiveness. *Prostate Cancer Prostatic Dis.* **17,** 70–74 (2014).

59.   Filella, X. & Giménez, N. Evaluation of [-2] proPSA and Prostate Health Index (phi) for the detection of prostate cancer: a systematic review and meta-analysis. *Clin. Chem. Lab. Med.* **51,** 729–739 (2013).

60.   Le, B. V. *et al.* [−2] Pro-psa is more accurate than total and free psa in differentiating prostate cancer from benign disease in a prospective prostate cancer screening study,. *J. Urol.* **183,** 1355–1359 (2010).

61.   Jansen, F. H. *et al.* Screening for Prostate Cancer in 2008 II: The Importance of Molecular Subforms of Prostate-Specific Antigen and Tissue Kallikreins. *Eur. Urol.* **55,** 563–574 (2009).

62.   Voeghtly, L. M. *et al.* Potential Clinical Importance of the Activation Peptide of Prostate-specific Antigen. *Int. J. Clin. Exp. Pathol.* **2,** 588–598 (2009).

63.   Balk, S. P., Ko, Y.-J. & Bubley, G. J. Biology of prostate-specific antigen. *J. Clin. Oncol. Off. J. Am. Soc. Clin. Oncol.* **21,** 383–391 (2003).

64.   Campuzano, S., Pedrero, M., Montemayor, C., Fatás, E. & Pingarrón, J. M. Characterization of alkanethiol-self-assembled monolayers-modified gold electrodes by electrochemical impedance spectroscopy. *J. Electroanal. Chem.* **586,** 112–121 (2006).

65.   Mendoza, S. M., Arfaoui, I., Zanarini, S., Paolucci, F. & Rudolf, P. Improvements in the characterization of the crystalline structure of acid-terminated alkanethiol self-assembled monolayers on Au(111). *Langmuir ACS J. Surf. Colloids* **23,** 582–588 (2007).

66.   King, D. S., Fields, C. G. & Fields, G. B. A cleavage method which minimizes side reactions following Fmoc solid phase peptide synthesis. *Int. J. Pept. Protein Res.* **36,** 255–266 (1990).

67.   Amblard, M., Fehrentz, J.-A., Martinez, J. & Subra, G. Methods and protocols of modern solid phase Peptide synthesis. *Mol. Biotechnol.* **33,** 239–254 (2006).

68.   Stathopoulos, P., Papas, S., Sakka, M., Tzakos, A. G. & Tsikaris, V. A rapid and efficient method for the synthesis of selectively S-Trt or S-Mmt protected Cys-containing peptides. *Amino Acids* **46,** 1367–1376 (2014).

69.   Sreejivungsa, K. *et al.* Light-Regulated Release of Entrapped Drugs from Photoresponsive Gold Nanoparticles, Light-Regulated Release of Entrapped Drugs from Photoresponsive Gold Nanoparticles. *J. Nanomater. J. Nanomater.* **2016, 2016,** e4964693 (2016).

70.   Kamon, Y., Matsuura, R., Kitayama, Y., Ooya, T. & Takeuchi, T. Precisely controlled molecular imprinting of glutathione-s-transferase by orientated template immobilization using specific interaction with an anchored ligand on a gold substrate. *Polym. Chem.* **5,** 4764–4771 (2014).

71.   Lv, Y., Tan, T. & Svec, F. Molecular imprinting of proteins in polymers attached to the surface of nanomaterials for selective recognition of biomacromolecules. *Biotechnol. Adv.* **31,** 1172–1186 (2013).

72.   Zhou, W.-H. *et al.* Mussel-inspired molecularly imprinted polymer coating superparamagnetic nanoparticles for protein recognition. *J. Mater. Chem.* **20,** 880–883 (2010).

73.   Tang, A., Duan, L., Liu, M. & Dong, X. An epitope imprinted polymer with affinity for kininogen fragments prepared by metal coordination interaction for cancer biomarker analysis. *J. Mater. Chem. B* **4,** 7464–7471 (2016).

74.   Nicholls, I. A. & Rosengren, J. P. Molecular imprinting of surfaces. *Bioseparation* **10,** 301–305 (2001).

75.   Nakanishi, K., Sakiyama, T. & Imamura, K. On the adsorption of proteins on solid surfaces, a common but very complicated phenomenon. *J. Biosci. Bioeng.* **91,** 233–244 (2001).

76.   Ball, V. *et al.* Deposition Mechanism and Properties of Thin Polydopamine Films for High Added Value Applications in Surface Science at the Nanoscale. *BioNanoScience* **2,** 16–34 (2011).

77.   Peng, H., Yin, F., Zhou, A. & Yao, S. Characterization of electrosynthesized poly- (o-aminophenol) as a molecular imprinting material for sensor preparation by means of quartz crystal impedance analysis. *Anal. Lett.* **35,** 435–450 (2002).

78.   Gvozdenović, M. M., Jugović, B. Z., Stevanović, J. S., Trišović, T. L. & Grgur, B. N. Electrochemical Polymerization of Aniline. Electropolymerization, Dr. Ewa Schab-Balcerzak (Ed.), *InTech*, (2011).

79.   Rourke, F. & Crayston, J. A. Cyclic voltammetry and morphology of polyaniline-coated electrodes containing [Fe(CN)6]3–/4– ions. *J. Chem. Soc. Faraday Trans.* **89,** 295–302 (1993).

80.   Łuczak, T. Preparation and characterization of the dopamine film electrochemically deposited on a gold template and its applications for dopamine sensing in aqueous solution. *Electrochimica Acta* **53,** 5725–5731 (2008).

81.   Li, Y., Liu, M., Xiang, C., Xie, Q. & Yao, S. Electrochemical quartz crystal microbalance study on growth and property of the polymer deposit at gold electrodes during oxidation of dopamine in aqueous solutions. *Thin Solid Films* **497,** 270–278 (2006).

82.   Wen, X.-L., Jia, Y.-H. & Liu, Z.-L. Micellar effects on the electrochemistry of dopamine and its selective detection in the presence of ascorbic acid. *Talanta* **50,** 1027–1033 (1999).

83.   Guenbour, A., Kacemi, A., Benbachir, A. & Aries, L. Electropolymerization of 2-aminophenol: Electrochemical and spectroscopic studies. *Prog. Org. Coat.* **38,** 121–126 (2000).

84.   Fischer, A. E., Saunders, M. P., Lytle, J. C., Rolison, D. R. & Long, J. Self-Limiting Electropolymerization of o-Aminophenol on Ultraporous Carbon Nanoarchitectures for Electrochemical Capacitor Applications. *ECS Trans.* **6,** 159–164 (2008).

85.   Barbero, C., Silber, J. J. & Sereno, L. Formation of a novel electroactive film by electropolymerization of ortho-aminophenol. *J. Electroanal. Chem. Interfacial Electrochem.* **263,** 333–352 (1989).

86.   Thiemann, C. & Brett, C. M. A. Electropolymerisation and properties of conducting polymers derived from aminobenzenesulphonic acids and from mixtures with aniline. *Synth. Met.* **125,** 445–451 (2001).

87.   Conducting polymers from aminobenzoic acids and aminobenzenesulphonic acids: influence of pH on electrochemical behaviour. Available at: http://www.sciencedirect.com/science/article/pii/S0022072802012159. (Accessed: 31st July 2016)

88.   A DNA diagnostic biosensor: development, characterisation and performance. Available at: http://www.sciencedirect.com/science/article/pii/S0925400500004688. (Accessed: 31st July 2016)

89.   Lynge, M. E., Westen, R. van der, Postma, A. & Städler, B. Polydopamine—a nature-inspired polymer coating for biomedical science. *Nanoscale* **3,** 4916–4928 (2011).

90.   Liu, Y. *et al.* Polydopamine-assisted deposition of heparin for selective adsorption of low-density lipoprotein. *RSC Adv.* **5,** 12922–12930 (2015).

91.   Campuzano, S., Pedrero, M., Montemayor, C., Fatás, E. & Pingarrón, J. M. Characterization of alkanethiol-self-assembled monolayers-modified gold electrodes by electrochemical impedance spectroscopy. *J. Electroanal. Chem.* **586,** 112–121 (2006).

92.   Stöckle, B. *et al.* Precise Control of Polydopamine Film Formation by Electropolymerization. *Macromol. Symp.* **346,** 73–81 (2014).

93.   Spégel, C. *et al.* On-Chip Determination of Dopamine Exocytosis Using Mercaptopropionic Acid Modified Microelectrodes. *Electroanalysis* **19,** 263–271 (2007).

94.   Steel, A. B., Herne, T. M. & Tarlov, M. J. Electrochemical quantitation of DNA immobilized on gold. *Anal. Chem.* **70,** 4670–4677 (1998).

95.   Eckermann, A. L., Feld, D. J., Shaw, J. A. & Meade, T. J. Electrochemistry of redox-active self-assembled monolayers. *Coord. Chem. Rev.* **254,** 1769–1802 (2010).

96.   Shin-ichiro Imabayashi *et al.* Reductive desorption of carboxylic-acid-terminated alkanethiol monolayers from Au(111) surfaces. *J. Electroanal. Chem.* **428,** 33–38 (1997).

97.   Kawaguchi, T., Yasuda, H., Shimazu, K. & Porter, M. D. Electrochemical Quartz Crystal Microbalance Investigation of the Reductive Desorption of Self-Assembled Monolayers of Alkanethiols and Mercaptoalkanoic Acids on Au. *Langmuir* **16,** 9830–9840 (2000).

98.   Imabayashi, S., Hobara, D., Kakiuchi, T. & Knoll, W. Selective Replacement of Adsorbed Alkanethiols in Phase-Separated Binary Self-Assembled Monolayers by Electrochemical Partial Desorption. *Langmuir* **13,** 4502–4504 (1997).

99.   Electrochemical Desorption of Proteins from Gold Electrode Surface - Balasubramanian - 2006 - Electroanalysis - Wiley Online Library. (Accessed: 2nd August 2016)

100.   Jolly, P. *et al.* Aptamer-MIP hybrid receptor for highly sensitive electrochemical detection of prostate specific antigen. *Biosens. Bioelectron.* **75,** 188–195 (2016).

101.   Valincius, G., Meškauskas, T. & Ivanauskas, F. Electrochemical impedance spectroscopy of tethered bilayer membranes. *Langmuir ACS J. Surf. Colloids* **28,** 977–990 (2012).

102.   Roling, B., Drüschler, M. & Huber, B. Slow and fast capacitive process taking place at the ionic liquid/electrode interface. *Faraday Discuss.* **154,** 303-311-333, 465–471 (2012).

103.   Miodek, A. *et al.* Optimisation and Characterisation of Anti-Fouling Ternary SAM Layers for Impedance-Based Aptasensors. *Sensors* **15,** 25015–25032 (2015).

4. Chapter: Development of Hybrid Receptor for Electrochemical Detection of PSA

4.1. Introduction

4.1.1. General overview

Protein imprinting is a challenging area of molecular imprinting due to their large size and complex nature and has been one of the stumbling blocks in realising the full potential of MIPs as a feasible alternative to antibodies.[1] Challenges associated with protein imprinting have been highlighted in Chapter 1. Chapter 2 and 3 explored epitope imprinting of PSA protein as an alternative to whole protein imprinting, however, some of the biggest challenges with epitope imprinting were maintaining the conformation of the epitope with respect to whole protein, solubility in conventional solvents and sensitivity of the imprinted system to detect clinically relevant concentrations. An alternative approach proposed by our lab was to build a more sophisticated type of bio-receptor with an improved affinity using a technique termed hybrid imprinting.[2] Hence, the chapter explores surface imprinting of PSA using aptamers as 'super monomers' in the hybrid imprinting strategy. An electrochemical sensor was built with the hybrid receptor (apta-MIP) as the recognition unit and evaluated for detection of PSA. This project was carried out in collaboration with colleagues at the University of Bath, Dr. P. Estrela and Dr. P. Jolly and results of this study have been published in "Aptamer–MIP hybrid receptor for highly sensitive electrochemical detection of prostate specific antigen", Biosensors and Bioelectronics, Volume 75, 15 January 2016, Pages 188-195.

4.1.2. Hybrid molecular imprinting:

Hybrid imprinting utilises a bio-receptor, with an established affinity towards the template, to confine the template in its preferred conformation during the imprinting

process. Post extraction of the template, the polymeric cavity lined with the bio-receptor displays a higher affinity than the bio-receptor or MIP alone.[3] The hybrid imprinting technique allows for localisation of the template in its preferred conformation allowing for the formation of uniform binding sites which improves the binding characteristics of the hybrid-MIP.[4] Furthermore, it is proposed that the bio-receptor receptor acts synergistically with the polymer to lend higher affinity to the resulting imprinted polymer. Bowen *et al.* used Merrifield resin to co-immobilise iniferters and peptide (as the receptor) for application in hybrid imprinting.[2] The short peptide (polymyxin) was used to trap LPS (lipopolysaccharide) on the resin while the iniferter enabled control growth of a surface 'imprinting' polymer layer. It was proposed that the covalently immobilised peptide conferred greater selectivity to the resulting polymer. An imprinting effect was observed with hybrid polymyxin MIPs demonstrating an improved binding affinity compared to polymyxin alone. Over the years, various other groups have successfully demonstrated hybrid imprinting using aptamers[5,6], lectins[7] and small molecules[4] for proteins with varying degrees of success.

4.1.3. Aptamers

Aptamers are short oligonucleotide sequences resulting from SELEX (systematic evolution of ligands by exponential enrichment) process displaying high affinity for their target molecules.[8] The word aptamer is derived from the Latin word 'aptus' which means to fit which is appropriate as the aptamer fit into their target much like the lock-and-key analogy from enzymes.[9] SELEX technology identifies particular nucleotide sequences, from an extensive library of oligonucleotide sequences, which bind to a target, through an iterative process of *in vitro* selection and amplification (Figure 4.1).[10]

Using this technology aptamers can be raised for a variety of targets in a short period of time. The expiry of patents on SELEX technology has triggered much-needed research in this field.
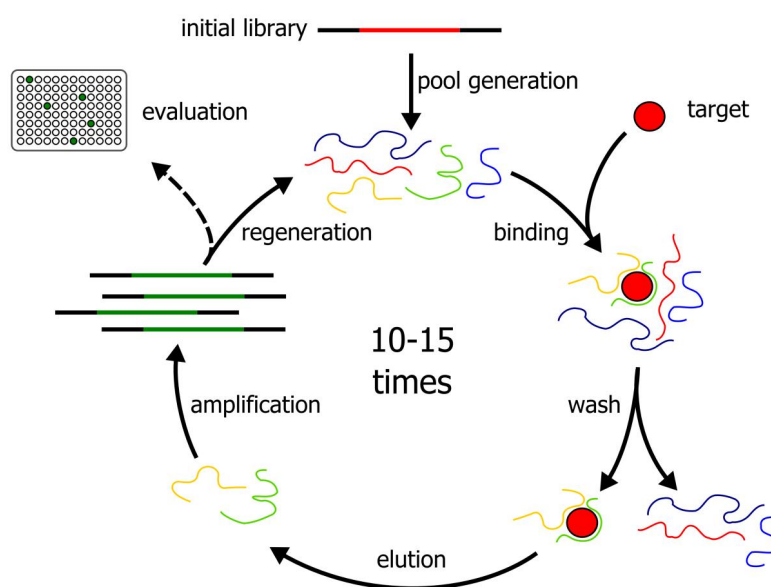
Figure 4. 1 Generation of aptamers using the SELEX process. The aptamers are chosen from a pool of nucleotides sequence and checked for binding to the target repeatedly till a high-affinity sequence is identified and amplified. Figure adapted from (http://www.creative-biogene.com/Services/Aptamers/Technology-Platforms.html)

Aptamers target the molecules at an atomic level by changing conformation upon binding to form a pocket for the ligand to fit in, allowing them to discriminate closely related molecules.[11] Certain functional groups on the aptamer come into close proximity upon the conformational change, which favours binding to the target. This is a simple explanation for the binding mechanism for small molecule aptamers. However, the structural basis for specific discrimination in cases of complex molecules such as proteins could be based on the combination of different effects such as pi-pi stacking,

hydrogen bonding, electrostatic interactions and shape similarity.[11,12] While there is a complete change in conformation of the aptamer to form a pocket surrounding the target in case of small molecules[13], the protein aptamer interactions are confined to a smaller region with unique interactions between the nucleotides and amino acids.[14] This difference in binding can be well exploited in hybrid protein imprinting to create polymer cavities with steric and chemical selectivity towards the protein.

4.1.4. Aptamers for hybrid imprinting

Use of a peptide as the bioreceptors for hybrid imprinting was observed to be challenging due to rigid conformation adopted by peptides and the difficulty in finding peptide receptors with high template affinity. Aptamers have various advantages over antibodies/peptides as the choice of bioreceptors for diagnostic and sensing applications. They are produced by chemical synthesis with high accuracy and reproducibility and can be chemically modified for different sensing platforms.[10] They are chemically stable at room temperature and have a longer shelf life than antibodies.[8] They can be regenerated for use by denaturing them at high temperatures and they are more flexible in their structure as compared to peptides. The chemical stability of the aptamers also makes them a good choice for the receptor as they can withstand harsh washing conditions required for template removal in MIP fabrication. Aptamers also face certain drawbacks such as they are easily denatured by nuclease enzymes and they demonstrate optimum binding only in buffers used for raising them, making their application for sensing somewhat limited. It is proposed that by combining aptamers with MIPs drawbacks of both technologies could be overcome to generate sensitive and efficient synthetic receptors. Wei *et al.* first used the aptamers in a double imprinting method to

detect Apple Stem Pitting Virus (ASPV).[5] Polymerisable aptamers were first used to isolate the virus and subsequently build an imprinted hydrogel. The resulting hydrogel was engineered into a diffraction-gating sensor using imprinting lithography. The sensor showed comparable sensitivity to ELISA with LOD of 10 ng/ml. Similarly, Poma *et al.* used polymerisable aptamers for surface imprinting of cocaine which, was detected by QCM sensor.[3] The apta-MIP nanoparticles were produced by polymerising acrylated aptamers on surface immobilised template and eluting them post polymerisation. The apta-MIPs nanoparticles showed a higher affinity (apparent Kd of 26.4 mM) than aptamer only / MIP only nanoparticles suggesting an improved effect due to the aptamer integration into the polymer. The study also demonstrated that the aptamers were protected from enzymatic degradation inside the polymer, as incubation with endonucleases did not alter the binding capability of MIP nano-particles. Both studies demonstrated the scope for hybrid aptamer imprinting for protein imprinting application.

4.1.5. PSA aptamer

Savory *et al.* first developed the fPSA aptamer that was used in the current study.[15] The group studied the use of a genetic algorithm to increase the selectivity and sensitivity of aptamers selected by the SELEX process.[15] Five aptamers were found, out of which one showed 48 times higher binding than the parent sequence. The PSA aptamer is a 34-nucleotide sequence, which forms a stable loop secondary structure (Figure 4.2) on binding to fPSA as predicted by Mfold program (prediction based on lowering of Gibbs free energy). The binding affinity, K_d of 40 nM, was determined using ELISA and LOD

of 10 nM was reported. However, the exact mechanism of PSA binding to the aptamer

has yet to be elucidated.

Figure 4. 2: PSA aptamer folds into a secondary structure upon binding to PSA predicted by

Mfold program, obtained from Savory et al. (2010),[15] with permission from Elsevier.

Various groups have investigated this particular aptamer for fPSA detection using

different sensing platforms such as optical, piezoelectric and electrochemical. A

summary of published literature demonstrating the use of aptamer for electrochemical

detection of PSA has been listed in Table 4.1. It can be observed that the PSA aptamer is

highly sensitive for PSA detection on various electrochemical platforms.

Sensing Platform: Electrochemical	Detection technique	Sensing strategy	LOD
Glassy carbon electrodes	DPV, CV	Gold NPs immobilised on mesoporous carbon deposited on GCE followed by immobilisation streptavidin and biotinylated aptamer.[16]	7.6 pM
Gold electrodes	EIS	Co-immobilisation sulfobetaine SAM with thiolated aptamers.[17]	30 pM
Gold electrodes	Squarewave voltammetry	Deposition of polymer to covalently attach amine terminated aptamers.[18]	33 pM
Gold electrodes	EIS	Use of DNA hybridisation for immobilisation of DNA aptamers.[19]	0.1 pM

GCE	Electrochemical: DPV/EIS	Graphene chitosan composite deposited on GCE to form antibody-PSA-aptamer (biotin) sandwich assay.[20]	DPV: 300aM EIS: 150fM
Gold surface on silicon dioxide/lithium tantalite wafer	Electrochemical: Love-wave sensor	$LiTaO_3$ substrate with SiO_2 film as wave guide layer, two set of inter-digital transducers (IDT), a gold film for immobilisation of the aptamer and a polydimethylsiloxane (PDMS) microfluidic channels. [21]	330 pM

Table 4. 1: Summary of PSA aptamer sensors, detection technique and their sensitivity.

4.1.6. Hybrid imprinting for PSA detection

Due to various advantages offered by aptamers, and the availability of an established aptamer for PSA with known affinity, it was decided to investigate PSA-aptamer combination for the hybrid imprinting approach. In the current study, an electrochemical sensing platform was investigated to understand the feasibility of the hybrid imprinting approach for detection of PSA at clinically relevant concentrations. It was hypothesised that the improved bioreceptors 'apta-MIPs' would exhibit greater selectivity because of the aptamer trapped in the favourable binding conformation and the recognition ability of the imprinted polymer, as a result of steric and chemical selectivity. The proposed technique also demonstrates a targeted one step immobilisation strategy specifically for macromolecular surface imprinting applications, which has not been studied by other hybrid MIP techniques reported in the literature. It was further hypothesized that the particular orientation of the aptamer-bound-PSA on the sensor surface would allow for uniform binding site formation during the imprinting process, which is not observed in bulk imprinting (conventional or hybrid) technique. An electrochemical-sensing platform used for rapid detection of protein binding events. Studying and understanding such a sensing platform could help in the development of highly sensitive and selective MIP sensors that could be translated to other biomarkers in the future.
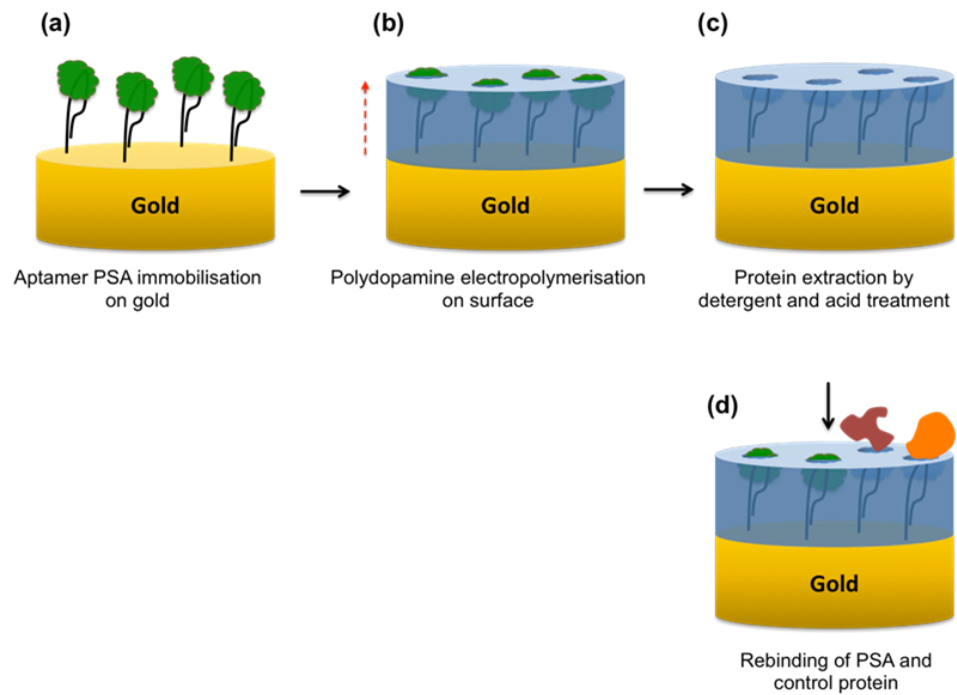
Figure 4. 3: Schematic of apta-MIP electrode preparation process: aptamer-PSA complex is immobilised via thiol chemistry (a) dopamine is electropolymerised to entrap the PSA (b) PSA is extracted by washing with detergent and acid (c) Post template extraction sensor is tested for rebinding of proteins (d)

4.2.   Aims And Objectives Of Chapter 4

The overall aim of this chapter is to construct a hybrid apta-MIP sensor for sensitive and selective detection of PSA.

Key objectives of this chapter are:

1. To study surface immobilisation strategies of PSA-aptamer complex on electrode surface.

2. To understand polymerisation strategies for molecular imprinting of aptamer-PSA.

3. Characterisation of surface post molecular imprinting of aptamer-PSA complex.

4. Evaluation of apta-MIP sensor performance by performing dose response studies with PSA and performing cross-reactivity studies with homologous proteins as well as serum proteins.

4.3. Materials And Methods

4.3.1. Reagents

Thiol terminated DNA aptamer with the sequence (5'-HS-$(CH_2)_6$-TTT TTA ATT AAA GCT CGC CAT CAA ATA GCT TT-3') was obtained from Sigma Aldrich, UK. Prostate specific antigen (PSA) was obtained from Merck Chemicals Ltd, UK. Human glandular kallikrein 2 (hK2) was obtained from RnD systems, UK. Human serum albumin (HSA), dopamine hydrochloride, trisma base, concentrated sulphuric acid, potassium phosphate monobasic solution (1 M), potassium phosphate dibasic solution (1 M), potassium hexacyanoferrate (III), potassium hexacyanoferrate (II) trihydrate, hexaammineruthenium (III) chloride, TWEEN 20 , potassium chloride and magnesium chloride were all purchased from Sigma–Aldrich, UK. All reagents were of analytical grade. All aqueous solutions were prepared using ultra-pure water 18.2 MΩ cm from Milli-Q system with Pyrogard filter (Millipore, MA, USA). Gold working electrodes were obtained from CH Instruments, USA and mechanical electrode polishing kit from Buehler, UK.

4.3.2. Electrochemical setup

All electrochemical measurements were performed with the µAUTOLAB III / FRA2 potentiostat (Metrohm Autolab, The Netherlands) with a three-electrode cell setup (Figure 4.4) consisting of an Ag/AgCl reference electrode (BASi, USA), connected via a salt bridge filled with 10mM phosphate buffer saline (PBS) pH 7.4, and a platinum (Pt) counter electrode (ALS, Japan). The impedance spectrum was measured in 10 mM PBS measurement buffer pH 7.4 containing 10 mM ferro/ferricyanide $[Fe(CN)_6]^{-3/-4}$ in a

frequency range from 100 kHz to 100 mHz, with a 10 mV a.c. voltage superimposed on a bias D.C. Voltage of -0.200 V *vs* Ag/AgCl reference electrode (corresponding to the formal potential of the redox couple). All measurements were performed at 20 ºC in 10 ml glass beakers as shown in Figure 4. 4.
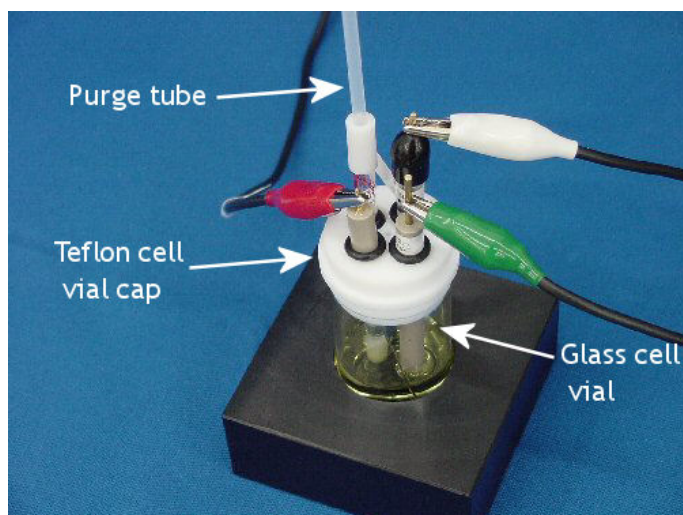
Figure 4. 4: Three-electrode setup with working (green), counter (white) and reference (red) electrodes. The set-up is connected to a potentiostat measures electrochemical changes in the system.

4.3.3. Fabrication of capacitive apta-MIP sensors

4.3.3.1. Electrode cleaning

Gold-disk working electrodes with a radius of 1.0 mm were first mechanically polished for 5 min with 50 nm alumina slurry on a polishing pad. Electrodes were then sonicated first in ethanol for 5 min followed by 10 min sonication in ultrapure water to remove any residual alumina particles. The electrodes were subsequently incubated in piranha solution (three parts of concentrated sulphuric acid to one part of hydrogen peroxide) for 5 minutes for chemically oxidising the surface. Electrodes were then washed thoroughly

with ultra-pure water to remove any residual acid. Post mechanical and chemical cleaning, electrodes were subjected to electrochemical cleaning in 0.5 M H_2SO_4 by scanning the potential between the oxidation and reduction potential of gold, −0.05 V and +1.1 V, *versus* Ag/AgCl reference electrode for 50 cycles until no further change in the voltammogram was observed. Finally, electrodes were washed with ultra-pure water and dried under nitrogen.

4.3.3.2. Aptamer – PSA complex immobilisation

Aptamers were first activated by incubating at 95^0 C for 10 minutes in a water bath and then gradually cooling them to room temperature over a period of 30 minutes. Post activation, 1μM DNA aptamer in TBST (Tris buffered saline with TWEEN 20) buffer pH 7.4 (10 mM Tris-HCl, 10 mM KCl, 10 mM $MgCl_2$, 0.05 % TWEEN 20) was incubated with 1 μg/ml of PSA for 1 hour at 37^0 C. Clean gold electrodes were then immersed in the aptamer-PSA complex solution for one hour, before being rinsed with milliQ water. To ensure the saturation of all aptamer molecules by PSA, the electrodes were backfilled with 1 μg/ml PSA in TBST buffer for an additional 30 minutes. These bio-functionalized electrodes were then taken forward into an electropolymerisation strategy.

4.3.3.3. Imprinting of the aptamer – PSA complex

- Autopolymerisation:

Dopamine was dissolved in Tris buffer pH 8.5 to a final concentration of 5 mM. The aptamer-PSA functionalised gold electrodes with were dipped into the freshly prepared solution of dopamine and left for an hour to allow auto-polymerisation to occur.

244

Following polymerisation, the electrodes were washed with copious amount of water and left in washing buffer (5 % acetic acid and 5 % SDS) overnight to extract the PSA. A non-imprinted polymer (NIP) was made with aptamer but in the absence of PSA. The electrodes were washed with water to remove residual acid and detergent and stabilised in PBS buffer pH 7.4 before use.

- Electropolymerisation:

The method for electropolymerisation of dopamine on gold electrodes was adapted from the procedure reported by Liu *et al.*[22] PBS buffer (pH 7.4) containing 5mM dopamine was degassed with nitrogen gas for 10 minutes prior to polymerisation. The solution was added to the electrochemical setup such that the functionalised gold working electrode, reference and counter electrode were immersed in the monomer solution. Polydopamine was electrodeposited on gold electrodes by performing cyclic voltammetry with varying (7/13/25) cycles by sweeping the potential from -0.5 V to 0.5 V at a scan rate of 20 mV/sec vs Ag/AgCl as the reference electrode. Following polymerisation, electrodes were thoroughly rinsed with water and left in washing buffer (5 % acetic acid and 5 % SDS) on a stirrer overnight to extract PSA. Electrodes were then rinsed with excess water to remove any residues of SDS and acetic acid in the polymer and incubated in PBS buffer for stabilisation.

The non-imprinted biosensor (apta-NIP) was prepared under exactly the same experimental conditions in the absence of PSA but with aptamer. The DNA aptamer was first immobilised on the gold surface followed by electropolymerisation of dopamine. The apta-NIP sensor was also exposed to the same washing conditions as apta-MIP.

4.3.3.4. Chronocoulometry for confirming presence of aptamers

Chronocoulometry measurements were performed using a μAUTOLAB III / FRA2 potentiostat. To functionalise the gold electrodes, the aptamer-PSA complex was first immobilised on the surface. The complex was then backfilled with 1 mM 6-Mercapto-1-hexanol (MCH) to cover any free gold surface. The aptamer-PSA functionalized gold electrodes were then rinsed with 5 % acetic acid and 5 % SDS solution. Gold electrodes functionalised with DNA aptamer washed with water were used as a control. The electrodes measurement were conducted by stepping the potential from −300 to −800 mV *versus* Hg/HgSO$_4$ (K$_2$SO$_4$) reference electrode for 500 milli-sec (10 mM Tris–HCl buffer pH 7.4) and subsequently recording the resulting charge flow. The same electrodes were then immersed in a solution of 100 μM hexamineruthenium(III) chloride (Ru(NH$_3$)$_6^{3+}$) in Tris buffer pH 7.4, and the measurements repeated.

4.3.4. Apta-MIP characterisation

4.3.4.1. Scanning electron microscopy (SEM)

Scanning electron microscopy (SEM) was performed using a ZEISS SUPRA 40 instrument (Carl Zeiss AG, Germany) in vacuum mode with an acceleration voltage of 3kV and 1kV.

4.3.4.2. Fourier transform infrared spectroscopy (FTIR)

FTIR analysis was carried out on a Varian 3100 Excalibur FTIR (Agilent Technologies UK Limited, Cheshire, UK) using the Varian Resolutions Pro software.

4.3.4.3. Atomic force microscopy (AFM) characterisation

The thickness and root mean squared (RMS) roughness of washed and unwashed apta-MIP films on gold-coated glass slides (Au thickness 150 nm) were determined by (AFM) (Multimode Nanoscope V, Bruker, CA, USA). Before investigation, both samples were rinsed with MilliQ water and dried with a lateral flow of nitrogen. Small scratches were made in each film using a sharp cantilever tip, < 10 nm, on a rigid cantilever of spring constant 42 N/m (NuSENSE, NuNano, Bristol, UK). Keeping the applied force below 50 nN ensured that the scratching process did not damage the underlying gold film. The depth of the resulting scratches was investigated at high resolution utilising a compliant cantilever of spring constant 0.4 N/m with a sharper tip, < 2 nm, (SCANASYST-AIR-HR, Bruker, CA, USA). The greater compliance of the cantilever allows interaction forces normal to the sample to be maintained in the region of a few hundred pN, thus minimising possible film compression. Images were collected at a resolution of 2 nm/pixel.

4.3.5. Apta-MIP sensor evaluation with PSA

Capacitive changes in the apta-MIP sensor were measured by an electrochemical impedance spectroscopy technique. The electrodes were stabilized in 10 mM $Fe(CN)_6^{3-/4-}$ solution in PBS (pH 7.4) before conducting binding experiments. The apta-MIP sensor was mounted in a three-electrode configuration as the working electrode. After baseline stabilization, the electrodes were dipped in 100 μl volume of different PSA concentrations prepared in 10 mM $Fe(CN)_6^{3-/4-}$ solution in PBS buffer (pH 7.4) containing 0.05 % TWEEN 20.

4.3.6. Preparation of conventional MIP capacitive sensors

For the preparation of conventional capacitive MIP sensor, PSA (1 μg/ml) was mixed in 5mM dopamine solution in PBS buffer pH 7.4. The solution was degassed for 10 minutes with nitrogen. Dopamine solution containing PSA was then electropolymerised using cyclic voltammetry (13 cycles) from - 0.5 V to 0.5 V at a scan rate of 20 mV/sec vs Ag/AgCl as a reference electrode. The electrodes were washed with 5 % acetic acid and 5 % SDS solution for removal of protein, washed with water and checked for re-binding of PSA.

4.3.7. Apta-MIP sensor cross-reactivity evaluation

Capacitive changes in the apta-MIP sensor were measured by an electrochemical impedance spectroscopy technique. The electrodes were stabilized in 10 mM $Fe(CN)_6^{3-/4-}$ solution in PBS (pH 7.4) before conducting binding experiments. The apta-MIP sensor was mounted in a three-electrode configuration as the working electrode. After baseline stabilization, the electrodes were dipped in 100 μl volume of different concentration of control proteins: human kallikrein 2 (hK2) and human serum albumin (HSA) for sensor evaluation.

4.4.   Results And Discussion

4.4.1. Fabrication of hybrid imprinted sensor for PSA

4.4.1.1. Aptamer-PSA immobilisation

To characterise the fabrication of different layers of the sensor, cyclic voltammetry was used in the presence of a redox couple, 5 mM $Fe(CN)_6^{3-/4-}$ solution in PBS (pH 7.4). The redox couple allowed for sensitive measurement of current and resistance on the electrode surface. Figure 4. 5 shows the cyclic voltammograms obtained before and after immobilisation of the aptamer-PSA complex. The bare gold electrode (black line) showed distinct oxidation (0.28 V) and reduction peaks (0.2 V) with high current levels of the redox couple due to its conducting nature consistent with that found in the literature.[23] Following immobilisation of the aptamer-PSA complex on the gold surface (red line), a 70 % reduction in peak current along with a shift in peak voltage was observed indicating the formation of a SAM layer on the gold surface, which provided resistance to the flow of current.

The first step in fabrication process was optimisation of immobilisation of PSA-aptamer complex on the electrode surface in its most preferred conformation. Conventional aptasensors utilise thiolated spacer molecules such as alkane thiols to avoid over-packing of aptamers on the surface, which can impede sensor efficiency. However, these molecules have an inhibitory effect on the electropolymerisation of dopamine and therefore could not be used in the sensor fabrication process.[24] It was necessary to space the aptamers on electrode surface to prevent possible steric hindrance for efficient binding of PSA to densely packed aptamers. Hence, a pre-complexing step of PSA and

aptamer binding was introduced before functionalisation of gold electrodes with PSA-aptamer complex. It was hypothesised that the pre-complexed PSA-aptamer immobilisation would allow for a uniform SAM layer formation on the gold surface with auto spacing between the aptamer-PSA complex molecules due to electrostatic repulsion between aptamers and steric hindrance from proteins. The free gold space left between these aptamer-PSA complex would then be utilized to grow polydopamine.
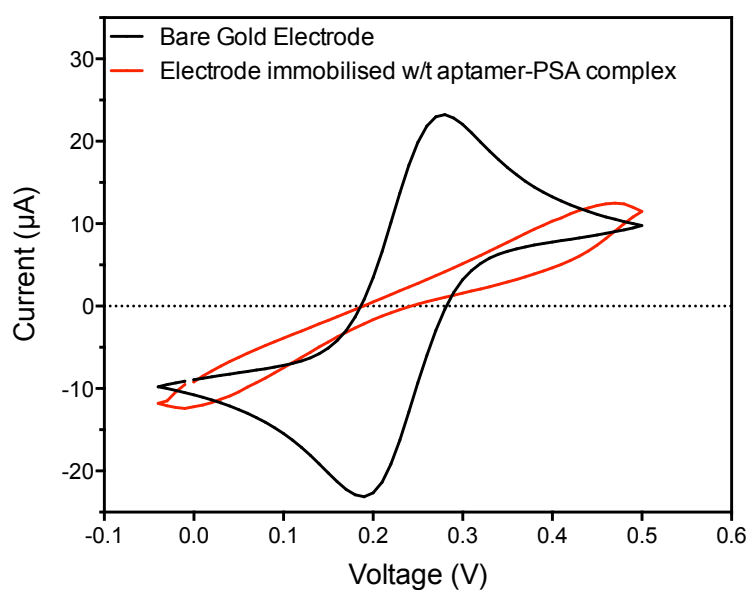
Figure 4. 5: Cyclic voltammograms showing a reduction in current and shift in peak voltage following immobilisation of complex performed in 10 mM PBS (pH 7.4) containing 10 mM ferro/ferricyanide [Fe(CN)6]$^{3-/4}$.

4.4.1.2. Molecular imprinting via autopolymerisation:

In 2007 Phillip Messersmith's group reported a simple method to coat virtually any surface with a thin layer of polydopamine by simply dipping the surface in an alkaline solution (pH 8.5) of dopamine.[25] The group demonstrated that surface-active polydopamine could coat various surfaces like noble metals (Au and Ag), metals with

native oxide surfaces (Cu and stainless steel), oxides (TiO$_2$ and SiO$_2$), semiconductors (GaAs) and glass. The mechanism of autopolymerisation is believed to be similar to the mechanism of formation of melanin for which dopamine serves as a precursor. Dopamine first oxidizes to dihydroxyindole and indolequinone, which then couple in a stepwise fashion, to form oligomeric mats that stack on top of each other to form melanin.[26] Due to simplicity of the process, initial imprinting studies were carried out with autopolymerisation process. The bio-functionalised electrodes fabricated with varying polydopamine thickness were measured for the reduction in peak current as a function of time as shown in Figure 4.6. It can be observed from Figure 4.6 that the current decreased with increase in polymerisation time and after 60 minutes there was minimal flow of current (~ 0.1 μA) through the electrode surface. This was a result of a non-conducting layer of polydopamine coating the electrode leading to passivation of the surface. From the literature it was determined that the polymer height could range from 50 - 100 nm after 60 minutes of polymerisation.[22,25,27] Hybrid imprinting studies were carried using polymerisation for 30 minutes to grow a thin polymer layer (~ 10 nm) close to the height of the aptamer-PSA complex. The aptamer-PSA complex height calculation and polymerisation optimisation has been elaborated in Section 4.4.31.
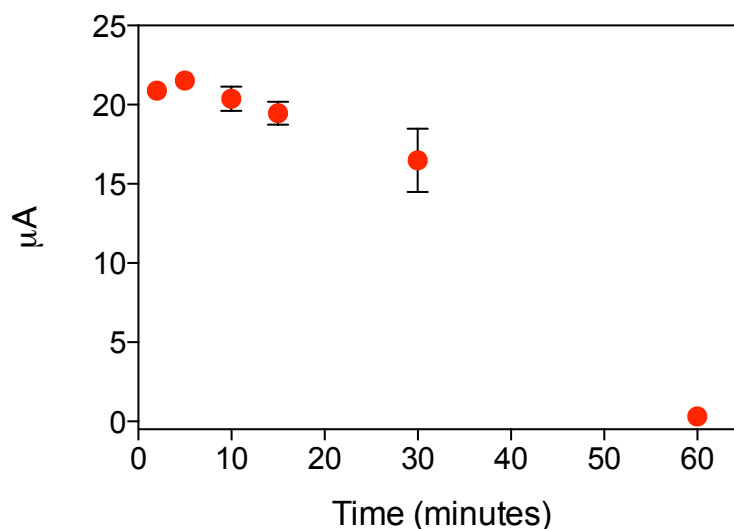
Figure 4. 6: Reduction of peak current with increase in polymerisation times

The apta-MIPs and apta-NIPs fabricated with the autopolymerisation process were evaluated for their binding efficiency to PSA. Electro-impedance spectroscopy (EIS) was used in this study to measure capacitive changes as a result of the re-binding process. When the protein (PSA) is introduced at different concentrations, the di-electric properties of the apta-MIP polymer changes, and this change were measured using EIS. The binding data plotted in Figure 4.7 showed no difference between apta-MIPs and NIPs with very large error bars, which is suggestive of non-specific binding of PSA to the polymer. A possible explanation could be the porous and non-uniform nature of polydopamine formed via autopolymerisation,[27] which, could lead to non-specific binding. A study by Zangmeister *et al.* demonstrated that after 10 minutes of autopolymerisation, polydopamine starts to deposit as agglomerates (formed in solution) of polymer onto the electrode surface.[27] This could be one of the reasons for the absence of imprinting effect due to large chunks of polymer depositing randomly on the

electrode surface leading to non-uniformity of the imprinted structure and lack of interaction between dopamine and PSA. Additionally, as these agglomerates are not covalently bound it was hypothesised that some of them could be washed away during the protein extraction process leading to further loss of imprinting effect.[27] The decrease in capacitance could be a result of non-specific binding of PSA to exposed gold and specific binding to the aptamer, which are still present on electrode surface of apta-NIP as well as apta-MIP. Shorter polymerisation periods also did not improve the imprinting process. This led us to explore electropolymerisation of polydopamine for further imprinting studies to get defined polymer characteristics for efficient imprinting.
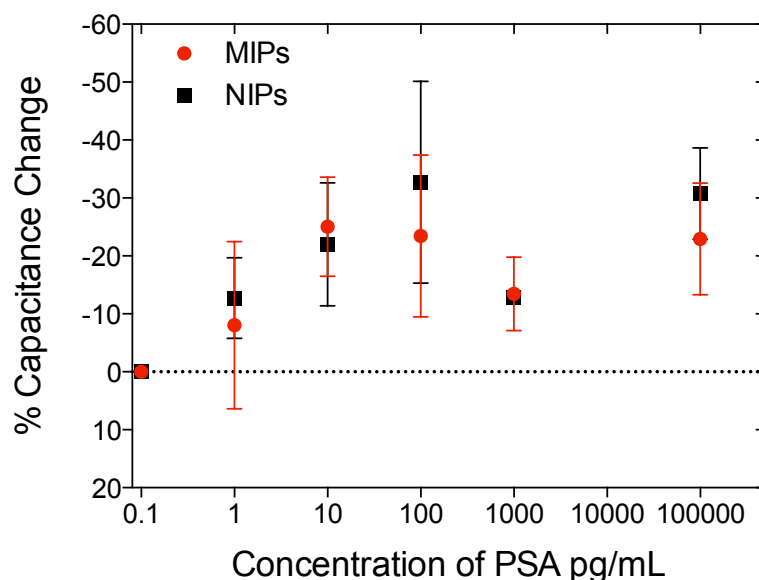
Figure 4. 7: Use of autopolymerisation of dopamine for imprinting. PSA binding results of apta-MIP and NIP

4.4.1.3. Molecular imprinting via electropolymerisation

Electropolymerised polydopamine has been used to generate molecular imprints on sensor surfaces such as gold, graphene oxide, silica for protein sensing.[22,28,29] For

surface imprinting, the oxidation/reduction potential applied for polymerisation of polydopamine is quite low, which prevents thiol oxidation of PSA-aptamer complex from the surface hence protecting the SAM layer orientation.[30] Polydopamine also has various functional groups for hydrogen bonding, hydrophobic and hydrophilic interaction with PSA making it a suitable functional monomer for imprinting. Cyclic voltammetry was used for the oxidation and reduction of polydopamine. The potential of the working electrode was swept from an initial value Eo (0V) to a set potential E1 (0.5 V) to a second set potential E2 (-0.5 V) after which the potential was reversed to its initial value. The potential values are set such that the oxidation and reduction potential of dopamine is within the range of the scanning potential of CV. Cyclic voltammogram of dopamine polymerisation is plotted in Figure 4.9 showing reduction in current with consecutive cycles. The distinct oxidation and reduction peaks represent oxidised species of dopamine during the polymerisation process. The peak at 0.39 V in the oxidation cycle represents DAQ, while the reduction cycle shows peaks at 0.08 V which represents LDAC and -0.38 V represents DAC. In the second cycle, an oxidation peak occurs at -0.18V which represents 5,6- dihydroxyindole which further undergoes polymerisation.[30] No new peaks were observed during polymerisation demonstrating that no conducting analogues were being produced during electropolymerisation. The polymer growth is self-limiting as the insulating polymer prevents electron transfer reactions for further oxidation of dopamine.
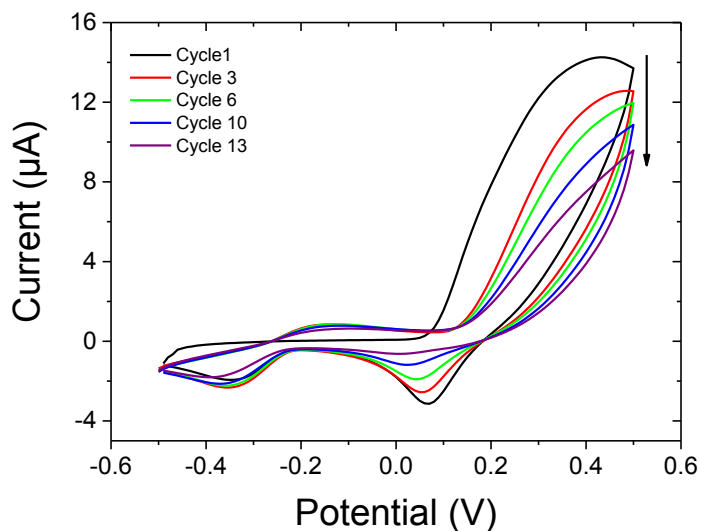
Figure 4. 8: Cyclic voltammograms showing electropolymerisation of dopamine on DNA aptamer-PSA modified gold electrodes. A reduction in peak current at 0.39V as well as at 0.07V and -0.35V was observed showing deposition of insulating polymer on the surface.

Post polymerisation of polydopamine on aptamer-PSA immobilised electrodes, cyclic voltammetry was used to characterise the electrode surface using 5 mM $Fe(CN)_6^{3-/4-}$ solution in PBS pH 7.4. The peaks were significantly reduced on polymerisation of dopamine on the gold surface due to the non-conducting nature of the polymer resulting into further insulation of the electrode surface (Figure 4. 9).
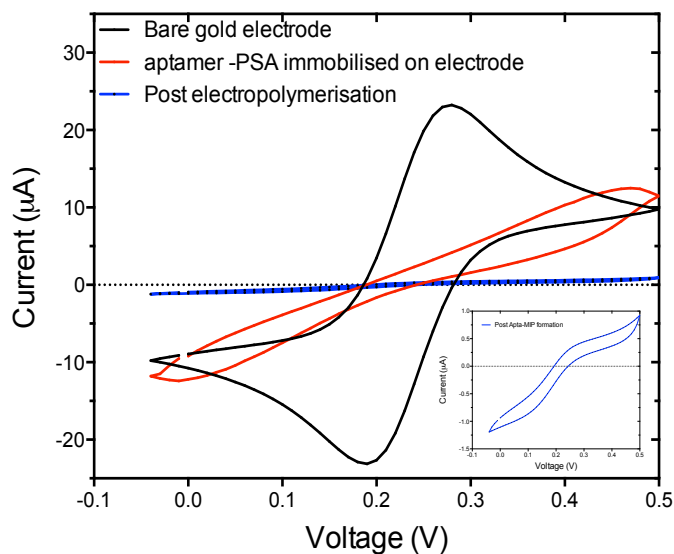
Figure 4. 9: Cyclic voltammograms showing steps of apta-MIP fabrication-. The blue curve shows the reduction in peak current post polymerisation of dopamine. There is a significant reduction in current compared to bare gold as a result of an insulating polymer being deposited. The inset shows the magnified view of the peaks post polymerisation.

4.4.1.4. Washing/Extraction step of PSA

For extraction of protein, a number of research articles have reported a combination SDS and acetic acid/sulphuric acid as an effective wash solution to remove imprinted proteins from MIPs.[31,32] Some articles have also reported the use of trypsin and proteinase K for digesting the protein.[33,4] However, incomplete digestion can lead to additional washing steps and incomplete template removal from the polymer. The incubation time for efficient protein extraction often depends on both protein and polymer properties. In the current study, the most successful result was observed with an overnight incubation in 5 % SDS and 5 % acetic acid for extraction of protein. This was observed through change in resistance of the apta-MIP sensor as well as the rebinding

efficiency of PSA. Removal of protein was observed as an increase in current in the reduction curve (0.6 µA, Figure 4.10a) of the apta-MIP electrode. However, an increase in current was also observed in apta-NIPs (0.1 µA, Figure 4.10b). As the only component of NIPs is DNA aptamer, which is covalently bound, it was concluded that some polymer was also being removed in the washing process (Chronocoloumetry in Section 4.4.2 further suggests that DNA aptamers are not being removed by washing solution). It is well known that dopamine can auto-polymerise over time in weakly basic pH (pH > 7) conditions[29], which could be getting removed during the washing process. Autopolymerisation, which can be observed by a change in colour of the polymerisation solution from transparent to slight brown, was observed during the last cycles of polymerisation in the experiments. The polymerisation solution was deoxygenated to retard the process but it could not be completely prevented. However, considering that increase in current in apta-MIP was larger than apta-NIP, it safe to conclude some protein was also removed from the apta-MIP surface. The electrochemical data alone cannot be used conclusively to understand the polymer removal, hence surface characterisation techniques like AFM and SEM were also explored.
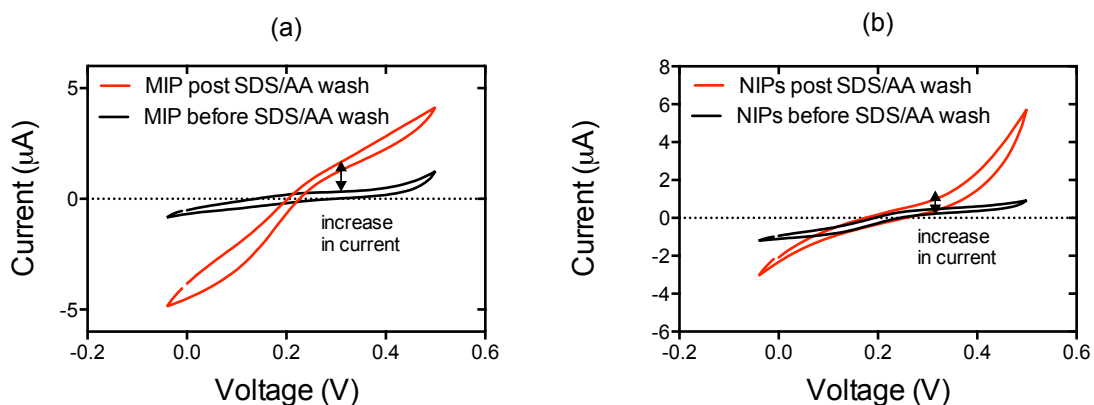
Figure 4. 10: Cyclic voltammograms showing steps of apta- MIP fabrication performed in 10mM PBS (pH 7.4) containing 10 mM ferro/ferricyanide [Fe(CN)6]$^{3-/4-}$. The Apta-MIP shows an increase in current indicating removal of protein. Apta-NIPs also show an increase in current, although smaller, which is attributed to the loss of some polymer during the wash process. The increase in current 0.5V is attributed to non-faradaic current.

4.4.2. Chronocoulometry for determination of aptamer surface coverage

The technique of chronocoulometry has been reported in the literature for determination of the surface density of nucleic acids on modified electrodes.[34,35] In this technique, the positively charged trivalent ruthenium redox molecule $Ru(NH_3)_6^{3+}$ preferentially exchanges its charge with the monovalent DNA counter ions which are negatively charged (phosphate group ion) in a low ionic strength buffer.[34] At −300 mV potential there is less reduction of ruthenium ions however when the potential is stepped to −800 mV potential, all surface confined $Ru(NH_3)_6^{3+}$ is reduced and a diffusion-limited current is produced. The charge (Q) as a function of time (t) is given as the sum of reduction of $Ru(NH_3)_6^{3+}$ diffusing from solution, the double layer charge and the charge due to

reduction of surface confined $Ru(NH_3)_6^{3+}$, which is given by the integrated Cottrell equation[36]:

$$Q = \frac{2nFAD_0^{1/2}C_0^*}{\pi^{1/2}} t^{1/2} + Q_{dl} + nFA\Gamma_0 \qquad (4.1)$$

Where **n** is the number of electrons per molecule for reduction, **F** the Faraday constant (C/mol), **A** the electrode area (cm^2), **D$_0$** the diffusion coefficient (cm^2/s), C_0^* the bulk concentration of $Ru(NH_3)_6^{3+}$ (mol/cm^3), **Q$_{dl}$** the capacitive charge (C) and **nFAΓ_0** the charge from the reduction of **Γ_0** (the amount of surface confined redox marker, in mol/cm^2).

Chronocoulometry was performed to calculate the number of aptamers immobilised on the surface as well as the effect of washing process on DNA aptamers. The technique was performed on DNA aptamer functionalised gold electrodes in the absence of polydopamine. The hypothesis was that if the washing buffer did not remove DNA aptamers from the gold surface in the free environment, DNA aptamers would not be removed from polymer layer either. Chronocoulometric data was plotted as an Anson plot of Q versus t$^{1/2}$ (Figure 4.11). Extrapolation of a least squares fit to the linear part was used to determine the intercept at time zero, which corresponded to Qdl+nFAΓ0.
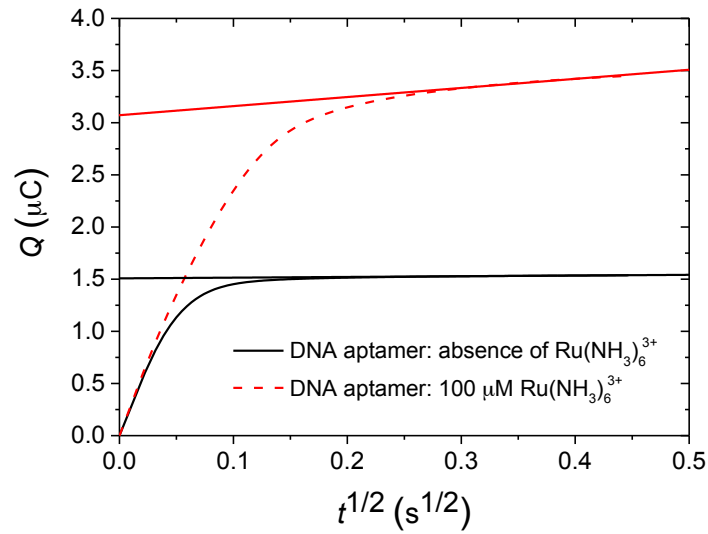
Figure 4. 11: Anson plot of Q versus $t^{1/2}$ for determination of surface charge. The measurements are taken before (black) and after the addition (red) of ruthenium redox molecules and the intercept can be extrapolated from the graphs which corresponds to $Q_{dl}+nFA\Gamma_0$

For calculation of surface charge it was assumed that the double layer capacitance was approximately equal in both measurements with and without $Ru(NH_3)_6^{3+}$, therefore **$nFA\Gamma_0$** was calculated as the difference in the two intercepts. The DNA surface density is determined using the following equation:

$$\Gamma_{DNA} = \Gamma_0 \, (z/m)N_A \quad (4.3)$$

Where **Γ_{DNA}** is the DNA aptamer surface density (molecules/cm^2), **m** the number of phosphate groups on the DNA aptamer, **z** the charge on the redox molecules $Ru(NH_3)_6^{3+}$ and **N_A** is Avogadro's number.

Two sets of electrodes one exposed to water and the second set exposed to 5 % acetic acid and 5 % SDS solution were measured. **Γ_0** (surface confined redox marker) was

calculated to be 5.31×10^{-10} molecules/cm^2, which corresponds to a DNA aptamer surface density of approximately 2.99×10^{13} molecules/cm^2 prior to washing. After washing (5 % acetic acid and 5 % SDS (aq)), Γ_0 was reduced to 2.30×10^{-10} mol/cm^2, which corresponds to 2.78×10^{13} molecules/cm^2 indicating an approximate decrease of 7 % (Figure 4.12). Electrodes washed only with water, showed an approximate decrease of 3 % in the number of DNA aptamer molecules. The higher percentage decrease when washed with acetic acid and SDS could be a result of distortion of the SAM layer because of drastic changes in pH and desorption of some aptamer molecules. However, the high number of molecules calculated on the surface (2.78×10^{13} molecules/cm^2) indicated the presence of DNA aptamer post washing of electrodes.
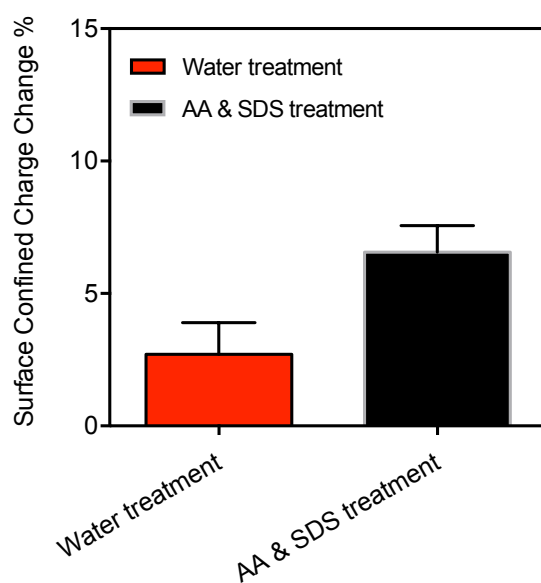
Figure 4. 12: Change in surface confined charged for electrodes washed with water (red) and electrodes washed with SDS and acetic acid (black). Change in surface confined charges indirectly represents the change in DNA molecules on the surface. The DNA molecules decreased from 2.99x1013 to 2.78x1013 post washing with SDS and acetic acid.

4.4.3. Apta-MIP surface characterisation

4.4.3.1. Polydopamine thickness optimisation

An approximate size/length determination of the DNA aptamer-PSA complex was calculated to design the polymer thickness on the surface for optimum imprinting efficiency. The DNA aptamer (single stranded DNA) consists of 32 bases, which corresponds to a length of 10 nm approximately. Upon undergoing conformational changes after binding to PSA, the secondary structure shortens to about 5-6 nm.[15] PSA is a 30 KDa protein, which corresponds to around 4 nm in size[37] making the total length of the complex about 9 -10 nm. The length is based on end-to-end measurement of the complex, which is based on the assumption that the PSA protein attaches on top of the aptamer. Although this gives the maximum theoretical length this may not be true in reality. Based on various models of aptamer-analyte binding, it is safe to assume that aptamers have multiple point interaction with various amino acid residues. Hence the actual length of the complex could be smaller than that calculated here. The electro-synthesized polydopamine film had to be designed similar the same height of the aptamer-PSA complex to allow the polymer to interact with the aptamer as well as PSA, permitting formation of a polymeric cavity that possessed chemical and steric selectivity for the protein. An optimum polymer thickness would also be helpful in facilitating complete removal of PSA from imprinted cavities preventing any leaching of the template in the re-binding step. From the literature, it was observed that 30 cycles of polymerisation produced a polymer ~ 40 nm in thickness.[22] The ideal scenario was to go for roughly half the polymerisation cycles however, as the surface was already pre-modified with aptamer-PSA, which could lead to different polymer height than that

observed in the literature, three different cycles of polymerisation - 25, 13 and 7 were investigated to evaluate the apta-MIP sensor performance. As can be seen in Figure 4.13a, the apta-MIP with 25 cycles of polymerisation showed good signal change however the apta-NIP also showed a high signal change leading to a low imprinting factor. Molecular imprinting with 7 cycles of polymerisation (Figure 4. 13b) demonstrated low imprinting efficiency with high initial capacitance change. It was proposed that this could be due to polymer layer not being thick enough to form uniform coverage on the entire electrode surface and some of it being removed in the washing step. The signal change being a result of PSA binding to aptamer and exposed gold surface non-specifically, indicating the absence of an imprinting effect. The results for 7 and 25 cycles of polymerisation are from one experiment (n of 4 electrodes) only and were not investigated further, however in the future it would be interesting to understand the imprinting effect as a function of polymer height using QCM/SPR techniques. Thirteen cycles of polymerisation showed the best apta-MIP versus apta-NIP signal change and was investigated further as shown in Section 4.4.
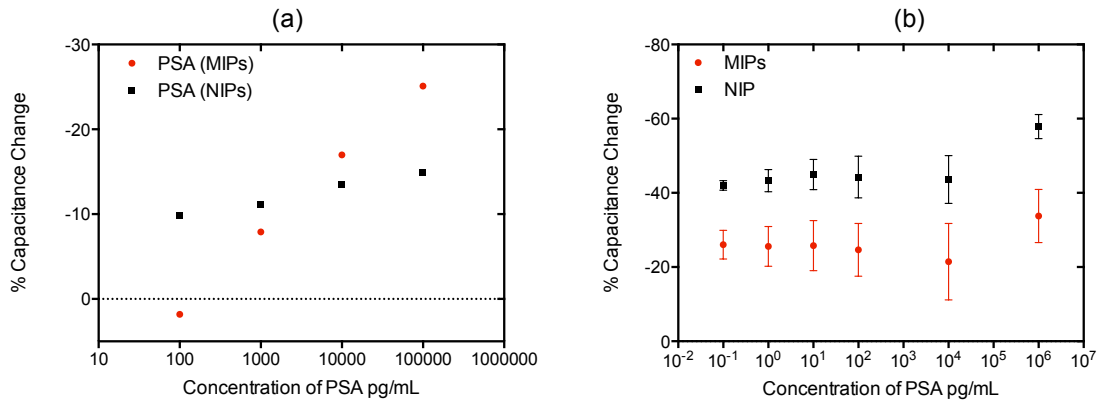
Figure 4. 13: (a) Dose response of PSA for apta-MIPs with 25 cycles of polymerisation. (b) Dose response for apta-MIPs with 7 cycles of polymerisation. Both show a loss in sensitivity in terms of changes in capacitance and poor imprinting effects compared to 7 cycles of polymerisation as described in section 4.4.5.

4.4.3.2. Scanning electron microscopy

SEM was used to understand the surface coverage of the polymer as well as estimate the thickness of the polymer in apta-MIPs with 13 cycles of polymerisation. Figure 4.14(a) shows SEM of bare gold before any polymerisation. Gold is a conductive material and thus absorbed electrons from SEM beam to produce an image with brighter contrast. The contrast of the SEM image changed post polymerisation (formation apta-MIP), appearing darker than bare gold as seen in Figure 4.14(b).
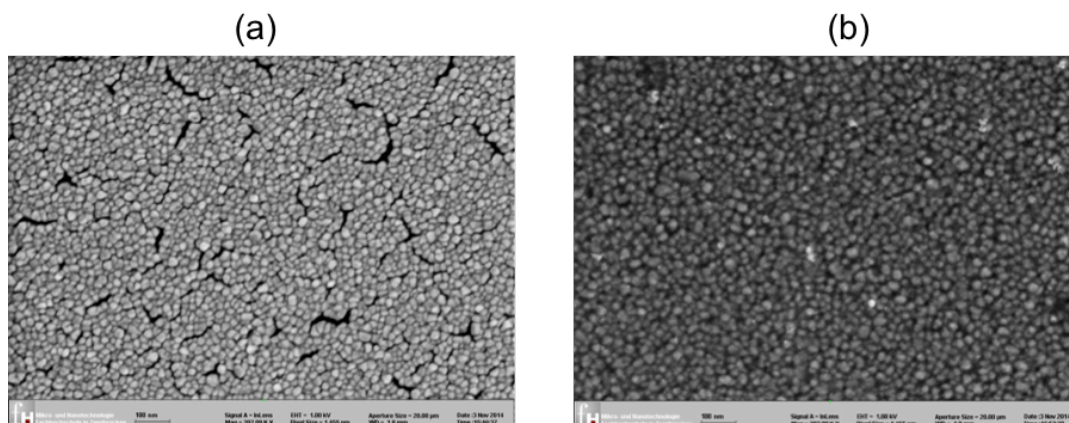
Figure 4. 14: Change in contrast of the image from bare gold (a) to gold coated with apta-MIPs (b) is indicative of a uniform polymeric layer on the surface

A cross section of the gold coated with apta-MIP was analysed to understand the thickness of the polymer layer (Figure 4.15). The bottom layer was glass followed by chrome and gold, which was covered by the apta-MIP layer. The slide was not kept at 180° but was slightly tilted below 180° to see the surface more clearly and differentiate the polymer from the gold surface. The thickness of the apta-MIP film was dd by calculating the change in contrast in the image and was estimated to be around 10 nm in dry format (average of 9 measurements from two samples).
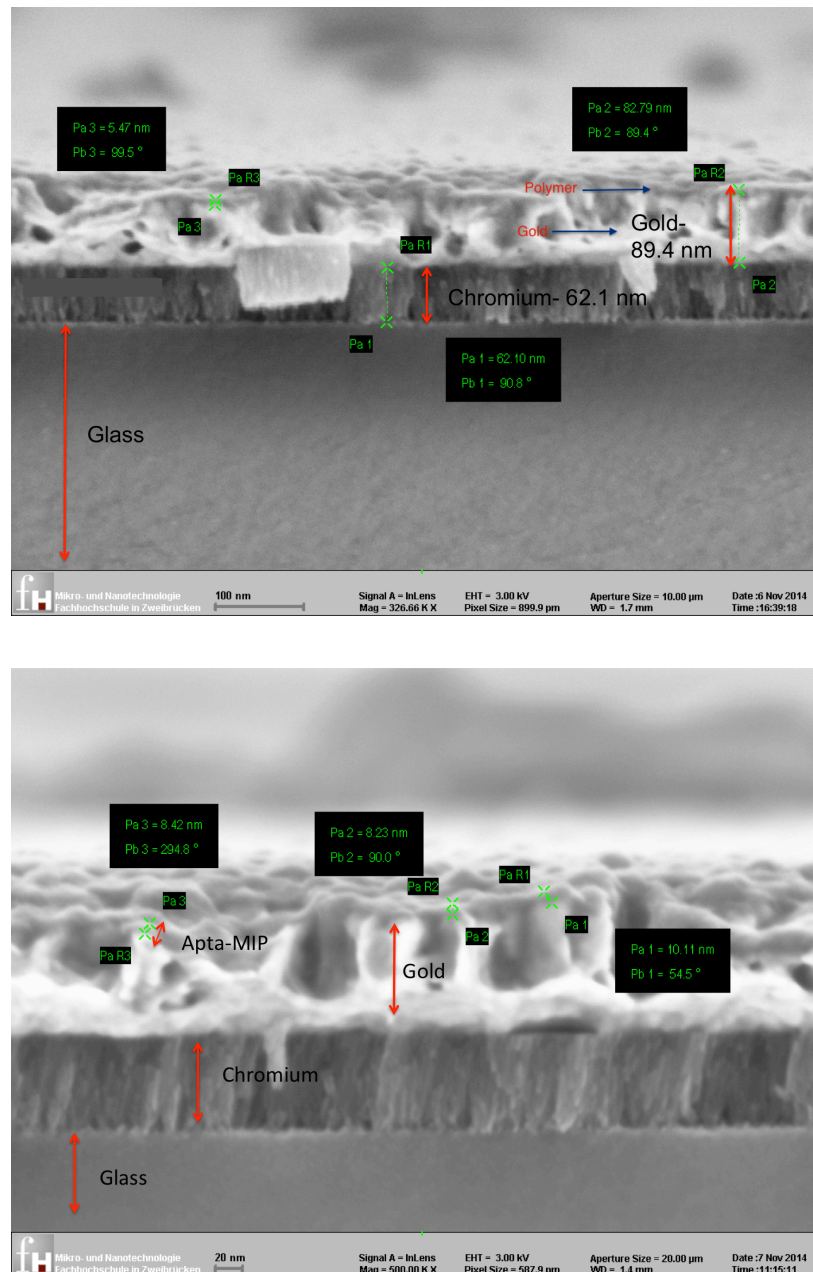
Figure 4. 15: SEM images of the cross-Section of polymer on gold. The bottom grey part is glass, followed by chromium (62 nm) and gold. The gold layer (90 nm) is the brightest as it becomes charged with electrons from the beam. The dark layer on top of the gold is the polydopamine layer showing thickness measurements of 8.42, 8.23 and 10.1 nm.

4.4.3.3. AFM

Tapping mode atomic force microscopy (AFM) was performed to calculate the thickness of the polymer layer for 13 cycles of polymerisation grown on the electrodes. For ease of measurement AFM analysis of apta-MIP was carried out on larger areas of gold-coated glass slides (10 mm in diameter). Post-polymerisation a clear difference in wettability was observed between the apta-MIP surface (hydrophilic) and bare-gold which remained unchanged post-washing of the apta-MIP suggesting the presence of a stable polydopamine layer. The root mean square (RMS) roughness of the bare-gold surface was 2.0 nm and this increased to 2.6 nm following the formation of the apta-MIP (Figure 4.16). Washing the apta-MIP with SDS and acetic acid resulted in a reduction in roughness to 2.2 nm. This reduction in height could be a combination of protein removal and some non-specifically bound polymer, which corresponds to the increase in current observed in Figure 4.11. The small changes in surface roughness suggest uniform surface coverage of the polymer on the gold electrode consistent with that observed in the literature.[38] The thickness of the polymer layer, measured as the step-depth between the base of a scratch and the flat surface of the top of the film, was 10.61 nm (n = 10; SD 1.23 nm) before washing, which decreased to 7.49 nm (n = 10; SD 0.42 nm) post washing. It was hypothesised that the change in thickness during the washing step was a result of PSA extraction and loss of some loosely associated polymer. It should be noted that the polymers were dried prior to their thicknesses measurement. It is, therefore, likely that the actual thickness would be a bit higher given that polydopamine has been reported to swell 1.12-1.25 times when hydrated.[39] It was difficult to measure the polymer thickness in its hydrated form due to hydrophilic nature

of the polymer dragging the AFM probe on the surface, preventing it from making a

scratch on the polymer.
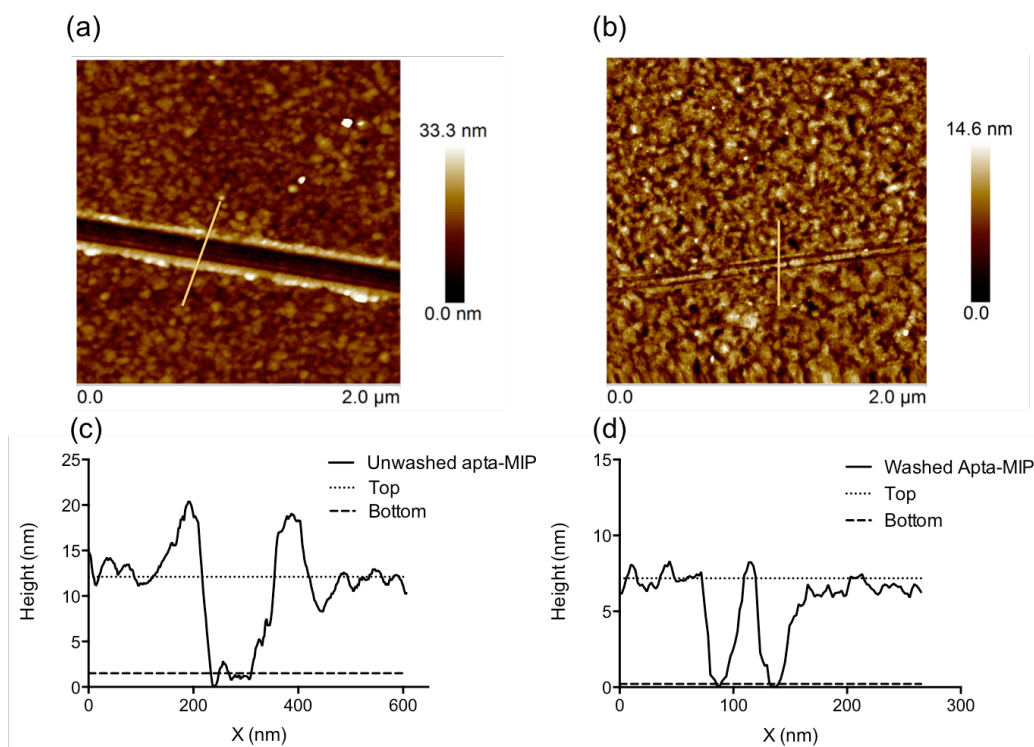
Figure 4. 16: The polymer depth was measured using AFM. A step edge on the polymer coated

electrode was created by making small scratches in each film using a sharp cantilever tip, < 10

nm, on a rigid cantilever of spring constant 42 N/m. AFM images (a,b) and graphs(c,d)

demonstrate the height profile of the step edge created on the surface of apta-MIPs before and

after the washing process.

4.4.3.4. Fourier-transform Infrared Spectroscopy (FTIR)

FTIR was performed on polymer modified gold surfaces to provide further evidence of

polymer deposition. The spectra of bare gold and polydopamine-modified gold is

presented in Figure 4.17 (a),(b). As the polymer layer was very thin (10 nm) it was

difficult to obtain strong bands for the IR spectrum, which could be due to the depth of

IR penetration during the measurements. The depth of penetration in the sample at the contact position is directly dependent on wavelength of the light and can vary from 0.5-5 μm (depending on the angle of incidence of light and the refractive index of the prism used).[40] A thicker polymer layer ($\approx$50 nm) was deposited to understand polymer properties on gold surface. An amide and hydroxyl stretch was observed from 3200-3600 cm^{-1}, which could be attributed to the NH and OH groups in the polydopamine film. An aromatic C=C and C=N stretch was also observed at 1200-1600 cm^{-1} from the aromatic ring.
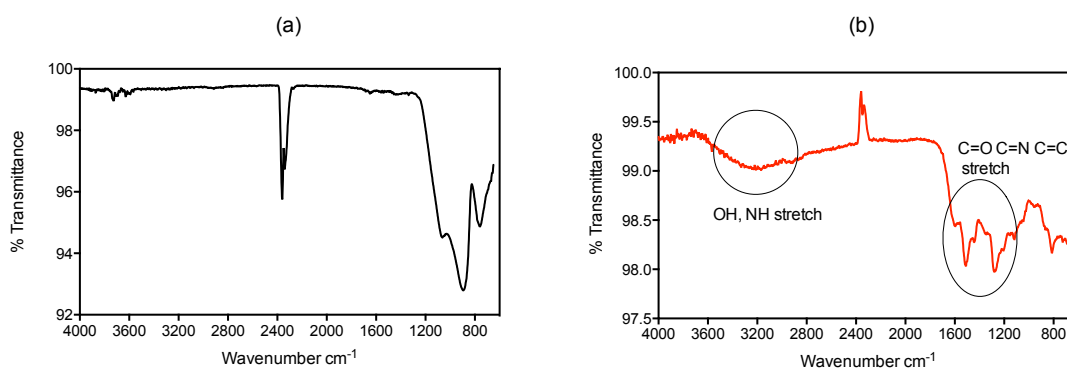
Figure 4. 17: FTIR spectrum of polydopamine on the gold surface (b) showing characteristic peaks for NH and OH groups (3200-3600 cm-1). A small C=O, C=C and C=N stretch is also observed from 1200-1600 cm-1. The corresponding peaks are absent in the FTIR spectrum of bare gold (a).

4.4.4. Evaluation of apta-MIP sensor performance

4.4.4.1. Apta-MIP sensor dose response with PSA

Apta-MIP with 13 cycles of polymerisation was fabricated and tested for PSA binding using EIS. Apta-MIP sensor response to PSA has been plotted in Figure 4.19. A

decrease in impedance was observed with increasing concentrations of PSA. As PSA

binds to the cavities of the apta-MIP, less DNA charge is exposed to the outer

electrolyte, causing a reduction in the resistance of the system. The screening of the

charge of the PSA-specific DNA aptamer has previously been reported in the

literature.[17,41] On the other hand apta-NIP sensor response plotted in Figure 4.18 shows

negligible response to increasing concentrations of PSA.
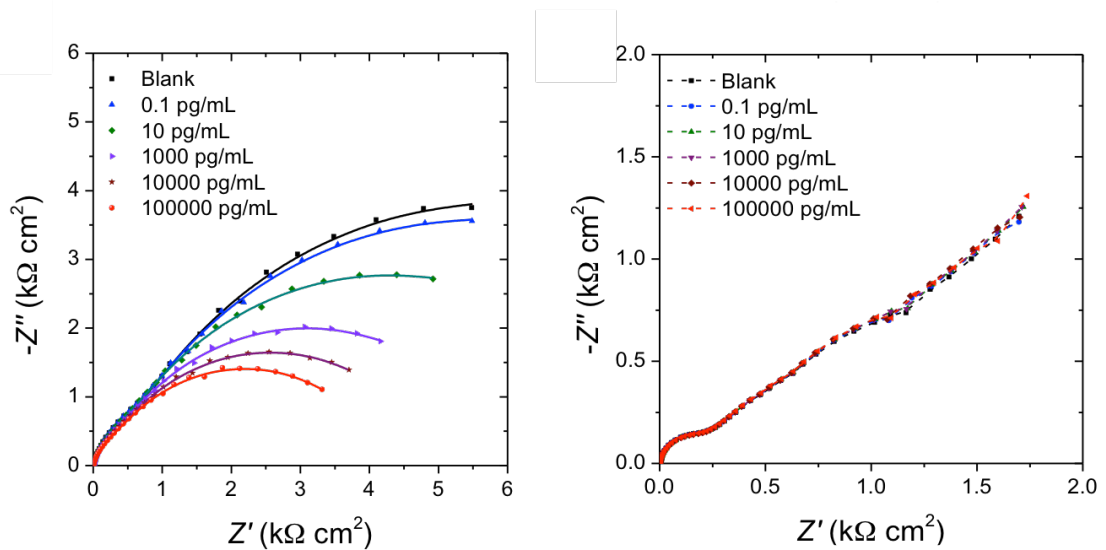
Figure 4. 18: Nyquist plots showing changes in impedance of the apta-MIP sensor for different concentration of PSA (0.1 pg/ml to 100000 pg/ml). The apta-NIP on the other hand shows negligible change on addition of PSA due to absence of polymeric cavities.

The Niquist data plot can be best fitted using a modified Randall's equivalent circuit

(Ivium modelling software, UK) comprising two R∥C (resistance in parallel with

capacitance) circuits in series, Rs (R1∥C1) (R2∥C2), where Rs is the solution resistance

C2 can be replaced by a constant phase element (CPE) with impedance

$Z(CPE) \equiv 1/Q(CPE)(j\omega)n$. The two curves (one at low frequencies and the other at

higher frequencies) are likely to be associated with the electrochemical double layer and

with the polymer itself. For the blank measurement of the sample shown in Figure 4.19

with a 1.0 mm radius, the fitted values are $R1 = 0.419\ k\Omega cm^2$, $R2 = 11.0\ k\Omega cm^2$,

$C1 = 86.9\ \mu F cm^2$, $QCPE = 4.00\ \mu Fsn\text{-}1cm^2$ and $n = 0.774$, which corresponds to an

estimated capacitance value of $C2 = 0.620\ \mu F cm\text{-}2$ by using the conversion

$C2 = (R2QCPE)1/n/R2$.[42] The high values of charge transfer resistance ($R2 =$

$11.0\ k\Omega cm^2$) observed for the system, are compatible with the presence of the insulating

polymer and the electrical potential barrier created by the negative charge of the

aptamers towards the negatively charged redox markers in solution.

Impedance is defined as a combination of real and imaginary part of impedance:

$$Z^* = Z' + jZ^{"}   \quad (4.4)$$

Given the high impedance values of the system, a better evaluation of the capacitance of

the system can be obtained by defining a complex capacitance[43,44]:

$$C^* = C' + jC^{"} \equiv \frac{1}{j\omega Z} = -\frac{Z^{"}}{\omega |Z|^2} - j\frac{Z'}{\omega |Z|^2} \quad (4.5)$$

Due to the high impedance values of the system and the relatively low exponent n of the

CPE, estimation of the capacitance of the system through fitting of the data with an

equivalent circuit yields large errors. The errors are then exacerbated by the calculation

of the capacitance through the fitted values of the constant phase element. Therefore, the

measured impedance at a fixed frequency (1 Hz) was used as the signal so that the

evolution of the electrochemical response could be monitored without the need for

fitting the data. The capacitance, calculated as $C^* = -1/j\omega Z^{"}$ at 1 Hz, was used for

plotting the dose response with the apta-MIP. The capacitance plots are characteristic of

a certain system and provide us with information on the nature of the electrochemical reaction occurring at the surface. Figure 4.20 shows the Cole–Cole capacitance plots at higher frequencies before and after PSA binding events and measurable changes in the capacitance can be observed upon PSA interaction with the sensor. On addition of PSA, it can be seen from Figure 4.19 that a greater change ($\approx$ 60 %) is observed at higher frequencies indicating a fast capacitive process, followed by another curve at lower frequencies (inset) which could be a result of a slow capacitive process (dominated by diffusion of an analyte). [45] The second curve that appears at lower frequencies shows an increase in capacitance of the system with increasing amount of PSA, which could be associated with the increase in conductive pathways of the apta-MIP polymer layer due to screening of the aptamer charges. This is a widely reported response of an impedance-based (biolayer containing) sensors when using redox markers such as $Fe(CN)_6^{3-/4-}$ in solution. [43,44]
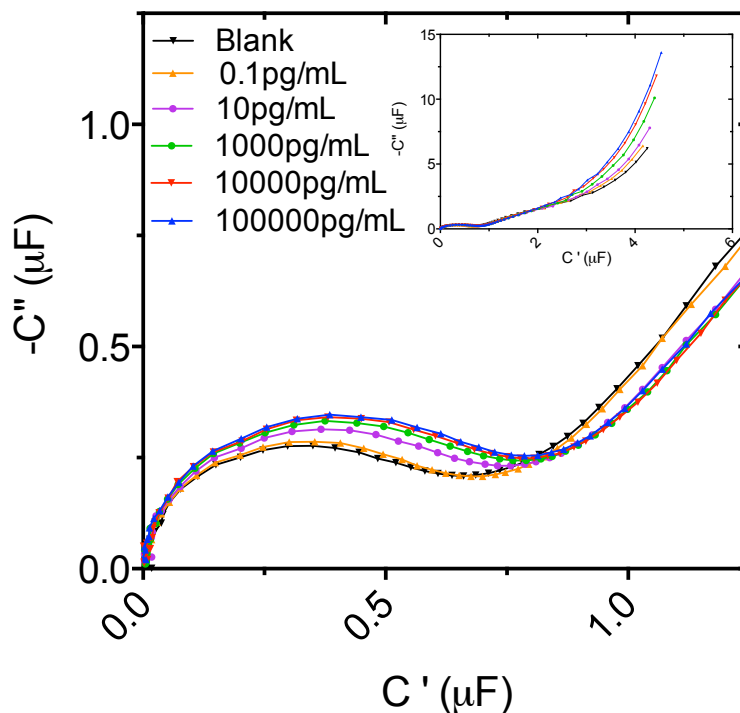
Figure 4. 19: Capacitance plots showing changes in capacitance of the apta-MIP and apta-NIP sensor for different concentration of PSA. The DNA aptamer folds into its conformation on binding to PSA which leads to increase conductive pathways for the redox couple leading to increase in capacitance the apta-MIP sensor.

It is hypothesised the negatively charged DNA aptamer as well the polymer pose an electrostatic potential barrier to the negatively charged redox marker $(Fe(CN)_6^{3-/4-})$. This causes resistance to the flow of redox markers to the sensor surface. When the aptamer binds to PSA the aptamer folds thus screening the negative charge, and allowing easier flow of redox markers.[17] This could explain the decrease in impedance of the system as PSA binds to the apta-MIP sensor (Figure 4.18).

The apta-MIP and apta-NIP sensor PSA dose response plots are shown in Figure 4.20. All measurements were normalised to the baseline signal after achieving stability. The

apta-MIP sensor incubated with 0.1 pg/ml showed a capacitance change of 5 % while 1 µg/ml showed a signal change of about 47 % showing high sensitivity in terms of sensor response. The apta-MIP sensor showed a linear response from 100 pg/ml to 100 ng/ml PSA, which covers the clinical range of PSA (4-10 ng/ml) for prostate cancer detection.[46] All protein-rebinding experiments were conducted in the presence of 0.05 % TWEEN 20 to prevent any non-specific interactions. The DNA aptamers (in the absence of PSA) immobilised on gold surface embedded in electropolymerised polydopamine were used as the control or apta-NIP. The apta-NIPs showed a decrease in capacitance with a signal change of just 6 % when incubated with 1 µg/ml PSA, which could be due to non-specific interaction of the protein with the polydopamine. The low signal change for apta-NIPs could be a result of densely packed polydopamine with the DNA aptamer posing a significant diffusional barrier to PSA. It is proposed that during polymerisation, in absence of PSA, the aptamers lie flat on the electrode surface and subsequently get buried in the polymer preventing any interaction with PSA.

The PSA aptamer used in this study was investigated by a collaborating group for development of an electrochemical aptamer only sensor.[17] The aptamer alone sensor had limit of detection of 1 ng/ml PSA, which was 100 fold lower than the apta-MIP sensor. The aptamers were co-immobilised with sulfobetaine molecules (using different aptamer/thiol ratios), as an anti-fouling chemistry for covering any free gold surface and preventing non-specific binding of proteins. Although, the aptamer alone sensor does not have the same aptamer distribution as compared to apta-MIP due to difference in immobilisation strategies, it is hypothesised that the aptamer distribution would be close

to if not similar to apta-MIP to get maximum signal change upon binding to PSA. Hence, improved sensitivity suggests that there is an improvement in affinity of the new hybrid receptors when compared to aptamer alone receptor.

The high sensitivity of the apta-MIP sensor could be result of a hybrid system exhibiting two levels of recognition towards PSA. The DNA aptamer has high affinity toward PSA while the polymeric cavity could be acting synergistically with the aptamer conferring shape and chemical selectivity. As PSA is a large macromolecule it is hypothesised, the aptamer has a small contact point where it docks to the protein after changing conformation as described in Section 5.2. This means that maximum interaction of the polymer could occur with the bulk protein allowing for non-covalent interaction such as hydrogen bond and hydrophobic interaction to be established during the polymerisation process. This could allow for the creation of highly selective polymeric cavity lined with an aptamer locked into its preferred conformation. This is in contrast to the aptamers for small molecules, which have multiple contact points leading to less interaction of template with the polymer during the imprinting process and the binding being dominated by the aptamer only as demonstrated in imprinting of hybrid MIP nanoparticles for cocaine.[3] The polymer thickness also contributes to the imprinting effect as we see a loss in recognition with 7 cycles of polymerisation. The thickness determined by AFM (9 -10 nm) suggests that there is potential for significant interaction between PSA and polydopamine for the formation of the specific cavity. Additionally, growth of the polymer post binding of PSA and the aptamer leads to protection of the aptamer-protein interaction site preventing any hindrance during re-binding. After the protein is released it is hypothesised the aptamer is locked in its most favourable

conformation hence thermodynamically lowering its Gibb's free energy. When the PSA is re-introduced it is thermodynamically favourable for it to bind to cavity with the aptamer resulting is higher sensitivity. Furthermore, a 100-fold increase in sensitivity from an aptamer alone sensor strongly suggests that the affinity of the new aptamer-MIP receptor is greater than the affinity of the aptamer alone system.
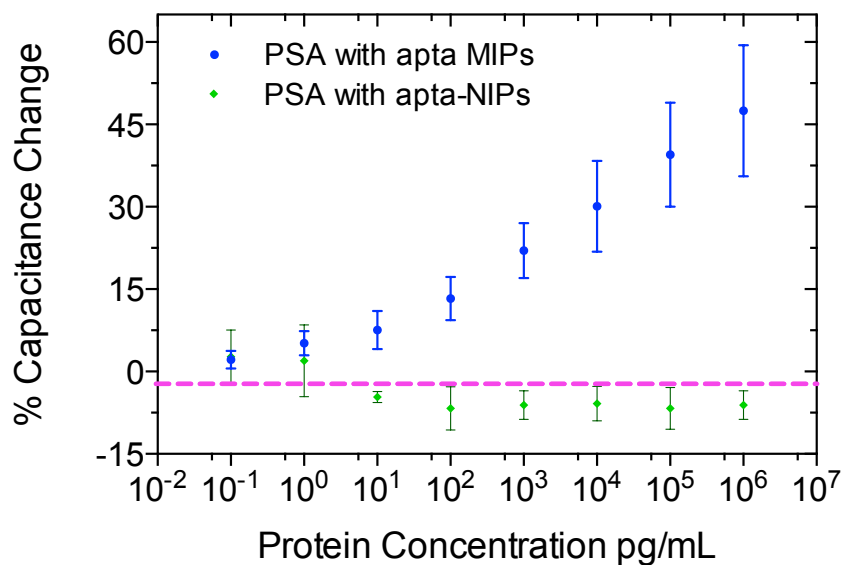
Figure 4. 20: Dose response of apta-MIPs (blue) and apta-NIPs (green) with different concentrations of PSA. The apta-MIP sensor shows an increase in capacitance with different concentration of protein while the apta-NIP shows a negligible response to PSA. The horizontal pink line represents the baseline signal obtained after stabilisation of the sensor.

To ensure that the apta-MIP sensor response was a result of an imprinting effect and not due to protein-protein interaction with any residual PSA trapped in the polymer, apta-MIPs were washed only with water so as to retain the protein in the polymer. A control polydopamine layer without any PSA was washed with water to understand the effect washing on the polymer. It can be observed from Figure 4.21 that there was no change is

CV of the polymer pre and post washing suggesting that the polymer remains intact. It was known from the PSA extraction optimisation studies that PSA was difficult to extract without fairly harsh washing steps indicating that the protein was intact in the polymer layer.
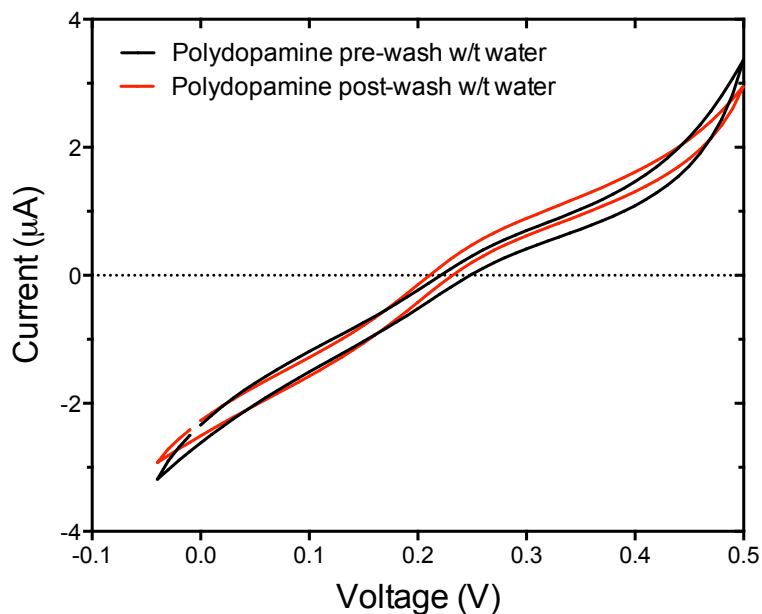
Figure 4. 21: Polydopamine coated electrode washed only with water shows negligible change in cyclic voltammetry curves before and after washing indicating no removal of polydopamine.

PSA was introduced at the same concentrations to see if the apta-MIP sensor showed a response. Figure 4.22 demonstrates that apta-MIP sensors washed with water showed no response to PSA with a maximum signal change of 1.3 % confirming that the response was not a result of protein-protein interaction but due to steric and chemical selectivity of the apta-MIP hybrid polymer.
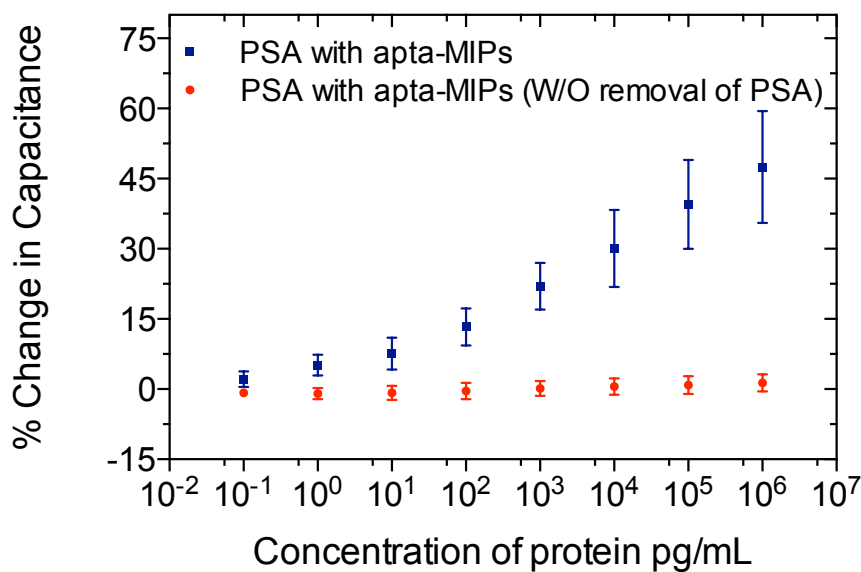
Figure 4. 22: The blue curve represents the apta-MIP sensor response to PSA while the black curve is the apta-MIP PSA response without extraction of PSA. It can be seen when PSA is not extracted from the apta-MIP there is a significantly decreased response on addition of PSA suggesting that protein-protein interactions do not play a role in the recognition of PSA.

4.4.4.2. Determining the dissociation constant (K_d) of the Apta-MIP system.

A number of different models were used for deducing the apparent K_d of the hybrid polymer system. One of the most basic adsorption model is the Langmuir adsorption model, which assumes one site specific binding and relies on saturation capacity (B) and equilibrium constant (K). [47,48] The model however does not take into account any binding site heterogeneity that commonly exists within molecularly imprinted polymer systems, leading to sites of different affinities and selectivity.[49] The Freundlich-Langmuir (FL) model, which is a combination of Freundlich and Langmuir adsorption models, takes into account this heterogeneity observed with most MIP systems.[50] In the

FL model, saturation capacity (B) and equilibrium constant (K) are the same, however n (0<n<1) is the heterogeneity factor. The equation used for this model is,

$$B = \frac{Bmax(KFLC)^n}{1 + (KFLC)^n} \qquad (4.2)$$

where; C = Concentration, B = amount of protein bound, B_{max} = maximum protein bound, K_{FL} = $1/K_d$. Applying the FL model to the apta-MIP sensor data produced the isotherms shown in Figure 4.24. The R^2 value obtained using this model was 0.998. The apparent K_d value obtained was 0.3 nM, which was much lower than the aptamer alone sensor 2 nM (Figure 4.23).
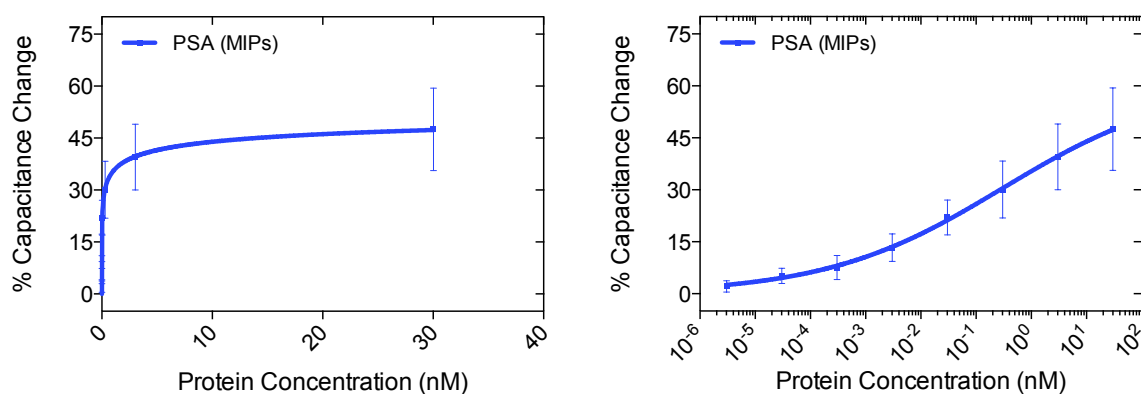
Figure 4. 23: FL model applied to the dose response data. The data is shown on linear as well as logarithmic scale. The dose response curve fits well with the model (R^2 value of 0.99).

The Imprinting Factor (IF) is defined as the amount bound by MIP divided the amount bound by NIP, which is also known as the selectivity factor.[51] As the polymer had a biomolecule (aptamer) incorporated in it, the selectivity is much higher than conventional polymer only systems as an IF of 7.8 was obtained for the apta-MIP

sensor. This value is similar to that reported for the hybrid mannose - polymer MIP system.[4]

4.4.5. Conventional molecular imprinting of PSA

A standard protocol to fabricate conventional electrochemical MIP sensors is to solubilize the template in the monomeric solution and subsequently apply a potential to deposit a polymer on the electrode surface. The template gets trapped into the polymer during polymerisation, which upon extraction leaves a cavity, which displays an affinity and selectivity for the template. This process works very well with small molecules as they can be mixed at known molar ratios with the monomer for maximum template entrapment and subsequent extracted. A similar protocol has also been applied for surface protein imprinting with higher concentration of protein (1-10 mg/ml) being used to ensure maximum entrapment of protein and creation of binding sites.[52,53] This however may not feasible in certain cases where protein templates are expensive (PSA) or difficult to purify in large quantities. Studies were undertaken to understand the performance of the apta-MIP sensor *versus* conventionally prepared MIPs (without the aptamer and surface immobilisation of PSA) on gold surfaces. For the purpose of direct comparison between the conventional system and the apta-MIP sensor, the protein concentration was maintained at 1 μg/ml. The conventional MIPs showed a poor response when compared to apta-MIP sensors with a maximum signal change of 2 % when incubated with 1 μg/ml PSA (Figure 4.24). One reason for this could be the absence of any aptamers displaying high affinity towards PSA in the MIP sensor and second being poor entrapment of PSA into polymer during electropolymerisation.

Considering only some liquid is in contact with the electrode surface where the electrochemical reactions are occurring the amount of protein getting trapped is going to be less than that present in the bulk liquid. A large degree of variation was observed in the rebinding experiments (see error bars in Figure 4.24 inset), which is strongly suggestive of binding site heterogeneity. Conventional protein imprinting does not allow for creation of homogenous binding sites as the template is not uniformly presented at the surface nor evenly distributed through the polymer layers, leading to binding cavities of varying depth and shapes.[54] This could further lower the sensitivity of the conventional MIP sensor. Preparation conventional MIP sensors may require longer incubation times and higher protein concentrations for imprinting to show significant signal change as a result of the imprinting effect. Although this comparison study is not perfectly designed, as we are not comparing conventional monomer imprinting or an optimised template concentration for imprinting, it does point towards various shortcomings of conventional imprinting protocols that one needs overcome when imprinting proteins. This study also suggests that the immobilisation technique used for imprinting in the hybrid MIP system is more efficient than conventional imprinting for sensitive protein detection
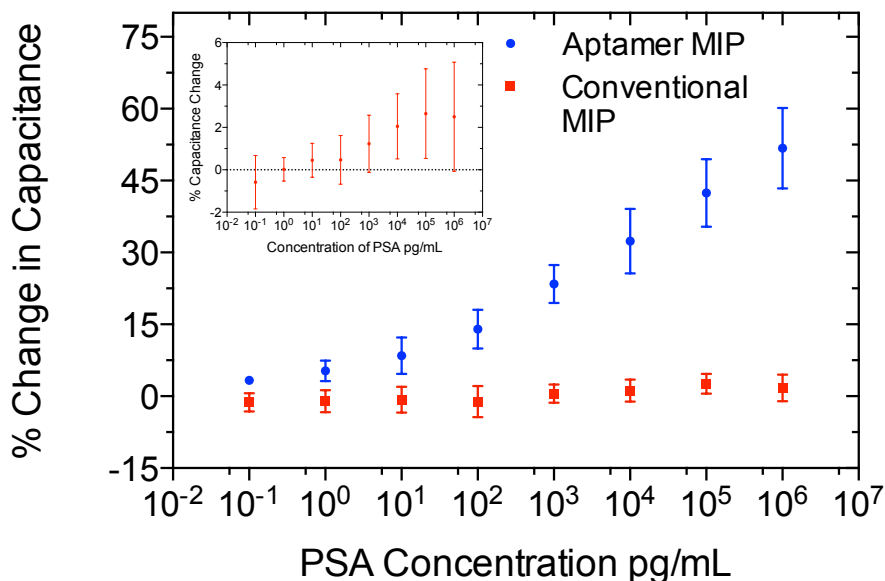
Figure 4. 24: Comparison of conventional MIP (red) and apta-MIP (blue) sensor performance with different concentrations of PSA. The inset shows the magnified response data from conventional MIP sensors. The conventional MIP shows low signal change in comparison to apta-MIP and high error bars, possibly indicative of increased heterogeneity in the binding site population.

4.4.6. Apta-MIP evaluation with control proteins

4.4.6.1. Selectivity study with hk2

To evaluate the selectivity of the apta-MIP sensor, a control protein was introduced to the system in a non-competitive assay. The control protein used in the study was human kalikrien2 (hK2), which is a kallikrein family protein sharing 80 % homology with PSA.[55] This protein although found in 100 fold lower concentration than PSA in clinical samples was a stringent control to check apta-MIP sensor selectivity than a more generic protein like BSA. On challenging the apta-MIP sensor in a non-competitive assay, hk2

showed a much lower response approximately 15 % compared to 45 % signal change upon incubation with 1 μg/ml PSA (Figure 4.25).
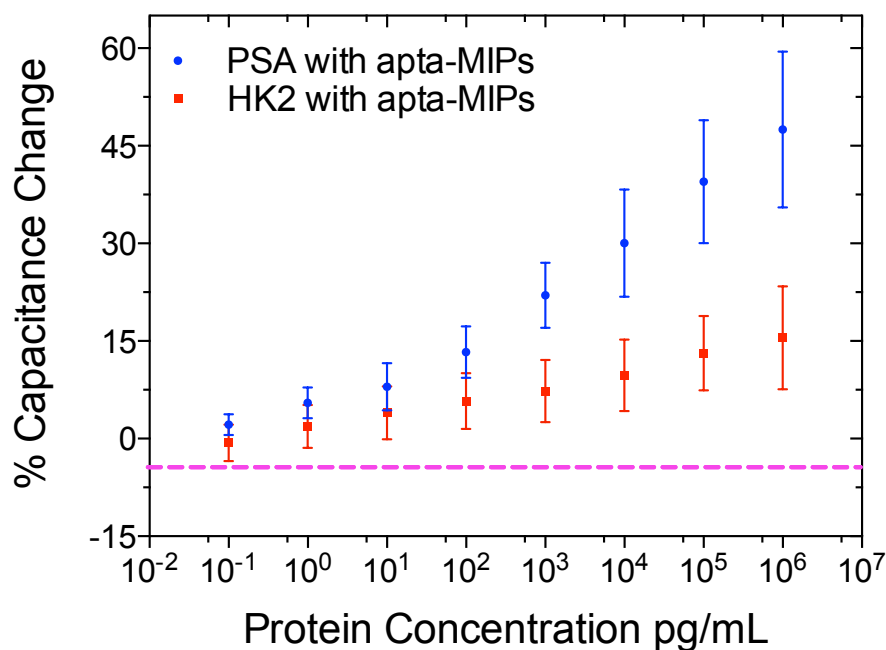
Figure 4. 25: Selectivity study of apta-MIP with different concentrations of hK2 (red) and respective PSA concentrations (blue). A lower response was observed with hK2 than PSA following incubation with apta-MIPs in a non-competitive binding assay.

To understand the source of cross-reactivity the 'aptamer only' sensor's response to hK2 was studied. This demonstrated a signal change (Rct) of 1.6 %, when incubated with 100 ng/ml of hk2 suggesting high selectivity of the aptamer for PSA.[17] Due to the absence of a polymeric layer in the aptamer alone sensor capacitance change at lower frequencies could not be measured, hence a ratio of the signal change of PSA *versus* hK2 was obtained based on the assumption that both signal changes are a result of specific interaction only. The PSA aptamer only sensor had signal ratio of 0.18

(PSA/hk2) while the aptamer-MIP system signal ratio was 0.28 (Figure 4.26(a)). This suggested that the cross-reactivity was not a result of hK2 interacting with the DNA aptamer, but a combination of interaction with the MIP cavity and polydopamine.
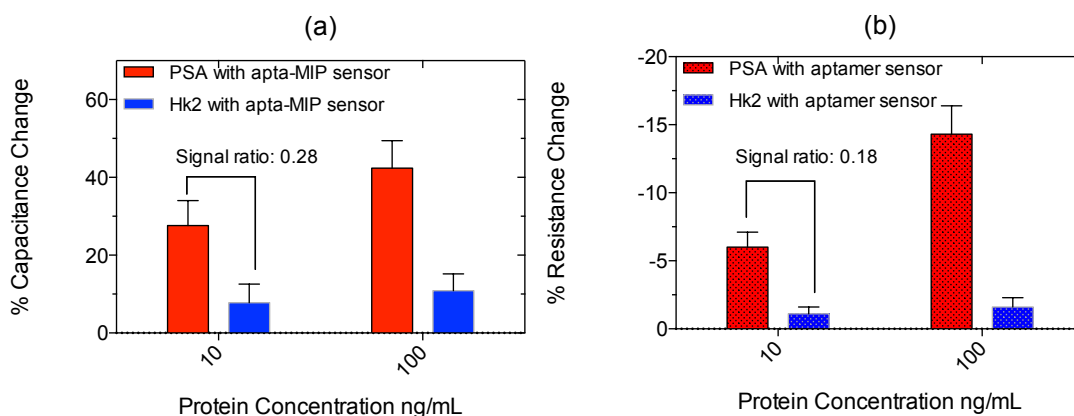
Figure 4. 26: hK2 cross-reactivity with the aptamer-MIP was compared with the aptamer sensor. The aptamer only sensor (b) showed a lower hK2/PSA ratio than apta-MIP sensor (a) indicating an increased cross-reactivity to hk2 with the apta-MIP sensor.

The source of cross-reactivity in apta-MIP could be is could be explained by the mechanism of aptamer interaction with PSA as elaborated in the Section 4.2. The DNA aptamer relies on highly specific interactions between amino acids and nucleotides in a small region of the protein making the binding event highly specific to a protein. It is proposed that during the imprinting process the polymer first surrounds the lower portion of the protein where it binds the aptamer and as the polymer thickness increases it surrounds the protein, allowing for establishment of more non-covalent interactions between polymer and protein. As a result, the more specific interaction of the aptamer is possibly dominated by non-covalent interactions of the polymer. As most non-covalent bonds formed with the polymer are a result of general hydrogen bonds and given the

significant homology with PSA, it is not surprising that hK2 cross reacts with the MIP cavity. This is also observed in antibody assays where antibodies raised for PSA cross-react with hK2 due to similar epitopic regions.[56] This could be improved in the future by using electroactive monomers/ conventional monomers with alternative functional groups giving rise to higher differentiation capacity to MIP cavity. Additionally from a clinical point of view the concentration of hK2 is 100 fold lower in blood compared to PSA, which would prevent major interference from hK2 to PSA binding.[57]

To further distinguish the source of cross reactivity, hK2 was incubated with polydopamine only (apta-NIPs) to understand non-specific binding to the polymer. Hk2 showed a signal change of about 1.5 % (Figure 4.27) with polydopamine, which indicates that remaining response could be a result of cross-reactivity with the binding sites. The decrease in capacitance can be explained by increase in impedance (resistance). As the protein sticks to the polymer non-specially it provides resistance to the diffusion of the redox couple through an already insulated polymer layer causing an increase in resistance. This behaviour is observed in most EIS sensors where binding of proteins to surface immobilised receptor causes an increase in resistance.[58,59] Protein cross-reactivity is not uncommon in MIP sensors due to shape of the MIP cavity. Moreover, a competitive binding assay will help us better understand the ability of the hybrid apta-MIP sensor to discriminate between PSA and hk2, however a labelled technique would be required to carry out such experiments for discriminating the two proteins which is expensive.
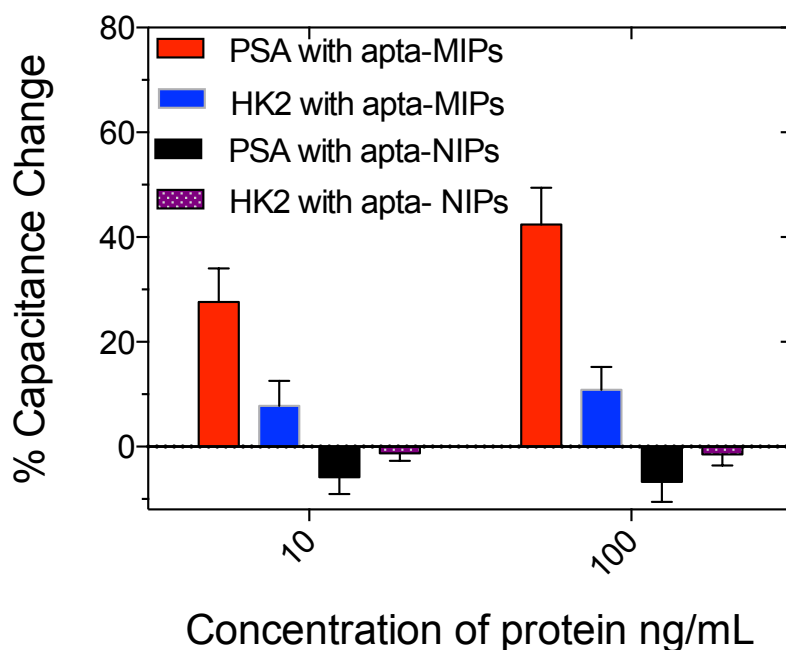
Figure 4. 27: Hk2 reactivity with apta-NIP sensor (purple) shows a signal change of 1.5 %
showing low cross-reactivity to the polymer. The decrease in capacitance was similar to that
observed with PSA with apta-NIPs (black)

4.4.6.2. Selectivity study with HSA

Another key aspect to take into account is the investigation of antifouling properties of
the fabricated apta-MIP sensor for its application with blood samples. Human serum
albumin (HSA) was used as a control protein to study non-specific binding, as it is one
of the major constituents of human blood (3.5-5.0 g/dL) and helps us to understand
whether the apta-MIP sensor could be used with clinical samples. HSA at 0.1 μg/ml and
1 μg/ml showed signal changes of 3 % and 5 % respectively (Figure 4.28). HSA is a
negatively charged protein at pH 7.4,[60] which could lead to electrostatic repulsion
between the polymer DNA layer and the protein leading to low signal change. When
tested at higher concentrations of 6.7 mg/ml, HSA showed a maximum capacitive

change of 11 %, which could be a result of non-specific interaction with polymer as well as protein-protein interactions. The low signal change is beneficial as HSA is a large protein which is abundantly found in blood and usually lowers the sensitivity of biosensors.[61] HSA interaction with apta-NIPs was similar to PSA interaction with apta-NIPs showing negligible change at lower concentrations and an increase in capacitance with a signal change of 3.5 % at the highest concentration of 6.7 mg/ml HSA, however, further studies PSA spiked serum are required to help understand the potential for loss in sensitivity in clinical samples. Regardless, the low non-specific binding of HSA at very high concentrations is very encouraging for application of the apta-MIP sensor in measuring clinical samples.
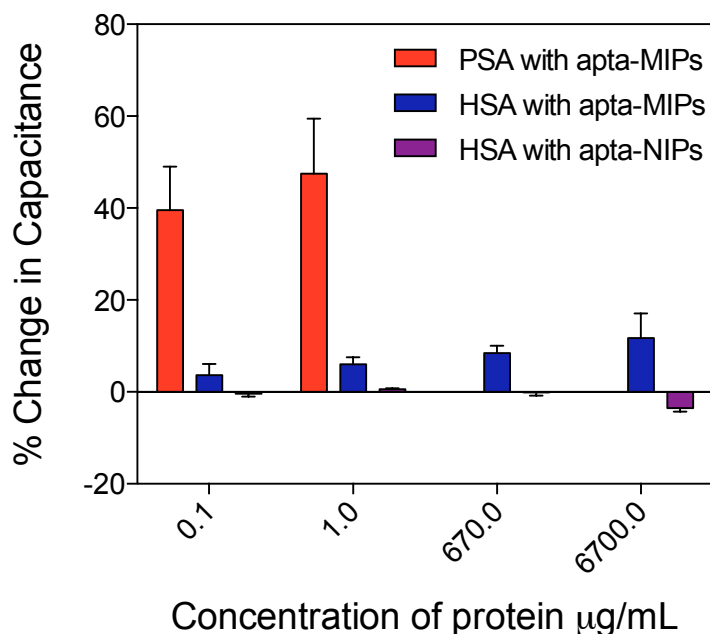
Figure 4. 28: Apta-MIP response to HSA (blue) shows some non-specific binding at higher concentrations of HSA. A signal change of 11 % is observed for HSA concentration of 6.7 mg/ml with apta-MIPs. Apta-NIPs showed a lower response to HSA (purple), which is mostly due to absence of polymeric cavities.

4.5.   Challenges Associated With Sensor Evaluation

Dissociation constants (Kd) could not be estimated using conventional bound vs free isotherms as it is difficult to estimate the actual concentration of protein bound to the apta-MIP sensor in these experiments. A labelled antibody or a labelled protein is required to estimate total amount of protein bound. Furthermore, even if a labelled antibody was used for detection PSA, it would difficult for it to bind to PSA entrapped in the polymer. A secondary technique such as SPR (surface plasmon resonance) or QCM (quartz crystal microbalance) could also be used to evaluate and validate apta-MIP sensor performance in the future. The best way to find if the polymer contributed

towards the affinity of apta-MIP would be use the same protocol for fabricating the apta-MIP sensors and substituting the aptamer with a molecule that has no affinity for PSA. This could be conducted using alkanethiols for immobilising PSA via EDC/NHS chemistry. However, this is challenging due to overcrowding of thiols on gold surface preventing polymerisation of polydopamine and subsequent removal protein would require enzymatic digestion due to covalent binding. Another technique that could be evaluated would be to use a peptide to create hybrid-MIP receptor for PSA and compare the two systems (This work is still on-going at University of Bath).

4.6.   Conclusion

The study presents the successful use of the aptamers in the application of imprinting PSA for building a sensitive electrochemical sensor. The apta-MIP receptor developed in this study was highly sensitive with LOD of 1 pg/ml, which is well below the clinical range. The apta-MIP receptor is also 100 times more sensitive to the aptamer alone sensor highlighting the advantage of imprinting. Furthermore, the low cross-reactivity with homologous protein suggests high selectivity of the sensor. The low non-specific binding to high concentration serum proteins is highly encouraging for future clinical use. There has been a significant amount of work published in the field of protein imprinting. However, some of the challenges have remained such as imprinting homogenous binding sites, attaching the polymers to transducer surface, controlled polymerisation and efficient removal of the template. Researcher has overcome some of these hurdles whereas some remain to be solved. Hybrid imprinting helps overcome majority of these challenges creating a new brand of synthetic receptors that can be aptly termed as 'super-receptors'. The apta-MIP receptor developed in this project is one such step towards creating the next generation of receptors for clinically relevant biomarkers. The apta-MIP sensors can be easily adapted for various templates with existing aptamers to make a multiplexed biosensor or by using different affinity receptors for imprinting.

4.7. References

1. Turner, N. W. *et al.* From 3D to 2D: a review of the molecular imprinting of proteins. *Biotechnol. Prog.* **22,** 1474–1489 (2006).

2. Kelly, M., Bowen, J., Gumbleton, M. & Allender, C. Molecularly imprinted polymers: macromolecule recognition. *Drug Discov. Today* **15,** 1112 (2010).

3. Poma, A., Brahmbhatt, H., Pendergraff, H. M., Watts, J. K. & Turner, N. W. Generation of Novel Hybrid Aptamer–Molecularly Imprinted Polymeric Nanoparticles. *Adv. Mater.* n/a-n/a (2014). doi:10.1002/adma.201404235

4. Dechtrirat, D., Gajovic-Eichelmann, N., Bier, F. F. & Scheller, F. W. Hybrid Material for Protein Sensing Based on Electrosynthesized MIP on a Mannose Terminated Self-Assembled Monolayer. *Adv. Funct. Mater.* **24,** 2233–2239 (2014).

5. Bai, W. & Spivak, D. A. A Double-Imprinted Diffraction-Grating Sensor Based on a Virus-Responsive Super-Aptamer Hydrogel Derived from an Impure Extract. *Angew. Chem.* **126,** 2127–2130 (2014).

6. Zhang, Z. & Liu, J. Molecularly Imprinted Polymers with DNA Aptamer Fragments as Macromonomers. *ACS Appl. Mater. Interfaces* **8,** 6371–6378 (2016).

7. Miyata, T., Jige, M., Nakaminami, T. & Uragami, T. Tumor marker-responsive behavior of gels prepared by biomolecular imprinting. *Proc. Natl. Acad. Sci. U. S. A.* **103,** 1190–1193 (2006).

8.   Jayasena, S. D. Aptamers: An Emerging Class of Molecules That Rival Antibodies in Diagnostics. *Clin. Chem.* **45,** 1628–1650 (1999).

9.   Tan, W. *et al.* Molecular aptamers for drug delivery. *Trends Biotechnol.* **29,** 634–640 (2011).

10.   Baldrich, E., Restrepo, A. & O'Sullivan, C. K. Aptasensor Development: Elucidation of Critical Parameters for Optimal Aptamer Performance. *Anal. Chem.* **76,** 7053–7063 (2004).

11.   Hermann, T. & Patel, D. J. Adaptive recognition by nucleic acid aptamers. *Science* **287,** 820–825 (2000).

12.   Lin, P.-H. *et al.* Studies of the binding mechanism between aptamers and thrombin by circular dichroism, surface plasmon resonance and isothermal titration calorimetry. *Colloids Surf. B Biointerfaces* **88,** 552–558 (2011).

13.   Lin, P.-H. *et al.* Microcalorimetrics Studies of the Thermodynamics and Binding Mechanism between l-Tyrosinamide and Aptamer. *J. Phys. Chem. B* **112,** 6665–6673 (2008).

14.   Xu, W. & Ellington, A. D. Anti-peptide aptamers recognize amino acid sequence and bind a protein epitope. *Proc. Natl. Acad. Sci.* **93,** 7475–7480 (1996).

15.   Savory, N., Abe, K., Sode, K. & Ikebukuro, K. Selection of DNA aptamer against prostate specific antigen using a genetic algorithm and application to sensing. *Biosens. Bioelectron.* **26,** 1386–1391 (2010).

16.   Liu, B., Lu, L., Hua, E., Jiang, S. & Xie, G. Detection of the human prostate-specific antigen using an aptasensor with gold nanoparticles encapsulated by graphitized mesoporous carbon. *Microchim. Acta* **178,** 163–170 (2012).

17.   Jolly, P. *et al.* Label-Free Impedimetric Aptasensor with Antifouling Surface Chemistry: A Prostate Specific Antigen Case Study. *Sens. Actuators B Chem.* doi:10.1016/j.snb.2014.11.083

18.   Souada, M. *et al.* Label-free electrochemical detection of prostate-specific antigen based on nucleic acid aptamer. *Biosens. Bioelectron.* **68,** 49–54 (2015).

19.   Yang, Z., Kasprzyk-Hordern, B., Goggins, S., Frost, C. G. & Estrela, P. A novel immobilization strategy for electrochemical detection of cancer biomarkers: DNA-directed immobilization of aptamer sensors for sensitive detection of prostate specific antigens. *Analyst* **140,** 2628–2633 (2015).

20.   Kavosi, B., Salimi, A., Hallaj, R. & Moradi, F. Ultrasensitive electrochemical immunosensor for PSA biomarker detection in prostate cancer cells using gold nanoparticles/PAMAM dendrimer loaded with enzyme linked aptamer as integrated triple signal amplification strategy. *Biosens. Bioelectron.* **74,** 915–923 (2015).

21.   Zhang, F. *et al.* A Microfluidic Love-Wave Biosensing Device for PSA Detection Based on an Aptamer Beacon Probe. *Sensors* **15,** 13839–13850 (2015).

22.   Liu, K., Wei, W.-Z., Zeng, J.-X., Liu, X.-Y. & Gao, Y.-P. Application of a novel electrosynthesized polydopamine-imprinted film to the capacitive sensing of nicotine. *Anal. Bioanal. Chem.* **385,** 724–729 (2006).

23.   Zhang, S., Wang, N., Niu, Y. & Sun, C. Immobilization of glucose oxidase on gold nanoparticles modified Au electrode for the construction of biosensor. *Sens. Actuators B Chem.* **109,** 367–374 (2005).

24.   Spégel, C. *et al.* On-Chip Determination of Dopamine Exocytosis Using Mercaptopropionic Acid Modified Microelectrodes. *Electroanalysis* **19,** 263–271 (2007).

25.   Lynge, M. E., Westen, R. van der, Postma, A. & Städler, B. Polydopamine—a nature-inspired polymer coating for biomedical science. *Nanoscale* **3,** 4916–4928 (2011).

26.   Waite, J. H. Surface chemistry: Mussel power. *Nat. Mater.* **7,** 8–9 (2008).

27.   Zangmeister, R. A., Morris, T. A. & Tarlov, M. J. Characterization of Polydopamine Thin Films Deposited at Short Times by Autoxidation of Dopamine. *Langmuir* **29,** 8619–8628 (2013).

28.   Lu, C.-H. *et al.* Sensing HIV related protein using epitope imprinted hydrophilic polymer coated quartz crystal microbalance. *Biosens. Bioelectron.* **31,** 439–444 (2012).

29.   Ball, V. *et al.* Deposition Mechanism and Properties of Thin Polydopamine Films for High Added Value Applications in Surface Science at the Nanoscale. *BioNanoScience* **2,** 16–34 (2012).

30.   Łuczak, T. Preparation and characterization of the dopamine film electrochemically deposited on a gold template and its applications for dopamine sensing in aqueous solution. *Electrochimica Acta* **53,** 5725–5731 (2008).

31.   Cai, D. *et al.* A molecular imprint nanosensor for ultrasensitive detection of proteins. *Nat. Nanotechnol.* **5,** 597–601 (2010).

32.   Hawkins, D. M., Stevenson, D. & Reddy, S. M. Investigation of protein imprinting in hydrogel-based molecularly imprinted polymers (HydroMIPs). *Anal. Chim. Acta* **542,** 61–65 (2005).

33.   Zayats, M., Kanwar, M., Ostermeier, M. & Searson, P. C. Molecular Imprinting of Maltose Binding Protein: Tuning Protein Recognition at the Molecular Level. *Macromolecules* **44,** 3966–3972 (2011).

34.   Keighley, S. D., Estrela, P., Li, P. & Migliorato, P. Optimization of label-free DNA detection with electrochemical impedance spectroscopy using PNA probes. *Biosens. Bioelectron.* **24,** 912–917 (2008).

35.   Goda, T. & Miyahara, Y. Label-free and reagent-less protein biosensing using aptamer-modified extended-gate field-effect transistors. *Biosens. Bioelectron.* **45,** 89–94 (2013).

36.   Inzelt, G. in *Encyclopedia of Applied Electrochemistry* (eds. Kreysa, G., Ota, K. & Savinell, R. F.) 207–214 (Springer New York, 2014). doi:10.1007/978-1-4419-6996-5_217

37.   Erickson, H. P. Size and Shape of Protein Molecules at the Nanometer Level Determined by Sedimentation, Gel Filtration, and Electron Microscopy. *Biol. Proced. Online* **11,** 32–51 (2009).

38.   Kotál, V. *et al.* Gold Coating of Poly(ethylene terephthalate) Modified by Argon Plasma. *Plasma Process. Polym.* **4,** 69–76 (2007).

39.   Bernsmann, F. *et al.* Characterization of Dopamine−Melanin Growth on Silicon Oxide. *J. Phys. Chem. C* **113,** 8234–8242 (2009).

40.   Buffeteau, T., Desbat, B. & Eyquem, D. Attenuated total reflection Fourier transform infrared microspectroscopy: Theory and application to polymer samples. *Vib. Spectrosc.* **11,** 29–36 (1996).

41.   Formisano, N. *et al.* Optimisation of an Electrochemical Impedance Spectroscopy aptasensor by exploiting Quartz Crystal Microbalance with Dissipation Signals. *Sens. Actuators B Chem.* doi:10.1016/j.snb.2015.05.049

42.   Hsu, C. H. & Mansfeld, F. Technical Note: Concerning the Conversion of the Constant Phase Element Parameter Y0 into a Capacitance. *Corrosion* **57,** 747–748 (2001).

43.   Fernandes, F. C. B., Santos, A., Martins, D. C., Góes, M. S. & Bueno, P. R. Comparing label free electrochemical impedimetric and capacitive biosensing architectures. *Biosens. Bioelectron.* **57,** 96–102 (2014).

44.   Valincius, G., Meškauskas, T. & Ivanauskas, F. Electrochemical Impedance Spectroscopy of Tethered Bilayer Membranes. *Langmuir* **28,** 977–990 (2012).

45.   Roling, B., Drüschler, M. & Huber, B. Slow and fast capacitive process taking place at the ionic liquid/electrode interface. *Faraday Discuss.* **154,** 303–311 (2011).

46.   Prostate-Specific Antigen (PSA) Test. *National Cancer Institute* Available at: http://www.cancer.gov/cancertopics/factsheet/detection/PSA.   (Accessed: 16th November 2014)

47.   Langmuir, I. The constitution and fundamental properties of solids and liquids. LI. Liquids.1. *J. Am. Chem. Soc.* **39,** 1848–1906 (1917).

48.   Sajonz, P., Kele, M., Zhong, G., Sellergren, B. & Guiochon, G. Study of the thermodynamics and mass transfer kinetics of two enantiomers on a polymeric imprinted stationary phase. *J. Chromatogr. A* **810,** 1–17 (1998).

49.   Umpleby, R. J., Baxter, S. C., Chen, Y., Shah, R. N. & Shimizu, K. D. Characterization of molecularly imprinted polymers with the Langmuir-Freundlich isotherm. *Anal. Chem.* **73,** 4584–4591 (2001).

50.   Sips, R. On the Structure of a Catalyst Surface. *J. Chem. Phys.* **16,** 490–495 (1948).

51.   Schneider, H.-J. & Yatsimirsky, A. K. in *Artificial Receptors for Chemical Sensors* (eds. Mirsky, V. M. & Yatsimirsky, A. K.) 17–65 (Wiley-VCH Verlag GmbH & Co. KGaA, 2010).

52.   Bossi, A., Piletsky, S. A., Piletska, E. V., Righetti, P. G. & Turner, A. P. F. Surface-Grafted Molecularly Imprinted Polymers for Protein Recognition. *Anal. Chem.* **73,** 5281–5286 (2001).

53.   Wu, S., Tan, W. & Xu, H. Protein molecularly imprinted polyacrylamide membrane: for hemoglobin sensing. *Analyst* **135,** 2523–2527 (2010).

54.   Umpleby II, R. J. *et al.* Characterization of the heterogeneous binding site affinity distributions in molecularly imprinted polymers. *J. Chromatogr. B* **804,** 141–149 (2004).

55.   Hong, S. K. Kallikreins as Biomarkers for Prostate Cancer. *BioMed Res. Int.* **2014,** e526341 (2014).

56.   Väisänen, V., Peltola, M. T., Lilja, H., Nurmi, M. & Pettersson, K. Intact free prostate-specific antigen and free and total human glandular kallikrein 2. Elimination of assay interference by enzymatic digestion of antibodies to F(ab')2 fragments. *Anal. Chem.* **78,** 7809–7815 (2006).

57.   Klee, G. G. *et al.* Highly sensitive automated chemiluminometric assay for measuring free human glandular kallikrein-2. *Clin. Chem.* **45,** 800–806 (1999).

58.   Liao, H., Zhang, Z., Li, H., Nie, L. & Yao, S. Preparation of the molecularly imprinted polymers-based capacitive sensor specific for tegafur and its characterization by electrochemical impedance and piezoelectric quartz crystal microbalance. *Electrochimica Acta* **49,** 4101–4107 (2004).

59.   Lisdat, F. & Schäfer, D. The use of electrochemical impedance spectroscopy for biosensing. *Anal. Bioanal. Chem.* **391,** 1555–1567 (2008).

60.   Fogh-Andersen, N., Bjerrum, P. J. & Siggaard-Andersen, O. Ionic binding, net charge, and Donnan effect of human serum albumin as a function of pH. *Clin. Chem.* **39,** 48–52 (1993).

61.   D'Orazio, P. Biosensors in clinical chemistry. *Clin. Chim. Acta* **334,** 41–69 (2003).

5. Chapter: Hybrid Synthetic Receptors on (Bio)-FET Devices For Detection Of PSA

5.1. Introduction

5.1.1. General overview

The chapter extends the application of hybrid imprinting to metal-oxide-semiconductor field effect transistor (MOSFET) devices. MOSFET devices are more sensitive than EIS sensors and provide scope for miniaturisation. PSA sensing with MOSFET devices was carried out in order to investigate the compatibility of the hybrid-MIP system with a different sensing platform and to explore improvement in sensitivity of the apta-MIP system. Additionally, encouraging results with human serum albumin (HSA) of the apta-MIP EIS sensor led to the testing of PSA in human plasma to explore the potential for clinical applications.

5.1.2. MOSFET devices:

Field effect transistors (FET) are semiconductor devices made up of two highly conducting regions separated (source and drain) by a channel, whereby the potential applied to an external gate controls flow of current between the two conducting channels.[1] There are various types of FETs of which metal-oxide semiconductor FET devices are the most popular, finding use in practically every electronic appliance today (for data processing and storage).[2] MOSFET devices have also found applications in biosensing as a result of their stability, sensitivity and scope for miniaturization.[3, 4]

There two types of semiconductor FET devices: n-channel and p-channel depending on the type of charge carriers present in the conducting channel. The charge carriers of the conducting channel constitute an inversion charge, that is, electrons in the case of a p-type substrate (n-channel device) or holes in the case of an n-type substrate (p-channel device), which can be obtained by manufacturing the device with different impurities that

control the amount and type of charge in the device.[5] MOSFETs are made with silicon as the semiconductor material due to various advantages such as accessibility, ease of manipulation of conductivity by controlled addition of impurity and the ability to change charge carrier (p and n channel) by doping with different impurities.[5]

A common n-channel MOSFET is fabricated on a p type substrate (silicon) with heavily doped n^+ regions, which act as source and drain (Figure 5.1).[6] A thin layer of silicon oxide (SiO_2) or glass (typically between 2 and 50 nm) is placed on the surface of the substrate, between the drain and the source regions, which acts as the insulator from the gate electrode. Metal or polysilicon (which is a conductor) is deposited on top of the silicon oxide layer to form the gate electrode. Metal contacts are also made in the source and drain regions (Figure 5.1) to form three channels: source, drain and gate. The current that flows from source to drain is then controlled by application of voltage on the external gate terminal (Figure 5.1). To put in simple terms the flow of charge in a MOSFET device can be compared to tank carrying water, which is separated into two sections (source and drain terminal) by a barrier in the middle (gate terminal). When the barrier is closed there is no flow of water between the two sections of water, but when the barrier is opened (external voltage), water flows from higher to the lower section much like flow of charge in MOSFET devices.
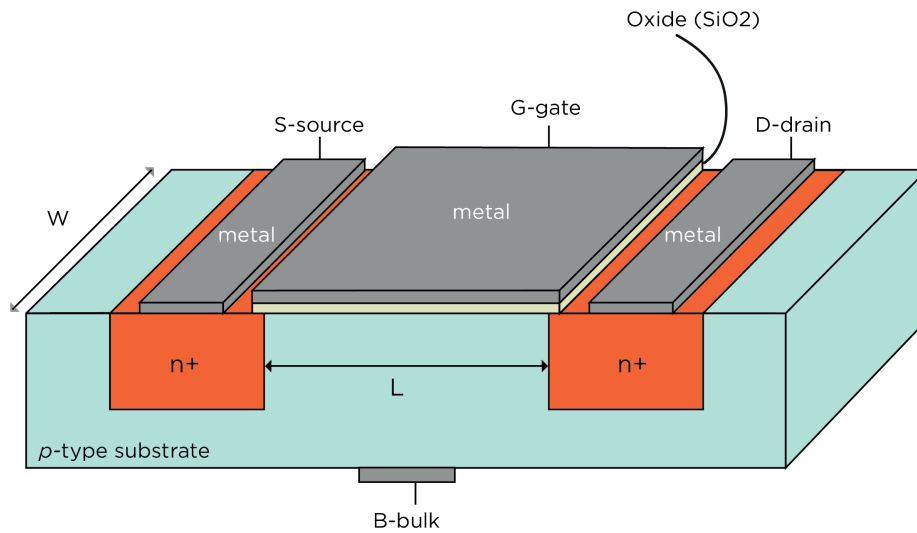
Figure 5. 1: Schematic of n-MOSFET device containing the source and the drain through which current flows when an external voltage is applied across the gate terminal

In a simple n-type MOSFET device the source terminal and the body of the device are grounded. The gate and drain voltages are applied with respect to the source. Under DC conditions, the source and drain are separated by the p-type substrate, which prevents flow of electrons between the two terminals. This is also termed as the cut-off mode. When a suitable external voltage is applied through the gate terminal (Vgs), the barrier to flow of current is lowered and electrons flows through the semiconductor channel as can be seen in Figure 5.2.[6] The onset of current flow is defined in terms of threshold voltage (Vt), which is the minimum voltage (applied with respect to other terminals) required to induce the inversion charge.[5] When Vgs is greater that Vt and a potential (Vds) is applied at the drain terminal (Vds > 0), current starts flowing through the channel, which is denoted as 'Id'. The electrons pass from the source to drain though the channel, while no

current flows through the gate (gate current or Ig = 0). Gate current is zero because the gate is insulated from the conducting channel. Increasing the amount of Vds increases the channel conductivity, which leads to increase in source-drain current (Id) following Ohms law. This mode is also called the triode mode. Ohm's law is followed till (Vgs-Vt) > Vds, inducing the electrons to flow from source to drain. However, when (Vgs-Vt) < Vds, there is competition between gate and drain to attract the electrons leading to a pinch-off condition (end of Ohm's law) as seen in Figure 5.3.[5] As drain attracts more electrons due to higher voltage the channel conductivity is diminished, however as a result of potential different between the source and the drain a constant current (Id = constant) flows through the channel, which is also called the saturation current. This mode is termed the saturation mode.[5,6]
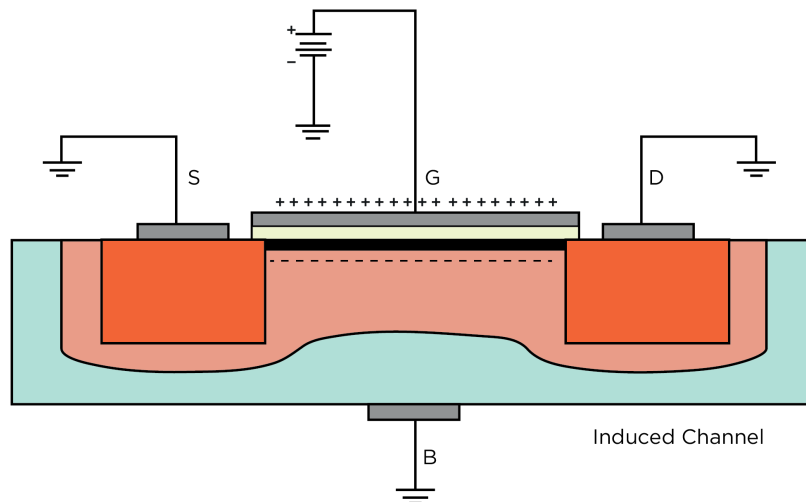
Figure 5. 2: Induced channel created as a result of Vgs applied at the gate terminal.

There are three modes of operation for MOSFET devices as seen in Figure 5.3:

1) A cut-off mode, Vgs-Vt < 0, no induced channel is created hence no flow of current;

2) Triode mode, Vgs-Vt > Vds > 0, current flows through the induced channel proportional Vds;

3) Saturation mode, 0 < Vgs-Vt < Vds , Id current becomes constant
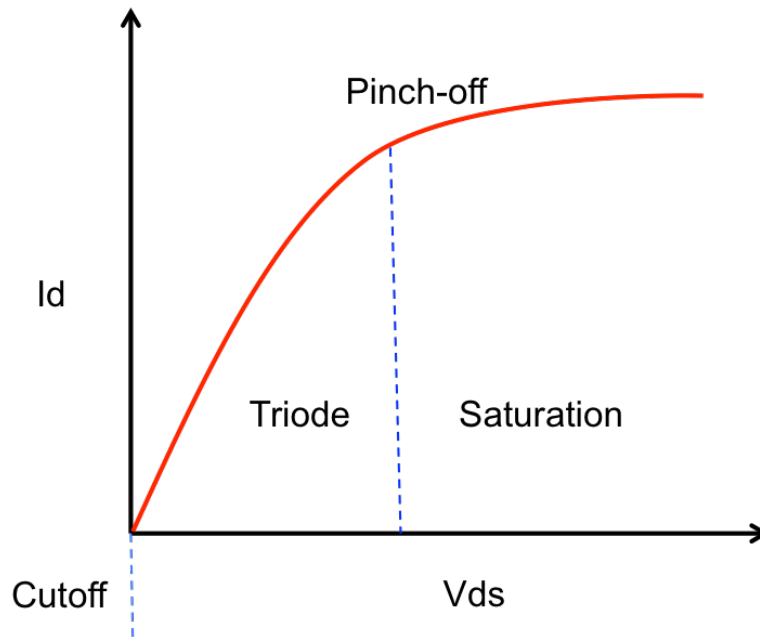
Figure 5. 3: Id vs Vgs characteristic of MOSFET devices with three modes of operation: cutoff, triode and saturation.

5.1.3. *Application of a MOSFET device in biosensing*

MOSFET devices have been used for detection of various biomolecules such as DNA[7], proteins[8], small molecules[9] and cells[10] in the field of biosensing. For the purpose of biosensing, bio-receptors need to be immobilised on the surface of the MOSFET devices. The surface used for immobilisation is usually the gate terminal, which modulates the channel conductivity. The interaction of the bio-functionalised gates with the analyte of interest changes the effective surface potential of the gate terminal (open circuit potential)

due to changes in charge density and charge distribution of the immobilised biolayer.[11] The change in surface potential at the gate in turn modulates the channel conductivity causing changes in the current between source and drain terminal. This change in channel conductivity can be easily measured and is directly proportion to the amount of analyte bound to the receptor at the gate terminal. Non-covalent or covalent immobilisation of bio-receptors directly on the gate terminal has been widely reported in the literature for biosensing.[11,12,13] However, this setup faces certain disadvantages like low environmental stability and lack of flexibility in chemical modification of the gate surface. An alternative strategy that is utilised is the use of an extended gate for immobilisation of biomolecules. The extended gate set up permits the incorporation of biocompatible surfaces to facilitate easy bio-functionalisation of the gate surfaces.[14] The use of extended gate surface leads to improved stability of the MOSFET device, which permits sensitive detection of biomolecules. The extended gate setup also provides flexibility in bio-functionalisation strategy by allowing the use of different materials like gold, titanium, carbon nano-tube, zinc in different configurations to be integrated with the device.[9, 15, 16] Extended gate FETs have been widely used for DNA hybridisation[17], aptamer-protein interaction[16], and enzymatic activity detection[18] demonstrating wide application in field of biosensing. One significant advantage of MOSFETs is their suitability for use in miniaturized measurement systems, thereby allowing ease of integration with electronic readouts[12]. In this regard, a bio-FET device could be applicable to a range of point-of-need healthcare applications.

5.1.4. Apta-MIP on MOSFET devices

Chapter 4 developed and explored the use of impedance-based sensors for aptamer hybrid imprinting strategy for detection of PSA. Although a highly sensitive biosensor was developed for detection PSA, the sensor suffered from certain drawbacks such as low stability due to the use of redox couple solution (photosensitive), low scope for miniaturisation and difficulty integration with point-of-care electronic systems. MOSFET devices on the other hand overcome some of these drawbacks and have not been well studied for molecular imprinting in the literature. A recent report by Z. Iskierko *et al.* demonstrated the integration of electropolymerised bis(bithiophene) molecularly imprinted polymers (MIPs) within extended field effect devices for sensitive detection of inosine.[19] The MIP-FET sensor reported an imprinting factor 4.9 with limit of detection (LOD) of 0.62 µM, which is suitable for inosine detection in biological samples. The study highlighted the advantages of using MOSFET for molecular imprinting application. Protein imprinting with MOSFET devices has not been explored yet, hence MOSFET with apta-MIPs were fabricated to test their suitability for MIP sensing. It was hypothesised that the MOSFET devices would be more stable and sensitive than impedimetric sensors, allowing for detection of PSA in diluted biological samples. Figure 5.4 shows the development of apta-MIP on gold electrodes that were integrated into the extended gate MOSFET device setup.
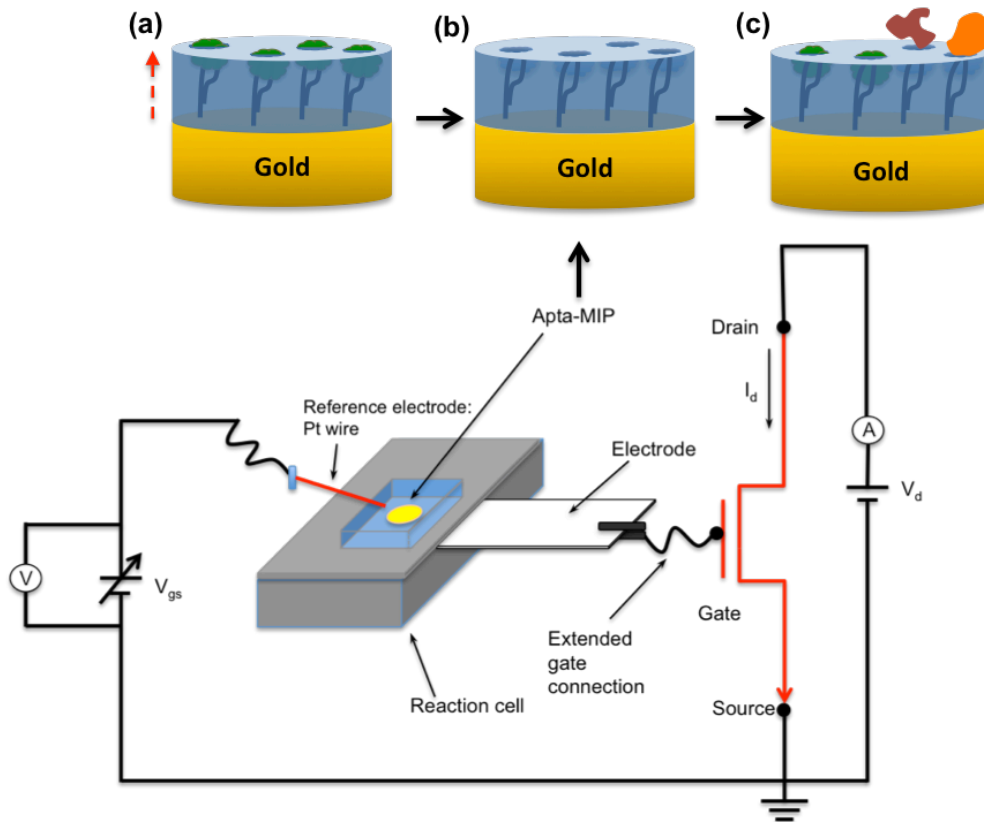
Figure 5. 4: (a) In the first step the gold surface was functionalised with PSA-aptamer complex in a flow cell followed by electropolymerisation of polydopamine on surface to imprint the aptamer-PSA complex (b) Post imprinting, PSA was extracted using detergent and acid to expose the imprinted site (c) The electrodes modified with apta-MIP were then utilized in an extended gate MOSFET setup to check for rebinding of PSA.

5.2.   Aims And Objectives

Chapter 5 extends apta-MIP hybrid impedance sensing on field effect transistor devices (FET). The overall aim of this chapter is to fabricate a MOSFET apta-MIP sensor and evaluate the sensor's sensitivity and selectivity.

Main objectives are chapter 5 are:

1. Evaluation of MOSFET for apta-MIP PSA sensing.

2. Comparison with aptamer alone MOSFET sensor.

3. Comparison of MOSFET apta-MIP sensor's performance to EIS apta-MIP sensor from Chapter 4.

4. Detection of PSA in human plasma to understand fouling by serum proteins.

4.4.

5.3. Materials And Methods

5.3.1. Reagents:

Thiol terminated DNA aptamer with the sequence (5'-HS-$(CH_2)_6$-TTT TTA ATT AAA GCT CGC CAT CAA ATA GCT TT-3') was obtained from Sigma Aldrich, UK. Prostate specific antigen (PSA) was obtained from Merck Chemicals Ltd, UK. Human glandular kallikrein 2 (hK2) was obtained from RnD systems, UK. Human plasma albumin (HSA), dopamine hydrochloride, trisma base, mercaptohexano (MCH), concentrated sulphuric acid, potassium phosphate monobasic solution (1 M), potassium phosphate dibasic solution (1 M), potassium hexacyanoferrate (III), potassium hexacyanoferrate (II) trihydrate, hexaammineruthenium (III) chloride, tween 20, potassium chloride and magnesium chloride were all purchased from Sigma–Aldrich, UK. All reagents were of analytical grade. All aqueous solutions were prepared using ultra-pure water 18.2 MΩ cm from Milli Q system with Pyrogard filter (Millipore, MA, USA). Gold working electrodes were obtained from CH Instruments, USA and mechanical electrode polishing kit from Buehler, UK.

5.3.2. Gold slide electrode preparation

Evaporated gold electrodes (Figure 5.5) were prepared in-house on glass slides supports using a thermal evaporator (BOC Edwards, UK). The process was performed under fine vacuum (2.0×10^{-6} mbar) consisting of an initial deposition of 20 nm of chromium on glass followed by a deposition step of a thicker layer (usually between 100 and 200 nm) of gold. Chromium was used for easy adhesion of gold to the glass surface and thickness of gold was determined based on uniform coverage of gold and to prevent lift off during

the washing process.[20] The slides were washed with ethanol and water before being used for apta-MIP preparation.
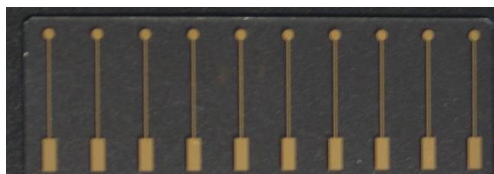
Figure 5. 5: Gold evaporated electrodes used in apta-MIP electrode preparation

5.3.3. MOSFET experimental setup

Colleagues at the University of Bath fabricated the MOSFET devices. The extended gate was produced by connecting modified gold electrodes immobilized in a reaction cell to the gate of the n-MOSFET device via a metal wire (Figure 5.4). n-MOSFETs were made using 0.8 μm semiconductor switch from AMS Technologies, Germany. The threshold voltage (Vt) of the transistor was determined to be 0.82 V and transconductance calculated was 69 μA/V. The length-by-width ratio of the transistor was 10:2 μm. The terminals of the transistor were provided with diode protection circuitry and were packaged in a standard complementary-metal-oxide-semiconductor (CMOS)_ chip. A voltage of 50 mV was applied between the drain and source (Vd or Vds) to operate the transistor and the gate-source voltage (Vgs) was swept from 0.0 to 5.0 V. These settings prevented the current from increasing more than 75 μA, avoiding any changes in Vgs by heating. All electrical measurements were conducted using an Agilent B1500A semiconductor device analyzer. Detailed information on the specifications of the CMOS chip can be found in the literature.[21]

5.3.4. *Apta-MIP fabrication and sensor performance*

The apta-MIPs were prepared using the protocol provided in Chapter 4, section 4.3.3. Briefly the apta-PSA complex was immobilised on the gold electrodes followed by electropolymerisation of dopamine. This was followed by extraction of PSA with acetic acid and SDS. The electrodes were extensively washed with water to remove residual acid/SDS before incubating with PBS pH 7.4 for stabilising the electrodes. Apta-NIPs were prepared in the same manner in the presence of aptamer but in the absence of PSA. The gold evaporated electrodes modified with apta-MIPs were immobilised in a flow cell (Figure 5.6) and then connected to the MOSFET device. Three stability measurements were conducted in PBS (pH 7.4) before incubating electrodes with PSA. Increasing concentration of PSA (0.1 fg/ml to 1 μg/mL) in PBS (pH 7.4) was incubated for half an hour on the electrodes. Post incubation, PSA solution was removed and electrodes were rinsed with PBS before measuring the response using the extended gate MOSFET setup. For detection of binding, a voltage of 50 mV was applied between the drain and source (Vd or Vds) to operate the transistor and the gate-source voltage (Vgs) was swept from 0.0 to 5.0 V. All electrical measurements were conducted using an Agilent B1500A semiconductor device analyzer. Measurements for all experiments were recorded for 4 different devices.
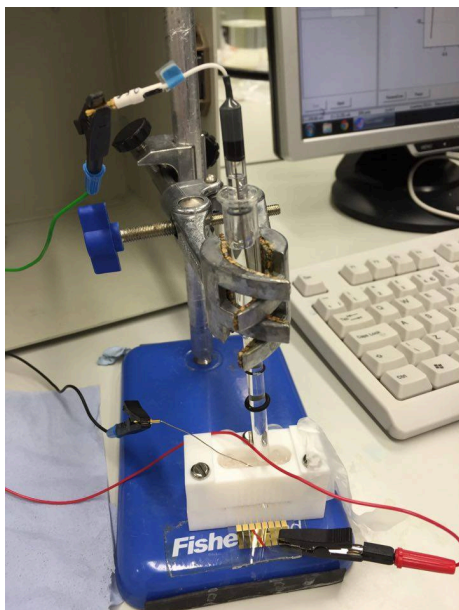
Figure 5. 6: Gold evaporated electrodes immobilised in a flow cell for electropolymerisation of dopamine. The electrodes were fixed in the flow cell and all binding experiments were conducted in situ.

5.3.5. Control studies with hk2 protein

For control studies 1μg/ml PSA was incubated with apta-NIP for 30 minutes before measuring the response. hK2 protein at a concentration of 1μg/mL was used to understand cross-reactivity of the apta-MIP sensor.

5.3.6. Aptamer/MCH immobilised electrode for PSA binding

Experiments with PSA aptamer alone were performed using the same gold evaporated electrodes following the protocol reported previously in Chapter 4. Briefly, electrodes were exposed to thiolated DNA aptamer/6- mercapto-1-hexanol (MCH, Sigma, U.K.) immobilization solution for 16 h in a humidity chamber. An optimized (1:100) DNA aptamer to total thiol was used to fabricate the biosensor. A high concentration of MCH was prepared in ethanol, which was diluted to working concentrations in 10 mM PBS

(pH 7.4). Prior to addition of MCH, DNA aptamers were heated to 95 °C for 10 min followed by gradual cooling over 30 min to room temperature. After immobilization, electrodes were rinsed with excess Milli-Q water to remove unattached thiols. In order to ensure complete thiol coverage of the gold surface, the electrodes were thereafter backfilled with 1 mM MCH for 1 h. Electrodes were then rinsed with Milli-Q water and placed in the 10 mM PBS (pH 7.4) for stabilization

5.3.7. PSA binding study in human plasma

For plasma experiments, blood obtained from a healthy female volunteer was spun down in a centrifuge (3200 rpm, 20 min) to remove the red blood cells. The resultant plasma was diluted 1000 times in a PBS buffer of pH 7.4 and then spiked with varying concentrations of PSA (1, 5, and 10 pg/mL PSA). For detection of binding, a voltage of 50 mV was applied between the drain and source (Vd or Vds) to operate the transistor and the gate-source voltage (Vgs) was swept from 0.0 to 5.0 V. All electrical measurements were conducted using an Agilent B1500A semiconductor device analyzer. Measurements for all experiments were recorded for 4 different devices.

5.4.   Results And Discussion

5.4.1. Apta-MIP fabrication and PSA binding study

The electrode fabrication process was kept consistent with the optimised apta-MIP EIS sensor in Chapter 4 to allow comparison between the two sensing methodologies. Dose response curves were generated for the apta-MIP MOSFET sensor with PSA. Fig. 5.7 (a) depicts the response of the device upon incubation with increasing concentrations of PSA. Figure 5.7 (b) shows the transfer characteristics of the device upon binding to PSA, demonstrating a positive shift in voltage upon introduction of PSA. Following the lag region of the plot, a linear response was obtained from 0.1 to 10 pg/ml of PSA after which no further significant change in signal was observed. A maximum voltage change (ΔVg) of 158 ± 42.5 mV was observed at concentration of 1 μg/mL of PSA and negligible changes in voltage shift was observed beyond 100 pg/ml suggesting saturation of binding sites. When compared to apta-NIP a change of 7.6 ± 3.21 mV (Fig. 2) was observed upon incubation with concentration 1 μg/mL PSA, which was 20 times lower apta-MIP indicating high selectivity of apta-MIPs towards the template. A high concentration of PSA was used with apta-NIP control to obtain maximum possible interaction/signal change with the sensor. The initial change of 30 mV at concentrations 1-10 fg/mL could be an effect of PSA interacting with the apta-MIP surface. It is hypothesised that when PSA comes closer to the polymer surface, it causes a change in the distribution of charges in the bilayer leading to an initial shift in voltage. The other reason for initial shift in voltage could be that there are two types of binding sites present on the sensor surface, where high affinity binding sites fill preferentially to a population of lower affinity sites. The initial lower shift in voltage to analyte has been observed in

other FET sensors suggesting that there could be some binding (specific/non-specific) event occurring at lower concentration which the sensor is not able to distinguish due to device limitations.[15] The initial change of 30 mV at concentrations between 1 and 10 fg/mL in the MOSFET sensor could be attributed to small amounts of weak binding of PSA to the aptamer causing a conformational change and hence changes in the distribution of charges in the biolayer. Beyond 0.1 pg/ml a shift in voltage could be a result of PSA filling the slightly lower binding affinity sites and specifically interacting with the apta-MIP surface. Increase in the shift of Vgs could be a result of aptamer charges being screened and PSA binding to the polymeric cavity, which dominates the charge behaviour at the gate surface. This is consistent with other aptamer FET sensor where an increase voltage shift is observed upon increasing concentration of analyte.[22,23] The current flowing through the MOSFET is based on the electric field established by the voltage applied to the gate electrode. Hence, the net charge of protein can modulate the flow of current through the device causing a shift in voltage. The FET sensors can detect local net-charges of PSA because of the smaller sensing depth (the Debye length) compared to the size of protein[24]. The direction of the voltage shift depends on net charge of PSA at pH 7.4 binding to the apta-MIP and the charge of DNA. It is hypothesised that upon rebinding of PSA (with a certain net charge) to the apta-MIP, there is a change in the electrochemical double layer and in the charge distribution of the bilayer, which causes a variation in the potential drop at the gate of the MOSFETs. A positive shift in voltage is observed upon binding of PSA to apta-MIP that corresponds to an increase in negative charges on the surface of the sensor; it is hypothesised that this is an effect of net negative charge of PSA.[16] MOSFET devices also permit rapid sensing in PBS buffer

316

as there is no need to stabilize the system in redox couple solution. The lack of requirement of redox couple for sensing ahead of testing, which could take up to an hour in case of apta-MIP EIS sensors, permits rapid sensing using the apta-MIP MOSFET system. The apta-MIP bio-FET device was also 100 times more sensitive than apta-MIP impedance sensor. The increase in sensitivity could be explained by the smaller sensing depth (Debye length) of FET devices whereby small changes in charge behaviours can be easily/quickly detected upon binding of aptamer to protein.[25] However, in the case of EIS sensor, the sensing is based on a bulk effect where the redox-couple diffuses through the polymer layer to detect the binding event, which could be slower, and less sensitive than MOSFET devices. The results from our study suggest that MOSFET devices could be a better platform for apta-MIP sensing that EIS, however there have not been any comparisons of polymeric FET and EIS sensing in the literature to support our findings.
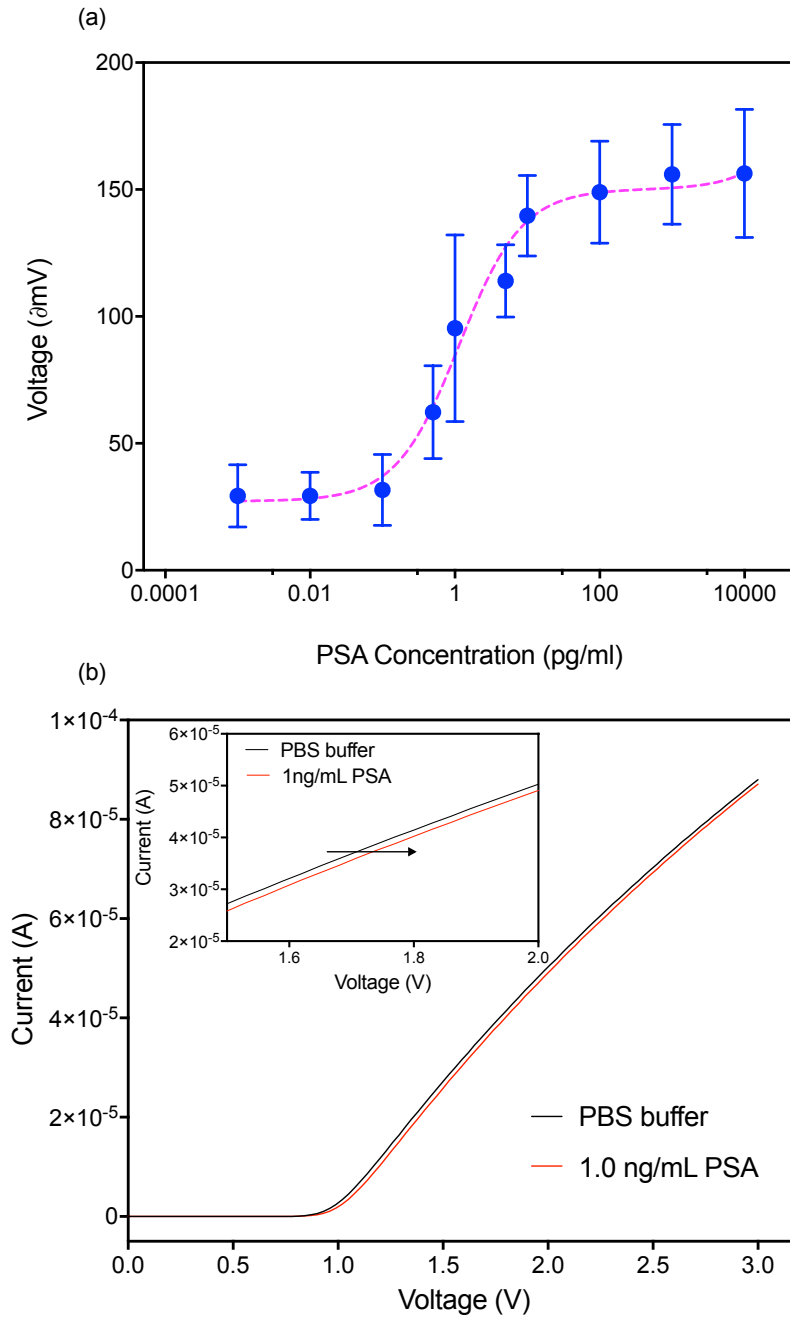
Figure 5. 7: (a) Dose response of PSA with apta-MIP FET device. (b) Transfer characteristics curve of apta-MIP FET device binding to PSA (Error bars represent SD, n = 4)

In the case of the apta-NIPs, it is proposed that the aptamer lies flat on the surface in the absence of PSA and get buried in the polymer during the polymerisation process. In the

absence of a polymeric cavity PSA does not bind to the aptamer in the apta- NIP leading

to a lower shift in voltage (Figure 5.8). This is consistent with impedance response of

apta-NIP EIS sensor to PSA as seen in Chapter 4.
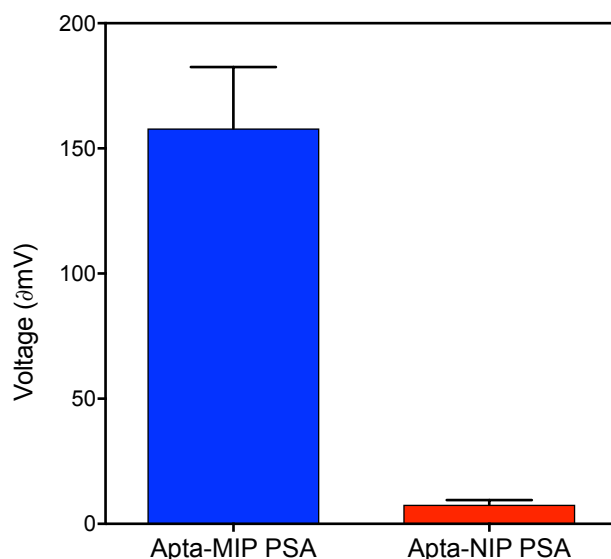
Figure 5. 8: Apta-MIP response versus apta-NIP response to 1µg/mL PSA. (Error bars represent SD, n = 4)

5.4.2. Control studies with hk2 protein

To understand the selectivity of the sensor, the apta-MIP bio-FET device was subjected

to stringent controls similar to EIS sensor by comparing the response with a homologous

protein hK2 (80 % homologous) in a non-competitive assay. The response to 1 µg/mL

hK2 was much lower with a change of 56 ± 13.6 mV compared to PSA (158 ± 42.5 mV)

at the same concentration as shown in Figure 5.9. The lower hK2 response suggested that

the apta-MIP device was more selective towards PSA. As can be observed from the

impedance based sensors in chapter 4 the PSA aptamer reported negligible cross

reactivity towards hK2, which therefore suggests that polymer interactions could be

contributing to hK2 recognition in MOSFET apta-MIP device too. The shape and chemical selectivity of the apta-MIP cavity, coupled with the high dependence on non-specific hydrogen bonding likely leads to this small degree of cross-reactivity.
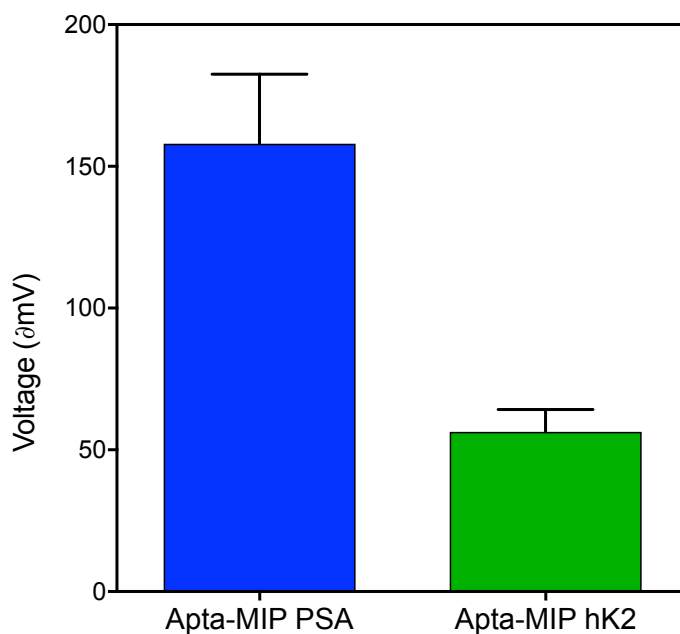
Figure 5. 9: Apta-MIP response to 1µg/mL hK2 protein was significantly lower than apta-MIP response to PSA. (Error bars represent SD, n = 4)

5.4.3. *Aptamer/MCH immobilised electrode for PSA binding*

It was important to compare the apta-MIP sensor with an aptamer alone sensor to understand whether an improvement in affinity was achieved as a result of imprinting. The ratio of aptamer/thiols was chosen based on work by P. Jolly *et al.* to obtain even distribution of aptamers with maximum binding to PSA[26]. On comparison of apta-MIP with an aptamer alone FET sensor a significant increase in sensitivity was observed for an aptamer-MIP sensor (Figure 5.10). Aptamer only FET displayed a shift of 18 mV compared to 150 mV shift of apta-MIP at 1 ng/ml PSA. A negative shift in voltage was

observed at 0.1 pg/ml, which could be a result of non-specific binding of PSA to MCH SAM (self-assembled monolayer), which has been reported in literature [26,27]. A positive shift in voltage was observed upon increasing the concentration beyond 0.1 pg/ml, however the response was much lower than apta-MIP sensor, suggesting an improvement in affinity of the hybrid receptors. Typically, low ionic strength buffers (I) are used for FET aptasensors that yield the solution Debye length κ^{-1} which allows for effective measurement of the intrinsic charges of the target protein by making the binding reaction on the surface within the electric double layer.[28] The low response of aptamer only sensor could be a result of higher ionic strength of the buffer, which leads to screening of charges and a lowering of the sensor sensitivity.
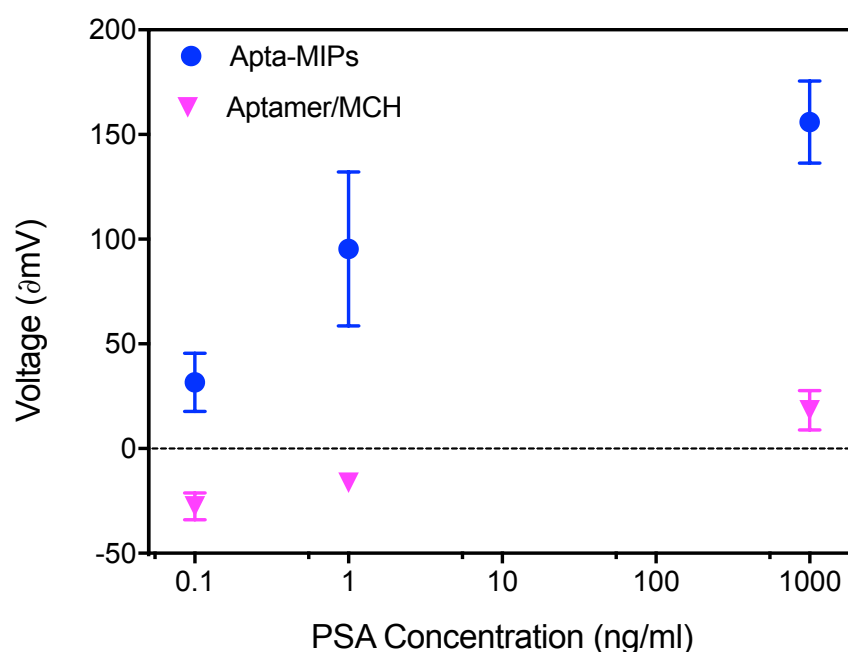
Figure 5. 10: Comparison of apta-MIP response to PSA with respect aptamer/MCH modified surface. The aptamer only device displays lower sensitivity than the apta-MIP device. (Error bars represent SD, n = 4)

5.4.4. *PSA binding study in human plasma*

The sensor was further tested in human plasma to evaluate its use in clinical applications. Human plasma from a healthy female volunteer was used for the experiments due low background PSA levels. Spiking the plasma with PSA from a healthy female volunteer allowed for the measurement of known level of PSA in the plasma (low background PSA) while maintaining the ratio of PSA/plasma proteins. Plasma diluted 1000 times displayed very low change in signal of -2 mV as shown in (Fig. 4) which indicated good resistance to fouling of the apta-MIP surface by plasma proteins. The negative shift in voltage could be explained by the net charge of serum proteins like albumin disturbing the distribution of charges in the bilayer. However, the shift is negligible, which suggest that there is not significant interaction between the apta-MIP and serum proteins. PSA concentrations between 1 and 10 pg/ml of PSA could be detected linearly in diluted plasma. 1 pg/ml PSA demonstrated a shift of 13 mV, which was still 2 times higher than the apta-NIP response at 1 μg/mL maintaining selectivity of the sensor (Figure 5.11). Although there was loss of recognition when compared to the response in PBS (pH 7.4), the results are highly encouraging due to detection of clinically relevant concentrations. Considering the concentration PSA in healthy men in 4 -10 ng/ml[29], diluting the plasma by a thousand fold would enable measurement in the linear range of the sensor. The loss in sensitivity observed is likely explained by protein-protein interactions, which have also been observed in aptamer ELISA assays in serum[28] and plasma[30]. Free PSA, which is derived from human plasma for the experiments, will interact with complement proteins, anti-chymotrypsin and albumin in plasma lowering the sensitivity of the sensor. However, free PSA present in the blood of patient samples is internally cleaved and

hence could escape interactions with anti-chymotrypsin[31] potentially allowing for detection of PSA at a lower sensitivity.

Nevertheless the experiment highlights the potential use of apta-MIP devices for sensitive detection of biomarkers in human blood at clinically relevant concentrations. The majority of MIP sensors have not been evaluated with human plasma due to low sensitivity and high non-specific binding observed with plasma proteins[32,33,34]. The apta-MIP sensors demonstrated in this work are capable of detecting clinically relevant concentrations of protein with minimal fouling of sensor surface by plasma proteins. Hybrid MIP sensors may hold the key to forming the next generation of robust label free biosensors. The sensors were also stable at 4 ^{0}C in PBS buffer for more than 3 days without any observable drop in signal suggesting that these sensors could be stored for longer period of time. However, long-term stability measurements would be required to confirm these results.
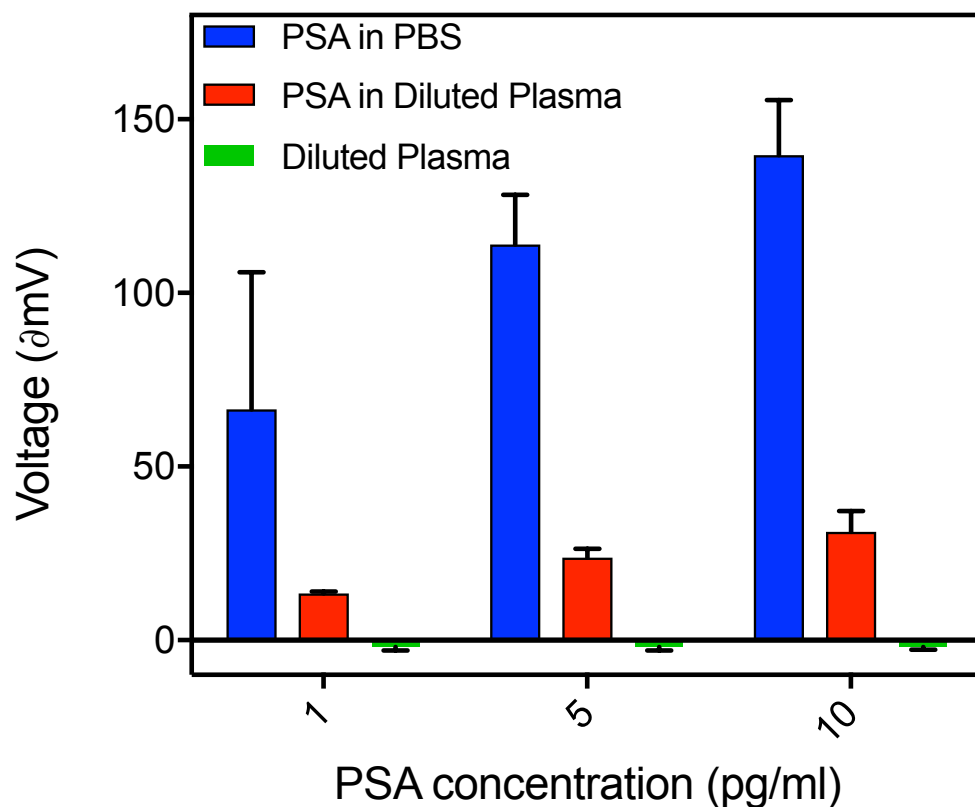
Figure 5. 11: Apta-MIP response in 1000X diluted plasma spiked with PSA. The sensor showed a lower response to PSA in diluted plasma (red) when compared to PSA in buffer (blue). The plasma on its own showed very little signal change (green). (Error bars represent SD, n = 4)

5.5.   Conclusion

In conclusion, a sensitive MOSFET apta-MIP device was developed with a higher sensitivity than an aptamer alone MOSFET sensor and also an apta-MIP EIS sensor. In addition, negligible response of the apta-MIP surface to the diluted plasma suggested high selectivity of the sensor towards PSA. The sensor was capable of detecting between 1-10 pg/ml PSA in diluted plasma, which falls in the clinical range of PSA levels in men demonstrating potential application in clinical use. This study showcases that the combination of hybrid MIP receptors with MOSFET devices could help develop next generation of robust label free sensors that can be translated to other clinical biomarkers.

5.6.　　References

1.　　　　Horowitz, P. & Hill, W. *The Art of Electronics*. (Cambridge University Press, 1989).

2.　　　　Foty, D. P. *MOSFET Modeling with SPICE: Principles and Practice*. (Prentice-Hall, Inc., 1997).

3.　　　　Yuqing, M., Jianguo, G. & Jianrong, C. Ion sensitive field effect transducer-based biosensors. *Biotechnol. Adv.* **21,** 527–534 (2003).

4.　　　　Bergveld, P. The impact of MOSFET-based sensors. *Sens. Actuators* **8,** 109–127 (1985).

5.　　　　Ytterdal, T., Cheng, Y. & Fjeldly, T. A. in *Device Modeling for Analog and RF CMOS Circuit Design* 1–45 (John Wiley & Sons, Ltd, 2003).

6.　　　　Anderson, B. & Anderson, R. *Fundamentals of Semiconductor Devices*. (McGraw-Hill, Inc., 2005).

7.　　　　Barbaro, M. *et al.* A CMOS, fully integrated sensor for electronic detection of DNA hybridization. *IEEE Electron Device Lett.* **27,** 595–597 (2006).

8.　　　　Park, K.-Y., Kim, M.-S. & Choi, S.-Y. Fabrication and characteristics of MOSFET protein chip for detection of ribosomal protein. *Biosens. Bioelectron.* **20,** 2111–2115 (2005).

9.　　　　Ali, S. M. U., Nur, O., Willander, M. & Danielsson, B. Glucose Detection With a Commercial MOSFET Using a ZnO Nanowires Extended Gate. *IEEE Trans. Nanotechnol.* **8,** 678–683 (2009).

10.   Campanella, L., Favero, G., Mastrofini, D. & Tomassetti, M. Further developments in toxicity cell biosensors. *Sens. Actuators B Chem.* **44,** 279–285 (1997).

11.   Schöning, M. J. & Poghossian, A. Bio FEDs (Field-Effect Devices): State-of-the-Art and New Directions. *Electroanalysis* **18,** 1893–1900 (2006).

12.   Lee, C. S., Kim, S. K. & Kim, M. Ion-Sensitive Field-Effect Transistor for Biological Sensing. *Sensors* **9,** 7111–7131 (2009).

13.   Veigas, B., Fortunato, E. & Baptista, P. V. Field Effect Sensors for Nucleic Acid Detection: Recent Advances and Future Perspectives. *Sensors* **15,** 10380–10398 (2015).

14.   Arya, S. K., Wong, C. C., Jeon, Y. J., Bansal, T. & Park, M. K. Advances in Complementary-Metal–Oxide–Semiconductor-Based Integrated Biosensor Arrays. *Chem. Rev.* **115,** 5116–5158 (2015).

15.   Goda, T. & Miyahara, Y. Label-free and reagent-less protein biosensing using aptamer-modified extended-gate field-effect transistors. *Biosens. Bioelectron.* **45,** 89–94 (2013).

16.   Maehashi, K. *et al.* Label-Free Protein Biosensor Based on Aptamer-Modified Carbon Nanotube Field-Effect Transistors. *Anal. Chem.* **79,** 782–787 (2007).

17.   Uslu, F. *et al.* Labelfree fully electronic nucleic acid detection system based on a field-effect transistor device. *Biosens. Bioelectron.* **19,** 1723–1731 (2004).

18.   Senillou, A., Jaffrezic-Renault, N., Martelet, C. & Cosnier, S. A miniaturized urea sensor based on the integration of both ammonium based urea enzyme field effect transistor and a reference field effect transistor in a single chip. *Talanta* **50,** 219–226 (1999).

19.   Iskierko, Z. *et al.* Extended-gate field-effect transistor (EG-FET) with molecularly imprinted polymer (MIP) film for selective inosine determination. *Biosens. Bioelectron.* **74,** 526–533 (2015).

20.   Balasubramania, S. G. Development of Smart Functional Surfaces for Biosensor Applications. (2008).

21.   Estrela, P. *et al.* Label-Free Sub-picomolar Protein Detection with Field-Effect Transistors. *Anal. Chem.* **82,** 3531–3536 (2010).

22.   Ozsoz, M. S. *Electrochemical DNA Biosensors*. (CRC Press, 2012).

23.   Peng Li, Piero Migliorato & Pedro Estrela. in *Electrochemical DNA Biosensors* 141–162 (Pan Stanford Publishing, 2012).

24.   Stern, E. *et al.* Importance of the Debye Screening Length on Nanowire Field Effect Transistor Sensors. *Nano Lett.* **7,** 3405–3409 (2007).

25.   Schöning, M. J. & Poghossian, A. Recent advances in biologically sensitive field-effect transistors (BioFETs). *Analyst* **127,** 1137–1151 (2002).

26.   Zayats, M., Huang, Y., Gill, R., Ma, C. & Willner, I. Label-Free and Reagentless Aptamer-Based Sensors for Small Molecules. *J. Am. Chem. Soc.* **128,** 13666–13667 (2006).

27.   Jolly, P. *et al.* Label-free impedimetric aptasensor with antifouling surface chemistry: A prostate specific antigen case study. *Sens. Actuators B Chem.* **209,** 306–312 (2015).

28.   Formisano, N. *et al.* Optimisation of an Electrochemical Impedance Spectroscopy aptasensor by exploiting Quartz Crystal Microbalance with Dissipation Signals. *Sens. Actuators B Chem.* **220,** 369-375 (2015).

29.   Goda, T. & Miyahara, Y. Label-free and reagent-less protein biosensing using aptamer-modified extended-gate field-effect transistors. *Biosens. Bioelectron.* **45,** 89–94 (2013).

30.   Kim, E. H. & Andriole, G. L. Prostate-specific antigen-based screening: controversy and guidelines. *BMC Medicine* **13**, 61 (2015).

31.   Savory, N., Abe, K., Sode, K. & Ikebukuro, K. Selection of DNA aptamer against prostate specific antigen using a genetic algorithm and application to sensing. *Biosens. Bioelectron.* **26,** 1386–1391 (2010).

32.   Balk, S. P., Ko, Y.-J. & Bubley, G. J. Biology of prostate-specific antigen. *J. Clin. Oncol. Off. J. Am. Soc. Clin. Oncol.* **21,** 383–391 (2003).

33.   Alexander, C. *et al.* Molecular imprinting science and technology: a survey of the literature for the years up to and including 2003. *J. Mol. Recognit.* **19,** 106–180 (2006).

34.   Bossi, A., Bonini, F., Turner, A. P. F. & Piletsky, S. A. Molecularly imprinted polymers for the recognition of proteins: The state of the art. *Biosens. Bioelectron.* **22,** 1131–1137 (2007).

35.   Blanco-López, M. C., Lobo-Castañón, M. J., Miranda-Ordieres, A. J. & Tuñón-Blanco, P. Electrochemical sensors based on molecularly imprinted polymers. *Trends Anal.   Chem.   **23,**   36–48   (2004)*

6. Chapter: General Discussion and Overall Conclusions

6.1.   General Overview Of Thesis

Detection of prostate cancer depends primarily on early screening, which is currently based on detection of PSA despite various controversies surrounding the biomarker as discussed in Chapter 1. Looking at drawbacks of PSA, it is evident that there is an urgent need to look at newer biomarkers for disease stratification to help patients make informed decisions. The discovery of new biomarkers was outside the scope of the current project. However, the project could focus on building robust diagnostic platforms for currently available biomarkers such as t-PSA, fPSA and pro-PSA that could be then easily transferred to newly discovered biomarkers of PCa in the future. It was hypothesised that by using artificial receptors, the resulting biosensor would be more stable, robust and sensitive than traditional antibody biosensors. It was also proposed that integrating the MIPs with an electrochemical platform would allow for rapid detection of the biomarker and easy integration in a point-of-care device setting.

Synthesising MIPs for protein biomarkers is a challenging task as elaborated in Chapter 1. Various groups have used different approaches such as bulk imprinting, epitope imprinting, surface imprinting, MIP nanoparticles to achieve imprinting of large proteins.[1,2,3] However each approach has its own advantages and disadvantages, which need to be carefully considered before applying them for imprinting large proteins such as PSA. In the current work, three approaches: epitope imprinting, surface imprinting and hybrid imprinting were studied to imprint PSA and engineer a MIP biosensor that was capable of detecting PSA at clinically relevant concentrations and in clinically relevant media. The merits of each approach and further suggestions have been discussed in this section.

The initial work in Chapter 2 focussed on molecular imprinting of short PSA epitopes to screen monomers and understand imprinting efficiency using conventional bulk imprinting methods. This was the simplest approach to molecular imprinting of a large and complex biomolecule like PSA as the epitopes sequences could be readily synthesised in the laboratory and imprinted using fairly inexpensive monomers. A four amino acid epitope sequence (VANP) from C-terminus of PSA was selected for epitope imprinting. However, initial solubility studies demonstrated that the peptide was not soluble in non-polar solvents. As a result, DMSO was used a co-solvent with acetonitrile to imprinting VANP with MAA and AAm as the functional monomer. MAA and AAm demonstrated an apparent Kd of 102 μM and 154 μM with imprinting factors of 2.62 and 2.02 respectively. It was proposed that the low affinity could be a result of imprinted cavity relying heavily on hydrogen bond formation between peptide and monomers. As a result, a urea monomer was used to introduce ionic interaction in combination with AAM to obtain a polymer with better binding characteristic than MAA, AAm MIPs. However, an improvement in affinity (apparent Kd 194 μM) was not observed, and lower imprinting factors (1.42) were reported with this approach. The bulk imprinting technique allowed us to screen certain monomers and conduct simple binding experiments. However, the methods were too cumbersome and the template too scarce and expensive to undertake a larger monomer screening study. This would have been crucial for finding the right monomer-template combination to obtain high performing MIPs. One approach to overcome this hurdle in the future would be to use computational methods to obtain a pool of monomers that have a theoretical high affinity for the template and further performing an experimental screen to obtain high-affinity MIPs as described by Nicholls *et al.*[4]. However, it could be still quite challenging to

achieve MIPs with nM affinity using conventional bulk imprinting techniques and a shift in surface imprinting may be required with the selected monomers.

In Chapter 3, surface imprinting of PSA epitopes was undertaken to overcome some of the challenges faced with bulk imprinting techniques. Surface imprinting has been demonstrated to be a better alternative to bulk imprinting techniques due to low solubility issues, faster binding kinetics and low diffusional and mass transfer barriers.[3] Furthermore, surface imprinted MIPs can be integrated with sensing platforms to obtain efficient signal transduction and readouts.[5] The initial experiments in Chapter 3 focused on using the pro-PSA peptide, which in itself is a biomarker for cancer aggressiveness. It was proposed that results from pro-PSA epitope imprinting, if successful, could be easily transferred to the C-terminus PSA epitopes selected in Chapter 1. Dopamine was selected as a monomer for imprinting due to its low oxidation potential, the presence of functional groups that could interact with the template to form a highly selective cavity, ease of polymerisation in PBS pH 7.4 and superior electrochemical properties than other electroactive monomers. The pro-PSA peptide was modified with MUA (thiol) linker to confine the peptide to the surface to build more homogenous binding to sites to improve binding kinetics and sensitivity of the sensor. The pro-PSA MIP sensor showed specificity towards the pro-PSA peptide when compared to the NIP sensor (IF of 14). The sensor also demonstrated higher binding affinity (apparent Kd 10 μM) and LOD (1 μM) than bulk-imprinted polymers from Chapter 1. The pro-PSA sensor also exhibited selectivity when challenged with a test peptide containing a random amino acid sequence. Surface confinement of the template was also seen to have a positive effect (LOD 1 μM) when compared to conventionally prepared (no surface immobilisation) surface imprinted sensor (LOD 10 μM). However,

the inability to discriminate between two closely related or homologous peptides and low repeatability of the sensor suggests that further optimisation maybe required for efficient binding. However, one major drawback of E-MIP is the lack of functionality and over dependence on hydrogen bonding and π-π stacking for a selective cavity formation. This could be addressed by the use of electropolymerisable RAFT agents[6] to build a surface-imprinted polymer with highly specific functional monomers while retaining control over the thickness of the polymer using electrochemical stimulus. This technique could be the key to building different layers of polymers with varying functionality to build next generations MIPs on electrically conducting transducer surfaces.

In Chapter 4, the work on surface imprinting and electroactive monomers were continued for detection of fPSA. However, an alternative and more sophisticated imprinting technique called hybrid imprinting was explored to achieve higher sensitivity with the (E)-MIP sensors. It was proposed that to achieve greater sensitivity (nM range) with MIPs, an added level of functionally would be beneficial to enhance the overall affinity of the imprinted polymer. The hybrid imprinting technique allowed for the incorporation of a receptor (aptamer) with an established affinity towards fPSA to build a polymeric cavity with superior recognition properties than the polymer or aptamer alone. The hybrid imprinted MIP demonstrated an apparent Kd of 0.3 nM could discriminate between closely related protein such as hK2 and also detected clinically relevant concentrations of PSA (4-10 ng/ml). Moreover, the sensor showed very little fouling to serum protein HSA. The apta-MIP sensors exhibited great promise in detecting clinically relevant proteins such as PSA at clinically relevant concentrations with high selectivity. However, the use of redox solution in the system slowed the detection process and reduced the stability of the sensor.

Hence, in Chapter 5, the apta-MIP technique was further extended to MOSFET devices to increase sensitivity and provide scope for miniaturisation without the need of redox solution. The MOSFET devices were found to be 100 times more sensitive that EIS sensor and allowed the detection of PSA in PBS pH 7.4. These results encouraged some preliminary experiments in diluted plasma. PSA concentrations between 1 and 10 pg/ml of PSA could be detected linearly in diluted plasma using the MOSFET apta-MIP sensors. Although, a loss of sensitivity was observed when samples were measured in plasma (compared to PBS buffer), the experiments highlighted the potential use of apta-MIP devices for sensitive detection of biomarkers in human blood at clinically relevant concentrations.

Despite the good sensitivity and selectivity achieved with the hybrid-MIP electrochemical sensing technique, further work is required to understand the mechanism of binding and the contribution of the polymer towards the total affinity of the MIP. Use of techniques such as QCM and SPR techniques could help determine binding characteristics and also help calculate actual affinity constants for the hybrid polymers, which could further support the data obtained from electrochemical sensors. Comparison studies also need to be carried out using different receptors such an antibodies, peptides and small molecules to investigate if aptamers are the most efficient receptors for hybrid imprinting technique.

In conclusion, the current work showcases that surface imprinting has a clear advantage over bulk imprinting for detection of biomolecules such as peptides and proteins in terms of ease of fabrication, overall sensitivity and affinity. However, the combination of hybrid-MIP receptors with electrochemical platforms gives the added advantage of detecting biomolecules that are found in extremely low concentrations in the human body with high

sensitivity and selectivity. It is proposed that hybrid imprinting could help develop the next generation of MIP sensors that are robust, sensitive and stable and can be translated to other clinical biomarkers. Furthermore, the integration of the hybrid-MIP with an electrochemical platform permits rapid detection of template and scope for miniaturisation, which allows for fabrication of a point-of-care device. It is proposed that further advances in the field of hybrid imprinting and sensing could allow for development of portable MIP sensors for clinical biomarkers in the near future.

6.2.   References

1.   Erdőssy, J., Horváth, V., Yarman, A., Scheller, F. W. & Gyurcsányi, R. E. Electrosynthesized molecularly imprinted polymers for protein recognition. *TrAC Trends Anal. Chem.* **79,** 179–190 (2016).

2.   Nishino, H., Huang, C.-S. & Shea, K. J. Selective protein capture by epitope imprinting. *Angew. Chem. Int. Ed Engl.* **45,** 2392–2396 (2006).

3.   Turner, N. W. *et al.* From 3D to 2D: A Review of the Molecular Imprinting of Proteins. *Biotechnol. Prog.* **22,** 1474–1489 (2006).

4.   Nicholls, I. A. *et al.* Theoretical and Computational Strategies for the Study of the Molecular Imprinting Process and Polymer Performance. *Adv. Biochem. Eng. Biotechnol.* **150,** 25–50 (2015).

5.   Sharma, P. S., Pietrzyk-Le, A., D'Souza, F. & Kutner, W. Electrochemically synthesized polymers in molecular imprinting for chemical sensing. *Anal. Bioanal. Chem.* **402,** 3177–3204 (2012).

6.   Grande, C. D., Tria, M. C., Jiang, G., Ponnapati, R. & Advincula, R. Surface-Grafted Polymers from Electropolymerized Polythiophene RAFT Agent. *Macromolecules* **44,** 966–975 (2011).